

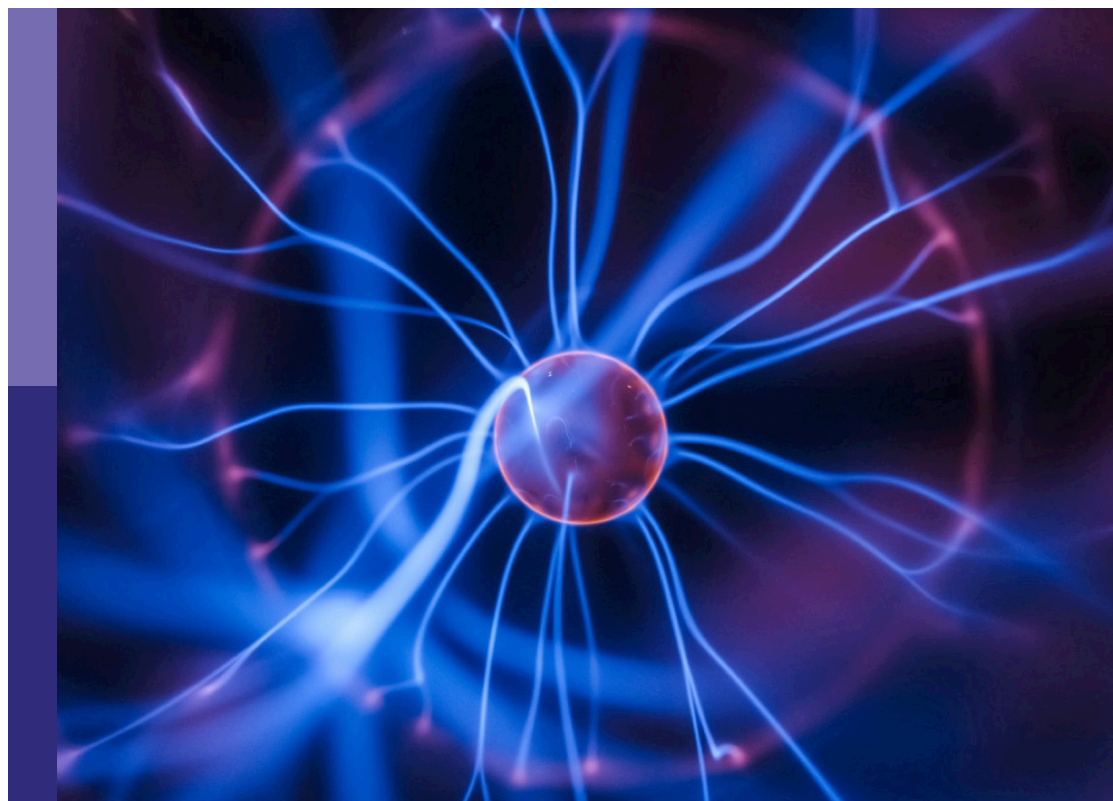
# Lost circulation control during drilling and completion in complex formations

**Edited by**

Chong Lin, Arash Dahi Taleghani, Zhenjiang You  
and Chengyuan Xu

**Published in**

Frontiers in Physics



## FRONTIERS EBOOK COPYRIGHT STATEMENT

The copyright in the text of individual articles in this ebook is the property of their respective authors or their respective institutions or funders. The copyright in graphics and images within each article may be subject to copyright of other parties. In both cases this is subject to a license granted to Frontiers.

The compilation of articles constituting this ebook is the property of Frontiers.

Each article within this ebook, and the ebook itself, are published under the most recent version of the Creative Commons CC-BY licence. The version current at the date of publication of this ebook is CC-BY 4.0. If the CC-BY licence is updated, the licence granted by Frontiers is automatically updated to the new version.

When exercising any right under the CC-BY licence, Frontiers must be attributed as the original publisher of the article or ebook, as applicable.

Authors have the responsibility of ensuring that any graphics or other materials which are the property of others may be included in the CC-BY licence, but this should be checked before relying on the CC-BY licence to reproduce those materials. Any copyright notices relating to those materials must be complied with.

Copyright and source acknowledgement notices may not be removed and must be displayed in any copy, derivative work or partial copy which includes the elements in question.

All copyright, and all rights therein, are protected by national and international copyright laws. The above represents a summary only. For further information please read Frontiers' Conditions for Website Use and Copyright Statement, and the applicable CC-BY licence.

ISSN 1664-8714  
ISBN 978-2-8325-3740-4  
DOI 10.3389/978-2-8325-3740-4

## About Frontiers

Frontiers is more than just an open access publisher of scholarly articles: it is a pioneering approach to the world of academia, radically improving the way scholarly research is managed. The grand vision of Frontiers is a world where all people have an equal opportunity to seek, share and generate knowledge. Frontiers provides immediate and permanent online open access to all its publications, but this alone is not enough to realize our grand goals.

## Frontiers journal series

The Frontiers journal series is a multi-tier and interdisciplinary set of open-access, online journals, promising a paradigm shift from the current review, selection and dissemination processes in academic publishing. All Frontiers journals are driven by researchers for researchers; therefore, they constitute a service to the scholarly community. At the same time, the *Frontiers journal series* operates on a revolutionary invention, the tiered publishing system, initially addressing specific communities of scholars, and gradually climbing up to broader public understanding, thus serving the interests of the lay society, too.

## Dedication to quality

Each Frontiers article is a landmark of the highest quality, thanks to genuinely collaborative interactions between authors and review editors, who include some of the world's best academicians. Research must be certified by peers before entering a stream of knowledge that may eventually reach the public - and shape society; therefore, Frontiers only applies the most rigorous and unbiased reviews. Frontiers revolutionizes research publishing by freely delivering the most outstanding research, evaluated with no bias from both the academic and social point of view. By applying the most advanced information technologies, Frontiers is catapulting scholarly publishing into a new generation.

## What are Frontiers Research Topics?

Frontiers Research Topics are very popular trademarks of the *Frontiers journals series*: they are collections of at least ten articles, all centered on a particular subject. With their unique mix of varied contributions from Original Research to Review Articles, Frontiers Research Topics unify the most influential researchers, the latest key findings and historical advances in a hot research area.

Find out more on how to host your own Frontiers Research Topic or contribute to one as an author by contacting the Frontiers editorial office: [frontiersin.org/about/contact](https://frontiersin.org/about/contact)

# Lost circulation control during drilling and completion in complex formations

## Topic editors

Chong Lin — CCDC Drilling & Production Technology Research Institute, China  
Arash Dahi Taleghani — The Pennsylvania State University (PSU), United States  
Zhenjiang You — Edith Cowan University, Australia  
Chengyuan Xu — Southwest Petroleum University, China

## Citation

Lin, C., Taleghani, A. D., You, Z., Xu, C., eds. (2023). *Lost circulation control during drilling and completion in complex formations*. Lausanne: Frontiers Media SA.  
doi: 10.3389/978-2-8325-3740-4

## Table of contents

04	<b>Editorial: Lost circulation control during drilling and completion in complex formations</b> Chong Lin, Arash Dahi Taleghani, Chengyuan Xu and Zhenjiang You
06	<b>Bridging performances of lost circulation materials (LC-LUBE and mica) and their blending in 80/20 and 60/40 oil-based drilling fluids</b> Mesfin Belayneh and Bernt Aadnøy
20	<b>Plugging efficiency of flaky and fibrous lost circulation materials in different carrier fluid systems</b> Saleh A. Alhaidari, Sulaiman A. Alarifi and Abdulaziz Bahamdan
39	<b>Study and application of temporary plugging agent for temporary plugging acid fracturing in ultra-deep wells of Penglai gas field</b> Yang Wang, Yu Fan and Weihua Chen
48	<b>Experimental studies on the performance evaluation of water-soluble polymers used as temporary plugging agents</b> Guangai Wu, Zhengrong Chen, Anshun Zhang, Jun Zhou, Yanan Hou, Xin Xie, Jianshu Wu, Xiangwei Kong and Song Li
61	<b>Composite stimulation technology for improving fracture length and conductivity of unconventional reservoirs</b> Yang Wang and Zefei Lv
70	<b>An experimental evaluation method of drilling fluid lost control efficiency considering loss types</b> Jingyi Zhang, Yili Kang, Yunhui Deng, Chengyuan Xu, Xiaopeng Yan, Chong Lin and Xiaojiang Cui
84	<b>Study on migration law of multiscale temporary plugging agent in rough fractures of shale oil reservoirs</b> Yang Wang, Yu Fan and Xiaojiao Wang
96	<b>Finite element study on the initiation of new fractures in temporary plugging fracturing</b> Xuesong Xing, Guangai Wu, Jun Zhou, Anshun Zhang, Yanan Hou, Xin Xie, Jianshu Wu, Xiangwei Kong and Song Li
109	<b>Optimization of degradable temporary plugging material and experimental study on stability of temporary plugging layer</b> Zhengrong Chen, Guangai Wu, Jun Zhou, Chuanzhi Ai, Anshun Zhang, Xin Xie, Jianshu Wu, Xiangwei Kong and Song Li





## OPEN ACCESS

EDITED AND REVIEWED BY  
Alex Hansen,  
Norwegian University of Science and  
Technology, Norway

\*CORRESPONDENCE  
Chong Lin,  
✉ linchong891020@163.com

RECEIVED 12 September 2023  
ACCEPTED 25 September 2023  
PUBLISHED 04 October 2023

CITATION  
Lin C, Dahi Taleghani A, Xu C and You Z  
(2023), Editorial: Lost circulation control  
during drilling and completion in  
complex formations.  
*Front. Phys.* 11:1293208.  
doi: 10.3389/fphy.2023.1293208

COPYRIGHT  
© 2023 Lin, Dahi Taleghani, Xu and You.  
This is an open-access article distributed  
under the terms of the [Creative  
Commons Attribution License \(CC BY\)](#).  
The use, distribution or reproduction in  
other forums is permitted, provided the  
original author(s) and the copyright  
owner(s) are credited and that the original  
publication in this journal is cited, in  
accordance with accepted academic  
practice. No use, distribution or  
reproduction is permitted which does not  
comply with these terms.

# Editorial: Lost circulation control during drilling and completion in complex formations

Chong Lin<sup>1\*</sup>, Arash Dahi Taleghani<sup>2</sup>, Chengyuan Xu<sup>3</sup> and  
Zhenjiang You<sup>4</sup>

<sup>1</sup>CCDC Drilling Production Technology Research Institute, Guanghan, China, <sup>2</sup>Department of Energy and Mineral Engineering, The Pennsylvania State University, University Park, PA, United States, <sup>3</sup>State Key Laboratory of Oil and Gas Reservoir Geology and Exploitation, Southwest Petroleum University, Chengdu, China, <sup>4</sup>Centre for Sustainable Energy and Resources, Edith Cowan University, Joondalup, WA, Australia

## KEYWORDS

lost circulation, wellbore strengthening, multiphase flow, geomechanics, granular mechanics

## Editorial on the Research Topic

### Lost circulation control during drilling and completion in complex formations

Well drilling is a common method for Earth exploration, underground mineral resource extraction, and geological storage of nuclear waste and carbon dioxide. Drilling fluid circulates in the well during drilling, cooling the drill bit, transporting rock cuttings, preventing wellbore collapse, and balancing formation pressure. Lost circulation occurs when less fluid returns from the wellbore than is pumped into it, resulting in economic losses due to drilling fluid wastage and nonproductive time. Untreated losses can cause well control issues, poor hole cleaning, pack-offs, and stuck pipe, impairing normal drilling. Lost circulation incidents are more likely to occur with the increasing share of difficult wells (deep-water, deviated, horizontal, high pressure, high temperature) in the drilling portfolio. It is one of the most troublesome drilling problems.

Lost circulation is a longstanding challenge in drilling that worsens under extreme conditions. To prevent and cure losses, we need to understand their causes, locations, and control methods. This entails elucidating four physical science issues: 1) multiphase flow in the drilling assembly-wellbore-formation system; 2) geomechanics, rock mechanics, and fracture mechanics during fracture initiation and propagation; 3) material and granular mechanics of the sealing zone formed by physical or chemical lost circulation materials; 4) fluid-structure interactions between multiphase fluid and rock. We present a Research Topic on lost circulation control during drilling and completion in complex formations that addresses these issues. This Research Topic aims to fill the gaps among fundamental theories, applied technologies and field practices, reporting recent innovations and advances related to lost circulation control during drilling and completion in complex formations.

We received 14 papers for this Research Topic and selected 9 for publication after careful review. The papers cover materials, experiments, mathematical models, and numerical simulations for lost circulation control.

The paper “*Study and application of temporary plugging agent for temporary plugging acid fracturing in ultra-deep wells of Penglai gas field*” by Wang et al. developed a temporary

plugging agent based on polyemulsion-modified polyvinyl alcohol resin for multi-stage acid fracturing. The agent, composed of fiber and granular resin, had an experimental fracture plugging strength of over 20 MPa. The paper “*Experimental studies on the performance evaluation of water-soluble polymers used as temporary plugging agents*” by Wu et al. tested a new temporary plugging agent made of degradable water-soluble polymer. The agent showed good temporary plugging performance due to its high plugging strength, temperature-controlled water degradation, stable reflux, and effective self-supporting after degradation. These two papers present two new lost circulation materials (LCMs) for enhancing temporary lost circulation control, especially in pay zones.

The paper “*Composite stimulation technology for improving fracture length and conductivity of unconventional reservoirs*” by Wang and Lv visualized ceramic proppant migration in vertical fractures. They found that non-uniform sized ceramic particles formed smoother sand dikes and migrated better to the fracture tip than uniform sized ones. The paper “*Study on migration law of multiscale temporary plugging agent in rough fractures of shale oil reservoirs*” by Wang et al. examined the effects of morphology, concentration, and combination of temporary plugging agents, as well as fracture width and roughness, on fracture plugging performance. Particles alone plugged fractures more effectively than fibers did, whereas a mixture of fibers and large and small particles yielded the best performance. Increasing fiber concentration in the mixture enhanced plugging pressure and reduced plugging time. Higher overall concentration of temporary plugging agents also increased plugging pressure. Rough fractures were easier to plug than smooth ones. These two papers offer insights for improving the placement and sealing efficiency of LCM slurry in fractures.

The paper “*An experimental evaluation method of drilling fluid lost control efficiency considering loss types*” by Zhang et al. quantified the main factors controlling lost circulation efficiency and proposed a new experimental method to evaluate it in fractured formations with different loss types. Their results showed a better agreement between indoor experimental lost circulation efficiency and on-site data. The paper “*Optimization of degradable temporary plugging material and experimental study on stability of temporary plugging layer*” by Chen et al. measured permeability under various confining pressures to optimize the temporary plugging material formula, and assessed the stability and degradability of the temporary plugging layer. They found that a mixture of hyperfine  $\text{CaCO}_3$  and walnut-shell particles formed a tight and stable plugging layer under increasing confining pressure, resulting in the best temporary plugging performance. These methods bridge the gap between experimental and real downhole conditions and improve the guidance of indoor experiments for on-site operations.

The paper “*Bridging performances of lost circulation materials (LC-LUBE and mica) and their blending in 80/20 and 60/40 oil-based drilling fluids*” by Belayneh and Aadnøy compared 80/20 and 60/40 oil-based drilling fluids (OBMs) on LCMs bridging performance, filtrate loss, barite sagging, and shale stability. They found that a mica and LC-LUBE blend had the best bridging performance, and that 60/40 OBM had better bridging stability, sagging, and filtrate loss than 80/20 OBM. The paper “*Plugging efficiency of flaky and fibrous lost circulation materials in different carrier fluid systems*” by Alhaidari et al. demonstrated the effect of carrier fluid on the plugging efficiency of flaky and fibrous LCMs. Carrier fluid exposure changed the particle size distribution, shape, specific gravity, fluid loss, and fracture plugging of LCMs, depending on the type of LCM and carrier fluid. These two papers highlight the importance of carrier fluid type for LCM and provide experimental evidence for selecting specialized LCM based on carrier fluid.

The paper “*Finite element study on the initiation of new fractures in temporary plugging fracturing*” by Xing et al. compared the stress field around the artificial fracture before and after production, and determined the mechanical conditions for new fracture initiation during temporary plugging fracturing. They discovered that stress field and pore pressure variations induced new fractures in re-fracturing processes, accounting for the increased lost circulation and difficulty in control in pressure-depleted formations.

## Author contributions

CL: Writing—original draft. AD: Writing—review and editing. CX: Writing—review and editing. ZY: Writing—review and editing.

## Conflict of interest

Author CL was employed by the company CCDC Drilling Production Technology Research Institute.

The remaining authors declare that the research was conducted in the absence of any commercial or financial relationships that could be construed as a potential conflict of interest.

## Publisher's note

All claims expressed in this article are solely those of the authors and do not necessarily represent those of their affiliated organizations, or those of the publisher, the editors and the reviewers. Any product that may be evaluated in this article, or claim that may be made by its manufacturer, is not guaranteed or endorsed by the publisher.



## OPEN ACCESS

EDITED BY  
Chong Lin,  
CCDC Drilling & Production  
Technology Research Institute, China

REVIEWED BY  
Xiaopeng Yan,  
Changzhou University, China  
Zhu Baiyu,  
Yangtze University, China

\*CORRESPONDENCE  
Mesfin Belayneh,  
mesfin.a.belayneh@uis.no  
Bernt Aadnøy,  
bernt.aadnøy@uis.no

SPECIALTY SECTION  
This article was submitted to  
Interdisciplinary Physics,  
a section of the journal  
Frontiers in Physics

RECEIVED 12 September 2022  
ACCEPTED 17 October 2022  
PUBLISHED 17 November 2022

CITATION  
Belayneh M and Aadnøy B (2022),  
Bridging performances of lost  
circulation materials (LC-LUBE and  
mica) and their blending in 80/20 and  
60/40 oil-based drilling fluids.  
*Front. Phys.* 10:1042242.  
doi: 10.3389/fphy.2022.1042242

COPYRIGHT  
© 2022 Belayneh and Aadnøy. This is an  
open-access article distributed under  
the terms of the [Creative Commons  
Attribution License \(CC BY\)](#). The use,  
distribution or reproduction in other  
forums is permitted, provided the  
original author(s) and the copyright  
owner(s) are credited and that the  
original publication in this journal is  
cited, in accordance with accepted  
academic practice. No use, distribution  
or reproduction is permitted which does  
not comply with these terms.

# Bridging performances of lost circulation materials (LC-LUBE and mica) and their blending in 80/20 and 60/40 oil-based drilling fluids

Mesfin Belayneh\* and Bernt Aadnøy\*

Department of Energy and Petroleum Engineering, University of Stavanger, Stavanger, Norway

In drilling wells, lost circulation, barite sagging, shale swelling, and formation damage are critical problems for the industry. These problems can be controlled by designing appropriate drilling fluids and lost circulation materials. In this study, the performance of 80/20 and 60/40 oil-based drilling fluids (OBMs) was compared based on the lost circulation materials' (LCMs) bridging performance, filtrate loss, barite sagging, and shale stability. The results show that in terms of LCM stability, the performance of LC-LUBE improved when blended with mica. Both drilling fluids inhibit shale swelling. The overall analysis showed that the 60/40 OBM is better and recommended.

## KEYWORDS

LCM, LC-lube, 80/20 OBM, 60/40 OBM, sagging, swelling, bridging

## 1 Introduction

Borehole instability problems occur during the drilling, completion, and production phases. Although in the past much progress has been made to solve the problem, it remains a challenging issue for the oil industry. The two main factors causing borehole instability are classified as mechanical and chemical effects. The physical-chemical fluid-rock interaction phenomena modify the near-wellbore rock strength. The main mechanisms are hydration, osmotic pressures, swelling, rock softening, and strength changes [1]. Knowledge of these helps for modeling and simulation of a wellbore stability study.

Drilling in natural fractures, highly permeable formation, and vugular and cavernous rocks, as well as drilling-induced fractures, result in undesired fluid loss, which is commonly called lost circulation. This could occur during drilling and cementing operations. Depending on the rate of losses, circulation losses are classified as seepage, partial, severe, or total circulation losses. Since the classification of circulation losses is not globally standardized, various classifications are documented by different authors [2–5]. A drilling-induced fracture occurs as the well pressure causes the minimum stress around the wellbore to exceed the tensile strength of the formation. Well fracturing can be controlled by designing appropriate mud density and fluid

properties (rheology and chemistry) that control the possible pore pressure build-up to reduce the well strength-weakening effect. However, when it comes to natural fractures, vugs, and cavern openings in dolomites and limestones, they exist *in situ*. Therefore, lost circulation is prevented or controlled by using lost circulation control materials (LCMs), which creates a self-healing/sealing mechanism in case the drilling formation contains micro-fractures.

Studies from the deep-water environments in the Gulf of Mexico showed that about one-third of the overall NPT incidents are due to lost circulation (>10%), kick (>10%), and stuck pipe (>10%) [6]. On average, the non-productive time associated with wellbore instability problems increases the drilling time by 15% [7], and Ref. [8] also reported that NPT increases the cost in the range of 10–20%.

Literature-documented laboratory experimental results have shown that lost circulation materials (LCMs) decrease fluid losses and also increase the wellbore strengthening effects [9–20]. The fracture initiation and propagation experimental studies conducted by [21] showed that both the OBM and water-based drilling fluid (WBM) recorded a similar fracture initiation pressure. However, the reopening pressures with the WBM fluids were higher. The authors interpreted the experimental data that the water-based fluids have fracture healing capability. Reference [22] presented experimental data from fracturing experiments using oil-based drilling fluids. The authors proposed operational guidelines and showed significant differences between oil- and water-based drilling fluids. Over the years, several experimental studies have been carried out at the University of Stavanger with penetrating and non-penetrating fluids. The results have shown that the penetrating fluids build up the formation pressure and, hence, recorded a lower fracturing pressure than the non-penetrating fluid [23]. This shows that the drilling fluid with a good sealing capacity at the face of the wellbore increases the wellbore strength. The sealing capacity of the drilling fluid is determined by how good enough the drilling fluid additives are to create a stronger and impermeable mud cake. Moreover, the fracturing pressure with three different commercial water-based drilling fluids' results showed that the fracturing pressure depends on the drilling fluids, which is associated with the quality of the mud cake it forms on the wellbore [24].

Recently, the applications of nanoparticles (1–100 nm size) have shown impressive performance in drilling fluids, cement, and enhanced oil recovery. Compared with microparticles such as LCM, the surface area-to-volume ratio of the nanoparticle is extremely high [25]. The impact of nanoparticles on OBM and WBM showed an improved rheological property [26–29], filtrate loss, and filter cake thickness reduction [26–31], plugging the pore spaces of shale and, hence, reducing its permeability [32–34], improving the lubricity [27, 28, 35–37], increasing the wellbore strength [38], enhancing the electrical conductivity and thermal conductivity of the conventional

drilling fluids [39–43], and inhibiting shale swelling [44, 45]. When it comes to wellbore strength, Ref. [38] reported that the addition of an optimal blend of iron III hydroxide nanoparticles and micro-sized graphite with a water-based drilling fluid increased the fracture strength by 70%. The fracture strength increased by 36% as the optimal calcium carbonate nanoparticles blended with micro-sized graphite in the oil-based drilling fluid. These results could be due to the improvement of the cake and the fluid's lost reduction properties as well, which reduced the communication between the well and the formation. Moreover, as reported in references [32–34], the plugging of the nanoparticles in shale inhibits water absorption and hence minimizes the shale swelling issue.

From the reviewed materials, the sealing/bridging performance of particulates (nano/micro) at a given fracture width depends on the type of the drilling fluid to be interacted with, the particle concentration, types, sizes, and the mechanical and chemical properties of the particles as well. The overall effect is associated with the strength of the LCM bridging in the mud cake. Oil-based drilling fluids are effective in maintaining wellbore stability and lubrication, which is suitable for drilling long-reach wells. However, oil-based drilling fluids are expensive and not environmentally friendly. The issues addressed in this study are the performances of the 80/20 and 60/40 OBMs concerning LCM stability at fracture gates, sagging potential, filtrate loss, and shale swelling inhibition performances. The comparisons of the two mud systems will be investigated through the single LCM and the blending of LCMs to investigate the effect of particle synergy.

## 2 Literature study

### 2.1 Lost circulation management

The commonly used methods to manage lost circulation are categorized as preventive and remedial action [3]. LCM and techniques are used to combat circulation loss problems. LCM testing and developing the best designs are the key to successful lost circulation management. The remedial action is conducted based on the severity of the loss rates in the formation.

#### 2.1.1 Preventive treatments

Preventive actions include using wellbore strengthening materials, drilling fluid selections, and best drilling practices. The reviewed materials indicate that the micro-sized LCM [46] and nanoparticle-based LCMs [38] increased the wellbore strength. Moreover, the bridging performance of the LCM particles assessed at the artificial slot and also the lost circulation material prevents huge mud loss by bridging at the gate of the fracture. The key elements for a good preventive method (i.e., wellbore strengthening and preventing losses) depend on selecting the right particle size spectrum, particles'

mechanical strength, shape, and size along with their interaction with the drilling fluids as well.

### 2.1.2 Remedial treatments

The remedial treatments for lost circulation management are performed by using lost circulation materials. The design of the LCM depends on the severity of the loss. The lost circulation cure/hindrane can be conducted by conditioning the drilling fluid with lost circulation materials or by using stop-loss pills. In this study, the preventive performance of pure LC-LUBE and mica and their mixture will be experimentally evaluated to investigate the synergy of particles. Different companies do have their own lost circulation treatment decision tree. When the loss is severe, the pill system is designed based on fibers, flakes, and particles that will be blended with a drilling fluid. However, before the application of the pill system, it is important to evaluate the LCM's bridging strength and optimize the design as well through an experimental study.

## 2.2 Lost circulation material selection approaches

The selection of a proper particle size, shape, and concentration along with a high-resilience LCM is of significant importance to achieve an effective bridge at the fracture gate. In the drilling fluid industry, theories have been developed to determine optimum particle sizes, namely, based on the ideal packing theory and particle size distribution (PSD). Based on the particle size distribution, the approaches to optimize bridging blends to seal the formation surface are based on  $D_{90}$ ,  $D_{50}$ , and  $D_{10}$ . The LCM selection approaches are documented in [47–50]. On the other hand, the ideal packing theory concept states that the median pore size can be estimated from the permeability by taking the square root of the permeability. The pore size is the median size of the pores, which is known as  $D_{50}$  [51]. The packing of the particle is affected by the size distribution and shape of the particles.

## 2.3 Lost circulation materials

In the industry, several lost circulation materials (LCMs) are developed and are in use. The LCMs are of particles, flaky, fibrous, and mixtures. Several investigators have reviewed the types and their bridging performance as well [52–58]. In this study, LC-LUBE (graphite), mica, and their blending are evaluated in two different oil-based drilling fluids. Both have different mechanical, structural, lubricity, and hardness properties. The particles are used in the industry.

## 2.4 Mud cake deposition and mechanism of particle bridging at the fracture gate

Due to differential pressures on a wellbore, particles and cuttings in a drilling fluid are filtered out and deposited in/at the gate fractures and on the wall of a wellbore (Figure 1). The filter cake eventually controls the flow between the well and the formation.

Figure 1 shows particle deposition on the wall of the unfractured wellbore (Figure 1A) and after wellbore fracturing at the fracture wings (Figure 1B). When a wellbore fractures, the mechanical strength and stability of the bridging at the mouth of the fracture play a key role in hindering the mudflow and healing the fracture to strengthen the wellbore.

The frictional force between the particles and the drilling fluid's properties such as viscosity and the coefficient of friction determines the net contact force between particles in a mud cake. At the right wing of the fracture (Figure 1B), stable bridging disconnects a pressure communication between the wellbore and the fracture tip. At the left wing of the fracture, the collapsed bridge allows pressure communication between the well and the fracture tip. The pressure applied on the walls of the fracture causes the fracture tip to grow and results in mud loss.

When particles plug at the gate of the fracture, the state of stress changes. The concept of stress caging due to particle deposition is shown in Figure 1B. Stress caging is the suggested mechanism for wellbore strengthening, which is by increasing the hoop stress around the borehole [46].

Studies at the University of Stavanger also indicated the importance of LCM properties and the developed plastic deformation of the filter cake as fracturing occurs. The strength of bridging depends on several factors including the mechanical and structural properties and concentration of the particles along with the drilling fluid properties.

Wellbore fracture, in general, occurs when the hoop stress exceeds the tensile strength of the wellbore. The hoop stress is a function of the wellbore pressure. In the presence of a mud cake, Aadnøy et al. presented a qualitative description of the fracturing process, which includes the fracture initiation, growth, and particle bridging phenomenon at the gate of the fracture [7].

## 3 Experimental design

Results obtained from several LCM bridging tests conducted at the University of Stavanger showed that the LCM plug fractures quite well when the fracture width size is around the  $D_{50}$  value of the PSD and the concentration of particles is about 5% by wt. of the drilling fluid. This is in line with Ref. [50]. However, the bridging performance of LCMs also depends on the characteristics of the particles (i.e., size, shape, hardness, and lubricity) and the drilling fluid. Experiments also showed that the blending of particles creates positive and negative synergies



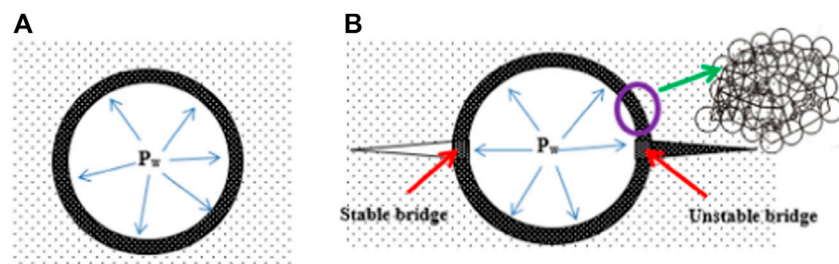


FIGURE 1

(A) Before fracturing and mud cake (particle deposition). Figure 1(B): After fracturing, the stable/unstable bridge at the fracture wings.

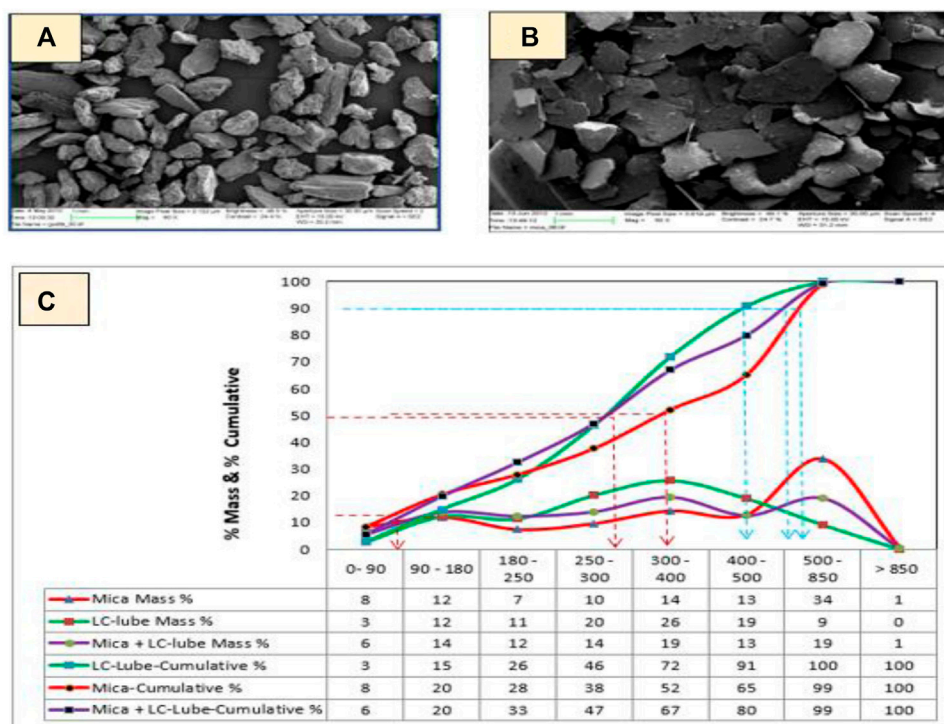


FIGURE 2

SEM picture of LC-LUBE (A) and mica (B), and cumulative particle size distribution (size is in micrometer) (C).

resulting in mechanically weak and stronger bridges, respectively. The selection of the right particle mix in terms of type and concentration is investigated through several experimental tests.

### 3.1 Material and methods

#### 3.1.1 Lost circulation materials

Quantifying the particle size and shape is important to evaluate the bridging performances of lost circulation

materials. In this study, the effect of mica, LC-LUBE, and their blending in 80/20 and 60/40 OBMs is investigated at different fracture slots.

LC-LUBE™ is a synthetic graphite particulate and is used as a fluid lost material. Mechanically, on the Mohs scale, the hardness of graphite is about 1–2. This allows the particle to be easily deformed at the gate of the fracture and shows a good bridging property [46]. The blending of LC-LUBE in drilling fluids has also a function as a solid lubricant. Figure 2 shows a scanning electron microscope (SEM) picture which provides an

**TABLE 1** Measured viscometer, density, and the calculated rheological parameters of drilling fluids.

Revolutions per minute (rpm)	Drilling fluid-1		Drilling fluid-2	
	60/40	80/20	60/40	80/20
600	261	160	261	80
300	161	98	149	44
200	124	76	109	32
100	81	50	67	20
6	23	17	18	5
3	19	15	16	4.5
<b>Rheological parameter</b>				
Density, sg	1.75	1.75	1.75	1.75
PV [lb/100 ft <sup>2</sup> ]	100	62	112	36
YS [lb/100 ft <sup>2</sup> ]	61	36	37	8
LSYS [lb/100 ft <sup>2</sup> ]	15	13	14	4
n [-]	0.696	0.707	0.81	0.86
k [lb.f.s <sup>n</sup> /100 ft <sup>2</sup> ]	2.09	1.194	0.96	0.20

insight into the structure of the particles. As can be seen from the SEM, the LC-LUBE (Figure 2A) particle is an irregular crystalline structure with a rough surface.

Mica is an aluminosilicate mineral. The SEM picture shows that the mica particle (Figure 2B) is irregular with a sheet or plate-like structure. Mica forms flat six-sided crystals with a significant cleavage in the direction of large surfaces, which permits them to easily split into flat films. Its hardness on the Mohs scale is 2–4.

To quantify the particle size distribution (PSD), a sieved analysis was performed. The particle cumulative weight percentage and the retention percentage are shown in Figure 2C. From the curve, one can observe the  $D_{10}$  values of all the particles lying within the same spectrum (0–90  $\mu\text{m}$ ). The  $D_{50}$  values of LC-LUBE and mica are within 250–300  $\mu\text{m}$  and 300–400  $\mu\text{m}$ , respectively, and their mixture is within 250–300  $\mu\text{m}$ . The drilling fluids contain a weight material, barite. The particle size distribution of barite shows small sizes. The PSD of barite showed that  $D_{10}$ ,  $D_{50}$ , and  $D_{90}$  values are 1.51  $\mu\text{m}$ , 14.52  $\mu\text{m}$ , and 65.18  $\mu\text{m}$ , respectively.

### 3.1.2 Drilling fluid-1 for lost circulation material and swelling evaluation

For the LCM performance study, two 1.75 sg oil-based mud systems with 80/20 and 60/40 oil-to-water ratios (OWRs) were prepared. The formulation is according to M-I SWACO, which is typically used for drilling operations.

#### 3.1.2.1 Drilling fluid-1 for lost circulation material, filtrate loss, and shale swelling evaluation

The drilling fluid-1 chemical composition analysis results showed that the brines (water-to-salt ratio) of the drilling fluid

systems are about 2.2, which is to obtain equal water phase salinity. The barite-to-water ratio of the 80:20 OBM is about twice that of the 60:40 OBM. Table 1 shows the viscometer responses of the drilling fluids measured at room temperature and the calculated Bingham plastic and power-law rheological parameters. Results showed that the Bingham plastic viscosity (PV), yield strength (YS), and lower shear stress (LSYS) of the 60/40 OBM are 1.6, 1.7, and 1.2 times higher than those of the 80/20 OBM, respectively. The power-law flow index parameters show closer values. On the other hand, the consistency index value of the 60/40 OBM is about 75% higher than that of the 80/20 OBM.

#### 3.1.2.2 Drilling fluid-2 for barite sagging evaluation

For the sagging evaluations, 60/40 and 80/20 OBM drilling fluids were obtained from M-I SWACO. The drilling fluids have the same density, which is 1,750 kg/m<sup>3</sup>, and different oil-to-water ratios (OWRs). Analysis of the chemical compositions of drilling fluid-2 showed that the brines (water-to-salt ratio) of the two drilling fluid systems are the same to obtain equal water phase salinity. The barite-to-water ratio of the 80:20 OBM is about twice that of the 60:40 OBM. As shown in Table 1, the calculated Bingham plastic viscosity (PV), yield strength (YS), and lower shear stress (LSYS) of the 60/40 OBM are 3.1, 4.6, and 3.5 times higher than those of the 80/20 OBMs, respectively. Except for the flow index, the power-law parameters such as the consistency index of the 60/40 OBM is 4.55 times higher than that of the 80/20 OBMs.

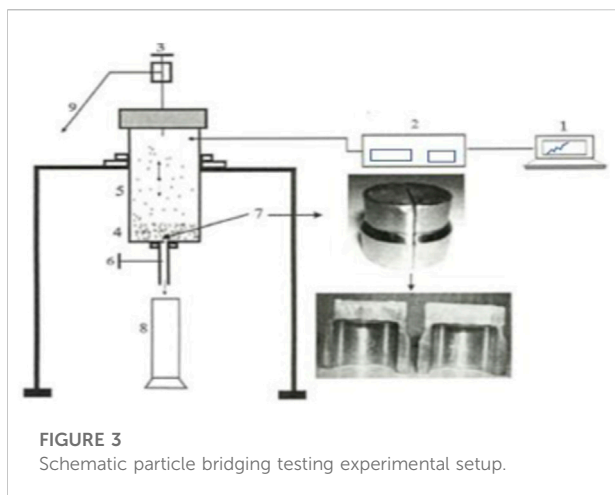
### 3.1.3 Characterization methods

#### 3.1.3.1 Lost circulation material bridging mechanical testing

Figure 3 shows a schematic diagram of the LCM bridging test experimental setup built at the University of Stavanger. The dimensions of the cylindrical drilling fluid holder (5) are 35 mm and 64 mm for the inner and outer diameters, respectively, and 150 mm long. The reason for the single-slot design was to simulate the fractured wing, as shown in Figure 1. The depth of the slots is 10 mm, and the length is 24.4 mm. The drilling fluid blended with the LCM filled in the drilling fluid holder forms a mud cake (4) at the gate of the slot (7), as shown at the fracture wings (Figure 1). The pressure response applied by the Gilson pump (2) on the mud cake was recorded using PC-control LabVIEW (1). The work process is as follows:

- First, we tested the system's maximum pressure that the experimental setup can hold without showing leakage during the testing and found it to be 50 MPa. We, therefore, set the maximum pressure limit during testing to be 50 MPa.
- From experience, we observed that LCM testing over 25 min sometimes showed water breakthrough. This is due to many bridge collapses resulting in both LCM





and drilling fluid losses. We, therefore, limited the testing to 25 min. We stop testing once the bridge pressure reaches the maximum limit. There is no API-standardized LCM testing procedure/guideline. Therefore, the purpose of the experimental work was just to evaluate the LCMs' performances in the drilling fluids under the considered temperature and the LCM (type and concentration) concerning the selected slot sizes.

- In order not to modify the rheological properties and the density of the drilling fluid, we added 2.5 g LCM to the 180 g drilling fluid. Converting this in pounds per gallon, it was 8.49. Different investigators recommended the size and concentration of LCM along with the fracture width. However, the selection of the LCM in this study is around the one proposed for flakes and particles by Howard and Scott [58].
- The selection of slot sizes was based on the ideal packing theory concept, which is the  $D_{50}$  value of the PSD of the LCMs (Figure 2), as suggested by Ref. [51]. The slots used for testing are  $300\mu\text{m}$ ,  $400\mu\text{m}$ , and  $500\mu\text{m}$ , which are above and below the  $D_{50}$  values.

### 3.1.3.2 Viscometer rheological properties

The viscosity of the drilling fluids is measured using the Fann 35 viscometer. Using the measured dataset, the rheological parameters were calculated with the Bingham plastic [59] and power-law models [59] and the Herschel–Bulkley model [60, 61] for comparison purposes.

### 3.1.3.3 Barite sagging

For the qualification of the drilling fluid in terms of bridging stability, it is also imperative to evaluate the sagging behaviors of the drilling fluids. The sag index is one of the methods used to assess the sagging potential. The dynamic sag measurement and sag factor determination are according to the M-I SWACO

procedure. In the VG-viscometer heating cup, the drilling fluid is allowed to maintain the temperature at  $50^\circ\text{C}$ . The bob was rotated at 100 rpm for 40 min. From the bottom of the cup, 20 ml of the sagged fluid was taken and the weight was measured. The sag factor determination was from the sagged fluid, and the initial mud weight is calculated as follows:

$$\text{Sag factor} = \frac{\text{Mud weight after 40 min (gm)}}{2 * \text{Initial mud weight (gm)}}$$

The change in density is calculated as follows:

$$\Delta\rho_{\text{mud}} [\text{sg}] = \frac{m_{\text{final}} - m_{\text{initial}}}{\text{Volume}}$$

where  $m_{\text{final}}$  is the mass of the fluid taken after testing,  $m_{\text{initial}}$  is the mass of the fluid taken before testing, and volume is the sample volume.

### 3.1.3.4 Shale swelling

A total of eight diverse types of synthetic pellets were used to study the swelling and disintegration behavior of shales in the drilling fluids presented in Section 3.1.2.1. Of these, six of the pellet types were prepared based on the literature data. Pierre, Texas, and Devonian shale compositions were obtained from Ref. [62], and three smectite-rich North Sea shales (A, B, and C) were obtained from Ref. [63]. This study's pellet type (I and II) contains a high concentration of bentonite. Except for the bentonite-I type, all the pellets were prepared by mixing bentonite and non-clay minerals (feldspar, quartz, and calcite) with water. After 24 h, the mixture was filled in a cylindrical-shaped tube and was pressed by hand to make pellets. The state of stress and the compaction strength will not represent the *in situ* condition. However, working on weak pellets is something like a worst-case scenario (which is soft, highly porous, and permeable pellets). The bentonite pellet type-I was prepared by pressing dry bentonite using a presser up to 10 bar. It is to be noted that the pellets used for the analysis in this study are modified versions of the ones proposed by Ref. [62] and Ref. [63], regardless of the formation fluid properties but only based on the mineralogical composition of the shales.

### 3.1.3.5 Static high-temperature and pressure filter test

To evaluate the filtrate loss of the two considered drilling fluids, a static high-temperature and pressure test was conducted. The drilling fluid was heated up to  $100^\circ\text{C}$ , and the applied differential pressure was 500 psi.

### 3.1.3.6 Rheological parameter determination

Bingham plastic model [59]: The model is described by plastic viscosity and yield stress parameters. According to the model, the shear stress varies linearly as the shear rate increases. The model reads as follows:

$$\tau = YS + PV\dot{\gamma}$$

The Bingham plastic (PV) and the yield stress (YS) are calculated from the 300 and 600 rpm viscometer dial readings, respectively, as follows:

$$PV [cP] = \theta_{600} - \theta_{300},$$

$$YS \left[ \frac{lbf}{100sqft} \right] = 2 \theta_{300} - \theta_{600}.$$

Power-law model [59]: According to the model, the shear stress varies in the power law as the shear rate increases. The model reads as follows:

$$\tau = k \dot{\gamma}^n,$$

where the parameters  $n$  and  $k$  describe the drilling fluid flow index and consistency index, respectively.

$$n = 3.32 \log \left( \frac{\theta_{600}}{\theta_{300}} \right),$$

$$k = \frac{\theta_{300}}{511^n} = \frac{\theta_{600}}{1022^n}.$$

Herschel–Bulkley model [60]: The Herschel–Bulkley model is a modified power-law model described by three parameters. According to the model, the fluid requires minimum applied pressure to set the fluid in motion when the shear rate is zero, and it is defined by a lower shear yield stress,  $\tau_y$ . The model reads as follows:

$$\tau = \tau_y + K \dot{\gamma}^n.$$

Zamora and Power [61] calculated the lower shear yield stress, LSYS, ( $\tau_y$ ) as follows:

$$\tau_y = 2 \theta_3 - \theta_6,$$

where  $\theta_3$  and  $\theta_6$  are the shear stress reading values at 3 and 6 rpm, respectively.  $n$  and  $k$  are determined from curve fitting.

## 4 Result and discussion

### 4.1 Lost circulation material bridging test

#### 4.1.1 The performance of LC-LUBE in the oil-based drilling fluids

For the drilling fluid lost circulation hindrance study, an 8.49 ppb LC-LUBE particle was mixed with the two selected drilling fluids. Bridging tests were conducted at 300  $\mu\text{m}$ , 400  $\mu\text{m}$ , and 500  $\mu\text{m}$  slots. The  $D_{50}$  value is within the range of 250–350 microns. Figures 4–6 show the test results. For a given particle concentration, as the fracture width increases and the size is higher than the  $D_{50}$  value, the particle becomes unstable and flows through the slots. Consequently, the bridging efficiency is reduced. From all tests, one can observe that the performance of the two mud systems is comparable. This could be the fact that the fluid flow between the particles has a

comparable coefficient of friction. Moreover, the reason for the bridge instability is due to the lubricity behavior of the LC lube. In general, it is important to remember that the bridging performance of particles depends on different parameters such as particle types, sizes, concentrations, and mechanical properties such as hardness and lubricity, which provide different results. Moreover, the chemistry of the particulate–drilling fluid may affect the particle–particle contact which as a result may affect the bridge stability.

#### 4.1.2 The performance of mica in the oil-based drilling fluids

As can be seen from the PSD (Figure 3), the  $D_{50}$  value is in the range of 300–400 microns. The majority of the mass % concentration (about 34%) is within 500–800 microns. The particle test results are shown in Figures 7–9. Compared with the test results obtained from LC-Lube (Figures 4–6), it can be seen that mica performs well showing a stable bridging pressure profile. The reason could be due to the wide particle size spectrum.

#### 4.1.3 Comparisons of the 80/20 and 60/40 OBM in different lost circulation material systems

The experimental pressure profile shows a zigzag shape, which is due to the formation and the collapse of a bridge at the mouth of the fracture. When sufficient LCM is deposited at the gate of the fracture, the bridge carries the applied load and the fluid will not be lost through the slot. The response of the bridge is the pressure building up and showing a positive slope, as shown in Figures 4–9. The pressure build-up phenomenon is called the bridging pressure. When the wellbore pressure reaches a certain critical peak value at which the bridge will not be able to carry the loading, the bridge will then collapse and result in a pressure drop (i.e., negative slope). As a result of the bridge collapse, the fluid will be lost through the slot. The degree of collapse varies. The measured dataset shows that when the bridge completely collapses, the pressure drops to zero and results in more fluid losses. On the other hand, when part of the bridge collapses and the LCM then quickly repairs the bridge, the pressure may not be reduced to zero but shows a minor reduction. The bridge healing process occurred as the LCM-laden fluid flows through the slot. The best analogy for unstable and stable bridges, along with the fluid loss and hindrance mechanisms, is shown in Figure 1B.

During LCM testing, the probability of particles' arrival at the gate of the fracture (in terms of concentration and size) varies from time to time. As we can see, the zigzag pressure behavior varies over testing time. To obtain more information and make a good evaluation, Mostafavi et al. [64] have analyzed the LCM bridging experimental data based on the number of peaks, the average of the maximum peaks, the maximum pressure, and the average pressure over the test period. For better comparisons of the performance of the LCMs in the two mud systems, in this

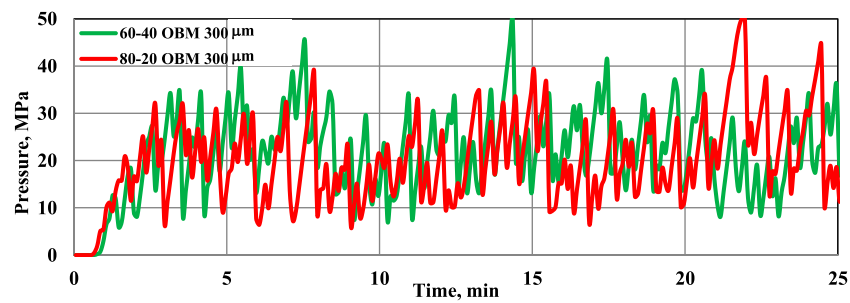


**FIGURE 4**  
Bridging test at the 300- $\mu\text{m}$  slot.

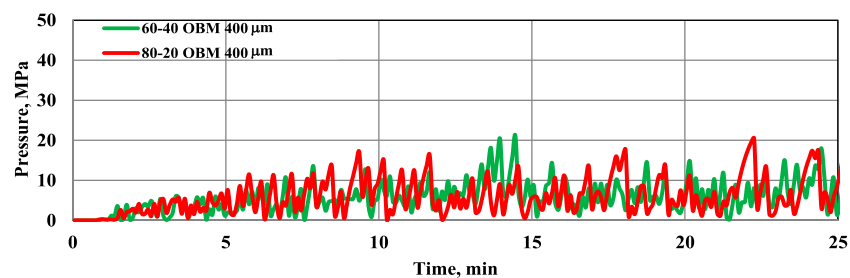


**FIGURE 5**  
Bridging test at the 400- $\mu\text{m}$  slot.

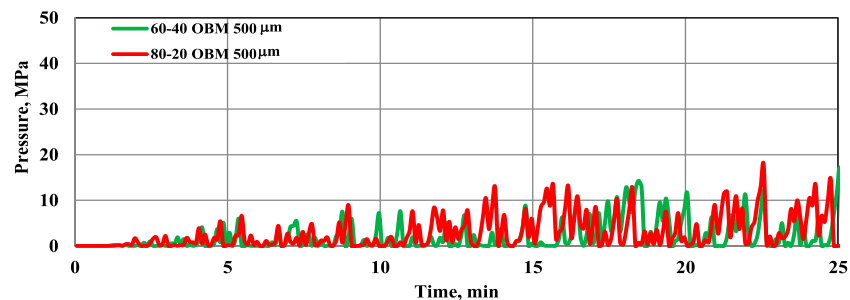


**FIGURE 6**  
Bridging test at the 500- $\mu\text{m}$  slot.

study, we just chose to present the average pressure over the test period. The average pressure is the measure of the mean of the bridge and collapse pressures during the test period.

Figures 10–12 show the comparisons of the LCM bridging performance in the two drilling fluids. The results show that the strength of the LC-LUBE LCM in the drilling fluids is quite

similar. On the other hand, mica shows different performances. This shows that the particle–drilling fluid interaction could be one factor when studying the mechanical strength of the mud cake. However, the detail and reason for this level of research are beyond the scope of this study.

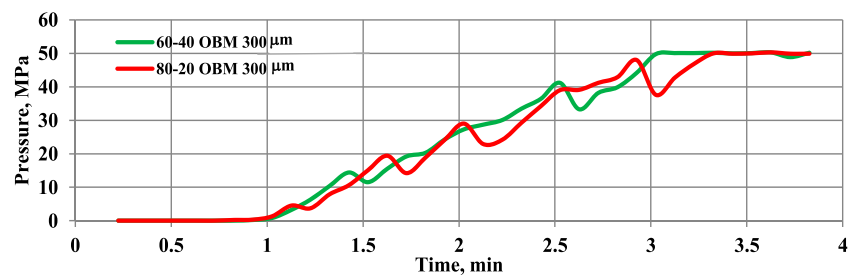


**FIGURE 7**  
Bridging test at the 300- $\mu\text{m}$  slot.

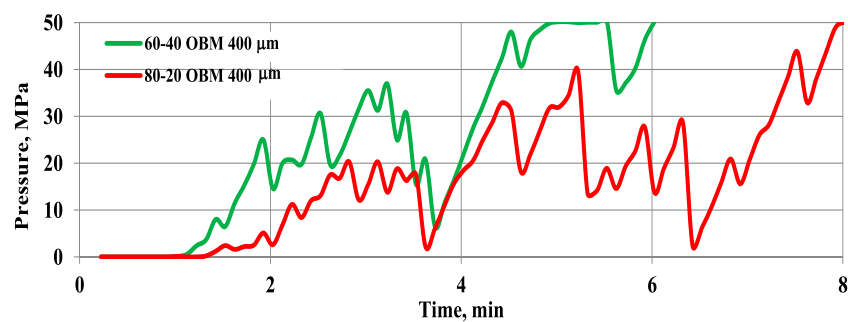


**FIGURE 8**  
Bridging test at the 400- $\mu\text{m}$  slot.

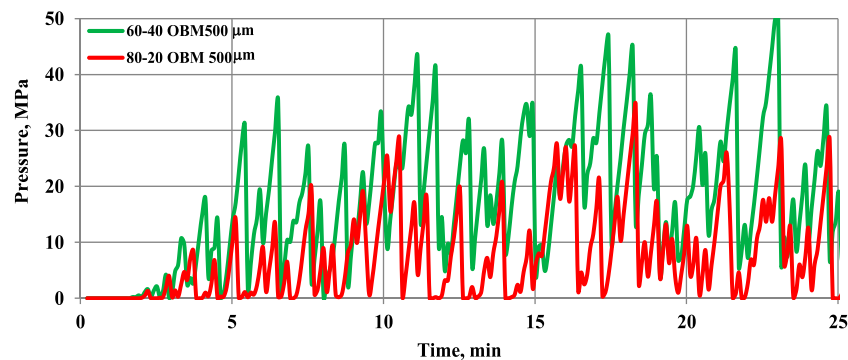


**FIGURE 9**  
Bridging test at the 500- $\mu\text{m}$  slot.

#### 4.1.4 Comparisons of the single LCM and the blending of lost circulation materials

To assess the synergy of LCMs, mica and LC-LUBE were mixed in a 1:1 ratio. The PSD and mass % concentration are shown in Figure 3, which is in between LC-LUBE and mica.

The blended LCM contains both flat and irregularly shaped particulates. The  $D_{50}$  value is within the range of 250–300  $\mu\text{m}$ , which is the same as that of the LC-LUBE particle. Compared with the separate test results performed with LC-LUBE (Figures 4–6), it can be shown that the

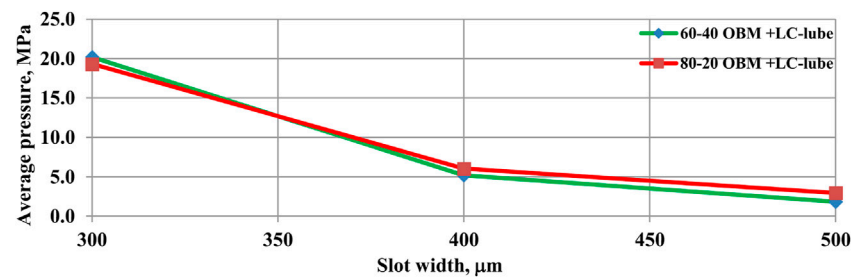


**FIGURE 10**  
Comparisons of 8.48-ppb LC-LUBE-treated 80/20 and 60/40 OBM systems.

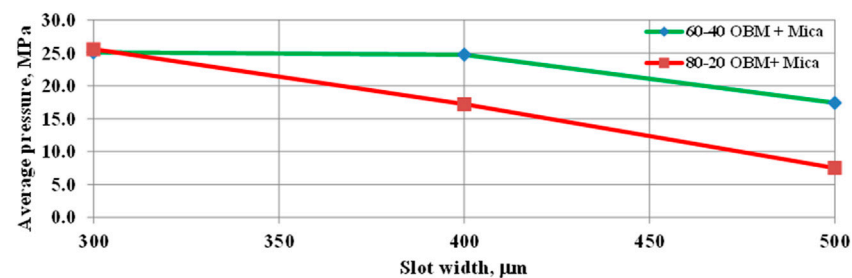


**FIGURE 11**  
Comparisons of 8.48-ppb mica-treated 80–20 and 60–40 OBM systems.

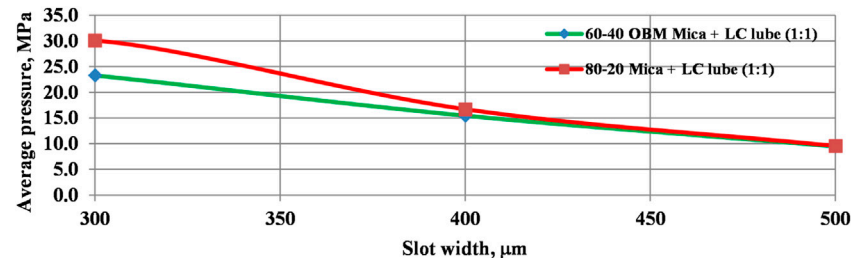


**FIGURE 12**  
Comparisons of 8.48-ppb LC-LUBE + mica (1:1 ratio)-treated 80/20 and 60/40 OBM systems.

addition of mica improves the pressure profile. However, compared with the single mica test results (Figures 7–9), the addition of LC-LUBE reduced the stability. The reason could be that the lubricity of LC-LUBE might have reduced the friction at the grain–grain contact at the fracture gate. Figures 13– Figure 14 show the analysis of the different LCM (separate and blending) stabilities in the two mud systems separately. As shown, the size, mechanical,

lubricity, and physical properties of particle additives are the major factors for the bridging strength and stability.

## 4.2 Barite sagging analysis

The rheological parameters, the dynamic sagging factor, and the change in the density of the drilling fluids are measured at 50°C. Scott et al. [65] have presented three field case studies to investigate sag occurrence and control methods. The study

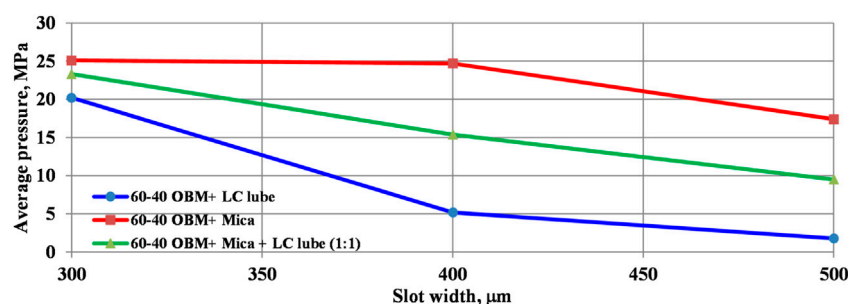


FIGURE 13

Bridging performance of the 60/40 OBM treated with 8.49 ppb LC-LUBE, mica, and a mixture of mica and LC-LUBE.

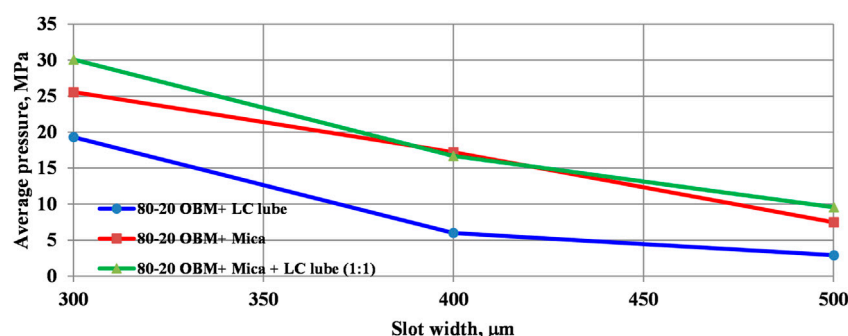


FIGURE 14

Bridging performance of the 80/20 OBM treated with 8.49 ppb LC-LUBE, mica, and a mixture of mica and LC-LUBE.

showed that the drilling fluid with an insufficient lower shear yield stress (LSYS) experiences a higher sagging tendency. The authors recommended an effective method to reduce sag tendencies by maintaining the LSYS value in the range of 7–15 lbf/100 sqft. From the measured rheological parameters, the LSYS of the 60/40 OBM is calculated to be 12 lbf/100 sqft, which is within the recommended range, and the LSYS of the 80/20 OBM is 4 lbf/100 sqft, which is below the recommended range. The change in the density of the 60/40 OBM and 80/20 OBM is 0.0888 sg, and 0.1887 sg, respectively.

According to Maxey [66], the sagging potential of the drilling fluid is higher when the sag factor is greater than 0.53. The dynamic sag test results showed that the sag factor of the 60/40 OBM is 0.52, which is below the sag limit, and the sag factor of the 80/20 OBM is 0.56, which is above the sag limit.

### 4.3 Filtrate loss

In the drilling well, the drilling fluid experiences elevated temperature and pressure. These thermodynamic variables affect the rheological and physical properties of the drilling fluid. The higher temperature decreases the viscosity and the density of the

fluid. Moreover, the fluid–solid phase separation will also increase. As a result, higher filtration rates will cause formation damage and the fluid property will also be changed. The cumulative filtrate loss collected during the 30-min testing results showed that the 60/40 OBM recorded 2.2 ml and the 80/20 OBM recorded 4.0 ml. The reason for the lower filtrate loss could be due to the reduction of the permeability/porosity of the mud cake, the reduction of the fluid–solid separation, and the higher viscosity of the filtrate. These parameters can be quantified through measurement and the Darcy law. Interested readers may refer to the study by Awais et al. (2020) [67].

### 4.4 Swelling inhibition of the drilling fluids

A total of eight pellets were synthesized, and their swelling phenomenon is investigated by immersing them in the 60/40 and 80/20 OBM drilling fluids. During testing, the pellets were immersed in the drilling fluids for 4 days. Results show that none of the pellets swelled, fractured, or disintegrated. By visual inspection and nail scratch testing, the strengths of the pellets are the same in the two drilling fluids.

## 5 Summary

Lost circulation occurs during the well construction process. It is one of the most challenging problems and costs the industry a lot. Investigators have tested several LCMs along with recommendations for the application. However, to have a better understanding of the bridging process, it is imperative to evaluate the performance of the LCM in the type of fluid systems to be mixed with.

In this study, the performance of 60/40 and 80/20 oil-based mud systems was compared. The analysis was based on bridging performance, shale stability, filtrate loss, and sagging effect to quantify the fluid for the application. Based on the overall analysis, results are as follows:

- The LC-LUBE bridging performance is quite similar in both fluid systems. This could be due to the lubricity of the fluids and the particle–particle grain contact being comparable.
- The performance of mica shows good bridging as compared with that of LC-LUBE.
- The performance of LC-LUBE is improved when blended with mica. This could be the mechanical, shape, size, and other properties that might play a role in improving the bridge's stability.
- The bridging stability in the 60/40 OBM is better than that in the 80/20 OBM.
- In terms of shale stability, both mud systems inhibit the shale swelling phenomenon.
- For field application, the experimental results reveal that it is important to test the performance of LCMs separately and their mixture to investigate positive synergy, as shown by mixing LC-LUBE with mica. Moreover, the selection of the LCM size, concentration, and testing at a slot should be based on the expected field formation fracture size. The LCM should also be tested by blending with the expected field drilling fluids to be used.
- The drilling fluids' performance analysis results show that the 60/40 OBM is better in terms of sagging, bridging stability, and filtrate loss. This agrees with the conclusion of [68].

## 6 Future work

It should be noted that the experimental work results presented in the study are valid for the considered testing temperature and pressures, the drilling fluids, the LCM types, and the concentration. Changing any one of these may produce a different result. The results obtained in the study are not a conclusion but a summary of the observation. To gain more insight into the understanding of the LCM performance and barite sagging issues, in the future, we plan

to conduct testing at elevated pressure and temperature, among others:

- Dynamic barite sagging and filtrate loss.
- Change the drilling fluids from the OBM to WBM and consider 70/30 and 90/10 OBMs.
- Change the LCM types and PSD.

## Data availability statement

The raw data supporting the conclusions of this article will be made available by the authors, without undue reservation.

## Author contributions

The paper is the result of the equal contribution of the authors in writing, experimental design as well as interpretation. MB: Contributions are experimental test design, testing, writing and interpretation. BA: Contributions are LCM experimental setup-design and construction, experimental test design, writing and interpretation.

## Acknowledgments

The authors acknowledge the University of Stavanger for the materials and the laboratory access.

## Conflict of interest

The authors declare that the research was conducted in the absence of any commercial or financial relationships that could be construed as a potential conflict of interest.

## Publisher's note

All claims expressed in this article are solely those of the authors and do not necessarily represent those of their affiliated organizations, or those of the publisher, the editors, and the reviewers. Any product that may be evaluated in this article, or claim that may be made by its manufacturer, is not guaranteed or endorsed by the publisher.

## Supplementary material

The Supplementary Material for this article can be found online at: <https://www.frontiersin.org/articles/10.3389/fphy.2022.1042242/full#supplementary-material>



## References

- Mc Lellan PJ, Wang Y. *Predicting the effects of pore pressure penetration on the extent of wellbore instability: Application of a versatile poro-elastoplastic model*. Delft, The Netherlands: Eurock SPE/ISRM Rock Mechanics in Petroleum Engineering (1994). p. 29–31.
- Catalin I, James B, Bloys B, Chevron T. *How can we best manage lost circulation?* (2003).
- Cook J, Growcock F, Guo Q, Hodder M, Van oort E. *Stabilizing the wellbore to prevent lost circulation*. Oilfield Review (2011).
- Al-Yami A, Wagle V, Al-Anqari K, Aljohar A. Salah elkatatny//Curing losses: Lab developments and best practices. In: International Petroleum Technology Conference Paper presented at the International Petroleum Technology Conference; February 21–23, 2022; Riyadh, Saudi Arabia (2022). Paper Number: IPTC-22007-MS.
- Hitchcock G. Additive manufactured shapes used to cure total lost circulation events. In: Publisher: Offshore Technology Conference Paper presented at the Offshore Technology Conference; May 4–7, 2020; Houston, Texas, USA (2020).
- Pilisi N, Wei Y, Holditch SA. Selecting drilling technologies and methods for tight gas sand reservoirs, IADC/SPE 128191. In: Proceedings of the 2010 IADC/SPE Drilling Conference held in New Orleans; 2–4 February 2010; LA, USA (2010).
- Aadnøy BS. *Modern well design*. Florida, United States: CRC Press (2010).
- Redden J. Advanced fluid systems aim to stabilize well bores, minimize nonproductive time. *The Am Oil Gas Reporter* (2009) 52(8):58–65.
- Nayberg TM. Laboratory study of lost circulation materials for use in both oil-based and water-based drilling muds. *SPE Drill Eng* (1986) 2:229–36. doi:10.2118/14723-PA
- Soroush H, Sampaio JHB. Investigation into strengthening methods for stabilizing wellbores in fractured formations. In: Proceedings of the 2006 SPE Annual Technical Conference and Exhibition; September 24–27, 2006; San Antonio, Texas (2006).
- Fuh GF, Morita N, Boyd PA, McGoffin SJ. A new approach to preventing lost circulation while drilling. In: Proceedings of the 67th Annual Technical Conference and Exhibition of the Society of Petroleum Engineers; October 4–7, 1992; Washington, DC (1992).
- Ivan CD, Bruton JR, Thiercelin M, Bedel J. Making a case for rethinking lost circulation treatments in induced fractures. In: Proceedings of the 2002 SPE Annual Technical Conference and Exhibition; September 29–October 2, 2002; San Antonio, Texas (2002).
- Scott PP, Jr., Lummus JL. New developments in the control of lost circulation//SPE 516-G. In: Proceedings of the 30th Annual Fall Meeting of the Petroleum Branch of the American Institute of Mining and Metallurgical Engineers; October 2–5, 1955; New Orleans (1955).
- Whitfill DL, Hemphill T. *Pre-treating fluids with lost circulation materials*. Drilling Contractor (2004).
- Alsaba M, Nygaard R, Saasen A, Nes O. Lost circulation materials capability of sealing wide fractures. In: SPE deepwater drilling and completions conference; September 10–11, 2014; Galveston (2014).
- Alsaba M, Nygaard R, Saasen A, Nes O. Laboratory evaluation of sealing wide fractures using conventional lost circulation materials. In: SPE annual technical conference and exhibition; October 27–29, 2014; Amsterdam (2014).
- Alsaba M, Nygaard R, Saasen A, Nes O. Experimental investigation of fracture width limitations of granular lost circulation treatments. *Pet Explor Prod Technol* (2016) 6:593–603.
- Clapper DK, Szabo JJ, Spence SP, Otto MJ, Creelman B, Lewis TG, McGuffey G. One sack rapid mix and pump solution to severe lost circulation. In: SPE/IADC drilling conference and exhibition; March 1–3, 2011; Amsterdam (2011).
- Kefi S, Lee JC, Shindgikar ND. Optimizing in four steps composite lost-circulation pills without knowing loss zone width. In: Asia Pacific drilling technology conference and exhibition; November 1–3, 2010; Ho Chi Minh (2010).
- Kageson-Loe N, Sanders MW, Growcock F, Taugbøl K, Horsrud P, Singelstad AV, et al. Particulate-based loss-prevention material-the secrets of fracture sealing revealed. *SPE Drill & Compl* (2009) 24(04):581–9.
- Morita N, Black AD, Fuh GF. Theory of lost circulation pressure. In: Proceedings of the 65th Annual Technical Conference and Exhibition of the Society of Petroleum Engineers; September 23–26, 1990; New Orleans, LA (1990).
- Onyia EC. Experimental data analysis of lost-circulation problems during drilling with oil-based mud. *SPE Drill & Compl* (1994) 9(01):25–31.
- Aadnøy BS. Geomechanics analysis for deepwater drilling//SPE 39392. In: IADC/SPE Drilling Conference; March 3–6, 1998; Dallas, TX (1998).
- Aadnøy BS, Belayneh M. Elasto-plastic fracturing model for wellbore stability using non-penetrating fluids. *J Pet Sci Eng* (2004) 45:179–92. doi:10.1016/j.petrol.2004.07.006
- Amanullah MD, Al-Tahini MA. Nano-technology—its significance in smart fluid development for oil and gas field application//SPE-126102-MS. In: Proceedings of the Saudi Arabia Section Technical Symposium; May 9–11, 2009; Al-Khobar, Saudi Arabia (2009).
- Vryzas Z, Zaspalis V, Nalbantian L, Mahmoud O, Nasr-El-Din HA, Kelessidis VC. A comprehensive approach for the development of new magnetite nanoparticles giving smart drilling fluids with superior properties for HP/HT applications, IPTC-18731-MS. In: Proceedings of the International Petroleum Technology Conference; 14–16 November 2016; Bangkok, Thailand (2016).
- Sadeghalvaad M, Sabbaghi S. The effect of the TiO<sub>2</sub>/polyacrylamide nanocomposite on water-based drilling fluid properties. *Powder Technol* (2015) 272:113–9. doi:10.1016/j.powtec.2014.11.032
- Mohamadian N, Ghorbani H, Wood DA, Khoshmardan MA. A hybrid nanocomposite of poly (styrene-methyl methacrylate-acrylic acid), clay as a novel rheology-improvement additive for drilling fluids. *J Polym Res* (2019) 26:33. doi:10.1007/s10965-019-1696-6
- Mohamud O, Mady A, Aftab ASDA. Al<sub>2</sub>O<sub>3</sub> and CuO nanoparticles as promising additives to improve the properties of KCl-polymer mud: An experimental investigation. *Can J Chem Eng* (2021) 2021:1–14. doi:10.1002/cjce.24285
- Mohamadian N, Ghorbani H, David Wood A, Khoshmardan MA. Rheological and filtration characteristics of drilling fluids enhanced by nanoparticles with selected additives//An experimental study. *Adv Geo-energy Res* (2018) 2:228–36. doi:10.26804/ager.2018.03.01
- Aftab A, Ali M, Sahito MF, Mohanty US, Jha NK, Akhondzadeh H, et al. Environmental friendliness and high performance of multifunctional tween 80/ ZnO-nanoparticles added water-based drilling fluid: An experimental approach. *ACS Sustain Chem Eng* (2020) 8:11224–43. doi:10.1021/acssuschemeng.0c02661
- Sharma MM, Zhang R, Chenevert ME, Ji L, Guo Q, Friedheim J. A new family of nanoparticle-based drilling fluids, SPE-160045-MS. In: Proceedings of the SPE Annual Technical Conference and Exhibition; 8–10 October 2012; San Antonio, TX, USA (2012).
- Hoelscher KP, de Stefano G, Riley M, Young S. Application of nanotechnology in drilling fluids, SPE- 157031-MS. In: Proceedings of the SPE International Oilfield Nanotechnology Conference and Exhibition; June 12–14, 2012; Noordwijk, The Netherlands (2012).
- Gao C, Miska SZ, Yu M, Ozbayoglu EM, Takach NE. Effective enhancement of wellbore stability in shales with new families of nanoparticles, SPE-180330-MS. In: Proceedings of the SPE Deepwater Drilling and Completions Conference; 14–15 September 2016; Galveston, TX, USA (2016).
- Taha NM, Lee S. Nano graphene application improving drilling fluids performance, IPTC-18539-M. In: Proceedings of the International Petroleum Technology Conference; 6–9 December 2015; Doha, Qatar (2015).
- Awais M, Belayneh M, Saasen A, Fjelde KK, Aadnøy S. Effect of MWCNT and MWCNT functionalized -oh and -cooh nanoparticles in laboratory water based drilling fluid. In: Proceedings of the ASME 2017 37th International Conference on Ocean, Offshore and Arctic Engineering; 17–22 June 2018; Madrid, Spain (2018).
- Sabah A, Alsawasiti A, Salam M. Improving drilling fluid properties at high-pressure conditions using selected nanomaterials. *IOP Conf Ser : Mater Sci Eng* (2019) 579:012004. doi:10.1088/1757-899x/579/1/012004
- Nwaoui CO, Hareland G, Husein M, Nygaard R, Zakaria ME. Wellbore strengthening-nano-particle drilling fluid. Experimental design using hydraulic fracture apparatus, SPE-163434. In: Proceedings of the SPE/IADC Drilling Conference; 5–7 March 2013; Virtual, Amsterdam, The Netherlands (2013).
- Halali MA, Ghotbi C, Tahmasbi K, Ghazanfari MH. The role of carbon nanotubes in improving thermal stability of polymeric fluids: Experimental and modeling. *Ind Eng Chem Res* (2016) 55:7514–34. doi:10.1021/acs.iecr.6b00784
- William JKM, Ponmani S, Samuel R, Nagarajan R, Sangwai JS. Effect of CuO and ZnO nanofluids in Xanthan gum on thermal, electrical, and high-pressure rheology of water-based drilling fluids. *J Pet Sci Eng* (2014) 117:15–27. doi:10.1016/j.petrol.2014.03.005
- Hassani SS, Amrollahi A, Rashidi A, Soleymani M, Rayatdoost S. The effect of nanoparticles on the heat transfer properties of drilling fluids. *J Pet Sci Eng* (2016) 146:183–90. doi:10.1016/j.petrol.2016.04.009
- Fazelabdolabadi B, Khodadadi AA, Sedaghatzadeh M. Thermal and rheological properties improvement of drilling fluids using functionalized carbon nanotubes. *Appl Nanosci* (2015) 5:651–9. doi:10.1007/s13204-014-0359-5

43. Ponmani S, Nagarajan R, Sangwai JS. Effect of nanofluids of CuO and ZnO in polyethylene glycol and polyvinylpyrrolidone on the thermal, electrical, and filtration-loss properties of water-based drilling fluids. *SPE J* (2016) 21:405–15. doi:10.2118/178919-pa
44. Boul PJ, Reddy BR, Zhang J, Thamelitz C. Functionalized nanosilicas as shale inhibitors in water-based drilling fluids. *SPE Drilling & Completion* (2017) 32: 121–30. doi:10.2118/185950-pa
45. Kang Y, She J, Zhang H, You L, Song M. Strengthening shale wellbore with silica nanoparticles drilling fluid. *Petroleum* (2016) 2:189–95. doi:10.1016/j.petlm.2016.03.005
46. Aston MS, Alberty MW, McLean MR, de Jong HJ, Armagost K. Drilling fluids for wellbore strengthening//IADC/SPE 87130. In: IADC/SPE Drilling Conference; 2–4 March 2004; Dallas, Texas (2004).
47. Abrams A Mud design to minimize rock impairment due to particle invasion. *J Pet Technol* (1977) 29(05):586–592. doi:10.2118/5713-pa
48. Smith P, Browne SV, Heinz TJ, Wise WV. Drilling fluid design to prevent formation damage in high permeability Quartz arenite sandstones. In: Proceedings of the SPE Annual Technical Conference; 6–9 October 1996; Denver, CO, USA (1996).
49. Vickers S, Cowie M, Jones T, Twynam AJ A new methodology that surpasses current bridging theories to efficiently seal a varied pore throat distribution as found in natural reservoir formations. *Wiertnictwo, Nafta, Gaz* (2006) 23(1):501–515.
50. Whitfill D. Lost circulation material selection, particle size distribution and fracture modeling with fracture simulation software//SPE-115039-MS. In: IADC/SPE Asia Pacific drilling technology conference and exhibition; August 25–27, 2008; Jakarta, Indonesia (2008).
51. Dick M, Heinz TJ, Svoboda CF, Aston M Optimizing the selection of bridging particles for reservoir drilling fluids. In: SPE International Symposium on Formation Damage Control; February 23–24, 2000; Lafayette, Louisiana (2000).
52. Messenger J. *Lost circulation*. 1st ed. Tulsa: Pennwell Corp (1981).
53. Alkinani HH, Abo Taleb Al-HameediDunn-Norman S, Mustafa A, Al-AlwaniMutar RA, Al-Bazzaz WH. State-of-the-Art review of lost circulation materials and treatments. In: Part I: General Trends and Uses/Paper presented at the Abu Dhabi International Petroleum Exhibition & Conference; November 11, 2019; Abu Dhabi, UAE (2019). Paper Number: SPE-197393-MS.
54. Alkinani HH, Al-Hameedi ATT, Dunn-Norman S, Waleed H, Al-Bazzaz. State-of-the-Art review of lost circulation materials and treatments. In: Part II: Probability and Cost Analyses Paper presented at the International Petroleum Technology Conference; January 13–15, 2020; Dhahran, Kingdom of Saudi Arabia (2020).
55. Alkinani HH. A comprehensive analysis of lost circulation materials and treatments with applications in Basra's oil fields, Iraq: Guidelines and recommendations. MSc Thesis. United States: Missouri University Of Science And Technology (2017).
56. Alsaba M, Nygaard R, Hareland G, Contreras O. Review of lost circulation materials and treatments with an updated classification. In: AADE fluids technical conference and exhibition; 15–16 April, 2014; Houston (2014).
57. Alkinani HH, Al-Hameedi AT, Flori RE, Dunn-Norman S, Hilgedick SA, Alsaba MT. Updated classification of lost circulation treatments and materials with an integrated analysis and their applications. In: Paper presented at the SPE Western Regional Meeting; April 22–26, 2018; Garden Grove, California, USA (2018).
58. Howard GC, Scott PP, Jr. An analysis and the control of lost circulation. *J Pet Technol* (1951) 3(06):171–82. doi:10.2118/951171-g
59. API. Api rp 13D. In: *Recommended practice on the rheology and hydraulics of oil-well drilling fluids*. 4th ed. Washington, D.C., United States: American Petroleum Institute (1995).
60. Gucuyener IH. A rheological model for drilling fluids and cement slurries. In: SPE 11487-MS Middle East Oil Technical Conference and Exhibition; 14–17 March 1983; Bahrain (1983).
61. Zamora M, Roy S, Slater K. Comparing a basic set of drilling fluid pressure-loss relationships to flow-loop and field data. In: AADE-05-NTCE-27 presented at the AADE 2005 National Technical Conference and Exhibition; 5–7 April, 2005; Houston (2005).
62. Chenevert ME, Osisanya SO. Shale/mud inhibition defined with rig-site methods. *SPE Drilling Eng* (1989) 4:261–8. doi:10.2118/16054-pa
63. Horsrud P, Bostrom B, Sonstebo EF, Holt R. Interaction between shale and water-based drilling fluids: Laboratory exposure tests give new insight into mechanisms and field consequences of KCl contents. In: SPE 48986, SPE Annual Technical Conference and Exhibition, New Orleans; 27–30 September 1998; Louisiana (1998).
64. Mostafavi V, Hareland G, Belayneh M, Aadnøy BS. Mechanistic modeling of fracture sealing resistance with respect to fluid and fracture properties. In: Paper presented at the 45th U.S. Rock Mechanics/Geomechanics Symposium; June 26–29, 2011; San Francisco, California (2011).Experimental and
65. Scott PD, Mario Z, Catalin A. Barite-sag management: Challenges, strategies, opportunities//SPE-87136-MS. In: IADC/SPE Drilling Conference; 2–4 March, 2004; Dallas, Texas (2004).
66. Maxey J. Rheological analysis of static and dynamic sag in drilling fluids. *Annu Trans Nordic Rheology Soc* (2007) 15.
67. Alvi MAA, Belayneh M, Bandyopadhyay KKS. Effect of hydrophobic iron oxide nanoparticles ( $\text{Fe}_2\text{O}_3$ )On the properties of 90/10 oil based drilling fluids. In: Proceedings of the ASME 2020 39th International Conference on Ocean, Offshore and Arctic Engineering OMAE2020; June 28–July 3, 2020; Fort Lauderdale, FL, USA (2020).
68. Aston M, Mihalik P, Tunbridge J, Clarke S. Towards zero loss oil based muds//SPE 77446. In: Presented at the SPE Annual Technical Conference and Exhibition; Sept 20–Oct 2, 2002; Texas (2002).



## OPEN ACCESS

EDITED BY  
Zhenjiang You,  
Edith Cowan University, Australia

REVIEWED BY  
Vishnu Chandrasekharan Nair,  
Indian Institute of Technology  
Kharagpur, India  
Mesfin Belayneh,  
University of Stavanger, Norway

\*CORRESPONDENCE  
Sulaiman A. Alarifi,  
✉ salarifi@kfupm.edu.sa

SPECIALTY SECTION  
This article was submitted to  
Interdisciplinary Physics,  
a section of the journal  
Frontiers in Physics

RECEIVED 09 October 2022  
ACCEPTED 16 November 2022  
PUBLISHED 13 December 2022

CITATION  
Alhaidari SA, Alarifi SA and Bahamdan A  
(2022), Plugging efficiency of flaky and  
fibrous lost circulation materials in  
different carrier fluid systems.  
*Front. Phys.* 10:1065526.  
doi: 10.3389/fphy.2022.1065526

COPYRIGHT  
© 2022 Alhaidari, Alarifi and Bahamdan.  
This is an open-access article  
distributed under the terms of the  
[Creative Commons Attribution License](https://creativecommons.org/licenses/by/4.0/)  
(CC BY). The use, distribution or  
reproduction in other forums is  
permitted, provided the original  
author(s) and the copyright owner(s) are  
credited and that the original  
publication in this journal is cited, in  
accordance with accepted academic  
practice. No use, distribution or  
reproduction is permitted which does  
not comply with these terms.

# Plugging efficiency of flaky and fibrous lost circulation materials in different carrier fluid systems

Saleh A. Alhaidari<sup>1</sup>, Sulaiman A. Alarifi<sup>2\*</sup> and  
Abdulaziz Bahamdan<sup>1</sup>

<sup>1</sup>Saudi Aramco, Dhahran, Saudi Arabia, <sup>2</sup>Department of Petroleum Engineering, King Fahd University of Petroleum and Minerals, Dhahran, Saudi Arabia

Lost circulation is one of the most significant contributors to wellbore instability and causes an increase in drilling operation costs. It is also a major contributor to the nonproductive time and must be minimized for improved economic and operational performance. The objective of this research is to provide tools and information about specific loss circulation management techniques that drillers can use to minimize lost circulation. This study involves comprehensive approaches to test the plugging efficiency of three different lost circulation materials (LCMs) from two groups of materials (flaky and fibrous). It also highlights the carrier fluids (drilling fluids) and the determination of the optimum drilling fluid properties. Different fracture sizes and the effect of the various LCM are analyzed. The impact of LCM's shape, size, and physical and chemical properties along with the fracture sizes is discussed. Examining the particle size distribution before and after mixing with the fluids shows the capability of the materials in plugging the fracture while maintaining the minimum porosity and permeability of the plug. It also helps to strengthen the fracture gradient of the formation by knowing the actual particle sizes. The primary objective of this work is to precisely study and analyze these factors on the three LCMs along with different carrier fluids to investigate their plugging efficiency and potentially resolve or minimize the severity of the lost circulation problem.

## KEYWORDS

lost circulation materials, particle size degradation, plugging efficiency, flaky material, fibrous material

**Abbreviations:** D<sub>s</sub>, maximum particle size of a percentage of the particles, μm; D<sub>10</sub>, maximum particle size of 10% of the particles, μm; D<sub>25</sub>, maximum particle size of 25% of the particles, μm; D<sub>50</sub>, median particle size, μm; D<sub>75</sub>, maximum particle size of 75% of the particles, μm; D<sub>90</sub>, maximum particle size of 90% of the particles, μm; LCM, lost circulation material; PSD, particle size distribution.

## 1 Introduction

To meet the world's energy needs, the oil and gas production industry is expected to provide the supply needed to meet this demand. Therefore, more wells with formidable challenges will be required. These wells, with extended vertical depth and extended reach laterals, make drilling operations more complex. Major obstacles contribute to the cost of the operation. Some of these obstacles are not controllable such as geological complexity and weak formations with low fracture gradients. Lost circulation events typically occur in these situations. One of the causes of lost circulation is tensile failure [1]. Aadnøy and Chenevert showed the types of borehole problems which cause lost circulation problems. When wellbore pressure exceeds the fracture pressure, the fracture occurs; on the other hand, with a lower wellbore pressure, wellbore collapse might occur.

### 1.1 Effects of lost circulation

Loss of drilling fluids into the formation has a tremendous impact on the drilling operation. This impact can be operational problems that can have an adverse effect on the well. In addition, another impact is the extra cost associated with this problem.

Lost circulation could cause an interruption to the well delivery or loss of the well. One of the examples that would be a result of lost circulation is a well control situation. Loss of hydrostatic pressure due to a mud level drop could cause a kick and the situation may become a blowout or result in the loss of lives [2].

The cost associated with lost circulation incidents is remarkable. It costs the industry about one billion dollars annually despite the fact that the treatment cost comes with no benefits [3]. According to Ivan et al., lost circulation treatments are causing a loss of 200 million dollars annually mainly due to the cost of materials [4]. The cost of mud lost into the formation comes with a high figure and is equivalent to 1.8 million barrels of drilling fluids lost into the formation [5]. The overall economic impact of the lost circulation problem is 20%–40% of total drilling costs [6]. Lost circulation events can occur while drilling, tripping, and during any other operational activity. Losses are classified according to the rate of losses; that is, seepage losses are in the range of 1–10 bbl/hr, partial losses are 10–500 bbl/hr, and complete losses are 500 bbl/hr or greater, as shown in Table 1 [7].

TABLE 1 Classification of losses [7].

Type of loss	Classification
Seepage losses	1–10 bbl/hr
Partial losses	10–500 bbl/hr
Complete losses	500 bbl/hr or greater

### 1.2 Wellbore strengthening techniques

Wellbore strengthening is a technique used to enhance the fracture gradient by sealing and plugging the pore throat in a weak formation to avoid the induced fracture. This technique results in widening the mud weight window [8]. The main objective is to increase the formation pressure so that the formation can sustain additional drilling fluid pressure without inducing a fracture and lost circulation events will be avoided [9]. Many models are presented in the literature to address the concept of wellbore strengthening. The first model is called the “stress cage model,” which is based on the linear elastic analysis. The model was introduced by Alberty and McLean [10] and based on the LCM forming a seal in the fracture mouth with the result of increasing the hoop stress, which leads to an increase in the fracture gradient. The second model is fracture closure stress developed by Dupriest [11]. This model explains the change of the hoop stress by sealing the fracture tip. The third model uses elastic–plastic fracture analysis and was introduced by Aadnøy and Belayneh [12]. The model drives the enhancement of the fracture gradient and increases fracture resistance by two main mechanisms. The mechanisms involve the mud-cake plastic deformation that seals the fracture mouth and the type and concentration of the LCM used. This model is pivotal to improving the fracture gradient [13].

The next model, named as “fracture propagation resistance,” was built based on the Drilling Engineering Association experimental work. In their experiments, they used 30-in<sup>3</sup> shale blocks to investigate lost circulation events [14]. The results showed rock failure analysis using Young's modulus and Poisson's ratio, and carrier fluids and wellbore diameter affect lost circulation event. The study also revealed that there is a relation between the mud-cake thickness and the fracture reopening pressure [15]. The fracture propagation resistance model emphasizes a new concept, which indicates that the increase in the fracture gradient is strongly related to the fracture propagation pressure at the fracture tip. The output of the fracture propagation resistance model implies that the sealing of the fracture mouth by LCM could enhance the hoop stress around the wellbore. The last model takes a different direction and uses the three-dimensional poroelastic finite-element model [16]. This work concluded that the wellbore hoop stress enhancement estimates fracture initiation, propagation, and sealing mechanism.

### 1.3 Lost circulation management

Proper lost circulation management considers all factors involved. Lost circulation management is not only based on how stiff and rigid the materials are but also considers other factors to cure the losses. The material selection, or the pill designed, is the last stage of lost circulation management and

comes after the preventive and proactive management stages. Lost circulation management starts with the best design of the drilling parameters, which encompasses the geomechanical model to avoid the creation of induced fractures. Then the drilling fluids are selected which involve the proper rheological properties and include the effect of the fluid and material interaction. The wellbore strengthening technique is the third factor to enhance the fracture gradient and to avoid inducing fractures. This technique depends on the LCM particle size distribution. All these stages are called lost circulation preventive design. The last stage, which is the selection of the lost circulation material, is called remedial action [17].

## 1.4 Lost circulation material

The solid particles that are mixed and pumped to control a lost circulation problem that has occurred are called LCM. Lost circulation management focuses on selecting the right material to cure the losses as an essential part of the treatment. The industry categorizes LCM into seven different types. Due to the different formations and situations of the problem, there is no single material that can be suitable to cure all types of losses. The history of LCM started in 1951 by Howard and Scott. The initial classification was based on four categories only: dehydratable, flaky, fibrous, and granular. Then in 1956, White added a mixture of all previous materials [19]. Alsaba added more types to the list of LCMs including water-soluble and acid-soluble types [5]. The distinctions of these types of LCMs are as follows: one of the LCM classifications is by appearance, and other ways to classify the materials are by application and physical and chemical properties. The chemical properties are the reactivity of the LCMs with other chemicals in the drilling fluids, which include acid solubility and swelling reaction. The physical properties are mainly the size and shape of the LCM [5] which is also one of the main parts of our study in this work. The selection of which material to use is dependent on many factors such as geological formation description, fluid loss mechanisms (fracture types), and rate of loss. In this work, the LCMs used are classified into two groups based on the raw material properties, that is, flaky and fibrous.

The physical description of flaky materials is that the particle shape has a large flat and thin surface area with low stiffness [7,18]. This type of material can be used to mat shingles over the formation face [19]; however, due to its low stiffness and strength, the flaky material usually provides optimal coverage during the placement process, which makes it a last option in the treatment plan [5,9].

The fibrous material can form a mat-like bridge across vugular and fractured formations to form an effective seal [9]. It has a long and slender shape with low stiffness. It is an organic material with a distinctive particle size distribution. Natural cellulose fiber is one of the fibrous materials [20].

## 1.5 Particle size and shearing effect

As shown in the literature, the particle size distribution of the LCM is the only widely used method to design and plan the sealing or plugging mechanism to stop a lost circulation event. One of the criteria for selecting which material to use is a correlation between the particle size and the fracture width. However, this assumes that the selected size will be maintained when it reaches the thief zone or fracture [21]. Many publications addressed that most of the materials are degrading with high shearing but did not confirm or quantify the material size degradation rate and its impact on the ability of the LCM to plug the fracture. This work will answer the question of the relationship between size degradation and its quantifying effect to plug the fracture [22].

Size degradation is due to mechanical shearing or a dynamic force that acts on the particles by the mud pumps, drill string, wellbore annulus, and bit nozzles [23]. Plugging the fracture or enhancing the fracture gradient by LCM may be affected by size degradation. However, the degradation rate of the material particle size does not necessarily demonstrate a low plugging efficiency [21].

As the LCM is degraded by the mechanical shear, not only does the size change, but the shape also deteriorates and becomes more rounded [2]. Gaurina-Medjimurec and Pasic showed the proper bridging mechanism and illustrated the optimum size selection that allows the material to bridge as shown in the upper right side, while the smaller size due to size degradation forms no seal [24]. Therefore, to achieve effective bridging, the material size distribution must be small enough to enter the fracture or pore throat while being large enough to build the bridge.

The two crucial terminologies which are often incorrectly used are bridge and seal. Bridging provides the mechanical strength to the formation having a large permeability technique by using large particles; small particles will fill the void spaces between the large ones to form the seal [2]. Lavrov demonstrated the bridging and sealing mechanism in three different situations. The first situation is the fracture before adding the material, the second situation is the ineffective bridging when only large particles are used, and the third situation is the optimum conditions required for bridging and sealing using large particles to create bridging and fine particles to develop sealing [2].

## 1.6 Size degradation

Selecting the proper size for a fracture or a permeable formation is the primary factor in minimizing fluid invasion. It has been noted that when the materials are exposed to high shear, they might experience size degradation [25]. The type of materials, shearing rate, the fluid used, and the dry particle size distribution (PSD) will drive the severity of the degradation and



lead to information on the corrective action that can be taken during the treatment to achieve the required plugging and sealing needed. Little data are published describing the LCM size degradation phenomena [25]. In this work, an industry-standard approach was followed to comprehensively measure and analyze the size degradation of the concerned materials with the designed fluids. The sieve analysis was conducted, including material behavior when exposed to the fluids, and the results revealed the size expansion or reduction of the LCMs. The minus sign represents the percentage of size reduction, and a plus sign is used to show the percentage of size expansion. A comprehensive experimental study on the LCM will add a significant value to performance of future drilling operations to eliminate lost circulation events or make the problem less severe. Controlling and curing the losses involves more than just selecting the proper size and strength of the LCM. Detailed engineering approaches and techniques are required to deeply understand available solutions, and the current lack of an encompassing methodology requires a re-examination of the related factors to implement the best solution based on a specific situation. The significance of this work lies in assisting the industry in developing the optimum lost circulation mitigation procedure and material utilization in an engineering approach.

## 2 Materials and methods

### 2.1 Materials

#### 2.1.1 Lost circulation materials

In this work, the LCMs used are classified into two groups based on the raw material properties, flaky and fibrous, as shown in Table 2. The flake group includes a sized grade of mica and flaked calcium carbonate. The fibrous group includes a raw material of natural cellulose fiber. Each of these raw materials is sold under a variety of trade names as many companies manufacture almost similar or even identical materials but with different trade names.

#### 2.1.2 Carrier fluids

For drilling fluids or carrier fluids, four different fluid systems are used which are the same fluids used in our previous publication [21]. The four water-based fluid systems: water–bentonite mix (clay system), water–polymer mix (polymer system), and polymer–salt

systems using NaCl and CaCl<sub>2</sub> salts. The polymer used was xanthan gum, which is a hydrocolloid polymer. For the first polymer–salt system, 15 wt% NaCl was added, while for the second polymer–salt system, 20 wt% CaCl<sub>2</sub> was added [21]. Table 3 shows the carrier fluid formulations and their properties (i.e., pH, plastic viscosity, yield point, and API fluid loss) were measured and are shown in Table 4.

### 2.2 Methods

#### 2.2.1 Particle size distribution measurements

The selected LCMs (sized grade of mica, flaked calcium carbonate, and natural cellulose fiber) were mixed for two time intervals with the four selected fluids (water–bentonite mix, water–polymer mix, polymer–salt system using NaCl salt, and polymer–salt system using CaCl<sub>2</sub> salt). All fluid systems were mixed with each LCM at 4,000 RPM for intervals of 10 and 30 min. It was mixed for 10 min which is believed to be an enough time to mix the fluids with the LCM at the high shear rate then it is mixed for longer time (30 min) to investigate the effect of longer mixing time. A Silverson advanced high shear multimixer was used to simulate the high shear that the drilling fluids and LCM would be subjected to in the field. This multimixer can simulate the mixing tank in the field and bit nozzles' shearing effect. This multimixer used could simulate the mixing tank in the field and the bit nozzles' shearing effects. The multimixer had six nozzles to produce the required force to shear the materials and the fluids [21]. For dry sieve testing, the material is kept in the oven for 24 h to dry the sample and extract the moisture. Then the sample is placed into a set of different sieves, or mesh-bottomed containers, with sieve sizes ranging from large to small openings. Then, the column of the screens is positioned on a mechanical shaker to allow the material to pour through the sieves and stay on the mesh that either matches the particle size or is smaller. The mixed LCM particle size distribution is almost following the same procedure as the dry PSD. The only difference is that the material was mixed first with the designed fluids and then dried to examine the size changes due to shearing, time, and fluid interaction.

#### 2.2.2 Shape analysis after fluid interaction

The microscopy analysis in this work was carried out to investigate the shape of the particles. The particle shape of all materials in the dry phase was investigated, and the results are

TABLE 2 LCM groups with corresponding raw materials and dry phase shape description.

Group	Material description	Shape description
Flaky	Sized grade of mica	Angular, thin, and flat in shape with a large surface area
	Flaked calcium carbonate	Angular, thin, and flat in shape with a small surface area
Fibrous	Natural cellulose fiber	Angular and sub-angular

**TABLE 3 Carrier fluid formulations [21].**

Additive quantity	Clay system	Polymer system	NaCl–polymer	CaCl <sub>2</sub> –polymer
Water, m <sup>3</sup>	0.154	0.157	0.148	0.138
Bentonite, kg	9.07	0	0	0
Polymer, kg	0	0.68	0.68	0.68
Starch, kg	2.72	2.72	2.72	2.72
NaCl, kg	0	0	26.31	0
CaCl <sub>2</sub> , kg	0	0	0	47.63

**TABLE 4 Properties of the four drilling fluids [21].**

Drilling fluid formulation	pH	Plastic viscosity (cP)	Yield point (lb/100 ft <sup>2</sup> )	API fluid loss (ml)
Clay system	11	17	26	4.4
Polymer system	10	8	20	8.8
Polymer system—15 wt% NaCl	10	15	20	8.8
Polymer system—20 wt% CaCl <sub>2</sub>	9	25	20	6.7

illustrated in Table 2. To continue the full investigation of the shape analysis, a new evaluation of the materials' shape after the fluid's interaction was required. Five fluids were mixed with each material for 30 min, and the shape was examined. The fluids are clay systems (7 pH and 11 pH), polymer system (7 pH), polymer–NaCl system (7 pH), and polymer–CaCl<sub>2</sub> system (7 pH).

### 2.2.3 Plugging efficiency testing

LCM plugging performance analysis studied the ability of the material to plug, or bridge, the simulated fracture width. A key challenge in testing LCM plugging efficiency is the lack of industry standards for defining LCM testing methods and specifications for interpreting the results [20]. Most companies use a piece of equipment called a permeability plugging apparatus (PPA) to evaluate LCM properties and plugging efficiency. The original design of this equipment was not able to simulate a fracture size of more than 2 mm. To simulate the fractures, a circular hole was opened (drilled) in the slotted discs with the different fracture diameters [21]. All materials were tested under test conditions of 500 psi pressure and ambient temperature.

### 2.2.4 Specific gravity testing

Specific gravity is a ratio of the material density (mass per volume) to the water density and it is a unitless parameter. In this work, the specific gravity was measured on a dry sample and also after the material was exposed to the fluids. For wet samples, the material is kept in the oven for 16 h to dry the sample and extract the moisture. The analysis will show material's volume expansion or reduction resulting from fluid interaction. AccuPyc 1330 is a fully

automated gas displacement pycnometer used to measure the specific gravity of an irregular powder material.

### 2.2.5 Fluid loss

To measure the amount of fluid loss resulting from the filtration process, the API fluid loss standard test was applied (API-RP-13B). The fluid loss test was conducted at 100 psi and room temperature for the fluid loss tests on the carrier fluids (Table 4). For the plugging performance test, fluid loss was measured after applying a pressure of up to 500 psi (Tables 9–14). The loss of liquid (filtrate) from a carrier fluid with LCM due to filtration is controlled by the filter cake formed of the solid constituents in the carrier fluid [26]. A Fann filter press was used to determine the fluid loss. A filter paper was inserted at the bottom of the filter cup assembly, followed by filling a filter cup with 350 ml of carrier fluid mixture to conduct the fluid loss experiment. The filter cup was fastened in place and the filtration experiment began using compressed air at 100 psi (raised to 500 psi for the plugging efficiency testing). After 30 min of the filtration experiment, the filtrate liquid was collected and its total volume was measured [27].

## 3 Results and discussion

### 3.1 Particle size distribution measurements

#### 3.1.1 Sized grade of mica

Mica is one of the flaky group materials. It has a wide particle size distribution and large particles up to 4,000  $\mu\text{m}$ . Its dry PSD



measurements showed that the material has a particle size distribution that covers a range of 4,000–149  $\mu\text{m}$ . The cumulative distribution of the five  $D_s$  values is  $D_{10}$  (768  $\mu\text{m}$ ),  $D_{25}$  (1,131  $\mu\text{m}$ ),  $D_{50}$  (1,751  $\mu\text{m}$ ),  $D_{75}$  (2,382  $\mu\text{m}$ ), and  $D_{90}$  (2,776  $\mu\text{m}$ ).

### 3.1.1.1 Water system

The material was mixed with the water system for 10 min and 30 min time intervals, and the PSD data were recorded. The cumulative size distribution of the samples is shown in Table 5. The percent of size changing of each  $D_s$  value and the average percent of the size degradation showed that the material's size degradation was high and lost more than 60% of its size (Table 5). The time was not a factor in size degradation in which both 10 min and 30 min results showed a similar average size reduction percentage.

### 3.1.1.2 Clay system

A total of five mixes were performed, and the time intervals were 10 and 30 min. The cumulative distribution ( $D_s$ ) for both clay systems and a comparison analysis of the average size degradation are shown in Table 5. It was noticed that the size degradation of mica with the clay system was 56% at 5 min, 62% at 10 min, and 66% at 30 min of shearing. The change in alkalinity did not affect mica size degradation performance. Overall, the mica performed as a low-strength material because it performed poorly during mixing and was not able to withstand the size degradation. The average size degradation exceeded 66% in reduction with clay systems.

### 3.1.1.3 Polymer system

In the polymer system, three different alkalinity points were tested: 7, 9, and 10 pH with mica. The comparison analysis between dry and mixed PSD showed the material

with polymer systems behaved almost the same as the clay and water system with a very high size reduction percentage. All in all, the alkalinity effect of the polymer systems does not influence mica size degradation performance. The size degradation percentage remained constant at around 66% size reduction (Table 5).

### 3.1.1.4 Polymer–salt system

Mica was mixed with two salt systems (NaCl and  $\text{CaCl}_2$ ) to study the material's size degradation behavior. Two salt sources with different alkalinity environments were tested and analyzed for the size degradation study. Sodium chloride with pH values of 7 pH and 10 pH and calcium chloride at 7 pH and 9 pH were tested for size degradation.

**3.1.1.4.1 NaCl–polymer system.** Sodium chloride systems with two different alkalinities showed an effect on mica size degradation. The maximum particle size attrition was 77% below the dry PSD measurement, resulting from the low pH fluids (Table 5). The 10 pH was slightly better than the 7 pH, in maintaining the particle size distribution by around 8% less degradation (Table 5).

**3.1.1.4.2  $\text{CaCl}_2$ –polymer–salt system.** The calcium chloride system showed similar performance to another salt system. The highest size reduction was 59% in 30 min mixing with 9 pH, while the low pH showed a degradation percentage of 69% (Table 5).

## 3.1.2 Flaked calcium carbonate

Flaked calcium carbonate is the second material of the flaky group materials. It has a wide particle size distribution. Its dry PSD measurements showed that the material has a particle size distribution that covers a range of 4,000–149  $\mu\text{m}$ . The cumulative

TABLE 5 Cumulative distribution of the mixed samples' PSD (mica) (all systems) and size percent change.

System	10 min mix		30 min mix	
	Value ( $\mu\text{m}$ )	% change from the dry sample	Value ( $\mu\text{m}$ )	% change from the dry sample
Water system	752	–60%	674	–64%
7 pH clay system	696	–62%	624	–66%
11 pH clay system	740	–61%	648	–65%
7 pH polymer system	749	–60%	573	–69%
9 pH polymer system	708	–64%	662	–66%
10 pH polymer system	803	–59%	730	–61%
7 pH–NaCl–polymer system	657	–65%	437	–77%
10 pH–NaCl–polymer system	721	–62%	574	–69%
7 pH– $\text{CaCl}_2$ –polymer system	877	–53%	593	–69%
9 pH– $\text{CaCl}_2$ –polymer system	841	–56%	765	–59%

distribution of the five  $D_s$  values is  $D_{10}$  (1,111  $\mu\text{m}$ ),  $D_{25}$  (1,512  $\mu\text{m}$ ),  $D_{50}$  (2,074  $\mu\text{m}$ ),  $D_{75}$  (2,805  $\mu\text{m}$ ), and  $D_{90}$  (3,420  $\mu\text{m}$ ).

### 3.1.2.1 Water system

The material was mixed with the water system for 10 min and 30 min time intervals, and the mixed LCM PSD data were recorded. The percent change of each  $D_s$  value and the average percent of the overall size degradation showed that the material's size degradation was high and lost more than 72% of its size due to shearing (Table 6).

### 3.1.2.2 Clay system

A total of five mixes were performed at the time intervals of 10 and 30 min. The data in Table 6 illustrate the results and observations of the mixed sample PSD of mica with clay systems. The cumulative distribution ( $D_s$ ) for both clay systems and a comparison analysis are shown in Table 6. The results showed that the size degradation of flaked calcium carbonate with the clay system with 7 pH alkalinity was a little high, in which the size was reduced by 60% from the original at 30 min of shearing. The size degradation result of the clay system with 11 pH showed a similar performance to the 7 pH system. However, the higher pH was slightly less by 6%, which is not considered a significant difference. Thus, the alkalinity effect was negligible on the flaked calcium carbonate's size degradation performance. Overall, the flaked calcium carbonate performed as a low-strength material, and the average size degradation exceed 60% in reduction with clay systems.

### 3.1.2.3 Polymer system

In the polymer system, three different alkalinity points were tested, that is, 7, 9, and 10 pH with flaked calcium carbonate. The comparison analysis between dry and mixed

samples' PSD showed the material with polymer systems behaved more efficiently than that with clay and water systems, as shown in Table 6. Overall, the alkalinity effect of the polymer systems influences flaked calcium carbonate's size degradation performance. The size degradation percentage of the higher alkalinity was better than that of the low pH.

### 3.1.2.4 Polymer–salt system

Flaked calcium carbonate was mixed with two salts systems (NaCl and  $\text{CaCl}_2$ ) to study the material's size degradation behavior.

**3.1.2.4.1 NaCl–polymer system.** The size degradation of sodium chloride systems with two different alkalinities results is recorded. The maximum particle size attrition is 40% below the dry PSD measurement, resulting from the 11 pH fluids (Table 6). Both NaCl–polymer systems showed similar results.

**3.1.2.4.2  $\text{CaCl}_2$ –polymer system.** The calcium chloride system showed similar performance to sodium chloride, as observed in the sieve results. The highest size reduction was 40% in 30 min of mixing with 10 pH, while the lowest degradation occurred in 30 min shearing time with 9 pH (Table 6). Therefore, the alkalinity showed no direct relation with size degradation performance of flaked calcium carbonate.

## 3.1.3 Natural cellulose fiber

Natural cellulose fiber is the only material in this research that falls in the fibrous group. It has a particle size distribution range from 2,830 to 105  $\mu\text{m}$ . The cumulative distribution of the five  $D_s$  values is  $D_{10}$  (427  $\mu\text{m}$ ),  $D_{25}$  (767  $\mu\text{m}$ ),  $D_{50}$  (1,159  $\mu\text{m}$ ),  $D_{75}$  (1,584  $\mu\text{m}$ ), and  $D_{90}$  (2,007  $\mu\text{m}$ ). It is considered one of the large

TABLE 6 Cumulative distribution of the mixed samples' PSD (flaked calcium carbonate) (all systems) and size percent change.

System	10 min mix		30 min mix	
	Value ( $\mu\text{m}$ )	% change from the dry sample	Value ( $\mu\text{m}$ )	% change from the dry sample
Water system	933	–61%	668	–72%
7 pH clay system	1121	–52%	935	–60%
11 pH clay system	1332	–43%	1094	–54%
7 pH polymer system	1565	–33%	1437	–40%
9 pH polymer system	1664	–29%	1543	–36%
10 pH polymer system	1812	–23%	1608	–33%
7 pH–NaCl–polymer system	1535	–35%	1484	–38%
10 pH–NaCl–polymer system	1470	–38%	1416	–40%
7 pH– $\text{CaCl}_2$ –polymer system	1616	–30%	1542	–34%
9 pH– $\text{CaCl}_2$ –polymer system	1667	–27%	1508	–35%

LCM that can be used in high permeable formation, due to its large  $D_{50}$ .

### 3.1.3.1 Water system

The material was mixed for 10 min and 30 min time intervals, and the mixed samples' PSD data are recorded. The percent change of each  $D_s$  value and the average percent of the size degradation are illustrated in Table 7. The results of the material with the water system showed that the fiber was able to maintain its original PSD. The size degradation only occurred at the large particle size ( $D_{75}$  and  $D_{90}$ ), where the small particles ( $D_{10}$  and  $D_{25}$ ) showed an increase in size, resulting in an overall increase in the average particle size of the material by 5% after 30 min of shearing.

### 3.1.3.2 Clay system

A total of five mixes were performed, and the time intervals were 10 and 30 min. Table 7 shows the cumulative distribution ( $D_s$ ) of both clay systems and comparison analysis. It was noted that the size reduction effect is minimum, and the maximum degradation was 5% at 30 min mixing. It was also observed that the low alkalinity fluid has a less size degradation percentage than 11 pH fluid. The change in alkalinity did affect the material's size degradation performance. Overall, the natural cellulose fiber material performed as a medium-strength material, and the average size degradation did not exceed 17% size reduction with clay systems.

### 3.1.3.3 Polymer system

Natural cellulose fiber was tested for size degradation with the polymer system at three different alkalinity points 7, 9, and 10 pH. The PSD profile of the dry sample and three different pH fluids showed similar performance. Therefore, the polymer systems with different alkalinities have no adverse effects associated with size degradation. The size degradation performance of natural cellulose

fiber with a polymer system showed that the material maintained the original particle size distribution. The material demonstrated a high reduction in the big particles ( $D_{90}$  and  $D_{75}$ ) and that redistributed in the small particles ( $D_{10}$  and  $D_{25}$ ) and maintained  $D_{50}$  almost constant, resulting in an overall increase in the average percent of the  $D_s$  values to be 6% (Table 7).

### 3.1.3.4 Polymer-salt system

Sodium chloride with pH 7 and 10 and calcium chloride with 7 and 9 pH were mixed and tested to study natural cellulose fiber size degradation.

**3.1.3.4.1 NaCl-polymer system.** The natural cellulose fiber size degradation results with sodium chloride systems are recorded. The average mixed samples' PSD decreased by 10% with low pH fluids, while it was slightly better at high pH, with only 2% size reduction (Table 7).

**3.1.3.4.2 CaCl<sub>2</sub>-polymer system.** Calcium chloride systems showed a better performance than sodium chloride systems, in maintaining their original size. The mixed samples' PSD was increased by 3% with high pH, while it was a 5% size reduction of the low pH. All these data were obtained at 30 min of shearing (Table 7).

## 3.2 Specific gravity after fluid interaction

### 3.2.1 Flaky group

Another material that experienced a specific gravity change after fluid interaction from the flaky group is a sized grade of mica. The mica dry phase specific gravity was 2.736, and the specific gravity increased by an average of 0.07 after mixing with the different fluid systems. This increase was due to a volume decrease from fluid

TABLE 7 Cumulative distribution of the mixed samples' PSD (natural cellulose fiber) (all systems) and size degradation percent.

System	10 min mix		30 min mix	
	Value ( $\mu\text{m}$ )	% change from the dry sample	Value ( $\mu\text{m}$ )	% change from the dry sample
Water system	1246	9%	1151	5%
7 pH clay system	1097	-2%	1075	-5%
11 pH clay system	994	-13%	919	-17%
7 pH polymer system	1154	4%	1107	-1%
9 pH polymer system	1201	8%	1144	6%
10 pH polymer system	1164	4%	1067	-4%
7 pH-NaCl-polymer system	1107	-2%	1018	-10%
10 pH-NaCl-polymer system	1178	4%	1093	-2%
7 pH-CaCl <sub>2</sub> -polymer system	1184	8%	1053	-5%
9 pH-CaCl <sub>2</sub> -polymer system	1185	8%	1134	3%

interaction. Furthermore, in the size degradation study of mica, a high percentage of the mica mixed samples' PSD was significantly decreased.

### 3.2.2 Fibrous group

The last material that showed a specific gravity decrease due to fluid interaction from the fibrous group is natural cellulose fiber. The average specific gravity reduction after mixing with the different fluid systems was 0.71 and that was due to the characteristic of water absorption by the cellulose to develop hydrogen bond interaction, resulting in the volume increase [28]. [29] Therefore, the specific gravity showed reduction (Table 8). Moreover, this material did not show a high size degradation which fits with the specific gravity results.

## 3.3 Shape analysis after fluid interaction

### 3.3.1 Flaky group

The flaky group has two materials: sized grade of mica and flaked calcium carbonate. The dry-shape analysis of the first material showed the LCM to be angular, thin, and flat in shape with a large surface area, where the shape of mixed samples is described as rounded and angular (Figure 1). The original particle shape of flaked calcium carbonate was angular, sub-angular, thin, and flat with a small surface area. The shape of mixed samples for all fluids was drastically changed to be sub-rounded and angular (Figure 2).

### 3.3.2 Fibrous group

The fibrous group has only one fiber material. Natural cellulose fiber is an organic material with dry particle shapes of angular and sub-angular; on the other hand, the mixed sample shape showed more angularity with curved corners (Figure 3).

## 3.4 Plugging performance

### 3.4.1 Sized grade of mica plugging performance

The first material of the flaky group, mica, showed a significant decrease in plugging efficiency. The mixture with

fluid and no shearing showed excellent performance and was able to plug a 5.0-mm fracture. After the material was sheared with the fluid, the sealing capability dropped to 1.5 mm (Table 9). The  $D_{50}$  for the material before and after degradation was recorded at 1,751 and 566  $\mu\text{m}$ , respectively. The median particle size over the fracture size must be equal to or greater than 1.2 [1.751 mm ( $D_{50}$  before degradation) divided by 1.5 mm (sealed fracture size)] to form effective bridging (Eq. 1). This is the highest ratio among all materials tested.

$$\frac{D_{50}}{\text{Fracture Size}} \geq 1.2. \quad (1)$$

### 3.4.2 Flaked calcium carbonate plugging performance

Flaked calcium carbonate is the second material in the flaky group. It has a better performance than mica. The no-shearing mixture of the material was able to seal a fracture size of 5.0 mm. After the material was sheared with the fluid, the sealing capability dropped to 3.0 mm (Table 10). The material plugging efficiency performance was remarkable, especially with the high size degradation of the material. The median size of the dry phase was 2,074  $\mu\text{m}$ ; the mixed sample's phase median size dropped to 973  $\mu\text{m}$  due to size degradation. The new mathematical relationship equation for flaked calcium carbonate is developed. The median particle size over the fracture size must be equal to or greater than 0.7 to form the bridging.

$$\frac{D_{50}}{\text{Fracture Size}} \geq 0.7 \quad (2)$$

### 3.4.3 Natural cellulose fiber performance

The last material in our study is the natural cellulose fiber. The overall size degradation results of the material revealed that the material had a 5% size increase when immersed in the fluid. The no-shearing mixture plugged a fracture size of 2.5 mm; likewise, the mixture sheared for 30 min. The material maintained the ability to plug the same fracture aperture with no effect caused by the shearing force (Table 11). The  $D_{50}$  of the dry phase was 1,159  $\mu\text{m}$ , while the size degradation caused a reduction in the  $D_{50}$  to 1,087  $\mu\text{m}$ . The developed mathematical relationship equation (Eq. 3) states that the median

TABLE 8 Specific gravity measurements.

Material	Dry	Clay system 7 pH	Clay system 11 pH	Polymer system—no salt	Polymer system—NaCl salt	Polymer system—CaCl <sub>2</sub> salt
Sized grade of mica	2.736	2.781	2.787	2.824	2.801	2.805
Flaked calcium carbonate	2.73	2.722	2.725	2.728	2.728	2.718
Natural cellulose fiber	2.028	1.329	1.344	1.309	1.308	1.314

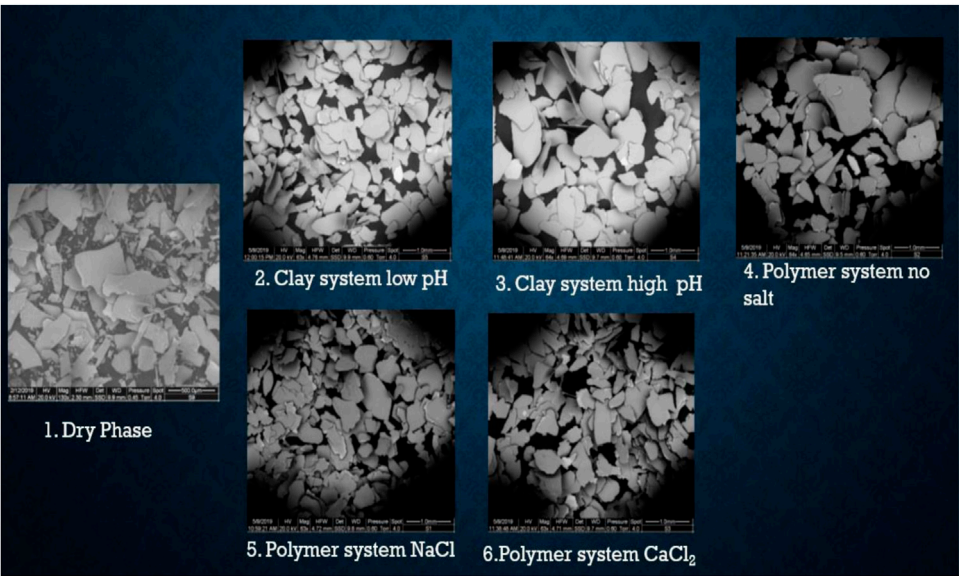


FIGURE 1  
Mixed and dry mica microscopy images.

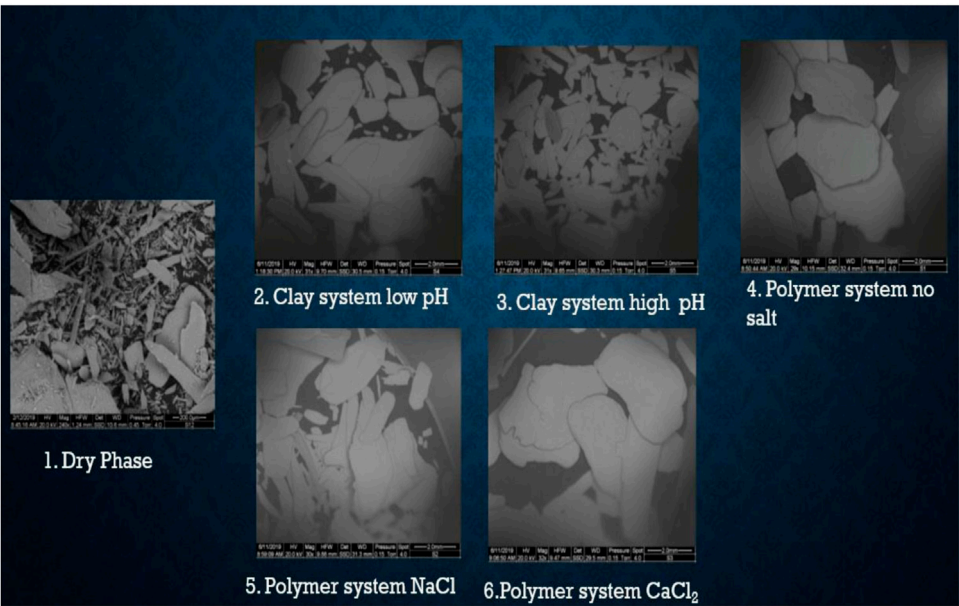


FIGURE 2  
Mixed and dry flaked calcium carbonate microscopy images.

size of the dry phase over the fracture size has to be equal to or greater than 0.5 in order to form the rigid plug with natural cellulose fiber.

$$\frac{D_{50}}{\text{Fracture Size}} \geq 0.5.$$

(3)

### 3.5 LCM overall performance

#### 3.5.1 Sized grade of mica

The original particle size distribution of mica covers a range from 4,000 to 149 μm. The overall performance of mica with the



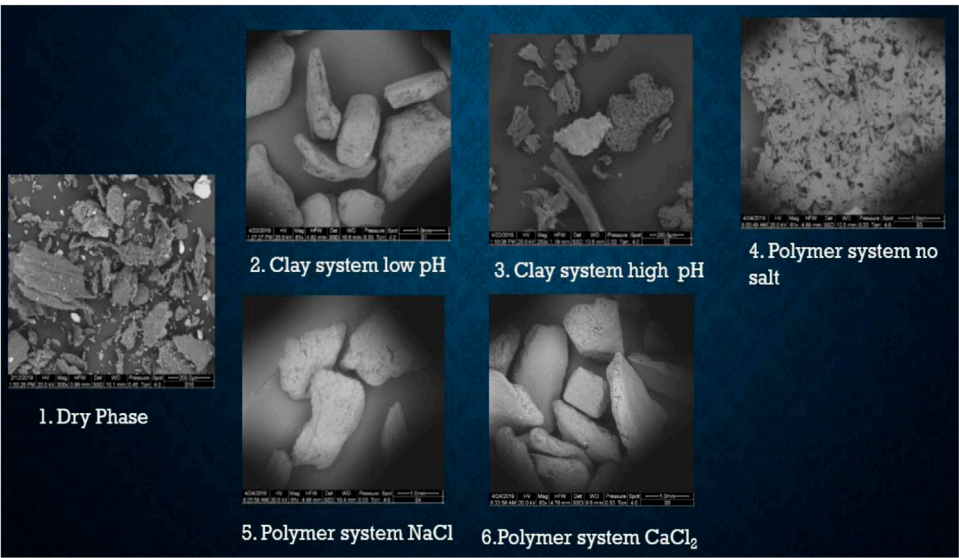


**FIGURE 3**  
Mixed and dry natural cellulose fiber microscopy image.

**TABLE 9** Sized grade of mica plugging performance.

No shearing		30 min shearing	
Size of fracture (slotted), mm	Fluid loss, cm <sup>3</sup>	Size of fracture (slotted), mm	Fluid loss, cm <sup>3</sup>
3.5	11	0.25	5
5.0	30	1.5	26
5.5	No control	2	No control

**TABLE 10** Flaked calcium carbonate plugging performance.

No shearing		30 min shearing	
Size of fracture (slotted), mm	Fluid loss, cm <sup>3</sup>	Size of fracture (slotted), mm	Fluid loss, cm <sup>3</sup>
2.5	8	3	28
3.5	19	3.5	No control
5.0	31		
5.5	No control		

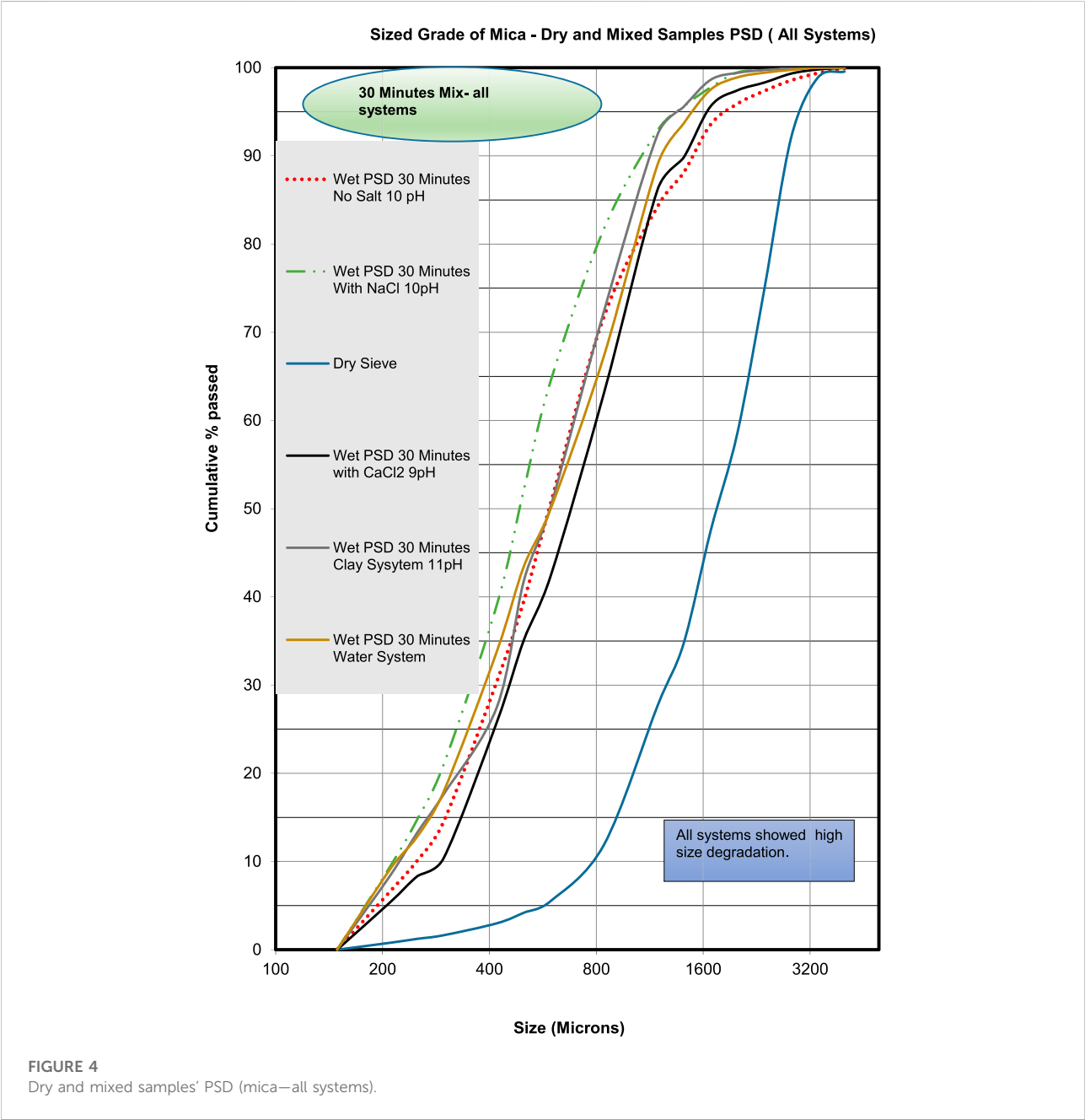
different carrier fluid systems showed that the material performed with very high size reduction with all fluids systems (Figure 4). The size degradation of mica was extraordinarily high which reached an average of 67% loss in particle size for all fluids. The cumulative distribution showed a high reduction, as shown in Figure 5 which showed a loss in D<sub>10</sub> at 71%, loss in D<sub>50</sub> at 70% and finally, the D<sub>90</sub> experienced a loss in particle size percent of 56%. This material was destroyed using this material as LCM will provide no benefits (Figure 5). The time interval analysis of mica size degradation performance showed that the material was not affected by time changing and acted as a

time-independent material. The size degradation results of the 10 min and 30 min shearing times were similar and no extra size degradation was encountered, as it can be observed in the clay system example (Supplementary Figure S1). The average size degradation of 10 min with all fluids showed a 60% decrease in size, while the 30 min showed an average of 67% decrease in size. The mass of the mica showed a high loss of 30% after shearing. Most of the particles went below the minimum (<149 μm), as it is shown in Supplementary Figure S2.

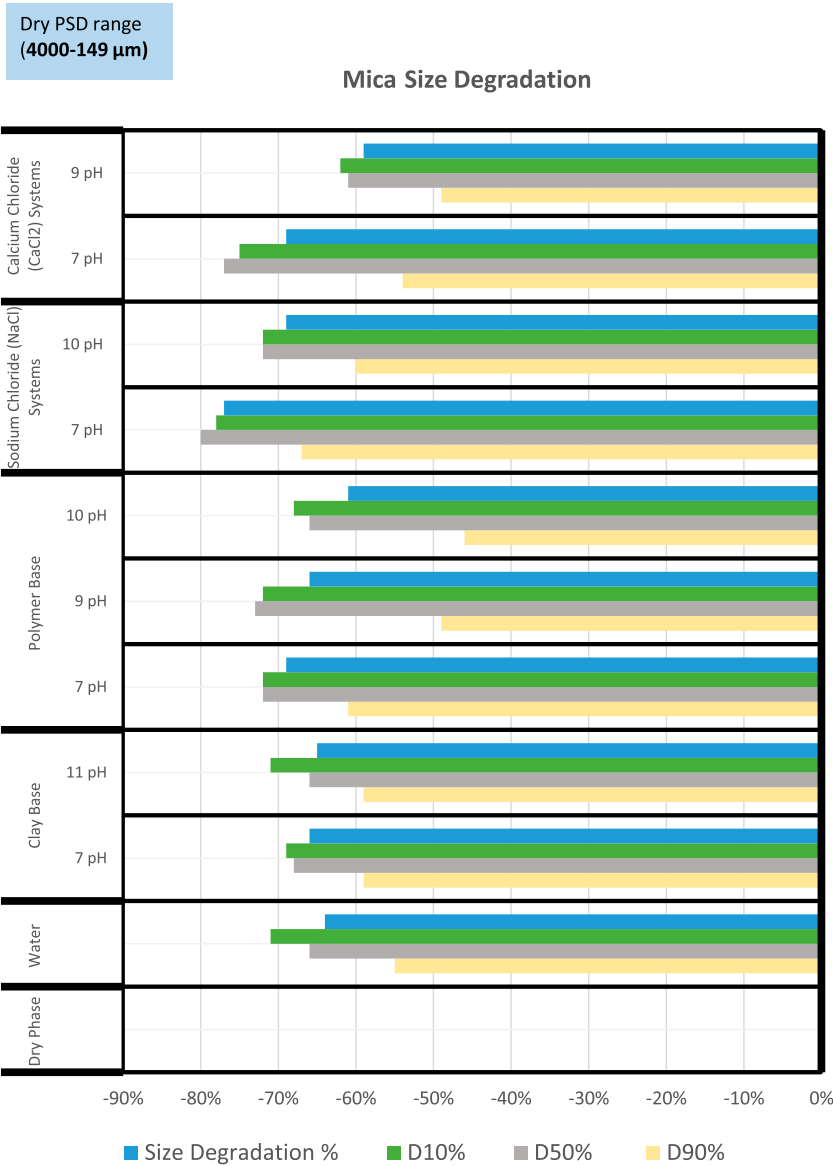
The shape of mica was changed from angular, thin, and flat with a large surface to rounded and angular because of

TABLE 11 Natural cellulose fiber plugging performance.

No shearing		30 min shearing	
Size of fracture (slotted), mm	Fluid loss, cm <sup>3</sup>	Size of fracture (slotted), mm	Fluid loss, cm <sup>3</sup>
2.5	23	2.5	25
3.0	No control	3.0	No control









**FIGURE 5**  
Mica—size degradation performance (30 min shearing).

**TABLE 12** Mica plugged fracture size before and after shearing force.

No shearing			30 min shearing		
Size of fracture (slotted), mm	Fluid loss, cm <sup>3</sup>	Plugging photo	Size of fracture (slotted), mm	Fluid loss, cm <sup>3</sup>	Plugging photo
5.0	30		1.5	26	

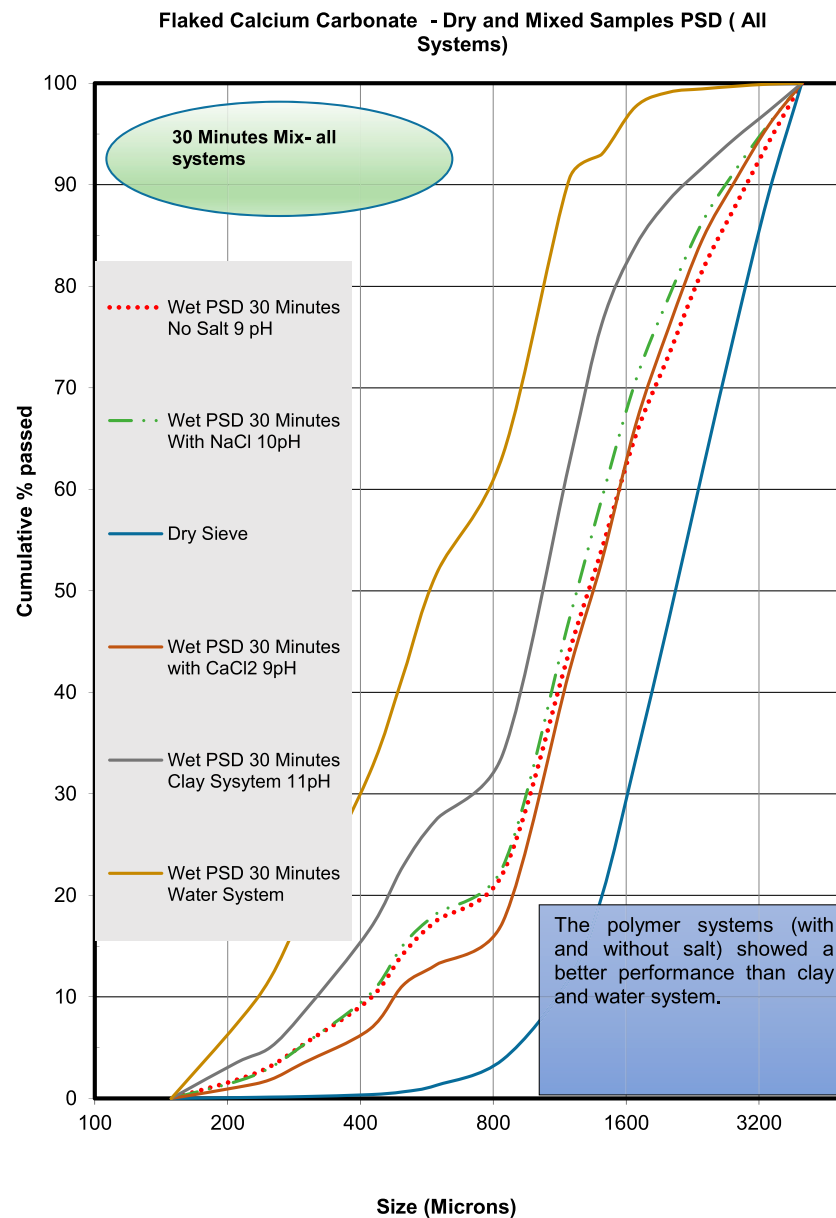


**FIGURE 6**  
Dry and mixed samples' PSD (flaked calcium carbonate—all systems).

shearing and the fluid's interaction. The specific gravity showed a slight increase, due to reduction in volume. The plugging efficiency of the no-shearing mixture was reported at 5.0-mm fracture size and then dropped significantly with the shearing effect to 1.5 mm. Moreover, a high fluid loss of 26 ml was observed. The new rounded shape was one of the reasons for the high fluid loss. The loss in plugging efficiency from 5.0 to 1.5-mm fracture size represents around 70% loss in efficiency, which is similar to the reduction in size degradation of 66%. Therefore, the relation between the

plugging efficiency to the material size is a one-to-one ratio (Table 12).

### 3.5.2 Flaked calcium carbonate

The PSD dry phase of flaked calcium carbonate has a particle size range of 4,000–149  $\mu\text{m}$ . The overall performance of flaked calcium carbonate with the different carrier fluid systems showed that the material performed with a very high size reduction in water and clay systems. However, it showed better performance with all polymer systems by almost 50% less in size degradation (Figure 6).

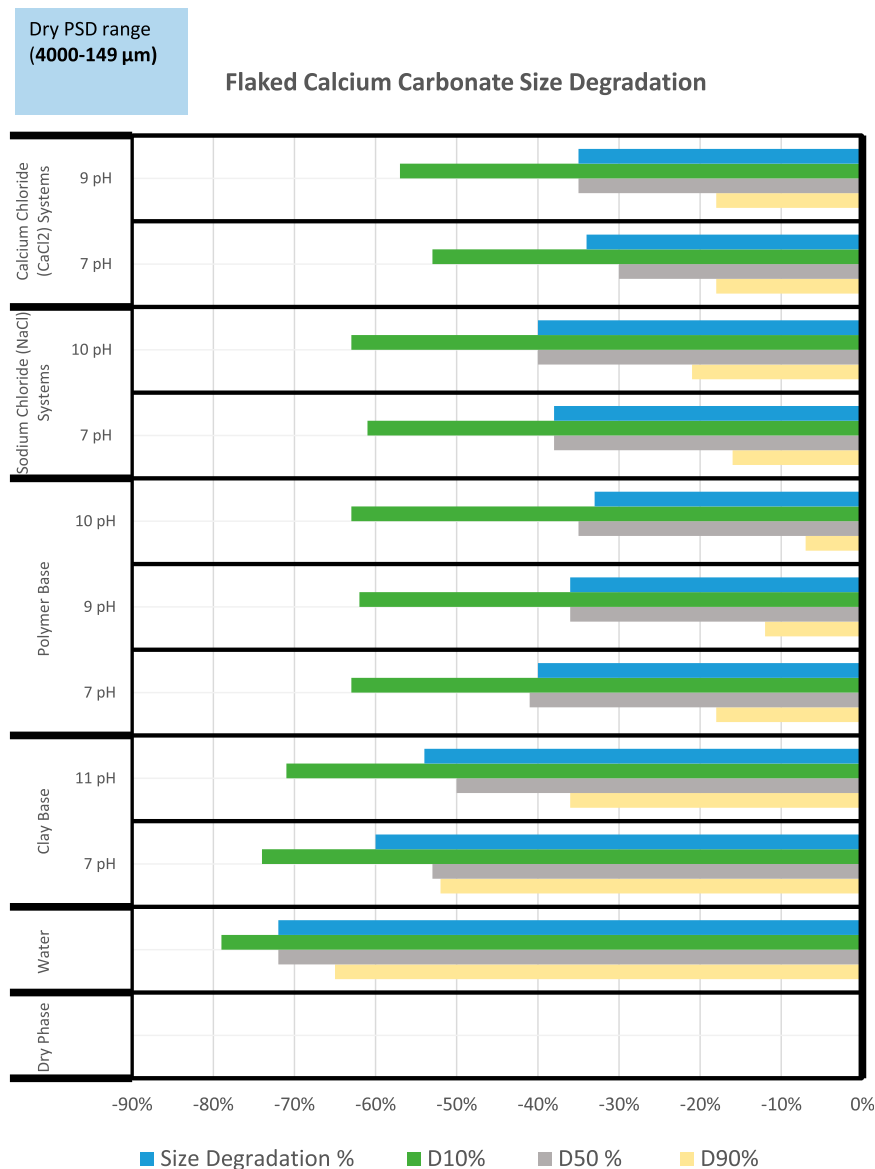




**FIGURE 7**  
Flaked calcium carbonate—size degradation performance (30 min shearing).

The mixed samples' PSD data revealed that the material behaved differently based on the fluid used. The water and clay systems showed more degradation and loss of the material durability than all polymer systems showing the comprehensive analysis of all fluids with flaked calcium carbonate. Since clay and water systems have similar performance, the average percentage of their data will be combined, and the same goes for polymer systems. Clay and water systems showed a size degradation of around 54%–72%, while polymer systems (both salt and no salt) showed an average of 33%–40% size reduction (Figure 7). The overall size degradation of the clay and water systems was reported at 62% size reduction, and that is considered a high loss in particle size. This was also shown in

$D_{90}$ ,  $D_{50}$ , and  $D_{10}$  with a size reduction of 51%, 58%, and 75%, respectively. On the other hand, the polymer systems only showed a loss of 37% in size reduction. The cumulative distributions showed a size reduction in  $D_{90}$ ,  $D_{50}$ , and  $D_{10}$  with a size reduction of 16%, 36%, and 60%, respectively.

The time interval analysis of flaked calcium carbonate size degradation performance showed that the material was not affected by time changing and acted as a time-independent material. The average difference of size degradation results of the 10 min and 30 min showed around 10% more degradation with shearing time changing, as it is shown in the clay system example

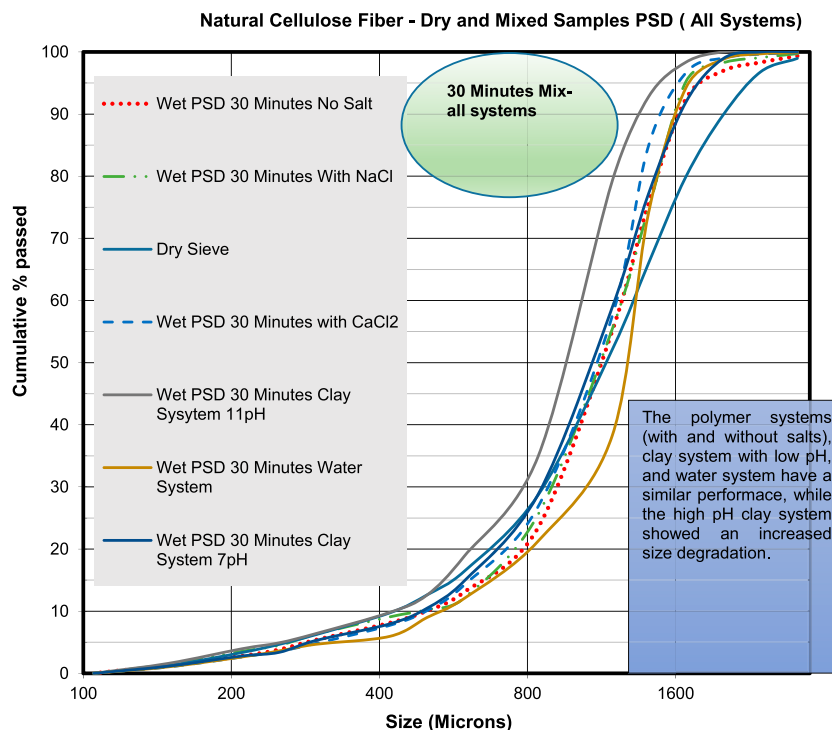
**TABLE 13** Flaked calcium carbonate plugged fracture size before and after the shearing force.

No shearing			30 min shearing		
Size of fracture (slotted), mm	Fluid loss, cm <sup>3</sup>	Plugging photo	Size of fracture (slotted), mm	Fluid loss, cm <sup>3</sup>	Plugging photo
5.0	31		3	28	

(Supplementary Figure S3). The average size degradation of 10 min with the first group (water and clay systems) showed a 52% reduction in size, while the 30 min showed an average of 62% reduction in size. The clay and water systems lost 31% of the material mass after shearing with only 70% of the particles that are above 149  $\mu\text{m}$ , while polymer systems maintained 85% of the particles above the minimum size (Supplementary Figure S4).

The original particle shape of flaked calcium carbonate was angular, sub-angular, thin, and flat with a small surface area. The mixed samples' shape for all fluids was drastically changed

to be sub-rounded and angular. The specific gravity measurements of flaked calcium carbonate did not change after the fluid's interaction and stayed constant at 2.73. The simulated plugged fracture was obtained at 5.0 mm by using the dry PSD (no shearing) of the material, but when the shearing force occurred, the material was able to plug 3.0-mm fractures. This drop in the fracture size was quantified to be a 40% decrease, while the size degradation of the fluids used in this test was 60% (Table 13). Thus, the size degradation percent of flaked calcium carbonate to plugging efficiency ratio is 1:0.6.

**FIGURE 8**

Dry and mixed samples' PSD (natural cellulose fiber—all systems).

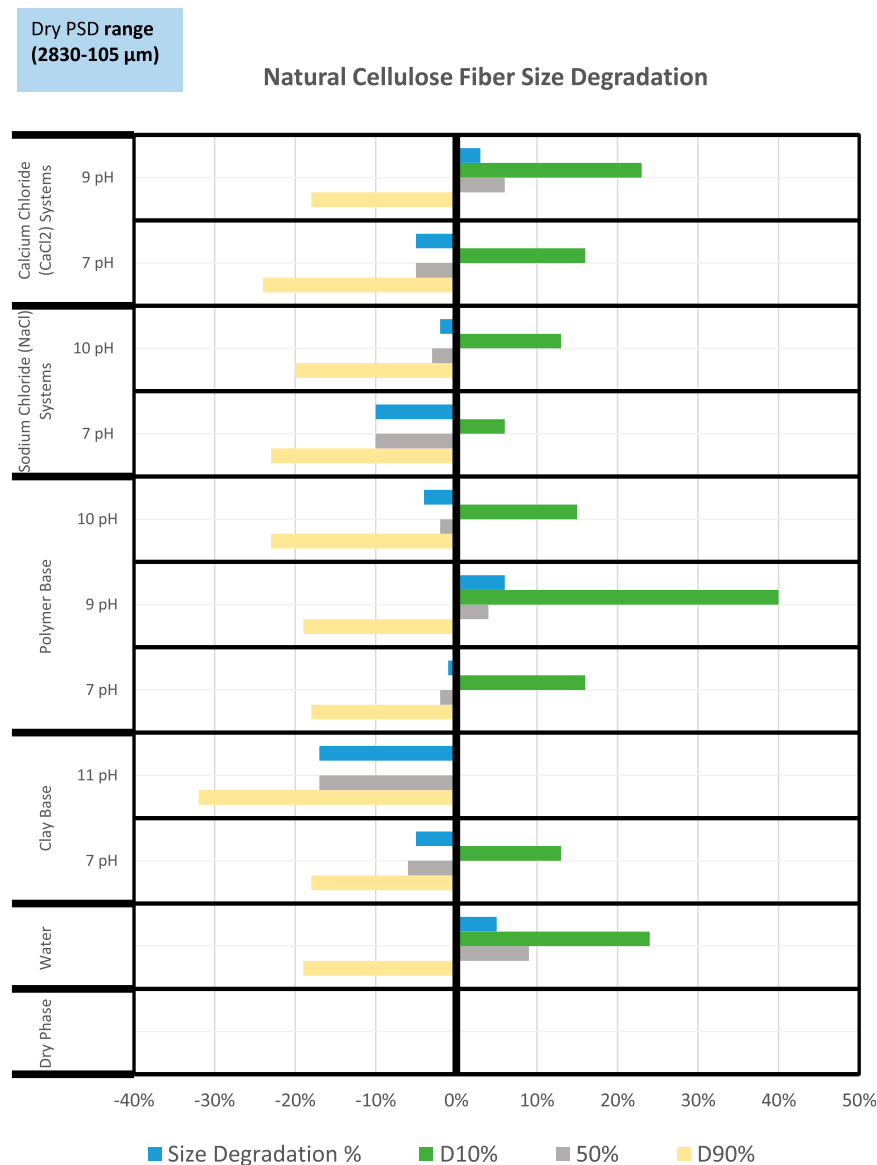




**FIGURE 9**  
Natural cellulose fiber—size degradation performance (30 min shearing).

### 3.5.3 Natural cellulose fiber

The dry size range of natural cellulose is from 2,830 to 105  $\mu\text{m}$ . The overall performance of natural cellulose fiber with the different carrier fluid systems showed that the material performed a minor size reduction with all systems with a maximum degradation of 17% with a high-pH clay system (Figure 8). The average size degradation of all fluids was reported at a 3% size reduction. The small particles ( $D_{10}$ ) showed a size increase of 17%. The big particles ( $D_{90}$ ) showed a loss of only 21% only, while the median particles ( $D_{50}$ ) showed a size decrease of 3%. This material showed particle redistribution between the big and small particles (Figure 9).

The time interval analysis of natural cellulose fiber size degradation performance showed that the material was not affected by time changing and acted as a time-independent material. The size degradation results of the 10 min and 30 min shearing time were similar and no extra size degradation was encountered, as it is shown in the clay system example (Supplementary Figure S5). The average size degradation of 10 min with all fluids was 1% reduction in size, while the 30 min showed an average of 3% reduction in size. The aspect of the natural cellulose fiber mass percentage loss study that went below the original PSD revealed that the material lost some of its mass and introduced new small

**TABLE 14** Natural cellulose fiber plugged fracture size before and after shearing force.

No shearing			30 min shearing		
Size of fracture (slotted), mm	Fluid loss, cm <sup>3</sup>	Plugging photo	Size of fracture (slotted), mm	Fluid loss, cm <sup>3</sup>	Plugging photo
2.5	23		2.5	25	

particles that are below the minimum dry particle size (105  $\mu\text{m}$ ). The average percentage of the lost mass was observed to be around 17%, that means after mixing and shearing, only 83% of the initial material mass will be reaching the target zone ([Supplementary Figure S6](#)).

The material showed a decrease in specific gravity with fluid interaction. The average specific gravity reduction is 0.71 and that was due to cellulose characteristics of water absorption to develop hydrogen bond interaction, resulting in an increase in volume (Caulfield 1978). Therefore, the specific gravity reflected that drop. The material dry phase shape was angular and sub-angular. Then due to fluid interaction, the mixed samples' shape showed more angularity with curved corners. The material's plugging efficiency was not affected by size degradation. The material was able to plug the same fracture size with and without the shearing force effect. The material plugged a simulated fracture size of 2.5 mm with a fluid loss of 2.5 ml ([Table 14](#)).

## 4 Conclusion

The overall impact of this work is to prove that applying these ways of investigation to the current lost circulation management can drive the industry to resolve some lost circulation problems by effectively and efficiently applying the right LCM in the specific situation.

The important and major findings of this work are as follows:

- The effect of carrier fluids was proven to be significant on the LCM size degradation. Flaked calcium carbonate was affected by the fluid selection. It showed high size degradation with water and clay systems, whereas it was less impacted with all polymer systems and showed even a better performance with high alkalinity polymer systems.
- Each material behaved differently under high shear. The material that did not experience significant size changes

was natural cellulose fiber. The other materials (mica and flaked calcium carbonate) showed a large size reduction.

- Two (natural cellulose fiber and mica) materials showed a change in their specific gravity results after mixing with fluids.
- All of the materials kept their initial shape after exposure to the fluids, except the flaky group that introduced more rounded shape particles.
- A new experimental mathematical observation was obtained for each material to enhance the plugging efficiency and can be used to simulate the fracture size.

## Data availability statement

The original contributions presented in the study are included in the article/[Supplementary Material](#); further inquiries can be directed to the corresponding author.

## Author contributions

Conceptualization: SaA; formal analysis: SaA, SuA, and AB; experimental investigation: SaA and AB; writing—original draft preparation: SaA and SuA; writing—review and editing: SaA, SuA, and AB; and supervision: SaA, SuA, and AB. All authors have read and agreed to the published version of the manuscript.

## Acknowledgments

The authors acknowledge and highly appreciate Saudi Aramco and King Fahd University of Petroleum & Minerals (KFUPM) for their support to publish this work. The company Saudi Aramco was not involved in the study design, collection, analysis, interpretation of data, the writing of this article or the decision to submit it for publication.



## Conflict of interest

SaA and AB were employed by Saudi Aramco.

The remaining author declares that the research was conducted in the absence of any commercial or financial relationships that could be construed as a potential conflict of interest.

## Publisher's note

All claims expressed in this article are solely those of the authors and do not necessarily represent those of their

affiliated organizations, or those of the publisher, the editors, and the reviewers. Any product that may be evaluated in this article, or claim that may be made by its manufacturer, is not guaranteed or endorsed by the publisher.

## Supplementary Material

The Supplementary Material for this article can be found online at: <https://www.frontiersin.org/articles/10.3389/fphy.2022.1065526/full#supplementary-material>

## References

- Aadnøy BS, Chenevert ME 1987. Stability of highly inclined boreholes. *SPE Drilling Eng* 2 (4): 364–74. SPE-16052-PA. doi:10.2118/16052-PA
- Lavrov A. *Lost circulation: Mechanisms and solutions*. Cambridge, MA: Gulf Professional Publishing, Elsevier (2016). doi:10.1016/C2015-0-00926-1
- Al Menhali S, Abdul Halim AO, A, Al Menhali S. Curing losses while drilling & cementing. Proceedings of the Paper presented at the Abu Dhabi International Petroleum Exhibition and Conference, Abu Dhabi, UAE, 10–13 November. SPE-171910-MS. doi:10.2118/171910-MS
- Ivan C, Bruton J, Bloys B 2003. How can we best manage lost circulation? Proceedings of the Paper presented at the AACE Technical Conference and Exhibition, Houston, Texas, USA, 1–3 April 2003.
- Alsaba M, Nygaard R, Hareland G. Review of lost circulation materials and treatments with an updated classification. Proceedings of the Paper presented at the AACE Fluids Technical Conference and Exhibition, Houston, Texas, USA, April 15–16. AACE-14-FTCE-24.
- Lecolier E, Herzhaft B, Rousseau L, Neau L, Quillien B, Kieffer J. Development of a nanocomposite gel for lost circulation treatment. Proceedings of the Paper presented at the SPE European Formation Damage Conference, Shevingen, Netherlands, 25–27 May 2005, 2387. SPE-94686-MS. doi:10.2118/94686-MS
- Nayberg TM, Petty BR 1986. Laboratory study of lost circulation materials for use in oil-base drilling muds. Proceedings of the Paper presented at the SPE Deep Drilling and Production Symposium, Amarillo, Texas, USA, 6–8 April 1986. SPE-14995-MS. doi:10.2118/14995-MS
- Salehi S, Nygaard R 2012. Numerical modeling of induced fracture propagation: A novel approach for lost circulation materials (LCM) design in borehole strengthening applications of deep offshore drilling. Proceedings of the Paper presented at the SPE Annual Technical Conference and Exhibition, San Antonio, Texas, USA, 8–10 October 2012. SPE-135155-MS. doi:10.2118/135155-MS
- Feng Y, Gray KE. *Lost circulation and wellbore strengthening*. Cham, Switzerland: Springer (2018). doi:10.1007/978-3-319-89435-5
- Alberty M, McLean M. *A physical model for stress cages*. Houston, Texas, USA: Paper presented at the SPE Annual Technical Conference (2004). p. 26–9. SPE-90493-MS. doi:10.2523/90493-MS September.
- Dupriest FE. Fracture closure stress (FCS) and lost returns practices. Proceedings of the Paper presented at the SPE/IADC Drilling Conference, Amsterdam, Netherlands, 23–25 February 2005. doi:10.2523/92192-MS
- Aadnøy BS, Belayneh M. Elasto-plastic fracturing model for wellbore stability using non-penetrating fluids. *J Pet Sci Eng* (2004) 45(3–4):179–92. doi:10.1016/j.petrol.2004.07.006
- Van Oort E, Friedheim JE, Pierce T, Lee J. Avoiding losses in depleted and weak zones by constantly strengthening wellbores. *SPE Drilling & Completion* (2011) 26(04):519–30. doi:10.2118/125093-PA
- Morita N, Black AD, Guh G-F. Theory of lost circulation pressure. Proceedings of the Paper presented at the SPE Annual Technical Conference and Exhibition, New Orleans, Louisiana, USA, 23–26 September 1990. SPE-20409-MS. doi:10.2118/20409-MS
- Onyia EC. Experimental data analysis of lost-circulation problems during drilling with oil-based mud. *SPE Drilling & Completion* (1994) 9(1):25–31. SPE-22581-PA. doi:10.2118/22581-PA
- Salehi S. *PhD dissertation*. Rolla, Missouri: Missouri University of Science and Technology (2012). Numerical simulations of fracture propagation and sealing: Implications for wellbore strengthening.
- Cook J, Growcock F, Guo Q, Hodder M, Van Oort E. Stabilizing the wellbore to prevent lost circulation. *Oilfield Rev* (2011) 23(4):26–35. <https://www.slb.com/-/media/files/oilfield-review/1-sealing-english>.
- Howard GC, Scott PP. An analysis and the control of lost circulation. *J Pet Tech* (1951) 3(06):171–82. SPE-951171-G. doi:10.2118/951171-g
- White RJ. Lost-circulation materials and their evaluation. *API Drilling Prod Pract* (1956) 56–52.
- Amer A, Hale A, Al Haidari S. Addressing the challenges of lost circulation using novel chemistries, test equipment and data science tools. Proceedings of the Paper presented at the AACE National Technical Conference and Exhibition, Denver, Colorado, USA, April 9–10 2019.
- Alhaidari SA, Alarifi SA. Experimental investigation of particle size degradation and plugging efficiency of three granular lost circulation materials. *Appl Sci (Basel)* (2021) 2021:119061. doi:10.3390/app11199061
- Alhaidari SA, Eustes AW. *PhD dissertation*. Golden, Colorado: Colorado School of Mines (2020). Lost circulation management: New engineering approaches and techniques for better bridging and sealing the fracture.
- Valsecchi P. On the shear degradation of lost circulation materials. Proceedings of the Paper presented at the SPE/IADC Drilling Conference and Exhibition, Amsterdam, Netherlands, March 8–22 2013, 5–7. doi:10.2118/163512-MS
- Gaurina-Medjimurec N, Pasic B. Lost circulation. In: *Risk analysis for prevention of hazardous situations in Petroleum and natural gas engineering*. PA: IGI Global (2014). p. 73–95. doi:10.4018/978-1-4666-4777-0.ch004
- Scott PD, Beardmore DH, Wade ZL, Evans E, Franks KD 2012. Size degradation of granular lost circulation materials. Proceedings of the Paper presented at the IADC/SPE Drilling Conference and Exhibition, San Diego, California, USA, 6–8 March 2012. doi:10.2118/151227-MS
- Murtaza M, Alarifi SA, Abozuhairah A, Mahmoud M, Onaizi SA, Al-Ajmi M. Optimum selection of H<sub>2</sub>S scavenger in light-weight and heavy-weight water-based drilling fluids. *ACS Omega* (2021) 6(38):24919–30. doi:10.1021/acsomega.1c03792
- Murtaza M, Alarifi SA, Kamal MS, Onaizi SA, Al-Ajmi M, Mahmoud M. Experimental investigation of the rheological behavior of an oil-based drilling fluid with rheology modifier and oil wetter additives. *Molecules* (2021) 26(16):4877. doi:10.3390/molecules26164877
- Caulfield DF. Interactions at the cellulose-water interface. *Paper Sci Technol Cutting Edge*. Appleton, WI: Inst Paper Chem (1980) 70–88.
- API. Recommended practice for field testing oil-based drilling fluids. In: *Standard API 13B-2*. Washington, DC, USA: American Petroleum Institute (2014).



## OPEN ACCESS

## EDITED BY

Chengyuan Xu,  
Southwest Petroleum University, China

## REVIEWED BY

Yuanqing Wu,  
Shenzhen University, China  
Chen Wang,  
University of Illinois at Urbana-  
Champaign, United States  
Daobing Wang,  
Beijing Institute of Petrochemical  
Technology, China  
Nanlin Zhang,  
Zhejiang University, China

## \*CORRESPONDENCE

Yang Wang,  
✉ wangyang0996@petrochina.com.cn

## SPECIALTY SECTION

This article was submitted to  
Interdisciplinary Physics,  
a section of the journal  
Frontiers in Physics

RECEIVED 16 February 2023

ACCEPTED 20 March 2023

PUBLISHED 30 March 2023

## CITATION

Wang Y, Fan Y and Chen W (2023), Study  
and application of temporary plugging  
agent for temporary plugging acid  
fracturing in ultra-deep wells of Penglai  
gas field.  
*Front. Phys.* 11:1167307.  
doi: 10.3389/fphy.2023.1167307

## COPYRIGHT

© 2023 Wang, Fan and Chen. This is an  
open-access article distributed under the  
terms of the [Creative Commons  
Attribution License \(CC BY\)](#). The use,  
distribution or reproduction in other  
forums is permitted, provided the original  
author(s) and the copyright owner(s) are  
credited and that the original publication  
in this journal is cited, in accordance with  
accepted academic practice. No use,  
distribution or reproduction is permitted  
which does not comply with these terms.

# Study and application of temporary plugging agent for temporary plugging acid fracturing in ultra-deep wells of Penglai gas field

Yang Wang\*, Yu Fan and Weihua Chen

Engineering Technology Research Institute of Southwest Oil and Gas Field Company, Chengdu, China

The burial depth of Penglai gas field reservoir in the Sichuan Basin of China exceeds 7,000 m, and the reservoir temperature is 160°C. Penglai gas field belongs to the fractured reservoir, and there are many natural fractures distributed in the reservoir. Natural fractures are not only the storage place of natural gas, but also the transportation channel of natural gas. Gas wells mainly increase natural gas production through acid fracturing. In the early stage, Penglai Gas Field mainly used gelled acid fracturing technology to create an artificial fracture in the reservoir by injecting a large amount of acid fluid. However, the stimulation range of gelled acid fracturing is very small. After acid fracturing, gas wells can only produce 120,000 cubic meters of natural gas per day. To obtain higher natural gas production, this paper proposes a multi-stage temporary acid fracturing technology that can greatly improve the effect of acid fracturing. The temporary plugging agent for acid fracturing has been developed to meet the high-temperature requirements of the Penglai gas field. Based on the simulation of fracture propagation, the feasibility of acid fracturing expansion of natural fractures in the Penglai Gas Field is clarified. Fiber and granular temporary plugging agents that meet the plugging strength greater than 20 MPa are selected by using the dynamic temporary plugging instrument. MultiFracS software is used to optimize the multi-stage temporary acid fracturing process parameters. The research results in this paper have been applied to wells PS101, PS102, and PS103. After fracturing, compared with the gelling acid fracturing, the natural gas production has increased by more than three times, and the multi-stage temporary plugging acid fracturing has achieved a very good stimulation effect.

## KEYWORDS

temporary plugging, fiber, acid fracturing, Penglai gas field, multifracs

## 1 Introduction

Penglai gas field is a newly discovered large carbonate reservoir in the Sichuan Basin, which is located in the north of the gentle slope of the central Sichuan paleo uplift [1, 2]. Sinian Dengying formation is the main production layer of Penglai Gas Field, and several wells have obtained natural gas in Sinian Dengying formation. The burial depth of the Penglai gas field reservoir reaches 7,000 m, the formation pressure coefficient is 1.27, and the reservoir temperature is about 160°C [3, 4]. The core and imaging logging shows that there

are a lot of natural fractures in the formation, and the average porosity of the reservoir is 4.8%. Natural fractures not only play an important role in the storage of natural gas, but also are the main channels for the migration of natural gas in the formation. In the early period of Penglai gas field development, gelling acid fracturing was the main method to increase production, but it was difficult for gas wells to maintain high production because of the short action distance of acid fluid at high temperatures and the low conductivity of acid etched fracture [5].

Carbonate reservoirs are very rich in oil and gas resources, and acid fracturing of ultra-deep carbonate reservoirs has been a hot research topic. Yang Wang et al. [6] proposed a technical method to improve the acid etching fracture length and conductivity of low permeability carbonate reservoirs by alternating injection of authigenic acid and gelling acid. Yang Wang et al. [7] carried out the visual test experiment of alternating injection acid fracturing and studied the influence of parameters such as injection displacement, acid ratio, and injection stage on acid fingering morphology. Lufeng Zhang et al. [8] conducted a research on long-term acid conductivity behavior and proposed a new method to raise acid fracture conductivity under high closure stress. Daobing Wang et al. [9] presented a comprehensive workflow to model hydraulic fracture by accounting for interactions with numerous crosscutting natural fractures or joint sets, as well as the effect of temporary plugging in opened fractures. This investigation provides new insight into the formation mechanism of fracture networks in naturally fractured formations. Fangzheng Jiao [10] proposed the idea of “volumetric development” which is based on years of study on the geological features, flow mechanisms, high-precision depiction, and the recovery mode of fractured-vuggy bodies. Yang Wang et al. [11] proposed a temporary plugging segmented acid fracturing technique for horizontal wells. Schlumberger company first proposed the temporary fiber plugging technology, using degradable fiber to temporarily seal the fracture, forcing the acid fracturing fracture extension direction to change [12]. Zhou Fujian et al. [13] carried out the liquid filtration experiment of temporary plugging artificial fracture with fiber, and analyzed the characteristics of liquid filtration in the process of temporary plugging. Daobing Wang et al. [14] presented a systematic study of the fracture diversion mechanisms of the fiber-diverting fracturing technique. Lei Qun et al. [15] put forward a new concept of “Fracture network” fracturing technology for low porosity, low permeability, and no natural fracture reservoirs. Jianye Mou et al. [16] designed a multi-stage triaxial fracturing system and experimental procedures to satisfy the requirements of diverted fracturing in horizontal wells. Nanlin Zhang et al. [17] proposed self-supporting fracturing technology, established a transient temperature model considering reaction heat based on the first law of thermodynamics, and clarified the impact of phase change reaction heat on wellbore temperature. Nanlin Zhang et al. [18] used Permian cores from Sichuan Basin to evaluate fracture conductivity under different conditions, such as proppant size and concentration, acid concentration and activity, and the separate or combined application of acid and proppant. Daobing Wang et al. [19] used the extended finite element method to investigate refracture propagation paths at different initiation angles. Daobing Wang et al. [20] established a comprehensive fracture index model that comprehensively considers the thermal

effect and fracture toughness under different temperatures and confining pressures. Yuanqing Wu et al. [21] used the CF model and DBF framework to simulate matrix acidification in fractured porous media, and the simulation results of this work were compared with Khoei’s work, which proved the rationality of this work. On the basis of improving the DBF framework, Yuanqing Wu et al. [22] introduced the energy balance equation into the improved DBF framework and gave the thermal DBF framework. The above research mainly focuses on how to improve the fracture conductivity and the test evaluation of a temporary plugging agent, but there is a lack of relevant research on the evaluation of temporary plugging agents for acid fracturing of ultra-deep and ultra-high temperature gas reservoirs like Penglai Gas Field and the temporary plugging acid fracturing technology based on fracture expansion.

Since there are many natural fractures in the reservoir of the Penglai gas field, this paper proposes a multi-stage temporary plugging acid fracturing technique and develops a temporary plugging agent to meet the high-temperature requirements of the Penglai gas field. The results of this study have been applied to three wells in the Penglai gas field and have achieved good results, further proving the success of multi-stage temporary plugging acid fracturing.

## 2 Introduction of gas reservoir

Penglai Gas Field is located in Sichuan Basin, China. The reservoir is buried at a depth of 7,000 m, with an average of 4.8% and an average permeability of 0.28mD. The lithology is mainly dolomite, with a small number of corrosion holes on the core. Both the core and the electric imaging logging show that there are a large number of natural fractures in the reservoir.

According to the measured data, the temperature in the middle part of the formation is 160°C, and the pressure coefficient is about 1.27, belonging to normal temperature and high-pressure gas reservoir.

The Young’s modulus of the Penglai gas field is  $4.7 \times 10^4$ MPa, and Poisson’s ratio is 0.0204. Young’s modulus of the Penglai gas field is lower than that of other gas fields in the Sichuan Basin. The acid corrosion rate of the core in the Penglai gas field is 95.76%. The high acid corrosion rate indicates that the Penglai gas field is suitable for acid fracturing stimulation.

## 3 Multi-stage temporary plugging acid fracturing

### 3.1 Solubility of temporary plugging agent

The reservoir temperature of Penglai Gas Field can reach 160°C, and the dissolution rate of the temporary plugging agent increases rapidly under high temperatures [23]. The technical principle of multi-stage temporary plugging acid fracturing is to add a temporary plugging agent in the acid fracturing, so as to achieve the purpose of fracture turning and expanding. Therefore, the temporary plugging agent with a slow dissolution rate under high temperatures should be selected first to carry out the experiment [24].

TABLE 1 Experiment on the solubility of the temporary plugging agents.

Experimental sample	Dissolution rate of test sample in 20%
	Hydrochloric acid at 160 °C (%)
Polyemulsion-modified polyvinyl alcohol resin	5.82
Urea methyl ester	93.12
Modified polyethylene glycol	96.19



Fiber



100 mesh



40/70 mesh

FIGURE 1  
Polyemulsion-modified polyvinyl alcohol resin of different shapes.

This paper evaluates the high-temperature solubility of three temporary plugging agents. These three temporary plugging agents are Polyemulsion-modified polyvinyl alcohol resin, Urea methyl ester, and Modified polyethylene glycol. We put the three temporary plugging agents in 20% hydrochloric acid at 160°C, and observed the dissolution of the temporary plugging agents after 1 h. The purpose of this experiment is to test the solubility of temporary plugging agent during acid fracturing. In order to ensure the plugging effect, the temporary plugging agent should be as insoluble as possible or have a low dissolution rate during acid fracturing. In this experiment, the temporary plugging agent is first weighed (M1), and then the temporary plugging agent soaked in acid solution is weighed again (M2) to determine the dissolved mass of the temporary plugging agent in acid solution (M1-M2). Define the solubility of temporary plugging agent as (M1-M2)/M2. The equipment used in this experiment mainly includes beaker, heater and electronic balance.

It can be seen from Table 1 that the dissolution rate of Polyemulsion-modified polyvinyl alcohol resin in high-temperature acid solution is the lowest, and the dissolution rate of the temporary plugging agent for the other two materials is more than 90%. Polyemulsion-modified polyvinyl alcohol resin is selected as the temporary plugging agent for acid fracturing in Penglai Gas Field. The low dissolution rate indicates that the temporary plugging agent will maintain good performance during acid fracturing.

Polyemulsion-modified polyvinyl alcohol resin can be processed into various shapes according to technical requirements, as shown in Figure 1. Polyemulsion-modified polyvinyl alcohol can be processed into fiber, 100 mesh particles, and 40/70 mesh temporary plugging agent.

### 3.2 Plugging performance test of temporary plugging agent

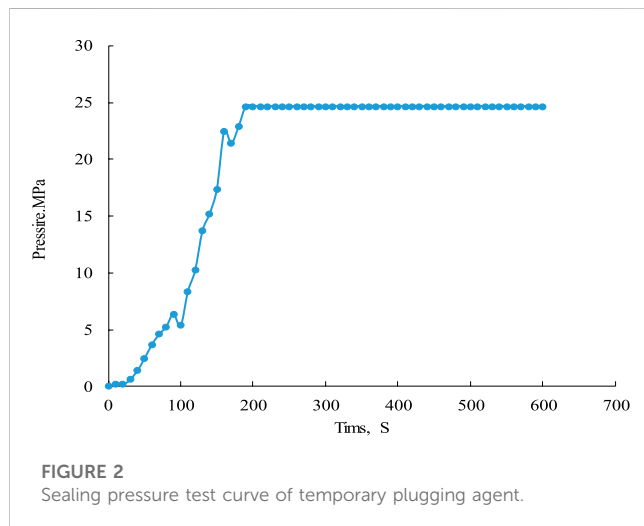
The key technology of multi-stage temporary plugging acid fracturing is to add a temporary plugging agent in natural fracture, so as to increase the net pressure in natural fracture and force the fracture to turn and extend [25]. The width of natural fracture in the Penglai gas field is about 2 mm according to the logging data of electrical imaging. Temporary plugging agents with different concentrations and combinations are selected for the plugging test, so as to select the temporary plugging agent combined with the strongest plugging ability.

The dynamic plugging evaluation instrument is used to carry out this test, and the test fracture width is set as 2 mm according to the natural fracture width of Penglai Gas Field. The dynamic plugging instrument is mainly composed of displacement pump, injection system and simulated fracture. The equipment is mainly used to evaluate the plugging performance of temporary plugging agent under high temperature and high pressure environment. This



**TABLE 2** Test results of plugging pressure with different temporary plugging agents.

Temporary plugging agent	Plugging pressure (MPa)
0.5% 40/70 mesh+1.5% 100 mesh	11.59
1.0% 40/70 mesh+1.0% 100 mesh	15.22
1.5% 40/70 mesh+0.5% 100 mesh	14.61
0.5%fiber+0.5% 40/70 mesh+1.0% 100 mesh	24.67



experiment first injects the temporary plugging agent into the simulated fracture, and records the plugging pressure data in real time through the electronic pressure gauge. The plugging ability is judged by the plugging pressure. The higher the plugging pressure is, the better the plugging performance of the temporary plugging agent for the fracture is. The temporary plugging agent with different

concentrations and combinations was used to test its plugging pressure.

It can be seen from Table 2 and Figure 2 that if only a granular temporary plugging agent is used, the plugging pressure will rise rapidly with the increase of 40/70 mesh granular temporary plugging agent concentration. At the same concentration, when the fiber is added into the granular temporary plugging agent, the plugging pressure increases significantly, and the plugging pressure of 0.5% fiber + 0.5% 40/70 mesh plugging agent + 1.0% 100 mesh plugging agent can reach 24.67 MPa.

It can be seen from Figure 3 that the fiber and granular temporary plugging agent are intertwined in the fracture, the filling layer formed by the temporary plugging agent is quite dense, and the granular temporary plugging agent is wrapped together by fibers. When the temporary plugging agent forms the plugging layer in the fracture, the first is that the fibers are intertwined and sealed in the fracture, and then the fibers catch the temporary plugging particles like fishing nets, and the temporary plugging particles further strengthen the plugging layer formed by the fibers.

### 3.3 Simulation of acid fracturing fracture propagation in fractured reservoirs

According to the thickness, porosity, permeability, water saturation and other reservoir geological parameters of Penglai Gas Field, the acid fracturing productivity prediction model of Penglai Gas Field is established using Petrel software. According to Petrel software simulation, natural fractures make a huge contribution to production, especially when acid fracturing communicates with a large number of natural fractures, the gas production can be increased by 340% compared with natural fractures without communication. Therefore, the design of acid fracturing scheme should ensure that as many natural fractures as possible will be opened.



**FIGURE 3**  
The placement form of temporary plugging agent in fracture.

TABLE 3 Input parameters of the model.

Porosity	4.8%
Permeability	0.28mD
Young's modulus	$4.7 \times 10^4$ MPa
Poisson's ratio	0.0204
Rock density	2746 kg/m <sup>3</sup>
Cohesion	72.56 MPa
Internal friction angle	36°
Acid viscosity	30 mPa s
Acid density	1100 kg/m <sup>3</sup>
Horizontal maximum principal stress	175.65 MPa
Horizontal minimum principal stress	162.42 MPa

The finite element software is used to simulate the expansion form of acid corrosion fractures in the Penglai Gas Field. Penglai Gas Field is a fractured gas reservoir, and there are many natural fractures in the reservoir. The dip angle of most natural fractures is NE 66°. The maximum horizontal principal stress direction of the Penglai Gas Field reservoir is NE 38°, and the approach angle between acid-etched fractures and natural fractures is 29°.

The finite element method is used to establish a square model with a length and width of 200 m. There is a natural fracture inside the model. The included angle between the natural fracture and the horizontal maximum principal stress is 29°, and the minimum element size is 0.5 m. The horizontal minimum principal stress and horizontal maximum principal stress are applied respectively in the X and Y directions of the model. The model parameters are set according to the reservoir parameters of

Penglai Gas Field, and the calculation parameters used are shown in Table 3.

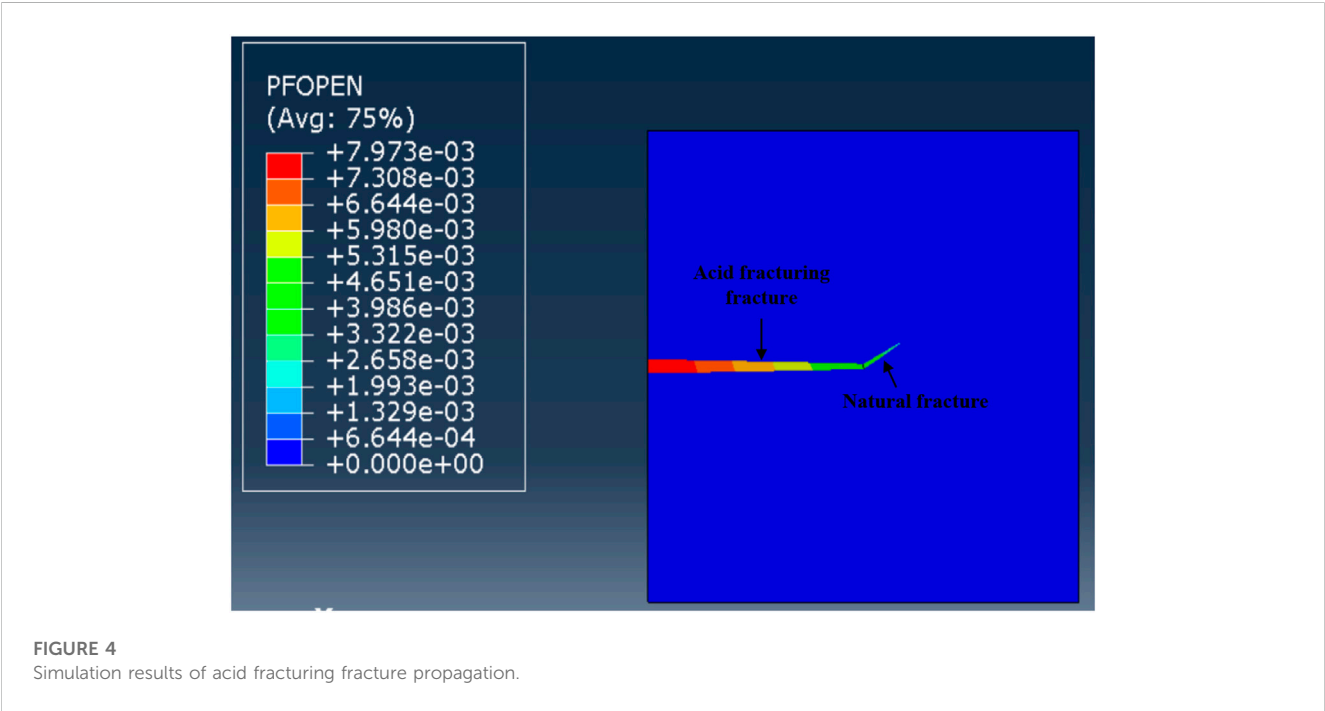
It can be seen from Figure 4 that the acid fracturing fracture of the Penglai Gas Field extends along the direction of the horizontal maximum principal stress before encountering the natural fracture. When the acid fracturing fracture meets the natural fracture, the natural fracture will break, then the acid fracturing fracture deviates from the original expansion direction, and the acid fracturing fracture will deflect along the natural fracture direction at the joint of the fractures, and extends to the end of the natural fracture. The simulation results of acid fracturing fracture propagation show that the natural fractures in the Penglai Gas Field will open during acid fracturing, and the stimulation range of acid fracturing will be significantly improved.

### 3.4 Optimization of multi-stage temporary plugging acid fracturing parameters

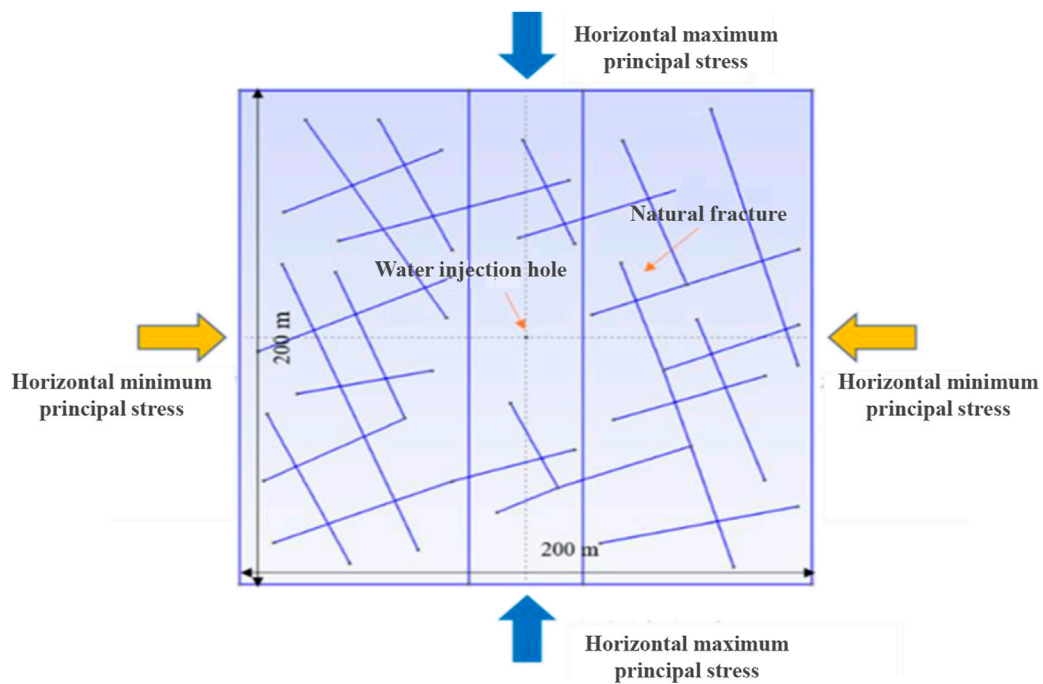
Multi-physical field fracture analysis software MultiFracS is used to optimize the parameters of multi-stage temporary plugging acid fracturing [26, 27]. MultiFracS software is a multi-physical field fracture analysis software based on the finite discrete element coupling method, which can consider the interaction of many factors such as heat, fluid, fracture, and fracture [28].

A rock model with a size of 200 × 200 m is established by using MultiFracS software (Figures 5). In the model, many connected natural fractures are randomly distributed, and the inclination angles of natural fractures are between 30° and 60°. A water injection hole is arranged in the middle of the model, and the whole model is divided into 16,851 triangular units.

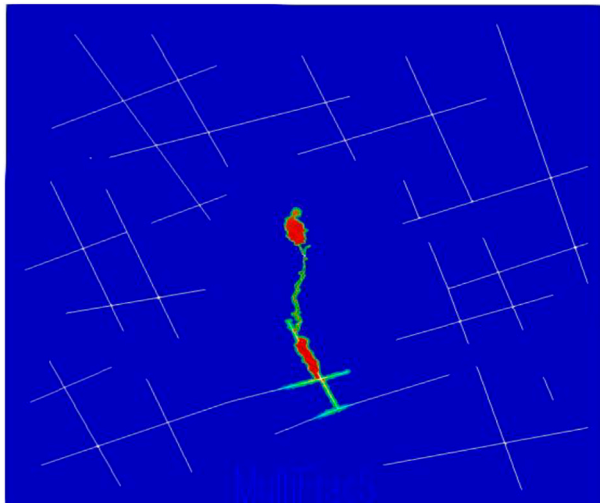
The key to multistage temporary plugging acid fracturing design is the temporary plugging time. The temporary plugging time is when the temporary plugging agent is added to obtain the maximum



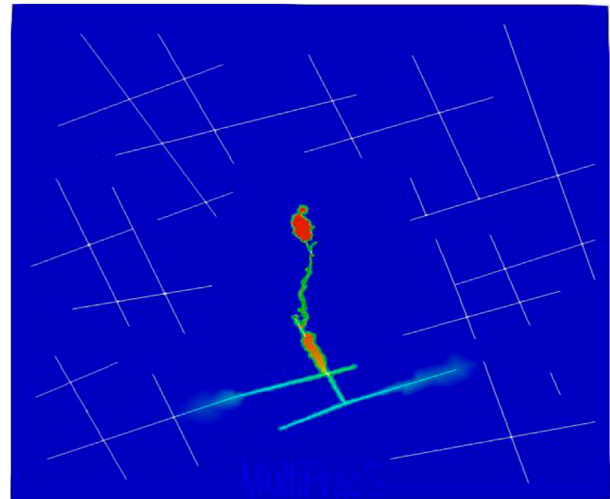




**FIGURE 5**  
Multi-stage temporary plugging acid fracturing model for fractured reservoir.



**FIGURE 6**  
Simulation of acid fracturing stimulation range when temporary plugging agent is added immediately after acid fracturing fracture pass through the natural fracture.

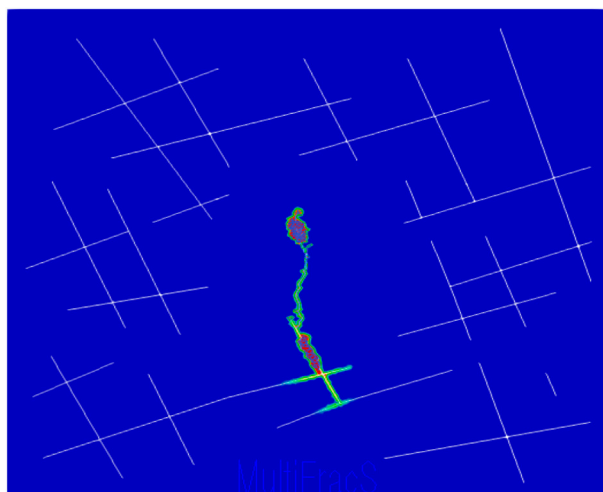


**FIGURE 7**  
Simulation of stimulation acid fracturing range by adding temporary plugging agent after injecting 100 m<sup>3</sup> acid.

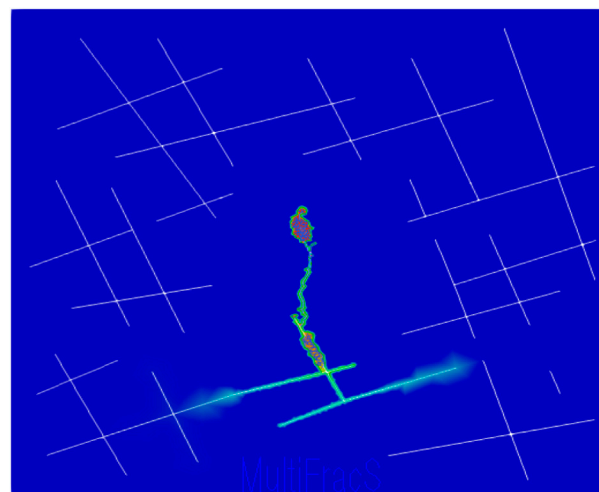
stimulation range. MultiFracS software is used to simulate the stimulation range of acid fracturing at different temporary plugging times. It can be seen from Figures 6, 7 that compared with adding a temporary plugging agent immediately after acid fracturing fracture pass through the natural fracture, adding a temporary plugging agent after continuing to inject 100 m<sup>3</sup> of

acid has significantly improved the range of acid fracturing stimulation, and the propagation length of natural fractures is significantly increased.

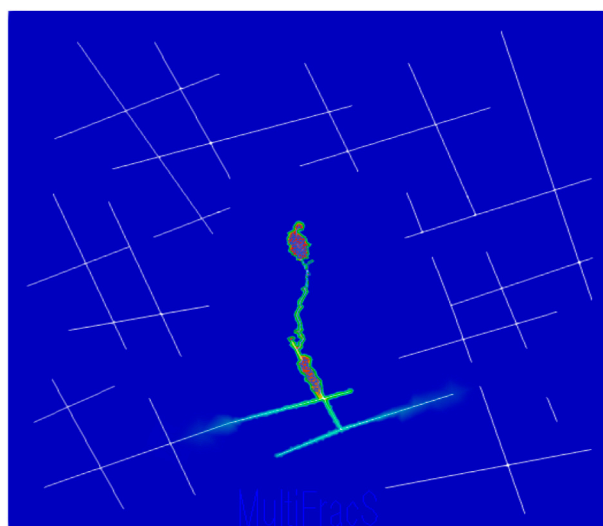
We simulated the acid fracturing stimulation range with different injection displacements after adding a temporary plugging agent. It can be seen from Figure 8, Figure 9, and Figure 10 that with the increase of

**FIGURE 8**

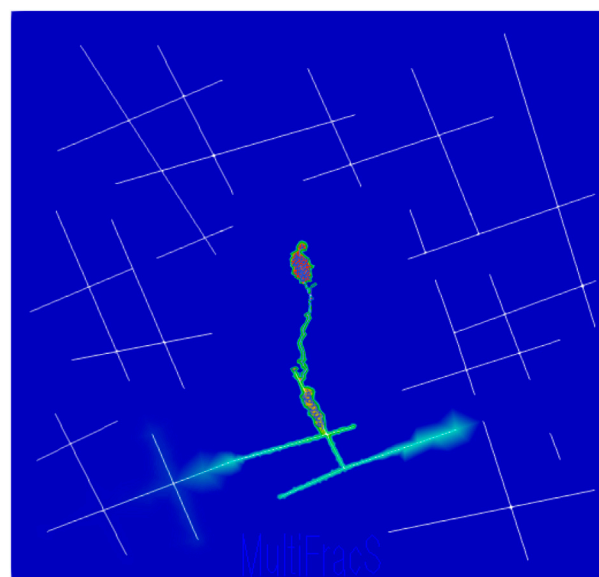
Acid fracturing stimulation range with injection displacement of 4 m<sup>3</sup>/min.

**FIGURE 10**

Acid fracturing stimulation range with injection displacement of 8 m<sup>3</sup>/min.

**FIGURE 9**

Acid fracturing stimulation range with injection displacement of 6 m<sup>3</sup>/min.

**FIGURE 11**

Acid fracturing stimulation range with temporary plugging pressure 15 MPa.

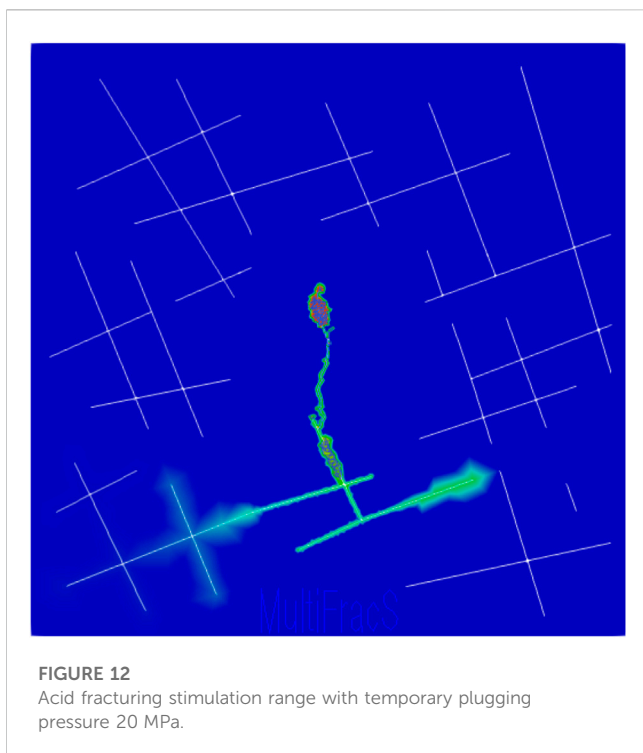
injection displacement, the expansion range of natural fracture becomes larger, and the acid fracturing stimulation range is significantly improved. Especially when the injection displacement is increased to 8 m<sup>3</sup>/min, the acid fracturing stimulation range is more than 60% of the injection displacement of 4 m<sup>3</sup>/min. In order to improve the acid fracturing stimulation range, it is suggested that the acid fracturing displacement of the Penglai gas field should reach 8 m<sup>3</sup>/min.

We simulated the acid fracturing stimulation range with different temporary blocking pressure. As can be seen from Figure 11 and Figure 12, with the increase of the temporary plugging pressure, the fracture expansion range becomes larger, especially the natural fracture is broken and activated. When the temporary plugging pressure is

increased to 20 MPa, the stimulation range of acid fracturing is 81% larger than that of 15 MPa. It is suggested that the temporary plugging pressure of acid fracturing in the Penglai gas field should reach 20 MPa, “0.5% fiber + 0.5% 40/70 mesh + 1.0% 100 mesh” is recommended as the temporary plugging agent for acid fracturing in the Penglai gas field.

## 4 Field application

PS101 is an evaluation well in the Penglai gas field, with a depth of 7,110 m, a reservoir temperature of 160.2°C, and a



reservoir porosity of 4.83%. PS101 uses multi-stage temporary plugging acid fracturing technology to increase production. The technical principle of multistage temporary plugging acid fracturing is to first inject fracturing fluid to form a fracture in the formation, then inject acid fluid to, etch the fracture wall, and then inject temporary plugging agent into the fracture to seal the hydraulic fracture tip, forcing the subsequently injected fluid into the natural fracture, thus expanding the stimulation range. PS101 is injected with 320 cubic meters of gelling acid, 100 kg of fiber, 200 kg of 100 mesh granular temporary plugging agent, and 100 kg of 40/70 mesh granular temporary plugging agent. The maximum pressure of acid fracturing in PS101 reaches 111 MPa, the maximum acid injection rate is 5.8 m<sup>3</sup>/min, and the bottom hole pressure rises by 9 MPa after injection of temporary plugging agent. The G function shows that acid fracturing fractures passes through the natural fractures, and a large number of natural fractures break and are activated, which indicates that multi-stage temporary plugging acid fracturing successfully improves the stimulation range.

PS101, PS102, and PS103 used the multi-stage temporary plugging acid fracturing. After acid fracturing, the average daily gas production of these three wells is 410,000 cubic meters. Compared with the gas wells using gelling acid fracturing technology in the early stage, the average gas production of gas wells using gelling acid fracturing is only 120,000 cubic meters, and the average daily gas production of the gas wells using multi-stage temporary plugging acid fracturing technology has increased by more than three times. The multi-stage temporary plugging acid fracturing technology has achieved success in the Penglai Gas Field.

## 5 Conclusion

- (1) There are a lot of natural fractures in the Penglai gas field reservoir. Fracture propagation simulation shows that acid fracturing fractures can pass through the natural fractures, and natural fractures will be damaged and activated.
- (2) "0.5% fiber + 0.5% 40/70 mesh + 1.0% 100 mesh" is recommended as the temporary plugging agent for acid fracturing in the Penglai gas field, and the temporary plugging pressure of this temporary plugging agent combination can reach 20 MPa.
- (3) The successful practice of PS101, PS102, and PS103 shows that multi-stage temporary plugging acid fracturing can greatly improve the production effect of the super-deep reservoirs such as the Penglai gas field.
- (4) It is suggested to implement microseismic or wide-area electromagnetic method to monitor fracture morphology during acid fracturing, so as to better guide the optimization of multi-stage temporary plugging acid fracturing parameters.

## Data availability statement

The original contributions presented in the study are included in the article/Supplementary Material, further inquiries can be directed to the corresponding author.

## Author contributions

YW: Conceptualization, funding acquisition, project administration, re-sources, writing—original draft and software. YF: Data curation, formal analysis, methodology. WC: Data curation. All authors have read and agreed to the published version of the manuscript.

## Funding

This work was financially supported by the project of the PetroChina Southwest Oil and Gas Field Company (Grant Nos. 20200302-14, 20210302-19).

## Conflict of interest

Authors YW, YF, and WC were employed by Engineering Technology Research Institute of Southwest Oil and Gas Field Company.

## Publisher's note

All claims expressed in this article are solely those of the authors and do not necessarily represent those of their affiliated organizations, or those of the publisher, the editors and the reviewers. Any product that may be evaluated in this article, or claim that may be made by its manufacturer, is not guaranteed or endorsed by the publisher.

## References

1. Yu Y, Long W, Zezhang S, Benjian Z, Wei Y, Gang Z, et al. Breakthrough and potential of natural gas exploration in multi-layer system of Penglai gas area in the north of central Sichuan paleo-uplift[J]. *Acta Petrolei Sinica* (2022) 43(10):1351.
2. Zengye X, Jian L, Chunlong Y, Xingwang T, Lu Z, Jin L, et al. Geochemical characteristics of Sinian-Cambrian natural gas in central Sichuan paleo-uplift and exploration potential of Taihe gas area[J]. *Nat Gas Industry* (2021) 41(7):1–14.
3. Yu Y, Long WEN, Jirong XIE, Bing L, Pinghui H, Qi R, et al. Progress and direction of marine carbonate gas exploration in the Sichuan Basin[J]. *China Pet Exploration* (2020) 25(3):44.
4. Luzi Z, Zecheng W, Yu Y, et al. Important discovery in the second member of Dengying formation in Well Pengtan1 and its significance, Sichuan Basin[J]. *China Pet Exploration* (2020) 25(3):1–12.
5. Wang Y, Zhou C, Yi X, Li L, Zhou J, Han X, et al. Research and Evaluation of a New Autogenic Acid System Suitable for Acid Fracturing of a High-Temperature Reservoir. *ACS omega* (2020) 5(33):20734–8. doi:10.1021/acsomega.0c00336
6. Wang Y, Fan Y, Wang T, Ye J, Luo Z. A New Compound Staged Gelling Acid Fracturing Method for Ultra-Deep Horizontal Wells. *J Gels* (2022) 8(7):449. doi:10.3390/gels8070449
7. Wang Y, Yang J, Wang T, Hu Q, Lv Z, He T. Visualization experiment of multi-stage alternating injection acid fracturing. *Energy Rep* (2022) 8:9094–103. doi:10.1016/j.egyr.2022.07.031
8. Zhang L, Zhou F, Mou J, Xu G, Zhang S, Li Z. A new method to improve long-term fracture conductivity in acid fracturing under high closure stress. *J Pet Sci Eng* (2018) 171:760–70. doi:10.1016/j.petrol.2018.07.073
9. Wang D, Dong Y, Sun D, Yu B. A three-dimensional numerical study of hydraulic fracturing with degradable diverting materials via CZM-based FEM. *Eng Fracture Mech* (2020) 237:107251. doi:10.1016/j.engfracmech.2020.107251
10. Fangzheng J. Practice and knowledge of volumetric development of deep fractured-vuggy carbonate reservoirs in Tarim Basin, NW China[J]. *Pet exploration Dev* (2019) 46(3):576–82.
11. Wang Y, Zhou C, Yi X, Li L, Chen W, Han X. Technology and Application of Segmented Temporary Plugging Acid Fracturing in Highly Deviated Wells in Ultradeep Carbonate Reservoirs in Southwest China. *ACS omega* (2020) 5(39):25009–15. doi:10.1021/acsomega.0c01008
12. Solares JR, Al-Harbi M, Al-Sagr AM, Amorochio R, Ramanathan V Successful application of innovative fiber-diverting technology achieved effective diversion in acid stimulation treatments in Saudi Arabian deep gas producers. In: SPE Asia Pacific Oil and Gas Conference and Exhibition; Perth, Australia (2008). p. 20–2.
13. Zhou F, Yi X, Yang X, Liu X, Wang D Dynamic filtration experiment of fiber temporary plugging artificial fracture[J]. *Drill Prod Technol* (2014) 37(4).
14. Wang D, Zhou F, Ge H, Shi Y, Yi X, Xiong C, et al. An experimental study on the mechanism of degradable fiber-assisted diverting fracturing and its influencing factors. *J Nat Gas Sci Eng* (2015) 27:260–73. doi:10.1016/j.jngse.2015.08.062
15. Lei Q, Xu Y, Jiang T, Ding Y, Lu H, et al. “Fracture network” fracturing technique for improving post-fracturing performance of low and ultra-low permeability reservoirs [J]. *Acta Petrolei Sinica* (2009) 30(2):237.
16. Zhang L, Zhou F, Mou J, Pournik M, Tao S, Wang D, et al. Large-scale true tri-axial fracturing experimental investigation on diversion behavior of fiber using 3D printing model of rock formation. *J Pet Sci Eng* (2019) 181:106171. doi:10.1016/j.petrol.2019.06.035
17. Zhang N, Chen Z, Luo Z, Liu P, Chen W, Liu F. Effect of the phase-transition fluid reaction heat on wellbore temperature in self-propping phase-transition fracturing technology. *Energy* (2023) 265:126136. doi:10.1016/j.energy.2022.126136
18. Zhang N, Luo Z, Chen X, Zhao L, Zeng X, Zhao M. Investigation of the artificial fracture conductivity of volcanic rocks from Permian igneous in the Sichuan Basin, China, with different stimulation method using an experiment approach. *J Nat Gas Sci Eng* (2021) 95:104234. doi:10.1016/j.jngse.2021.104234
19. Wang DB, Zhou FJ, Li YP, Yu B, Martyushev D, Liu XF, et al. Numerical simulation of fracture propagation in Russia carbonate reservoirs during refracturing. *Pet Sci* (2022) 19(6):2781–95. doi:10.1016/j.petsci.2022.05.013
20. Wang D, Zhou F, Dong Y, Sun D, Yu B. Experimental Investigation of Thermal Effect on Fractability Index of Geothermal Reservoirs. *Nat Resour Res* (2021) 30:273–88. doi:10.1007/s11053-020-09733-0
21. Wu Y, Kou J, Sun S. Matrix acidization in fractured porous media with the continuum fracture model and thermal Darcy-Brinkman-Forchheimer framework. *J Pet Sci Eng* (2022) 211:110210. doi:10.1016/j.petrol.2022.110210
22. Wu Y, Kou J, Sun S, Wu YS. Thermodynamically consistent Darcy-Brinkman-Forchheimer framework in matrix acidization. *Oil Gas Sci Technology—Revue d'IFP Energies nouvelles* (2021) 76:8. doi:10.2516/ogst/2020091
23. Wang Y, Fan Y, Zhou C, Luo Z, Chen W, He T, et al. Research and Application of Segmented Acid Fracturing by Temporary Plugging in Ultradeep Carbonate Reservoirs. *ACS omega* (2021) 6(43):28620–9. doi:10.1021/acsomega.1c03021
24. Yuan L, Zhou F, Li B, Gao J, Yang X, Cheng J, et al. Experimental study on the effect of fracture surface morphology on plugging efficiency during temporary plugging and diverting fracturing. *J Nat Gas Sci Eng* (2020) 81:103459. doi:10.1016/j.jngse.2020.103459
25. Barraza J, Capderou C, Jones MC, Lannen CT, Singh AK, Shahri MP, et al. Increased cluster efficiency and fracture network complexity using degradable di-verter particulates to increase production: Permian Basin Wolfcamp shale case study[C]. In: SPE Annual Technical Conference and Exhibition; OnePetro (2017).
26. Yan C, Zheng H, Sun G, Ge X. Combined Finite-Discrete Element Method for Simulation of Hydraulic Fracturing. *Rock Mech rock Eng* (2016) 49(4):1389–410. doi:10.1007/s00603-015-0816-9
27. Yan C, Zheng H. FDEM-flow3D: A 3D hydro-mechanical coupled model considering the pore seepage of rock matrix for simulating three-dimensional hydraulic fracturing. *Comput Geotechnics* (2017) 81:212–28. doi:10.1016/j.compgeo.2016.08.014
28. Yan C, Fan H, Huang D, Wang G. A 2D mixed fracture–pore seepage model and hydromechanical coupling for fractured porous media. *Acta Geotechnica* (2021) 16(10):3061–86. doi:10.1007/s11440-021-01183-z



## OPEN ACCESS

## EDITED BY

Chengyuan Xu,  
Southwest Petroleum University, China

## REVIEWED BY

Jinze Xu,  
University of Calgary, Canada  
Nanlin Zhang,  
Zhejiang University, China  
Jiajia Bai,  
Changzhou University, China

## \*CORRESPONDENCE

Zhengrong Chen,  
✉ chenzhr8@cnnooc.com.cn  
Xiangwei Kong,  
✉ kongxw\_yangtze@163.com

RECEIVED 26 February 2023

ACCEPTED 05 May 2023

PUBLISHED 12 May 2023

## CITATION

Wu G, Chen Z, Zhang A, Zhou J, Hou Y,  
Xie X, Wu J, Kong X and Li S (2023),  
Experimental studies on the performance  
evaluation of water-soluble polymers  
used as temporary plugging agents.  
*Front. Phys.* 11:1174268.  
doi: 10.3389/fphy.2023.1174268

## COPYRIGHT

© 2023 Wu, Chen, Zhang, Zhou, Hou, Xie,  
Wu, Kong and Li. This is an open-access  
article distributed under the terms of the  
[Creative Commons Attribution License](https://creativecommons.org/licenses/by/4.0/)  
(CC BY). The use, distribution or  
reproduction in other forums is  
permitted, provided the original author(s)  
and the copyright owner(s) are credited  
and that the original publication in this  
journal is cited, in accordance with  
accepted academic practice. No use,  
distribution or reproduction is permitted  
which does not comply with these terms.

# Experimental studies on the performance evaluation of water-soluble polymers used as temporary plugging agents

Guangai Wu<sup>1</sup>, Zhengrong Chen<sup>1\*</sup>, Anshun Zhang<sup>1</sup>, Jun Zhou<sup>1</sup>,  
Yanan Hou<sup>1</sup>, Xin Xie<sup>1</sup>, Jianshu Wu<sup>1</sup>, Xiangwei Kong<sup>2,3\*</sup> and Song Li<sup>2</sup>

<sup>1</sup>CNOOC Research Institute Co, Ltd., Beijing, China, <sup>2</sup>School of Petroleum Engineering, Yangtze University, Wuhan, China, <sup>3</sup>Hubei Key Laboratory of Oil and Gas Drilling and Production Engineering (Yangtze University), Wuhan, China

The performance of the temporary plug is a key factor in determining the success of loss-circulation control and temporary plug diversion fracturing. Due to the complexity of geomechanics and working conditions, current commonly used temporary plug agents face problems such as low plug strength and efficiency, large filtration losses due to failure to form filter cakes, and slow degradation affecting the recovery of fracture conductivity. A novel idea for the development of a novel water-soluble polymer plug for fracking is proposed, namely, low-to middle-molecule weight + reinforced chain rigidity + supramolecular aggregation. Using sodium bisulfite and potassium sulfate as initiators, AA, AM, and AMPS as grafting monomers, and SM as hydrophobic functional monomers, the AM-AA-AMPS-SM copolymer was prepared by polymerization. The developed new temporary plugging agent was completely degraded at 70°C for 5–8 h by carrying out experimental evaluation tests, such as water absorption expansion rate, swelling kinetics, density, post-dissolution viscosity, strength of the temporary plugging agent and post-degradation conductivity. After degradation, the viscosity of the solution is 2.5–3.6 mPa s with good fluidity and no gel remnants. The density of the temporary plug material is about 1.14 g/cm<sup>3</sup>. The absorption expansion rate was 25.8 g/g. The pressure is 60.1 MPa when the thickness of the granular temporary plug is 0.4 cm. Under experimental conditions, the fracture conductivity was found to be 69–123 D\*cm at a closing pressure of 30 MPa after degradation of the temporary plug. The test results demonstrate that the new temporary plug agent, with its high plug strength, temperature-controlled degradation, reflux stability and effective self-support after degradation, can meet the requirements of drilling plug and temporary plug fracturing technologies.

## KEYWORDS

water soluble, temporary plugging agent, plugging, diversion fracturing, polymer, degradable

## 1 Introduction

In the drilling fluid plugging and temporary plug diversion fracturing techniques, the performance of the temporary plug is a critical factor in determining the success of plugging and temporary plug diversion fracturing. Presently, commonly used temporary capping agents in temporary capping and fracturing techniques include: solid-sphere temporary



capping agents, which are characterized by high strength and small deformation, but suffer from easy detachment, low capping efficiency, and inability to degrade on their own. The disadvantages of suspended temporary plug agents are difficulty in forming large plug strengths due to turbulence and borehole deformation, low plug efficiency, inability to form filter cakes, and high filter loss. The disadvantage of underground cross-linked temporary plugs is that small doses don't achieve the required plug pressure, while large doses cause new damage to the reservoir. Although it can form filter cakes, the underground reaction is unstable and does not reach the required strength. The conventional surface cross-linked particle temporary plugging agent has the characteristics of easy injection and high plugging strength [1–6].

At present, it is mostly used in the process of temporary plugging and fracturing of oil wells, which is water-soluble polymer (gel forming agent) + inorganic or organic compounds (crosslinking agent) composed of gel type plugging agent [7–9]. After fracturing, the granular diverter slowly degrades under the action of water or oil, restoring the fracture conductivity. However, in low and ultra-low permeability natural gas wells, and especially in non-water producing natural gas wells undergoing diversion fracturing, this plug has the problem of difficult degradation, affecting the effect of diversion fracturing and even leading to invalid fracturing. In addition, another problem with the above-mentioned temporary plug is that the temporary plug portion of the fracture can easily close after the degradation of the temporary plug, resulting in a reduction in fracture conductivity and a reduction in oil and gas well production.

Tian M. et al. [10] studied a new heat and salt resistant water plugging and profile control agent. Based on AM (alkaline monomer), copolymer of 2-EHA (salt tolerant monomer) and VTEOS (temperature tolerant monomer) was introduced, which greatly improved the temperature and salt resistance. Wang C. et al. [11] developed a new heat-resistant plugging agent HTG using unsaturated amide monomer as the main agent, graft copolymerization and non-ionic fillers. The results show that HTG has strong salt and heat resistance, and maintains good gelling strength after being placed at 200°C for 72 h. HTG has a high plugging pressure. Xu et al. [12] established a flow regime-based gas apparent permeability model in high-pressure tight sandstone reservoirs, depending on bridging molecular kinetics, gas transport mechanisms, and apparent permeability. Their model was well validated against simulation and experimental data. Li et al. [13] rewritten the mass balance for determining the adsorbed amount, and two particular concepts, an “apparent excess adsorption” and an “actual excess adsorption,” were considered.

Zhang C. et al. [14] studied a new high-strength gel ABP system for fractured reservoirs with high salinity and low permeability. The temperature resistance, salt resistance and plugging characteristics of the gel system were studied at 29,500 mg/L salinity. The results showed that the crosslinking time was shortened and the gel strength was increased with increasing temperature. The core test results show that the ABP system has good plugging characteristics, and the plugging rate is more than 99%. Zhao T. H. et al. [15] studied a new type Poly (AM/O-MMT) composite by solution polymerization method, and X-ray diffraction analysis showed that the composite formed a completely stripped structure. Poly (AM/

OMMT) showed lower water absorption rate and better stability in 95°C distilled water and NaCl solution. From saturation to 90 days, the water absorption base did not change. Poly (AM/O-MMT) has better water plugging and profile control ability in high temperature (95°C) and high salinity (20% NaCl) environment. Xu et al. [16, 17] established a simulation model with periodic lean zones to analyze the effects of these lean zones on SAGD performance, which investigated the effects of vertical distribution, horizontal spacing and sizes, and spatial relationship with SAGD horizontal wells.

The polymer gel system has fluidity and low viscosity fluid state before gelation. In the reaction process, under the action of crosslinking agent, the linear polymer molecular chains are cross-linked at multiple positions, thus forming a gel with spatial network structure [18–21]. Colloids exhibit partial solid properties, with certain viscoelasticity, strength and bearing capacity. Crosslinking agents can usually be divided into two categories, one is the inorganic crosslinking agent based on metal ions such as chromium ions and aluminum ions; The other is organic crosslinking agent based on phenolic resin and other organic substances. Organic crosslinkers and polymer molecules are mostly connected in the form of covalent bonds, resulting in better gel stability and generally higher temperature resistance. Research and development of new crosslinking agents, using organic/inorganic crosslinking agents and other methods can effectively improve the temperature resistance of the gel system. Nasr-El-Din H A et al. [22] studied a gel type plugging agent with silicate/urea system, which can form gel over 70°C. The results showed that the maximum concentration of NaCl tolerated by sodium silicate/urea solution was 3%, while the maximum concentration of  $\text{CaCl}_2$  was 0.08%. Prajakta et al. [23] combined different activators with colloidal nano silica to prepare a non-toxic and environmentally friendly gel system with a gel formation time of 4–6 h at 200°F and 1 h at 300°F. The formation time of the system can be controlled by adjusting the pH. At 200°F, the formation time is less than 1 h in the pH 5–7 range and 2–8 h in the 8–10 range, which can meet the actual construction requirements. Guang Y. et al. [24] experimentally studied three kinds of polymer gel temporary plugging agents with different strengths. The core experiment shows that the polymer gels with different strength have good formation sealing property and erosion resistance. The formation sealing rate is increased by 90% after water erosion of 40 PV. Ayman et al. [25] synthesized a zirconia/graphene nanocomposite material and reacted it with low molecular weight polyacrylamide as a crosslinking agent to prepare a new gel system that can be used for high temperature water plugging. Adewunmi A et al. [26] studied and synthesized the CFA (fly ash) content (mass fraction 0.5%, 1%, and 2%) of pure polyacrylamide PAM/PEI hydrogel and PAM/PEI-CFA hydrogel (PEI as the crosslinking agent). Thermogravimetry analysis results show that the decomposition rate of PAM/PEI-CFA3 is less than 3% at 200°C, which may be due to the formation of strong chemical bonds between PAM/PEI and alumina and silica, which greatly improves the temperature resistance of hydrogels. Liu Y. et al. [27] studied a series of chemical gel plugging agents with temperature and salt resistance, using the low phase pair particle mass polymer {P (AM-coAMPS)} as the polymerization monomer and phenolic resin (linear) as the crosslinking agent. The results



show that the gel system can meet the diversity of water plugging requirements under different geological conditions by adjusting the dosage of each component. The gel system was tested by TG and DSC. It was proved that the gel system had good temperature resistance. Yang H. et al. [28] have poor performance under high salinity because of the rapid dehydration shrinkage of conventional polymer gels. Amphiphilic polymer gels have been studied by cross-linking the salt-tolerant amphiphilic polymer APP4 with organic chromium, with very low dehydration shrinkage at high salinity (80,000 mg/L NaCl) and temperature (85°C).

Water-soluble polymer gel particles have attracted a lot of attention due to their excellent hydrophilicity and have been widely used in agriculture, food, cosmetics, petrochemicals and other fields. Due to its unique swelling and dissolving properties, it can be used as a temporary plug or diverter for fracturing. The study of functional monomers and polymers forming composite systems has attracted much attention in recent years. After extensive preliminary experimental studies, we have prepared a novel water-soluble polymer temporary plug by polymerization in aqueous solution and optimized the preparation process conditions.

## 2 Preparation of water-soluble polymer temporary plugging agent

### 2.1 Design technical ideas

A new technical idea to develop a new water-soluble polymer plugging agent for fracturing is: medium and low molecular weight + reinforced chain rigidity + supramolecular aggregation.

- (1) medium and low molecular weight. The main purpose of reducing the molecular weight of polymer is easy to process, easy to degrade and reduce the viscosity of the degraded solution.
- (2) Enhance the chain rigidity. The enhancement of chain rigidity has two purposes: 1) to enhance the resistance of copolymer to mechanical degradation during the granulation process. 2) To enhance the chain rigidity and make the polymer chain more entangled, so as to control the dissolution time, especially by introducing different amounts of  $-\text{SO}_3^{2-}$  or  $-\text{COO}^-$  to the rigid groups used to increase the chain rigidity, so as to increase the electrostatic repulsion within and between the polymer chains, so as to control the dissolution time of the temporary stopper to a certain extent.
- (3) supramolecular aggregation. Although the molecular weight of the polymer is reduced, the dissociation time cannot be reduced or even increased. Clearly, it is no longer practical to rely solely on the entanglement of a single HPAM molecular chain, but must rely more on the interactions between the polymer chains. Hydrophobic groups with specific structures are introduced to achieve hydrophobic association and entanglement between the molecules and thus polymer molecules form supramolecular aggregates. The aggregates are not easily disentangled before entering the fracture pore, and have good hydrophilicity, which favors dispersion in a dispersive solution. Once inside the pore, it begins to swell and form a plug. As the fluid and the fracturing fluid continue to migrate, the swelling system formed by the

polymer temporary plug begins to dissolve and eventually disappears and the channel reopens.

### 2.2 Experimental materials and method

Acrylamide AM, acrylic acid AA, 2-acrylamide-2-methylpropane sulfonic acid AMPS, SM functional monomer (self-made),  $\text{Na}_2\text{CO}_3$ , urea, sodium bisulfite, potassium persulfate.

The temporary plug is prepared by solution polymerization, and the experimental workflow is as follows:

- (1) Under water bath cooling, add 0.3 Kg of acrylamide (AM) and 0.2 Kg of acrylic acid (AA) into a 5 L three-port reaction flask equipped with an agitator, thermometer and reflux condenser, and then add 80 g of water, 0.2 g of 2-acrylamide-2-methylpropane sulfonic acid (AMPS), 0.8 g of SM functional monomer, and 12 g of urea.
- (2) Start the agitator and add 46.5 g of sodium carbonate after stirring evenly for 1 h.
- (3) 0.014 g of sodium bicarbonate and 0.028 g of potassium bicarbonate were added to initiate polymerization to obtain the product.
- (4) After the reaction, pour the obtained mixture onto the container, spread it into a cake with a thickness of about 3 mm, after natural drying, cut it into blocks with a particle size of 3–6 mm, and bake it to constant weight in a 100°C oven to obtain a dry block, which is the finished product.

## 3 Experimental evaluation results and discussion

### 3.1 Infrared spectrum analysis

The structure of the synthesized temporary plug material was studied with the Perkin-Elmer 325 FI-IR infrared spectrometer, KBr plate, with measurements in the 400–4,000  $\text{cm}^{-1}$  range. It shows the IR spectra of polymer temporary plug agents synthesized in the laboratory. As can be seen in Figure 1, the absorption peak at 3,423  $\text{cm}^{-1}$  is attributed to the stretching vibration of the O-H bond, indicating the presence of the cross-linking functional group -OH-. The absorption peak at 2,932.7  $\text{cm}^{-1}$  is attributed to stretching vibrations of saturated C-H bonds in the polymer, and shifts towards higher wavenumbers as long carbon chains are introduced; The absorption peak at 1,642.8  $\text{cm}^{-1}$  belongs to the stretching vibration of the C = O bond. The absorption peak near 1,543.1  $\text{cm}^{-1}$  belongs to the bending vibration of the N-H bond in the secondary amide; the absorption peak at 1,451, 1,401  $\text{cm}^{-1}$  belongs to the internal bending vibration of the saturated C-H plane in the polymer, indicating that AA and AM are polymerized. Absorption peaks near 1,335  $\text{cm}^{-1}$  and 1,162  $\text{cm}^{-1}$  in the fingerprint region belong to stretching vibrations of the C=O bonds in the carboxyl group, which proves the presence of carboxylates. The absorption peak near 1,240  $\text{cm}^{-1}$  belongs to  $-\text{SO}_3$ , which justifies the introduction of the AMPS monomer. The absorption peak around 1,195  $\text{cm}^{-1}$  is attributed to asymmetric stretching vibrations of the C-O-C-bond. The absorption peak around 672  $\text{cm}^{-1}$  was attributed



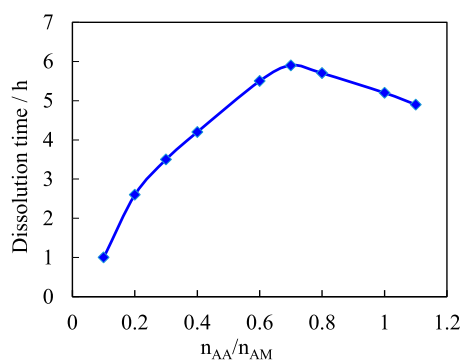


**FIGURE 3**  
Effect of monomer ratio on dissolution time.

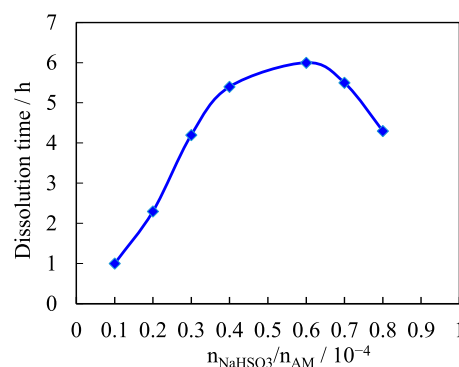


**FIGURE 5**  
Effect of initiator dosage on dissolution time.

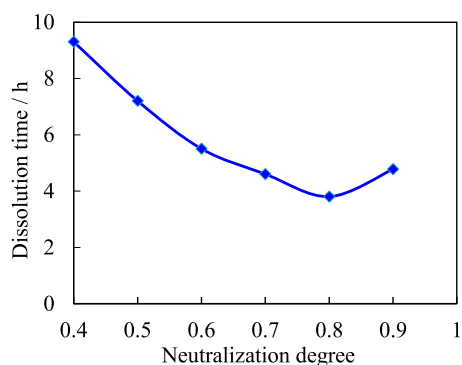


**FIGURE 4**  
Effect of neutralization degree of acrylic acid on dissolution time.

acrylic acid is increased to a certain extent, the molecular chains of the complex become elongated and the water molecules become more accessible, while the dissolution rate increases slightly. As for the dissociation time of the compound, it decreases after reaching its maximum because the hydrophilicity of acrylic is stronger than that of acrylamide, and water molecules are more likely to enter the network with a higher acrylic content. Comparing the requirements for the dissociation time of the temporary plug,  $n_{AA}/n_{AM} = 0.7$  was determined.

### 3.4 Effect of neutralization degree of acrylic acid on dissolution rate

Keep the dosage of other raw materials unchanged, change the dosage of sodium carbonate to change the neutralization degree (ND) of acrylic acid, and study the influence of the neutralization degree (ND) of acrylic acid on the solubility of copolymer. Figure 4 shows the effect of neutralization degree (ND) of acrylic acid on the solubility of polymer.

Figure 4 shows that the dissociation rate of copolymers increases with the neutralization degree of acrylic, with a

minimum occurring when the neutralization degree of acrylic reaches 80 percent. This is because when the degree of neutralization is low, the concentration of AA is high, the activity is high, the polymerization rate is fast, and it readily self-polymerizes to form a polymer with a high degree of cross-linking, which reduces the dissolution rate of the product. As the degree of neutralization continues to increase, it not only slows down the reaction and reduces the degree of cross-linking, but also increases the ionic group of sodium carboxylate, which increases the osmotic pressure inside the interconnecting network. Increasing the degree of neutralization also increases the osmotic pressure between the polymer and the water, which promotes polymer swelling and accelerates the dissolution rate of the products. However, if the neutralization of the system is too high, the carboxylic acid content increases and the coordination form is dominated by intermolecular coordination. As the degree of cross-linking of the complex increases, the network also becomes more contractive and access to water becomes difficult. The coordination bonds that need to be destroyed in the dissociation of the complex are also increased and the dissociation rate of the complex is correspondingly slowed down. The optimal neutralization of acrylic was determined to be 70% by comparing the required dissociation time of the temporary plug.

### 3.5 Effect of initiating dose on dissolution rate

The dosage of the other ingredients was kept constant, the dosage of the initiator sodium bisulfite was varied, and the effect of the initiator dosage on the dissolution rate was studied. Figure 5 shows the effect of the amount of initiator ( $n_{NaHSO_3}/n_{AM}$ ) on the solubility of the sample.

As the amount of initiator is gradually increased, the dissolution rate of the sample is accelerated. This is because the number of initiators is small, the decomposition rate of the initiators is low, the amount of radicals is small, the polymerization reaction is slow, the low-polymer content in the polymer is large, and the dissolution rate of the complex is fast. As the number of initiators increases, the

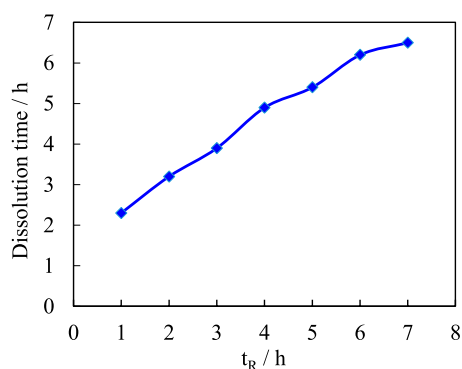


**FIGURE 6**  
Effect of reaction time on dissolution time.

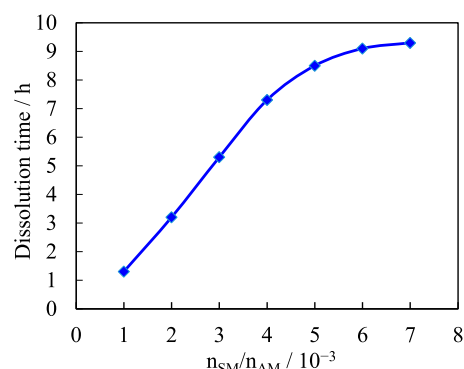


**FIGURE 7**  
Effect of functional monomer SM dosage on dissolution rate.

polymerization reaction speed is gradually accelerated, the low-polymer content of the polymer is gradually reduced, the chelating and cross-linking effects of the polymer are gradually enhanced, and the dissociation rate of the complex is increased. Increasing the number of initiators further, the molecular weight of the polymer will gradually decrease, the cross-linking network will contain more terminal groups, the solubility of the polymer will increase, and thus the dissolution rate will be accelerated. Compare the requirements for the dissolution time of temporary plugging agent, and determine that  $n_{NaHSO_3}/n_{AM} = 0.45 \times 10^{-4}$ .

### 3.6 Effect of reaction time on dissolution rate

The amount of other ingredients was kept constant, the reaction time was varied, and the effect of the reaction time on the dissociation rate of the copolymer was studied. Figure 6 shows the effect of reaction time ( $t_R$ ) on the dissolution rate of copolymer.

As the reaction time is extended, the polymer dissociation time gradually increases and eventually reaches a certain value. This is caused by a change in the polymerization of the initiator. The reaction time is short, the polymerization reaction is not balanced, and the structure of the compound is stable. There are high cross-linking regions with high cross-linking and low cross-linking regions with low cross-linking. Although high cross-linking regions are unfavorable for water entry, the presence of low cross-linking regions accelerates water entry. At the same time, due to the staggered and random distribution of the high and low cross-linking regions in the polymer, the effective distance of water entering the high cross-linking region is shortened, and finally the speed of water entering the high cross-linking region is accelerated, so the dissolution rate of the composite is fast. As the reaction time is extended, the coordination gradually reaches the most reasonable distributional state due to the gradual reduction of the residual monomers, and the degree of cross-linking increases compared to recombination with short reaction times. In this way, the polymer network structure is uniformly distributed, effectively blocking the entry of water, and the swelling and dissolution rate of the

compound is slowed down. A reaction time of 3 h is more reasonable compared to the requirement of a dissociation time for the temporary plug.

### 3.7 Effect of the amount of functional monomer SM on the dissolution rate

The functional monomer SM is varied while the other raw materials are kept constant, and the effect of the functional monomer SM on the dissociation rate of the copolymer is studied. Figure 7 shows the effect of the functional monomer SM on the dissociation rate of the copolymer. Figure 7 shows that the amount of functional monomer SM has a significant effect on the solubility of the copolymer temporary plug. Within the experimental range, as the functional monomeric SM content increases, the dissociation rate of the sample in water slows down significantly and the water absorption by the copolymer decreases significantly. This is because an increase in the hydrophobic functional monomeric SM content increases the physical cross-linking point of the copolymer, resulting in higher copolymer strength, lower water absorption, and lower dissolution rate. Compared with the requirements for the dissolution time of temporary plugging agent, the functional monomer SM ratio is optimized as  $3 \times 10^{-3}$ . Through experimental optimization, the optimum conditions of various influencing factors obtained are as follows: monomer ratio  $n_{AA}/n_{AM} = 0.7$ , the optimum neutralization degree of acrylic acid is 70%, initiator ratio  $n_{NaHSO_3}/n_{AM} = 0.45 \times 10^{-4}$ . Reaction time 3 h, functional monomer SM ratio  $3 \times 10^{-3}$ .

## 4 Performance evaluation of new temporary plugging agent

### 4.1 Determination of water absorption expansion

A sample of a certain quality is accurately weighed by placing it in a 200-g nylon bag, sealing the mouth of the bag and weighing it.

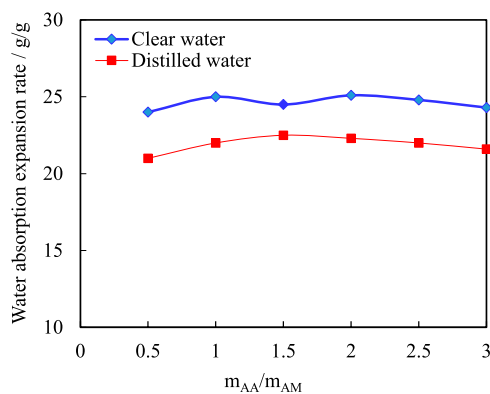


**FIGURE 8**  
Water absorption expansion rate of copolymer.

The sample was placed in the absorbable solution at a constant temperature of 30°C, sampled at regular intervals, removed free water from the surface, and then weighed. This is repeated several times until the mass is constant or has a steady downward trend. Calculate the water absorption expansion rate ( $Q_s$ , g/g) according to Formula 1.

$$Q_s = (m_2 - m_1)/m_0 \quad (1)$$

Where,  $m_0$  is the initial sample mass, g;  $m_1$  is the total mass of the initial nylon bag and sample, g;  $m_2$  is the total mass of nylon bag and sample after absorbing water for a period of time, g.

See Figure 8 for the water absorption expansion of copolymers. As can be seen from Figure 8, copolymers with different monomer ratios have a higher water absorption expansion rate in tap water than in distilled water, with a maximum water absorption rate of 25.8 g/g. This is because the hydrophobic interaction between the copolymer segments takes place between molecules, making the curled molecular chain extend and form a large spatial network - dynamic physical cross-linking network structure through the hydrophobic interaction, and the rich needle-like array on the surface increases the contact between the polymer and electrolyte ions such as  $\text{Na}^+$  and  $\text{Cl}^-$  in the solution, which enhances the hydrophobic association, so the water absorption capacity is also enhanced. The monomer ratios of AM and AA don't have a significant effect on their water absorption, which is due to the fact that the variation of water absorption not only increases with the number of hydrophilic functional groups, but is also limited by the degree of cross-linking of the polymers. When the degree of cross-linking is large, the density of polymer cross-linking points is large, the space formed by molecular chain swelling is small, and the volume of water contained is also small, so when the water absorption exceeds its tolerance limit, The water absorption capacity of the polymer tends to be stable without increasing.

## 4.2 Determination of swelling kinetics

The change in the water absorption of the polymer particles at different times allows to measure the water absorption and swelling

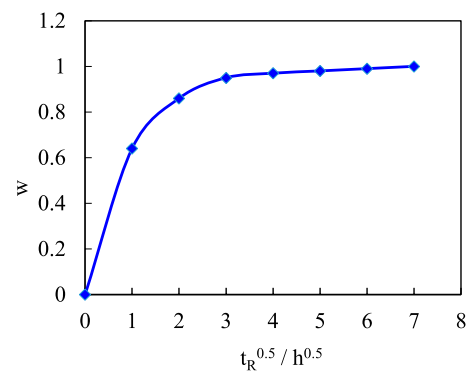


**FIGURE 9**  
Swelling kinetics curve of copolymer in tap water.

process of the polymer with the same specific measurement procedure as in Section 4.1. According to Formula 1, the water absorption ( $Q_t$ ) of polymer at time  $t$  can be calculated, and the ratio of water absorption of polymer at time  $t$  to water absorption at swelling equilibrium ( $w$ ) is:

$$w = Q_t/Q_e \quad (2)$$

Where,  $Q_e$  is the water absorption of polymer after swelling equilibrium, g/g.

Figure 9 shows that during the initial swelling process, the polymer particles exhibit a faster rate of water absorption and the swelling curve deviates from the ideal exponential change. As the swelling time continues to lengthen, the water absorption rate decreases and the swelling rate decreases. This variation is mainly related to the size of the copolymer sample particles and the structure of the copolymer cross-linking network. The swelling kinetics curves of copolymers show that copolymers have a fast water absorption rate and can reach swelling equilibrium in a short time.

## 4.3 Density

### (1) True density (particle density)

Five samples of 20–30 each were randomly selected from the product, their length, width and height were measured in the same way, the mean value was calculated and their mean volume was calculated. The sample was then weighed and the density of the sample was calculated using the density definition formula. The average density is:  $\rho = 1.15 \text{ g/cm}^3$ .

### (2) Bulk density

Randomly select 3 samples from the product, each containing 20–30 capsules, and weigh them. The bulk density of the sample was determined using the discharge volume method using tetrahydrofuran as the measuring medium. The average density is:  $\rho = 1.15 \text{ g/cm}^3$ .

The above experimental data show that the prepared crack steering control agent has uniform particle shape and density  $\rho = 1.14 \text{ g/cm}^3$ .



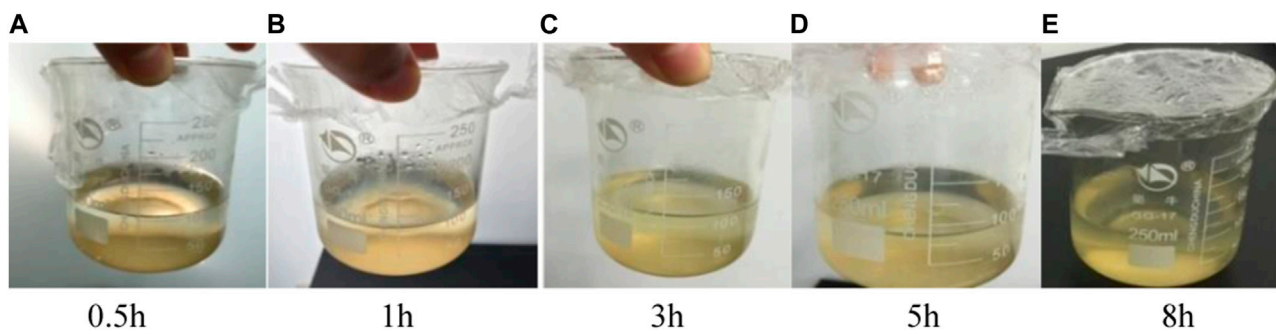


**FIGURE 10**  
Effect of dissolution of copolymer particles at 60°C.

#### 4.4 Determination of viscosity after dissolution

The solubility of the temporary plug is related to whether the temporary plug can effectively plug fractures and percolation channels, and whether it can achieve self-plugging. If the solubility of the temporary plugging agent is too good, the temporary plugging agent is completely dissolved before reaching the predetermined plugging area and cannot play a plugging role, or the effective plugging time isn't long enough to meet the construction requirements of the shift to re-fracturing shielding temporary plugging. If the solubility of the temporary plugging agent is too poor, it will not be able to remove the plug by itself or the plugging removal cycle will be very long after plugging, which will not only cause damage to the reservoir, but also have a certain impact on the increase of oil and gas productivity. If a temporary plug agent has poor solubility at low temperatures and good solubility at high temperatures, it can effectively plug fractures and percolation channels temporarily during the construction process. Upon completion of construction, the temperature in the near-well zone rises and returns to the formation temperature. At this point, the temporary plugging agent rapidly dissolves to achieve self-plugging.

The water solubility and high temporary plug strength of water-soluble temporary plug are the key technical difficulties of water-soluble temporary plug. Water-soluble temporary plugging agent generally consists of inorganic salts (slightly soluble in water at normal temperature, and the solubility gradually increases with the increase of temperature and solid-liquid ratio), organic acids (a mixture of organic acids and organic acid salts, with a high softening point and a small change in solubility with temperature) and other additives. The solubility of temporary plugging agent was tested at 30°C, 60°C, and 80°C. Experimental materials: temporary plugging agent, tap water. Experimental equipment: thermostatic water bath, electronic stirrer, electronic balance (minimum graduation 0.001 g), measuring cylinder, rubber tip dropper, glass rod.

Experimental steps:

- 1) Accurately weigh 3 parts of temporary plugging agent with electronic balance, 8 g each;
- 2) Use a measuring cylinder to measure 100 mL of tap water and put it into three 250 mL beakers;

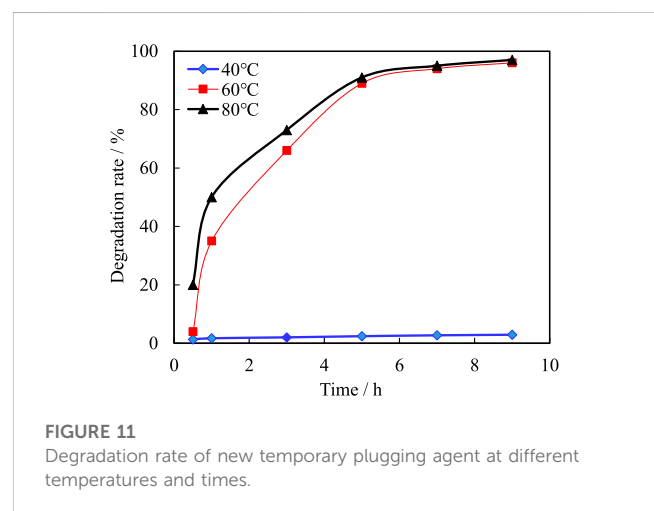


**FIGURE 11**  
Degradation rate of new temporary plugging agent at different temperatures and times.

- 3) Adjust the temperature of the three water bath pots to 30°C, 60°C, and 80°C, put the beaker containing tap water in the thermostatic water bath pot and connect the electronic stirrer. When the temperature is stable, stir into the beaker the temporary blocking agent and dissolve;
- 4) Observe the dissolution of temporary plugging agent in tap water at 0.5 h, 1 h, 3 h, 5 h and 8 h respectively, pass the insoluble substances through the 60-mesh screen, dry and weigh, and calculate the degradation ratio;
- 5) The liquid viscosity after the degradation of temporary plugging agent was measured by DV-II rotary Brinell viscometer (Brookfield Company, United States) at room temperature and 6r/min.

See Figures 10A–E for the dissolution effect of copolymer particles at 60°C.

See Figure 11 for the degradation ratio of the new temporary plug at different temperatures and times. It can be seen from Figure 12 that the degradation rate of temporary plugging agent is about 1%–4% at 30°C, which is difficult to degrade. After the temperature rises to 60°C and 80°C, the temporary plugging agent degrades rapidly in the early stage, and the degradation rate reaches more than 90% in about 5 h, and can be completely degraded in 5 h and 8 h. At the same time, the





**FIGURE 12**  
Physical picture of core displacement device.

experimental results show that the higher the temperature, the faster the degradation of the temporary plugging agent.

## 4.5 Strength of temporary plugging agent

The strength of the colloids formed after the injection of the temporary plug into the formation must be higher than the pressure value at the fracture of the pay formation to ensure the reorientation of the new fracture during re-fracture. At 60°C, the plugging strength of temporary plugging agent was studied by using artificial fracture core.

Experimental materials: New water-soluble temporary plug particles. Experimental equipment: electronic stirrer, electronic balance (minimum graduation 0.001 g), beaker, glass rod, natural core, core displacement device.

Experimental steps:

- 1) Cut the core with a diameter of  $D \approx 2.5$  cm axially for standby;
- 2) After drying the core, weigh the dry core mass  $M_1$ ;
- 3) Put the core into the formation water suction bottle and filter for 8 h. When the core is sufficiently saturated with water, the formation water on the surface of the core is drained off with a clean rag, and the mass  $M_2$  is weighed after the core has saturated with water;
- 4)  $(M_2 - M_1)/\rho_w$  Effective pore volume  $V$  of core obtained from formation water;
- 5) Add an appropriate amount of temporary plugging agent into the tap water, and fully mix for 5 min at 1,500 rpm;
- 6) Add appropriate thickness of mixed temporary plugging agent between two cores;
- 7) Put the core into the core holder, add a confining pressure of 3.0 MPa, place it in the thermostat at the temperature of the reservoir, use the core displacement device (Figure 12), and drive the formation water forward at a flow rate of 0.1 mL/min until the pressure is stable, and record the pressure value;
- 8) With the extension of displacement time, the temporary plugging agent gradually ages in the core, and continues to

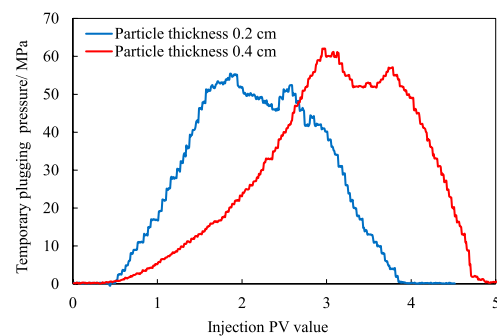


**FIGURE 13**  
Temporary plugging displacement pressure curve with different particle thickness.

inject formation water into the core at a flow rate of 0.1 mL/min, constantly observe the pressure change, record the pressure value at the time of breakthrough, and continue to displace until the pressure is stable, and record the stable pressure.

It can be seen from Figure 13 and Table 1 that in the early stages, the pressure increases significantly with the increase of the injected fluid, reaching the maximum pressure value, and the fluid breaks through the temporary plug, allowing the pressure decrease to gradually equalize. The break pressure for particles with thicknesses of 0.2 cm and 0.4 cm is 54.9 MPa and 60.1 MPa, respectively. This indicates that the temporary plug has the ability to seal the original fracture and cause the new fracture to deviate from the direction of maximum principal stress.

Then, with the extension of the displacement time at 70°C, the temporary plugging material gradually ages and loses its temporary plugging effect, resulting in a significant decrease in the injected fluid pressure. The number of breakthrough PV is between 1.2 and 1.5 PV, and the time is between 65 and 84 min. The aging failure time is shorter than the quiescent time and is mainly due to the incomplete degradation of the temporary plug at the time of rupture, but the partial temporary plug failure is caused by the high displacement pressure at the reservoir temperature. Later, as the injection time increases, the process of aging and degradation of the temporary plug continues until the pressure is stabilized. At the same time, the temporary plug pressure of the granular temporary plug is strongly dependent on the amount of the plug. The larger the amount, the higher the temporary plug pressure.

## 4.6 Preparation of coated temporary plugging agent and test of conductivity after degradation

After the copolymer is synthesized and before cooling, it is mixed with 20–40 mesh ceramics at 9:1, 8:2, and 7:3 and then pelletized to test the conductivity of the particle-temporary plug after degradation.

Experimental material: A novel water-soluble coated temporary plug particle, which is granulated after mixing with a ceramic

TABLE 1 Statistics of compressive strength of temporary plugging agent.

1# core parameter	Particle thickness/cm	Breakthrough pressure/MPa	Breakthrough PV value
L1 = 7.24 cm, D = 2.51 cm, V <sub>p</sub> = 5.94 cm <sup>3</sup>	0.2	54.9	1.83
2# core parameter	Particle thickness/cm	Breakthrough pressure/MPa	Breakthrough PV value
L1 = 7.32 cm, D = 2.48 cm, V <sub>p</sub> = 5.87 cm <sup>3</sup>	0.4	60.1	3.11

proppant. Experimental equipment: electronic stirrer, electronic balance (minimum graduation 0.001 g), beaker, glass rod, natural core, core displacement device.

Experimental steps:

- 1) Cut the core with a diameter of  $D \approx 2.5$  cm axially for standby;
- 2) After drying the core, weigh the dry core mass  $M_1$ ;
- 3) Put the core into the formation water suction bottle and filter for 8 h. When the core is sufficiently saturated with water, the formation water on the surface of the core is drained off with a clean rag, and the mass  $M_2$  is weighed after the core has saturated with water;
- 4)  $(M_2 - M_1)/\rho_w$  Effective pore volume  $V$  of core obtained from formation water;
- 5) Add an appropriate amount of temporary plugging agent into the tap water, and fully mix for 5 min at 1,500 rpm;
- 6) Add 0.3 cm thick mixed coated temporary plugging agent between cores;
- 7) Put the core into the core holder, add a confining pressure of 30 MPa, and place it in the thermostat at the temperature of the reservoir. Use the core displacement device (Figure 12) to drive the formation water forward at a flow rate of 2 mL/min. When saturated, let it stand for 5 h to dissolve the temporary plug;
- 8) As time goes on, the temporary plugging agent gradually ages in the core, continues to inject formation water into the core at a flow rate of 2 mL/min, constantly observes the pressure change, records the pressure value at the time of breakthrough, and continues to displace until the pressure is stable, and records the stable pressure.
- 9) After washing the rock sample, change the experimental conditions to conduct another group of experiments.

## Data processing:

According to Darcy's law, the conductivity of supporting fractures is measured, and its calculation formula is:

$$K_{fw} = \frac{5.555\mu Q}{\Delta p} \quad (3)$$

Where:  $K_{fw}$  is the conductivity of supporting fracture,  $\mu\text{m}^2\cdot\text{cm}$ .  $\mu$  is the working fluid viscosity, mPa·s.  $Q$  is the flow,  $\text{cm}^3/\text{min}$ .  $\Delta p$  is the pressure difference, kPa.

The results of the post-degenerate conductivity test are given in Table 2. Since the same rock sample was used, the data for each group is comparable. When the displacement fluid uses clean water (viscosity is 1 mPa s) and flow rate is 2 mL/min, the

displacement pressure of blank rock sample is 0.23 kPa, and the conductivity is about 48.30 calculated by formula 2-3  $\mu\text{m}^2\cdot\text{cm}$ . For rock samples using conventional temporary plugging agent, the particle temporary plugging agent is dissolved after 24 h, and the conductivity is 44.44  $\mu\text{m}^2\cdot\text{cm}$ , which is lower than that of the blank sample. It has been analyzed that part of the temporary plug is not completely degraded, which reduces the fracture conductivity to some extent. Change the coated temporary plugging agent with different proportions (9:1, 8:2, 7:3), and the core displacement pressure will be greatly reduced by 0.16, 0.12, and 0.09 MPa after 24 h, and the calculated conductivity is about 69  $\mu\text{m}^2\cdot\text{cm}$ , 93  $\mu\text{m}^2\cdot\text{cm}$ , and 123  $\mu\text{m}^2\cdot\text{cm}$  respectively, both of which have been greatly improved. It shows that the ceramics after the dissociation of the temporary plug act as a local support and significantly increase the fracture conductivity, reflecting that the developed coated temporary plug is in line with the original design intent and achieves the design purpose.

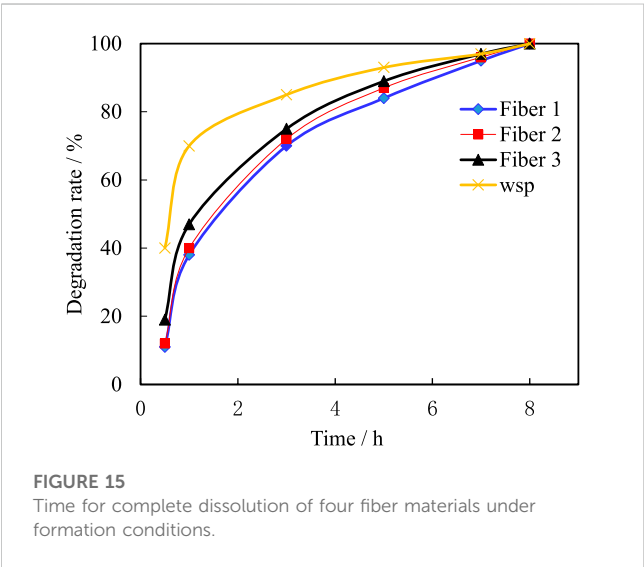
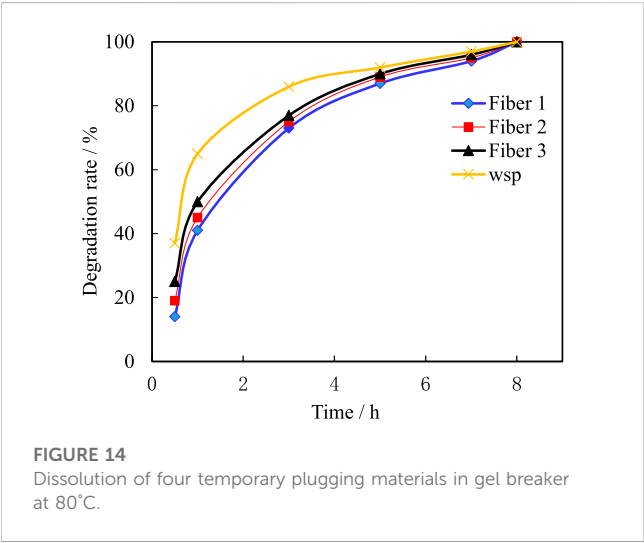
## 4.7 Compatibility evaluation of temporary plugging agent and fracturing fluid

The compatibility of temporary plugging agent and fracturing fluid to a certain extent reflects the controllability of temporary plugging fracturing construction and the damage to the formation. When the compatibility of the two is poor, it is easy to affect the cross-linking of the fracturing fluid, affect construction, or cause precipitation in the formation, damaging the formation. From the experimental results, it can be seen that the addition of particle temporary plugging agent does not affect the gel breaking of guar gum fracturing fluid, and the dissolution of temporary plugging agent in the fracturing fluid has no or micro precipitation, indicating that the temporary plugging agent has good compatibility with the fracturing fluid. At 80°C, after being placed for 3 h, the fiber changes into a colloidal block shape in the gel breaker, and is stirred to break in a lump shape. The gel breaker is thoroughly broken, and the viscosity of the gel breaker is equivalent to that of water. Under the same conditions, the particulate temporary plugging agent is almost completely dissolved after being placed for 3 h. The degradation of the four temporary plugging materials over time at 80°C after gel breaking is shown in Figure 14.

It can be seen from Figure 14 that, similar to the degradation process in water, the four temporary plugging agents degrade rapidly in the early stage of the gel breaker, with a degradation rate of over 90% within 3 h, and can be completely degraded within 5–8 h (According to the pH test results, guanidine glue

TABLE 2 Test results of conductivity after degradation.

Rock sample	Particle thickness cm	Particle type	Fluid viscosity mPa·s	Flow rate mL/min	Displacement pressure of 24 h/kPa	Conductivity $\mu\text{m}^2\cdot\text{cm}$
1	0	—	1	2	0.23	48.30
2	0.3	Routine	1	2	0.25	44.44
3	0.3	Coated type 9:1	1	2	0.16	69.44
4	0.3	Coated type 8:2	1	2	0.12	92.58
5	0.3	Coated type 7:3	1	2	0.09	123.44



and gel breaker are weakly alkaline, which is conducive to the degradation of acidic fibers.); At the same time, it was found that at 80°C, the degradation of particulate temporary plugging agent was faster than that of fibrous materials. In order to appropriately

reduce the degradation rate of particles, diesel immersion treatment measures can be taken.

#### 4.8 Time of complete dissolution of plugging agent under formation conditions

The formation temperature in the work area is about 80 °C. When the gel breaker containing four temporary plugging agents is heated to 80 °C, the degradation rates of the four temporary plugging materials at different times in the gel breaker are shown in Figure 15. It can be seen from the Figure 15 that the temporary plugging agent degrades rapidly in the early stage of the gel breaker, with a degradation rate of over 90% within 3 h, and can be completely degraded within 5–8 h.

### 5 Conclusion

- (1) A new idea for the development of a new water-soluble fracturing temporary plugging agent is proposed: medium and low molecular weight + enhanced chain rigidity + supramolecular aggregation. The AM-AA-AMPS-SM copolymer temporary plug is prepared by polymerization with sodium bisulfite and potassium sulfate as initiators, AA, AM and AMPS as grafting monomers, and SM as hydrophobic functional monomers. The FTIR and SEM results indicate that the synthesized product is an AM-AA-AMPS-SM copolymer.
- (2) Through experimental optimization, the optimum conditions of various influencing factors are as follows: monomer ratio  $n_{AA}/n_{AM} = 0.7$ , the optimum neutralization degree of acrylic acid is 70%, initiator ratio  $n_{NaHSO_3}/n_{AM} = 0.45 \times 10^{-4}$ . Reaction time 3 h, functional monomer SM ratio  $3 \times 10^{-3}$ .
- (3) The test results of water absorption expansion rate, swelling kinetics, density, viscosity after dissolution, strength of temporary plugging agent and conductivity after degradation of the new temporary plugging agent show that it is completely degraded at 70°C for 5–8 h, and the solution viscosity after degradation is 2.5–3.6 mPa s, with good fluidity and no gel residue. The density of the temporary plug material is approximately 1.14 g/cm<sup>3</sup>. The water absorption expansion rate reached 25.8 g/g. The pressure is 60.1 MPa when the

particle is 0.4 cm thick as a temporary plug. Under experimental conditions, the fracture conductivity at a closure pressure of 30 MPa after degradation of the temporary plug is 69–123 D\*cm, which meets the technical requirements for temporary plug and diversion fracturing.

- (4) The significant advantage of the new polymer is that the dissolution time and temperature in water can be controlled by the addition of functional monomers, and the addition of functional monomers can improve the interface performance between the solution and the proppant, contributing to the formation of coated temporary plugging agents. The new temporary fracture plugging agent has the characteristics of high plugging strength, temperature-controlled degradation in water, stable reflux, and effective self-supporting after degradation, which helps to ensure the success rate of temporary plugging fracturing and significantly improve the effect of temporary plugging fracturing.

## Data availability statement

The original contributions presented in the study are included in the article/supplementary material, further inquiries can be directed to the corresponding authors.

## Author contributions

GW and ZC: conceptualization, funding acquisition, project administration, resources, writing—original draft and software. YH: data curation, formal analysis, methodology. GW and SL: writing—original draft, and writing—review and editing. XK: project administration, resources. JZ: investigation, methodology, software, and visualization. XX and JW: conceptualization, funding acquisition, methodology. XK: investigation, methodology, project

administration. All authors have read and agreed to the published version of the manuscript.

## Funding

This research was funded by “Research on offshore large-scale fracturing engineering technology (KJGG2022-0704), Key parameter characterization and desert area evaluation technology of coalbed methane geological engineering (KJGG2022-1001), Research on Inter-well Disturbance Integral Fracturing Technology of Coalbed Gas (2021-YXKJ-010).”

## Acknowledgments

The authors are grateful for reviewers and editors for their careful review of this manuscript.

## Conflict of interest

GW, ZC, AZ, JZ, YH, XX, and JW were employed by CNOOC Research Institute Co, Ltd.

The remaining authors declare that the research was conducted in the absence of any commercial or financial relationships that could be construed as a potential conflict of interest.

## Publisher's note

All claims expressed in this article are solely those of the authors and do not necessarily represent those of their affiliated organizations, or those of the publisher, the editors and the reviewers. Any product that may be evaluated in this article, or claim that may be made by its manufacturer, is not guaranteed or endorsed by the publisher.

## References

- Huang X, Shen H, Sun J, Kaihe L, Liu J, Dong X, et al. Nanoscale laponite as A potential shale inhibitor in water-based drilling fluid for stabilization of wellbore stability and mechanism study. *Acs Appl Mater Inter* (2018) 10(39):33252–9. doi:10.1021/acsami.8b11419
- Chang X, Sun J, Xu Z, Zhang F, Wang J, Kaihe L, et al. A novel nano-ligninbased amphoteric copolymer as fluid-loss reducer in water-based drilling fluids. *Colloids Surf A Physicochemical Eng Aspects* (2019) 538:123979. doi:10.1016/j.colsurfa.2019.123979
- Huang X, Sun J, Lv K, Liu J, Shen H, Zhang F. Application of core-shell structural acrylic resin/nano-sio2 composite in water based drilling fluid to plug shale pores. *J Nat Gas Sci Eng* (2018) 55:418–25. doi:10.1016/j.jngse.2018.05.023
- An YX, Jiang GC, Agent P, Ge QY. Plugging agent of shale base on Nano flexible polymer. *Appl Mech Mater* (2016) 4254(1670):15–9. doi:10.4028/www.scientific.net/amm.835.15
- Lu Z. Progress and prospect study on temporary plugging agent for diverting fracturing. *Sci Tech Eng* (2020) 20(31):12691–701.
- Song L, Zhang H, Wang M, et al. Experimental investigation into temporary acidizing of fractured Carbonate reservoirs in Sichuan Basin. *Chem Eng Oil Gas* (2021) 50(3):90–5.
- Pu J, Geng J, Han P, Bai B. Preparation and salt-insensitive behavior study of swellable, Cr3+ - embedded microgels for water management. *J Mol Liquids* (2019) 273: 551–8. doi:10.1016/j.molliq.2018.10.070
- Hasankhani GM, Madani M, Esmailzadeh F, Mowla D. Experimental investigation of asphaltene-augmented gel polymer performance for water shut-off and enhancing oil recovery in fractured oil reservoirs. *J Mol Liquids* (2019) 275:654–66. doi:10.1016/j.molliq.2018.11.012
- Salehi MB, Soleimani M, Moghadam AM. Examination of disproportionate permeability reduction mechanism on rupture of hydrogels performance. *Colloids Surf A: Physicochemical Eng Aspects* (2019) 560:1–8. doi:10.1016/j.colsurfa.2018.09.085
- Tian M, Xu YJ. The preparation and characterization of AM/2-EHA/VTEOS copolymer as profile control agent. *Advanced Materials Research. Trans Tech Publications Ltd* (2013) 602:732–8.
- Wang C, Liu H, Zheng Q, Liu Y, Dong X, Hong C. A new high-temperature gel for profile control in heavy oil reservoirs. *J Energy Resour Tech* (2016) 138(2). doi:10.1115/1.4031706
- Xu J, Chen Z, Wu K, Li R, Liu X, Zhan J. On the flow regime model for fast estimation of tight sandstone gas apparent permeability in high-pressure reservoirs. *Energy Sour A: Recovery, Utilization, Environ Effects* (2019) 2019:1–12. doi:10.1080/15567036.2019.1687625
- Li J, Wu K, Chen Z, Wang K, Luo J, Xu J, et al. On the negative excess isotherms for methane adsorption at high pressure: Modeling and experiment. *SPE J* (2019) 24(06): 2504–25. doi:10.2118/197045-pa
- Zhang C, Qu G, Song G. Formulation development of high strength gel system and evaluation on profile control performance for high salinity and low permeability fractured reservoir. *Int J Anal Chem* (2017) 2017:1–9. doi:10.1155/2017/2319457
- Zhao TH, Xing JY, Pu WF, Dong ZM, Yuan CD, Peng GF, et al. Synthesis and property evaluation of a novel polyacrylamide-montmorillonite composite for water

shutoff and profile control in high salinity reservoirs. *Polym Composites* (2018) 39(2): 368–76. doi:10.1002/pc.23945

16. Xu J, Chen Z, Dong X, Zhou W. Effects of lean zones on steam-assisted gravity drainage performance. *Energies* (2017) 10(4):471. doi:10.3390/en10040471

17. Xu J, Chen Z, Cao J, Li R (2014). Numerical study of the effects of lean zones on SAGD performance in periodically heterogeneous media. In SPE Heavy Oil Conference-Canada. Adelaide, Australia, 10–12 June 2014.

18. Ahmed HS, Mohamad O, Samir MT. A cross link polymer sealant for curing severe lost circulation events in fractured limestone formations. In: SPE Asia Pacific Oil & Gas Conference and Exhibition; 14–16 October 2014; Adelaide, Australia (2014).

19. El-Karsani KS, Al-Muntasheri GA, Hussein IA. Polymer systems for water shutoff and profile modification: A review over the last decade. *Spe J* (2014) 19(01):135–49. doi:10.2118/163100-pa

20. ElKarsani KSM, Al-Muntasheri GA, Sultan AS, Hussein IA. Performance of PAM/PEI gel system for water shut-off in high temperature reservoirs: Laboratory study. *J Appl Polym Sci* (2015) 132(17):685–92. doi:10.1002/app.41869

21. Zhang X, Zhang S, Li L, Wu R, Liu D, Wu J, et al. High-temperature-resistant polymer gel system with metal–organic mixed cross-linking agents. *J Appl Polym Sci* (2015) 132(29):757–64. doi:10.1002/app.42261

22. Nasr-El-Din HA, Taylor K. Evaluation of sodium silicate/urea gels used for water shut-off treatments, Evaluation of sodium silicate/urea gels used for water shut-off treatments. *J Pet Sci Eng* (2005) 48(3):141–60. doi:10.1016/j.petrol.2005.06.010

23. Prajakta P, Rajendra K. Environmentally acceptable composition comprising nanomaterials for plugging and sealing subterranean formation. In: SPE Paper 154917 presented at the SPE International Oilfield Nanotechnology Conference; June 12–14, 2012; Noordwijk, The Netherlands (2012).

24. Yang G, Zhang J, Xue XS. Development and evaluation of salt-resisting polymer gel profile control agent[C]//Advanced Materials Research. *Trans Tech Publications Ltd* (2013) 781:426–30.

25. Almoshin AM, Alsharaeh E, Fathima A, Bataweel M. A novel polymer nanocomposite graphene based gel for high temperature water shutoff applications. In: SPE Kingdom of Saudi Arabia annual technical symposium and exhibition; 23–26 April 2018; Dammam, Saudi Arabia (2018).

26. Adewunmi A, Ismail S, Sultan AS. Crosslinked polyacrylamide composite hydrogels impregnated with fly ash: Synthesis, characterization and their application as fractures sealant for high water producing zones in oil and gas wells, characterization and their application as fractures sealant for high water producing zones in oil and gas wells. *J Polym Environ* (2018) 26(8):3294–306. doi:10.1007/s10924-018-1204-9

27. Liu Y, Jiao B, Chen D. Synthesis of phenolic resin/P(Am-Co-amps) temporary plugging agent and their properties of salt tolerance. *High Temperature Oilfield Chem* (2018) 35:427–32.

28. Yang H, Iqbal MW, Lashari ZA, Cao C, Tang X, Kang W. Experimental research on amphiphilic polymer/organic chromium gel for high salinity reservoirs. *Colloids Surf A: Physicochemical Eng Aspects* (2019) 582:123900. doi:10.1016/j.colsurfa.2019.123900





## OPEN ACCESS

## EDITED BY

Chengyuan Xu,  
Southwest Petroleum University, China

## REVIEWED BY

Xiaopeng Yan,  
Changzhou University, China  
Shuyu Sun,  
King Abdullah University of Science and  
Technology, Saudi Arabia

## \*CORRESPONDENCE

Yang Wang,  
✉ wangyang0996@petrochina.com.cn

RECEIVED 07 March 2023

ACCEPTED 02 May 2023

PUBLISHED 22 May 2023

## CITATION

Wang Y and Lv Z (2023), Composite  
stimulation technology for improving  
fracture length and conductivity of  
unconventional reservoirs.  
*Front. Phys.* 11:1181302.  
doi: 10.3389/fphy.2023.1181302

## COPYRIGHT

© 2023 Wang and Lv. This is an open-  
access article distributed under the terms  
of the [Creative Commons Attribution  
License \(CC BY\)](https://creativecommons.org/licenses/by/4.0/). The use, distribution or  
reproduction in other forums is  
permitted, provided the original author(s)  
and the copyright owner(s) are credited  
and that the original publication in this  
journal is cited, in accordance with  
accepted academic practice. No use,  
distribution or reproduction is permitted  
which does not comply with these terms.

# Composite stimulation technology for improving fracture length and conductivity of unconventional reservoirs

Yang Wang\* and Zefei Lv

Engineering Technology Research Institute of Southwest Oil and GasField Company, PetroChina,  
Chengdu, China

Unconventional reservoirs have strong heterogeneity, with significant differences in the distribution of porosity and permeability. Fracturing is an important technology for increasing natural gas production in unconventional oil and gas reservoirs. For unconventional reservoirs with high temperature and low permeability, the rapid increase in acid rock reaction rate leads to a significant decrease in the effective distance of acidic fluids and fracture conductivity, especially the inability to obtain effective support at the fracture tip, which restricts the increase in production of high-temperature unconventional oil and gas reservoirs. To address the above issues, a composite fracturing method is proposed, which first uses a proppant to support the crack tip, and then uses gelled acid to corrode the middle and rear parts of the crack. According to the fracture conductivity achievement test experiment and proppant migration experiment, when 40/70 mesh ceramsite and 100 mesh ceramsite are mixed at a mass ratio of 1:4, the fracture conductivity can reach  $21.8 \mu\text{m}\cdot\text{cm}^2$  under the effective closing pressure of 60 MPa, which is 123% higher than the fracture conductivity of cementitious acid corrosion. The gel is used to carry 40/70 mesh and 100 mesh ceramsite, and the Equilibrium level of the sand embankment can reach 38 cm. At the same time, the sand dike formed by different particle sizes of ceramic particles is smoother than the sand vein formed by a single particle size of proppant, and the migration ability of ceramic particles to the fracture tip is better. The composite stimulation technology has been applied to 9 wells in carbonate and shale oil and gas reservoirs. After fracturing, the production of oil and gas wells is 210% higher than that of gelled acid fracturing, and the composite stimulation technology has achieved good stimulation effects.

## KEYWORDS

fracture length, conductivity, unconventional reservoirs, low permeability, high temperature

## 1 Introduction

The unconventional reservoirs is rich in oil and gas resources, which is an important field to ensure the world energy security [1–3]. In the past 20 years, China has successively discovered several large carbonate oil and gas fields in the Tarim Basin and Sichuan Basin, such as Tahe Oilfield and Shunbei Oilfield in the Tarim Basin, Puguang Oilfield and Anyue Oilfield in the Sichuan Basin [4–7]. The burial depth of reservoirs in Shunbei Oilfield in Tarim Basin and Qixia Formation in Sichuan Basin even exceeds 8,000 m, and the reservoir temperature is as high as  $160^{\circ}\text{C}$ – $180^{\circ}\text{C}$  [8–11]. Acid fracturing stimulation mainly depends



on the formation of conductivity of fracture wall corroded by acid fluid, so as to establish oil and gas migration channel from formation to wellbore. The acid rock reaction speed increases sharply with the rise of reservoir temperature [12]. Under ultra-high temperature conditions, the acid solution reacts quickly after contacting the rock. The high temperature environment intensifies the consumption of acid solution, resulting in a very short effective action distance of acid solution in ultra-high temperature formation [13, 14], which affects the acid etching fracture length and oil and gas production.

Improving the length and conductivity of acid etched fractures is an important goal of acid fracturing in carbonate reservoirs, Aljawad et al. [15] indicated that different acid fluid systems should be selected according to the formation feature for improved fracture conductivity. Hou Bing et al. [16] investigated the fracture initiation and propagation in limestone formations under acid fracturing treatment. Lufeng Zhang et al. [17] proposed a new method to raise acid fracture conductivity under high closure stress and provided an insight into optimizing acid propped fracturing design and predicting well performance. Yang Wang et al. [18] proposed a technical method to improve the acid etching fracture length and conductivity of low permeability carbonate reservoirs by alternating injection of authigenic acid and gelling acid. Yang Wang et al. [19] carried out the visual test experiment of alternating injection acid fracturing and studied the influence of parameters such as injection displacement, acid ratio and injection stage on acid fingering morphology. Ye Jiexiao et al. [20], the influence of different injection stages, different liquid combinations and different displacement on the conductivity of acid corrosion fractures was studied by numerical scanning technology. Shahvir Pooniwal et al. [21] successfully performed proppant fracturing treatment for the first time in the Cretaceous carbonate formation of Kuwait. Lurui Dang et al. [22] established an acidizing fluid flow and reaction model taking the multiple leak-off effect of natural fracture, wormhole and matrix into account. Rencheng Dong et al. [23] developed a 3D acid transport model to compute the geometry of acid fracture for acid fracturing treatments with viscous fingering. The developed model couples the acid fluid flow, reactive transport and rock dissolution in the fracture. Daobing Wang et al. [24] proposed a simple iterative procedure to handle the non-linear characteristic of the hydraulic fracturing problem. Numeral validation illustrates that the results of PGD match well with these of standard finite element method in terms of fracture opening and fluid pressure in the hydro-fracture.

An Na et al. [25] developed a new type of solid granular acid which was prepared by taking sulfonic acid as the core material and using organic sulfonic acid/ethyl cellulose composite as capsule materials, and it could be solidified and granulated by adopting a spray drying process. Yang Wang et al. [26] established a kind of autogenic acid system through the hydrolysis of ester to acetic acid *in situ*, and the autogenic acid system possesses the desired characteristic in which hydrolysis can generate a small amount of acetic acid below 120°C and a large amount of acid above 140°C in 2 h. Zhiheng Zhao et al. [27] evaluated compatibility, temperature resistance, friction reduction of the high-temperature-resistant diverting acid (HTRDA), and the peak viscosity of the HTRDA can still reach 31 mPas at the temperature of 170 °C, which is higher than that of conventional diverting acid with about 10 mPas. Sui Yu et al. [28] developed a new high-temperature-resistant gelled acid system with modified xanthan gum, and the viscosity of the acid system at 160°C remains 21 mPas. Juan Du et al. [29] synthesized a

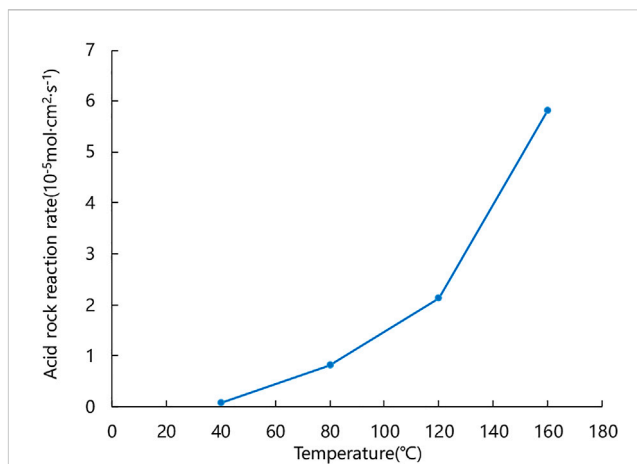


FIGURE 1  
Acid rock reaction rate at different temperatures.

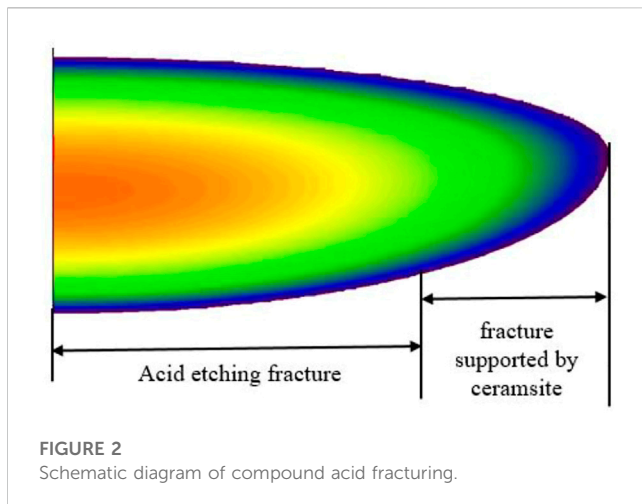
high-temperature autogenic acid system with formaldehyde and ammonium and chloride as the matrix, and the effective acid rock reaction time of this autogenic acid can reach 6 h.

At present, there are a lot of researches on acid fracturing technology and high-temperature resistant acid fluid of carbonate rock oil and gas reservoirs. However, there are few researches on acid fracturing technology of such ultra deep and ultra-high temperature carbonate rock oil and gas reservoirs with a buried depth of more than 7,000 m and a reservoir temperature of 180°C. In order to improve the recovery of ultra deep and ultra high temperature carbonate reservoirs, it is very necessary to study targeted acid fracturing stimulation technology.

In order to solve the technical problem of acid fracturing in ultra deep and ultra-high temperature wells, the author has developed high-temperature resistant gelling acid, which can meet the acid fracturing requirements of 180°C ultra-high temperature reservoirs. At the same time, a new acid fracturing technology combined with hydraulic fracturing and acid fracturing is proposed, which greatly improves the length and conductivity of fracturing fractures. The field test has achieved good application results, which has certain reference significance for the technology of improving oil recovery in ultra deep and ultra-high temperature carbonate rock reservoirs.

## 2 Results and discussion

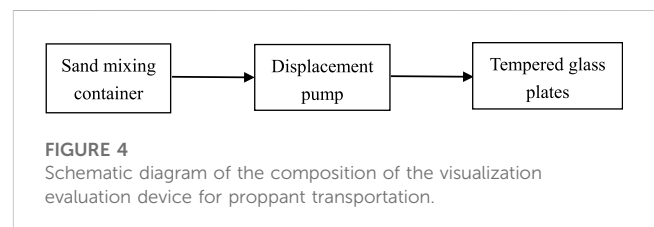
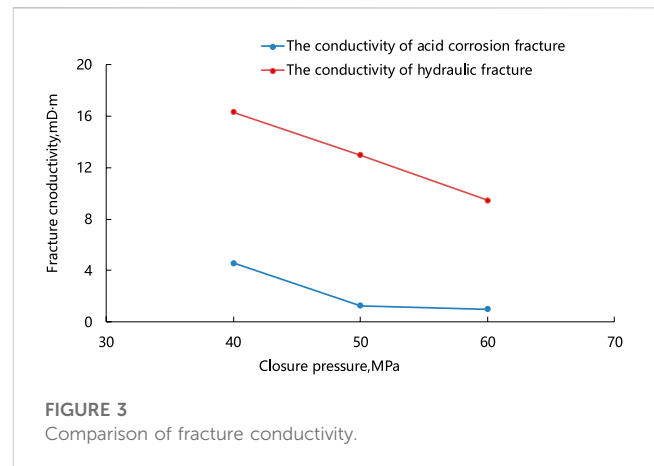
Acid fracturing forms grooves on the rock wall through acid rock reaction, thus establishing a channel for natural gas to flow from the reservoir to the wellbore. The length and conductivity of acid etched fractures determine the drainage area and control range of gas wells. For low permeability oil and gas reservoirs, the ultimate goal of acid fracturing is to improve the length and conductivity of acid etched fractures. However, the reaction speed of acid rock increases exponentially under ultra-high temperature environment, resulting in a significant reduction in the length of acid etched fractures and a rapid reduction in fracture conductivity, which is difficult to meet the requirements of ultra-high temperature and low permeability oil and gas reservoirs.



It can be seen from Figure 1 that the acid rock reaction rate at 160°C is 2.73 times that at 120°C, and the acid rock reaction rate increases sharply with temperature. This article uses FRACPRO to simulate the extension of acid corrosion fractures at different temperatures. FRACPRO is an acid fracturing design software. The single well geomechanical model is established by inputting parameters such as porosity, permeability, Young's modulus and crustal stress in the FRACPRO, and then the acid fluid performance is customized according to the experimental results such as acid rock reaction rate, so as to simulate the fracture length results under the same fluid volume and displacement. From the simulation results of the FRACPRO, it can be seen that under the same displacement and fluid scale, the length of acid corrosion cracks at 160°C is reduced by more than 20% compared to 120°C.

## 2.1 Technical principles

Under high temperature, acid rock reaction is fast, acid fluid is difficult to reach the fracture tip, and acid fluid cannot effectively dissolve the fracture tip. To solve the above problems, a new method of combined hydraulic fracturing and acid fracturing is proposed, and the schematic diagram of composite stimulation technology is shown in Figure 2. The process steps of compound acid compression are as follows: First, hydraulic fracturing is injected to open the formation to form artificial fractures; then, sand carrying fluid is injected to carry ceramicsite to support the fracture tip; finally, acid is injected to corrode the fracture wall. The ceramicsite is used to support the fracture tip, and the acid solution is used to dissolve the fracture wall, so as to produce a high conductivity fracture that can effectively support and corrode from the tip to the tail. This acid fracturing process combines the technical advantages of acid fracturing and hydraulic fracturing. It not only maintains the advantages of good effect of hydraulic fracturing to support fractures and high conductivity, but also forms high conductivity grooves on the fracture wall with the aid of acid solution to, etch the rock. The acid fracturing and hydraulic fracturing stimulation technologies complement each other well, and the compound acid fracturing technology greatly improves the fracture length and conductivity.



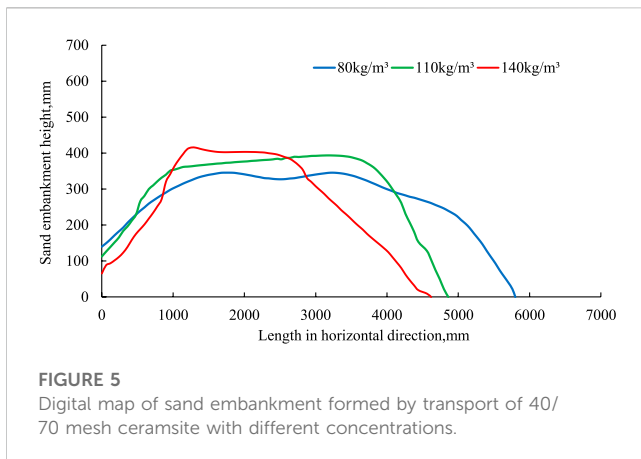
The core of the compound acid fracturing process is how to carry the proppant to the fracture tip, so as to improve the fracture length and conductivity. The transport of proppant in the fracture is affected by gravity, viscosity and other factors [30], and the proppant is distributed as a sand embankment in the fracture [31]. The equilibrium height of the sand dike and the position of the front edge of the sand dike are the key parameters to evaluate the transport of proppant [32].

In this paper, unconventional reservoir cores were selected to carry out acid corrosion fracture conductivity and hydraulic fracture conductivity tests. It can be seen from Figure 3 that hydraulic fracture conductivity is significantly higher than acid corrosion fracture conductivity, mainly because ceramicsite in hydraulic fractures can play a better supporting role under high closure stress, and grooves and bulges in acid etching fractures are easy to be crushed and deformed under high closure stress. The above experiment further proves that using ceramic particles to support the fracture tip can improve the fracture conductivity.

This article selected 70/140 mesh ceramic particles and 40/70 mesh ceramic particles to conduct proppant transport and fracture conductivity tests. The density of 70/140 mesh ceramic particles and 40/70 mesh ceramic particles is 2.7 g/cm<sup>3</sup>, and the proppant transport is mainly studied through the proppant plate transport experiment device. The fracture conductivity is tested using high-temperature and high-pressure conductivity equipment according to API standards.

## 2.2 Proppant transport evaluation

In this paper, the proppant plate transport experiment device was used to simulate the transport process of ceramicites with different particle sizes and different concentrations in fractures.



At the same time, the shape of sand embankment is quantitatively characterized by digital method.

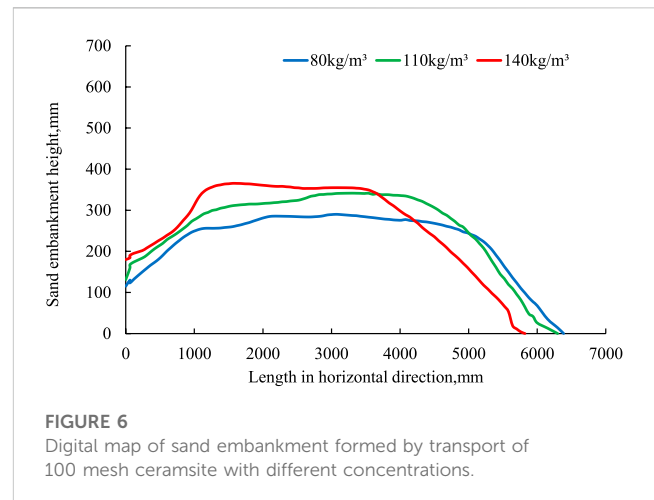
A visual evaluation device for proppant transport was designed to study proppant placement in fractures during fracturing. The equipment is mainly composed of sand mixing container, displacement pump and tempered glass plates (Figure 4). The tempered glass plates is the main part of the device. The fracture is simulated by two transparent tempered glass plates placed in parallel. The length of the tempered glass plate is 7 m and the height is 0.7 m.

Compared with the current conventional proppant transport evaluation equipment, the size of the experimental device designed in this study is larger. The length of the traditional transport evaluation device is about 3 m [33], and the length of this device is as high as 7 m. At the same time, the power of the displacement pump is larger, which can pump the sand carrying fluid with high displacement. At the same time, the inner wall of the tempered glass plate is rough, which can more truly simulate the transport of proppant in the fracture.

In the experiment, the fracturing fluid and ceramsite were mixed in the sand mixing container. The fracturing fluid was then displaced into the tempered glass plates by the displacement pump. The proppant in simulated fractures will fall under gravity, and during the experiment, a high-speed camera was used to record the shape of the sand embankment in real time, and the final shape of the sand embankment was described by digital method. In this experiment, the clean fracturing fluid with viscosity of 40 mPas is used as the sand carrying fluid, and the particle size of ceramsite is 40/70 mesh and 100 mesh. The injection displacement is constant at 50 L per minute.

The equilibrium height and non-uniform coefficient of sand embankment are used to describe the sand embankment [34]. The equilibrium height of the sand embankment is the height of the sand embankment when the proppant particles are in equilibrium. The non-uniformity coefficient is calculated by the variance of the sand embankment height per unit section length. The non-uniformity coefficient is used to measure the uniformity of the distribution of the sand embankment in the height direction. The smaller the non-uniformity coefficient, the more uniform the proppant placement.

It can be seen from Figure 5 that with the increase of 40/70 mesh ceramsite concentration, the transport length of ceramsite in the simulated fracture length direction gradually becomes shorter, and it



is difficult for high concentration ceramsite to be transported to the fracture tip. The total length of sand embankment formed by ceramsite with the concentration of 80 kg/cm<sup>3</sup> is 5,780 mm, which is about 28% longer than that formed by ceramsite with the concentration of 140 kg/cm<sup>3</sup>.

During the transport process in the simulated fracture, the proppant will gradually sink and accumulate at the bottom of the fracture, thus forming a sand embankment and gradually increasing the height of the sand dike. When the settlement speed of proppant and the forward speed of proppant carried by fracturing fluid balance each other, the height of sand embankment will not increase any more. At this time, the height of sand embankment is called the equilibrium height of sand embankment [35, 36]. The greater the equilibrium height of the sand embankment is, the better the proppant can support the fracture height. However, since the total amount of proppant is certain, the height and length of the sand embankment always show a trend of trade-off. Therefore, the height and length of the sand embankment should be taken into account when optimizing the concentration of proppant.

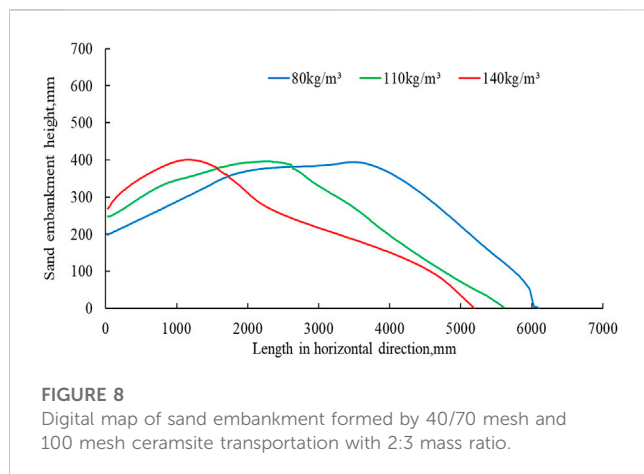
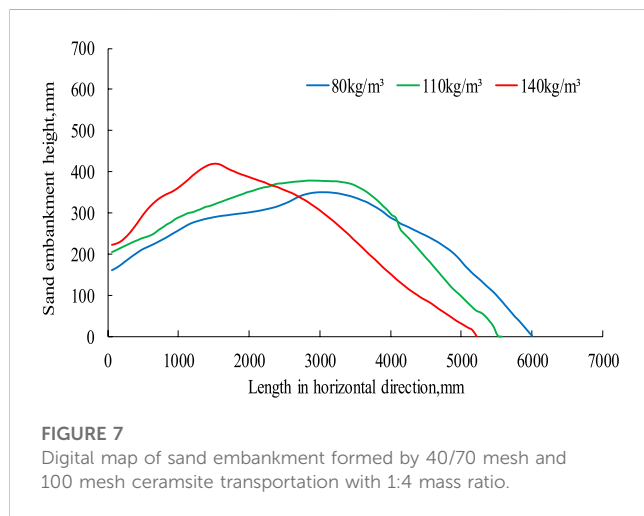
As shown in Figure 6 with the increase of 100 mesh ceramsite concentration, the transport length of ceramsite in the simulated fracture length direction gradually becomes shorter, but the difference in the length of sand embankment formed by ceramsite with different concentrations is very small. The total length of sand embankment formed by ceramsite with 80 kg/cm<sup>3</sup> concentration is only about 7% longer than that formed by ceramsite with 140 kg/cm<sup>3</sup> concentration.

It can be seen from Table 1 that with the increase of proppant particle size, the equilibrium height and non-uniformity coefficient of sand embankment gradually increase, and the overall length of sand embankment gradually decreases. This is because the ceramsite with small particle size is easy to carry, and it can move a large distance in the fracture. When the particle size of ceramsite increases, the increase of ceramsite settlement speed will lead to the sharp increase of the non-uniformity of the sand embankment at the same time.

The effective closure pressure of ultra deep carbonate reservoirs in China is approximately 50 MPa [37]. Small particle size proppant is difficult to obtain high conductivity under high closure pressure. Although large particle size proppant can provide higher fracture conductivity, the addition of large particle size proppant in ultra

**TABLE 1** Comparison of the sand embankment formed by ceramicsite transportation with different concentration and particle size.

Proppant type	Proppant concentration, kg/m <sup>3</sup>	Balance height of sand embankment, mm	Overall length of sand embankment, mm	Non-uniform coefficient
100 mesh ceramicsite	80	257	6,385	0.0009
	110	349	6,000	0.0015
	140	364	6,034	0.0021
40/70 mesh ceramicsite	80	329	5,764	0.0024
	110	378	4,981	0.0031
	140	412	4,668	0.0038



deep carbonate fracturing is easy to cause sand plug [38]. In order to effectively support the fracture tip, it is necessary to study the characteristics of proppant transport morphology and conductivity formed by mixing large and small particle size proppants.

In this paper, 40/70 mesh ceramicsite and 100 mesh ceramicsite are mixed according to the mass ratio of 1:4 and 2:3 to test the transport form and conductivity of the proppant with combined particle size

in the fracture. The experimental goal is to optimize the proppant combination that can not only transport to the fracture tip, but also provide high conductivity.

It can be seen from Figures 7, 8 that the transport patterns of ceramicsite with mixed particle size in the fractures are roughly the same. With the increase of proppant concentration, the horizontal transport distance of the sand embankment gradually decreases, and the time period for the sand embankment to maintain the equilibrium state gradually decreases.

It can be seen from Table 2 that with the increase of the mass proportion of 100 mesh ceramicsite in the proppant, the nonuniformity coefficient of the sand embankment formed by the proppant with the same concentration is lower, indicating that a more balanced sand embankment shape can be obtained by using a large number of small particle size ceramicsite.

There are many fractures and corrosion cavities in carbonate reservoir, so the fluid loss during stimulation is relatively large, which leads to sand plugging during fracturing [39]. Because the essence of compound acid fracturing is to support the fracture tip with proppant, and other parts of the fracture are etched with acid to form conductivity, it is unnecessary to add too much proppant to compound acid fracturing [40].

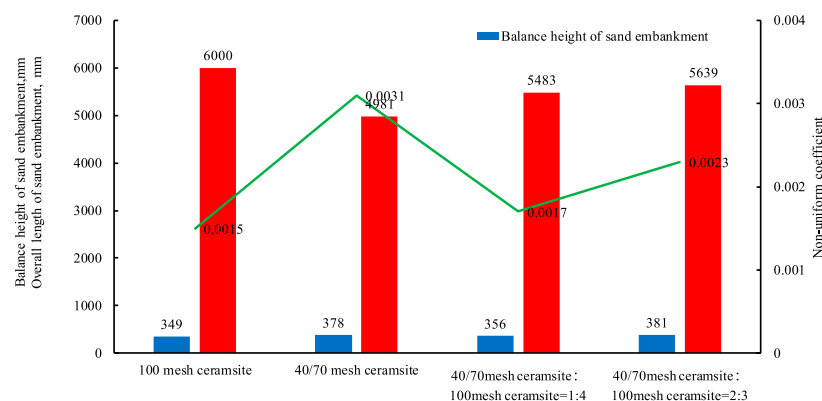
The purpose of compound acid fracturing is to deliver proppant to the fracture tip and form effective support at the fracture tip. In this way, the sand embankment not only has a large length and height, but also has a relatively small non-uniform coefficient [41]. It can be seen from Figure 9 that when only 100 mesh ceramicsite is added or the mass ratio of 100 mesh ceramicsite to 40/70 mesh ceramicsite is 4:1, the non-uniform coefficient of sand dike formed by proppant transport is small and the height and length of sand dike are large.

## 2.3 Fracture conductivity test

When only 100 mesh ceramicsite or the mass ratio of 100 mesh ceramicsite to 40/70 mesh ceramicsite is 4:1, the shape of the sand embankment is relatively balanced, and the height and length of the sand embankment have good extension effects. The concentration and combination of proppant are optimized according to the experimental results of compound acid fracturing conductivity test. This paper focuses on the fracture conductivity when adding different concentrations of 100 mesh ceramicsite or 40/70 mesh ceramicsite and 100 mesh ceramicsite with a mass ratio of 4:1, so as to select the best proppant combination and concentration.

**TABLE 2** Comparison of the sand embankment formed by ceramsite transportation with different concentration and particle size.

Mass ratio of 40/70 mesh and 100 mesh proppant	Proppant concentration, kg/m <sup>3</sup>	Balance height of sand embankment, mm	Overall length of sand embankment, mm	Non-uniform coefficient
1:4	80	309	6,001	0.0012
	110	356	5,483	0.0017
	140	388	5,162	0.0024
2:3	80	362	5,968	0.0018
	110	381	5,639	0.0023
	140	398	5,175	0.0029

**FIGURE 9**

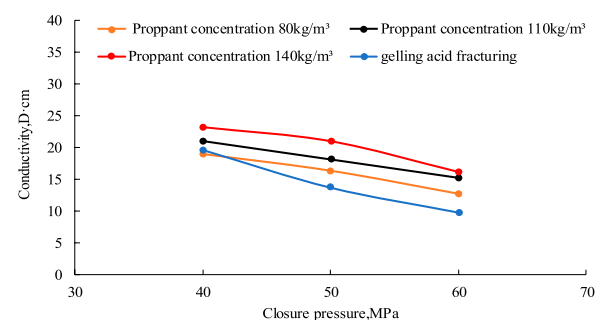
Comparison of sand dike parameters formed by different proppant.

The FCES-100 fracture conductivity meter produced by American Core Lab Company is used for the conductivity test. The maximum loading closure pressure of the instrument can be 120 MPa, and the ambient temperature can be heated to 160°C. The instrument meets the stress and temperature characteristics of ultra-deep and high-temperature carbonate reservoirs, and it can test the conductivity of proppant or the conductivity of acid etched fractures.

In order to ensure the reliability of the experimental results, carbonate rock slabs with the same rock mineral composition are used to carry out the experiment. First, drive the acid solution to corrode the surface of the carbonate rock slab, then pave ceramsite on the surface of the acid etched rock slab, and finally test the fracture conductivity.

We put 100 mesh ceramsite of three concentrations on the etched rock plate to test the fracture conductivity, so as to evaluate the change of the acid etched fracture conductivity after adding 100 mesh ceramsite. It can be seen from Figure 10 that with the increase of closure pressure, the fracture conductivity is generally declining. The fracture conductivity formed by acid + proppant is significantly higher than that of acid etched fractures. The fracture conductivity when the proppant concentration is 140 kg/m<sup>3</sup> is 64% higher than that of acid etched fractures.

The fracture conductivity with the proppant concentration of 140 kg/m<sup>3</sup> is only 5% more than that with the proppant concentration of 110 kg/m<sup>3</sup>. This is mainly because some proppant are filled into the grooves of acid etched fracture, which not only cannot improve the fracture conductivity, but may reduce the fracture conductivity [42].

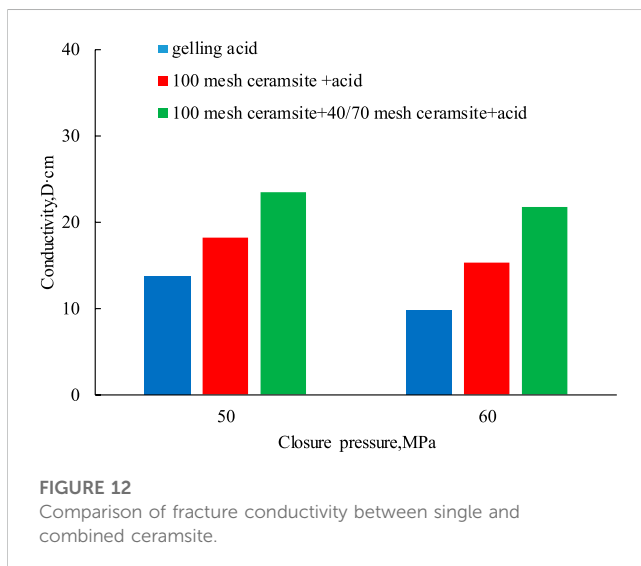
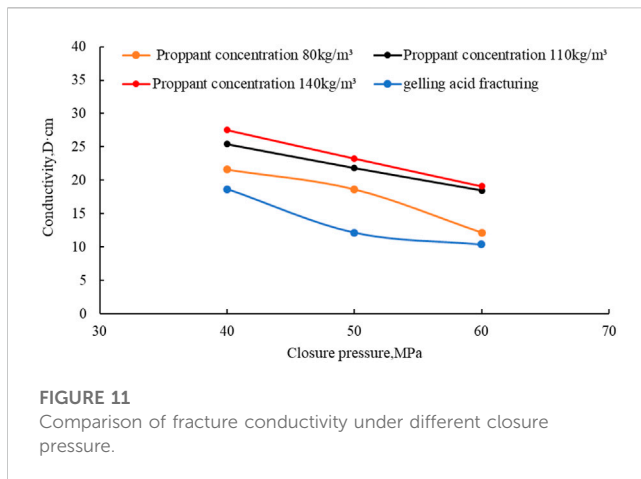
**FIGURE 10**

Comparison of fracture conductivity under different closure pressure.

We laid 40/70 mesh ceramsite and 100 mesh ceramsite on the etched rock slab in a 1:4 mass ratio to test the fracture conductivity, so as to evaluate the change of the fracture conductivity after adding 40/70 mesh ceramsite and 100 mesh ceramsite.

It can be seen from Figure 11 that the conductivity of proppant is greater than that of acid etched fracture. When the proppant concentration reaches 110 kg/m<sup>3</sup>, increasing the proppant concentration will not significantly improve the fracture conductivity.





It can be seen from Figure 12 that when the proppant concentration is also 110 kg/m<sup>3</sup>, the conductivity of 100 mesh ceramsite is significantly different from that of combined particle size ceramsite, and the combined particle size ceramsite is composed of 40/70 mesh and 100 mesh ceramsite in a 1:4 mass ratio. When the closure pressure is 50 MPa, the conductivity of composite ceramsite is 28.4% higher than that of 100 mesh ceramsite. When the closure pressure rises to 60 MPa, the conductivity of composite ceramsite is 43.0% higher than that of 100 mesh ceramsite, and 123% higher than the conductivity of gelling acid etched fracture.

## 2.4 Field application

The average buried depth of KL oil and gas field reservoir in China is 7,400 m, the reservoir temperature is 168°C, the average porosity is 2.7%, and the average permeability is 0.47 mD. The

reservoir is characterized by ultra deep, ultra high temperature and low permeability. In the early stage, KL Oilfield used gelling acid fracturing technology, and after acid fracturing, the gas well produced only about 40,000 m<sup>3</sup> of natural gas per day. Six wells in KL Oilfield with similar reservoir physical properties were selected for field test of composite acid fracturing technology. On average, 100 mesh ceramsite with a weight of 600 kg, 40/70 mesh ceramsite with a weight of 150 kg and 700 m<sup>3</sup> gelled acid were used in a single well, and the maximum injection displacement was 6 m<sup>3</sup>/min. After the completion of acid fracturing, the fracturing software is used to analyze the acid fracturing fracture parameters. The analysis results show that the fracture length of composite acid fracturing is 38% higher than that of gelled acid fracturing, and the fracture conductivity is 118% higher than that of gelled acid fracturing. The composite stimulation technology has been applied to 9 wells in carbonate and shale oil and gas reservoirs. After fracturing, the production of oil and gas wells is 210% higher than that of gelled acid fracturing, and the composite stimulation technology has achieved good stimulation effects.

## 3 Conclusion

- (1) By combining the advantages of hydraulic fracturing and acid fracturing, using proppant to fill the fracture tip that cannot be corroded by acid fluid, and using retarded acid to corrode the rest of the fracture. The compound acid fracturing can achieve full support of the fracture, especially improve the acid fracturing effect of the fracture tip.
- (2) Through the visualization experiment of proppant migration, it can be seen that the shape equilibrium height and migration length of sand dike formed by single particle size proppant are not ideal, and larger equilibrium height and migration length can be obtained by using combined particle size proppant.
- (3) When 100 mesh ceramsite and 40/70 mesh ceramsite are mixed, the fracture conductivity is significantly improved, especially 123% compared with the gelled acid etching fracture. The composite acid fracturing technology has achieved good application effect in ultra deep, high temperature and low permeability oil and gas fields, which can improve the gas production of such gas fields.
- (4) Compared to the existing acid fracturing and hydraulic fracturing technologies, the composite stimulation technology proposed in this article combines the advantages of the acid fracturing and hydraulic fracturing technology, which not only improves the conductivity and length of fractures, but also reduces the risk of sand plugging in low-permeability reservoir fracturing.
- (5) In order to accurately describe the migration of ceramic particles in rough fractures, it is recommended to combine PIV particle imaging technology to further finely describe the migration mechanism and influencing factors of ceramic particles in different viscosity fracturing fluids.

## Data availability statement

The original contributions presented in the study are included in the article/supplementary material, further inquiries can be directed to the corresponding author.

## Author contributions

YW: Conceptualization, funding acquisition, project administration, resources, writing—original draft and software. Data curation, formal analysis, methodology. ZL: writing—review & editing. All authors contributed to the article and approved the submitted version.

## Funding

This work was financially supported by the project of the PetroChina Southwest Oil and Gas Field Company (Grant Nos. 20200302-14,

20210302-19, 20220302-11). The funder was not involved in the study design, collection, analysis, interpretation of data, the writing of this article, or the decision to submit it for publication.

## Conflict of interest

Authors YW and ZL were employed by PetroChina Southwest Oil and Gas Field Company.

## Publisher's note

All claims expressed in this article are solely those of the authors and do not necessarily represent those of their affiliated organizations, or those of the publisher, the editors and the reviewers. Any product that may be evaluated in this article, or claim that may be made by its manufacturer, is not guaranteed or endorsed by the publisher.

## References

- Wang Y, Zhou C, Yi X, Li L, Chen W, Han X. Technology and application of segmented temporary plugging acid fracturing in highly deviated wells in ultradeep carbonate reservoirs in southwest China. *ACS omega* (2020) 5(39):25009–15. doi:10.1021/acsomega.0c01008
- Wang Y, Fan Y, Zhou C, Luo Z, Chen W, He T, et al. Research and application of segmented acid fracturing by temporary plugging in ultradeep carbonate reservoirs. *ACS omega* (2021) 6(43):28620–9. doi:10.1021/acsomega.1c03021
- Ningning Z, Dengfa H, Yanpeng S, Haowu L. Distribution patterns and controlling factors of giant carbonate rock oil and gas fields worldwide[J]. *China Pet Exploration* (2014) 19(6):54.
- Lu YUN. Controlling effect of NE strike slip fault system on reservoir development and hydrocarbon accumulation and its geological significance in the eastern Shunbei area, Tarim Basin[J]. *China Pet Exploration* (2021) 26(3):41.
- Li J, Wang X, Zhou K, Wang Y, Li N, Wu Y, et al. Characteristics of ultra-deep shale reservoir of marine-continental transitional facies[J]. *Pet Geology Exp* (2022) 44(1):72–82.
- Haitao L, Geng F, Shang K. Key factors and directions of exploration in the Cambrian pre-salt sequence, Tarim Basin[J]. *Oil Gas Geology* (2022) 43(5):1049–57.
- Xinhua MA, Haijun YAN, Jingyuan C. Development patterns and constraints of superimposed karst reservoirs in Sinian Dengying Formation, Anyue gas field, Sichuan Basin[J]. *Oil Gas Geology* (2021) 42(6):1281–94.
- Wang Y, Zhou C, Zhang H, He T, Tang X, Peng H, et al. Research and application of segmented acid fracturing technology in horizontal wells of ultra deep carbonate gas reservoirs in southwest China[C]. In: Proceeding of the International Petroleum Technology Conference; Virtual. OnePetro (2021).
- Jianzhong LI, Bin B, Ying B, Lu X, Zhang B, Shengfei Q, et al. Fluid evolution and hydrocarbon accumulation model of ultra-deep gas reservoirs in Permian Qixia Formation of northwest Sichuan Basin, SW China[J]. *Pet Exploration Dev* (2022) 49(4):719–30.
- Xiao D, Cao J, Luo B, Zhang Y, Xie C, Shuangling C, et al. Mechanism of ultra-deep gas accumulation at thrust fronts in the Longmenshan Mountains, lower Permian Sichuan Basin, China. *J Nat Gas Sci Eng* (2020) 83:103533. doi:10.1016/j.jngse.2020.103533
- Qi L, Structural characteristics and storage control function of the Shun I fault zone in the Shunbei region, Tarim Basin. *J Pet Sci Eng* (2021) 203:108653. doi:10.1016/j.petrol.2021.108653
- Li N, Feng Y, Liu P, Luo Z, Zhao L. Study of acid-rock reaction kinetics under high temperature and pressure conditions based on the rotating disk instrument. *Arabian J Sci Eng* (2015) 40(1):135–42. doi:10.1007/s13369-014-1504-x
- Xue H, Huang Z, Zhao L, Wang H, Kang B, Liu P, et al. Influence of acid-rock reaction heat and heat transmission on wormholing in carbonate rock. *J Nat Gas Sci Eng* (2018) 50:189–204. doi:10.1016/j.jngse.2017.12.008
- Deng J, Mou J, Hill AD, Zhu D. A new correlation of acid-fracture conductivity subject to closure stress. *SPE Prod Operations* (2012) 27(02):158–69. doi:10.2118/140402-pa
- Aljawad MS, Zhu D, Hill AD. Modeling study of acid fracture fluid system performance. In: Proceeding of the SPE 179109 presented at the Hydraulic Fracturing Technology Conference; Texas, USA. The Woodlands (2016).
- Hou B, Zhang R, Chen M, Kao J, Liu X. Investigation on acid fracturing treatment in limestone formation based on true tri-axial experiment. *Fuel* (2019) 235:473–84. doi:10.1016/j.fuel.2018.08.057
- Zhang L, Zhou F, Mou J, Xu G, Zhang S, Li Z. A new method to improve long-term fracture conductivity in acid fracturing under high closure stress. *J Pet Sci Eng* (2018) 171:760–70. doi:10.1016/j.petrol.2018.07.073
- Wang Y, Fan Y, Wang T, Ye J, Luo Z. A new compound staged gelling acid fracturing method for ultra-deep horizontal wells. *J Gels* (2022) 8(7):449. doi:10.3390/gels8070449
- Wang Y, Yang J, Wang T, Hu Q, Lv Z, He T. Visualization experiment of multi-stage alternating injection acid fracturing. *Energ Rep* (2022) 8:9094–103. doi:10.1016/j.egyr.2022.07.031
- Ye JX, Li L, Han HF, Zhang SQ, Xue H, Zhang ZC, et al. Optimization research of multistage alternating acid fracturing: A case study of reservoir reconstruction for longwangmiao Formation in moxi-longnvsi area[J]. *Reservoir Eval Dev* (2018) 8(3):46–50.
- Wu Y, Hu W, Wang M, Yao L, Fang H, Jia X, et al. Composite acid fracturing technology based on flow conductivity evaluation experiments[J]. *Science Technology and Engineering* (2018) 20(31):12276–12780.
- Dang L, Zhou C, Huang M, Jiang D. Simulation of effective fracture length of prepad acid fracturing considering multiple leak-off effect. *Nat Gas Industry B* (2019) 6(1):64–70. doi:10.1016/j.ngib.2019.01.009
- Dong R, Wheeler MF, Ma K, Su H. A 3D acid transport model for acid fracturing treatments with viscous fingering[C]. In: SPE Annual Technical Conference and Exhibition. Virtual. OnePetro (2020).
- Wang D, Zlotnik S, Diez P, Ge H, Zhou F, Yu B. A numerical study on hydraulic fracturing problems via the Proper generalized decomposition method. *CMES: Comput Model Eng Sci* (2020) 122(2):703–20. doi:10.32604/cmesci.2020.08033
- Na AN, Luo P, Yongshou LI, Fang Y, Jiao K. Development of solid granular acid for the deep acid-fracturing of carbonate reservoirs[J]. *Pet drilling Tech* (2020) 48(2):93–7.
- Wang Y, Zhou C, Yi X, Li L, Zhou J, Han X, et al. Research and evaluation of a new autogenic acid system suitable for acid fracturing of a high-temperature reservoir. *ACS omega* (2020) 5(33):20734–8. doi:10.1021/acsomega.0c00336
- Zhao Z, Sun C, Liu Y. High-temperature-resistant diverting acid for carbonate formation fracturing in sichuan basin: a property evaluation and field study[J]. *Geofluids* (2022).
- Sui Y, Cao G, Guo T, Li Z, Bai Y, Li D, et al. Development of gelled acid system in high-temperature carbonate reservoirs. *J Pet Sci Eng* (2022) 216:110836. doi:10.1016/j.petrol.2022.110836

29. Du J, Guo G, Liu P, Xiang G, Cheng P, Liu J, et al. Experimental study on the autogenic acid fluid system of a high-temperature carbonate reservoir by acid fracturing. *ACS omega* (2022) 7(14):12066–75. doi:10.1021/acsomega.2c00259
30. Qingzhi W, Yingtao Y, Feng W. Experimental study on an innovative proppant placement method for channel fracturing technique[J]. *J China Univ Pet (Edition Nat Science)* (2016) 40(5):112–7.
31. Wen Q, Jinjian GAO, Hua LIU, Liu X, Wang S, Wang F. Dynamic experiment on slick-water prop-carrying capacity[J]. *Oil Drilling Prod Tech* (2015) 37(2): 97–100.
32. Barboza BR, Chen B, Li C. A review on proppant transport modelling. *J Pet Sci Eng* (2021) 204:108753. doi:10.1016/j.petrol.2021.108753
33. Desheng Z, Zheng Z, Feng HUI, Yuhua S, Chaoneng Z, Yuan Z. Experiment and numerical simulation on transportation laws of proppant in major fracture during slick water fracturing[J]. *Oil Drilling Prod Tech* (2017) 39(4):499–508.
34. Zhang K, Zhang T, Wu S, Li N, He S. Simulation of proppant transport in fracture with different combinations of particle size[J]. *Reservoir Eval Dev* (2019) 9(6):72–7.
35. Liu X, Zhang X, Wen Q, Zhang S, Liu Q, Zhao L. Experimental research on the proppant transport behavior in nonviscous and viscous fluids. *Energy and Fuels* (2020) 34(12):15969–82. doi:10.1021/acs.energyfuels.0c02753
36. Suri Y, Islam SZ, Hossain M. Effect of fracture roughness on the hydrodynamics of proppant transport in hydraulic fractures. *J Nat gas Sci Eng* (2020) 80:103401. doi:10.1016/j.jngse.2020.103401
37. Tingxue J, Jun Z, Wenfeng J, Linbo Z. Deep penetration acid-fracturing technology for ultra-deep carbonate oil and gas reservoirs in the Shunbei Oil and Gas Field[J]. *Pet Drilling Tech* (2019) 47(3):140–7.
38. Yudi G, Linbo Z, Yang W. High conductivity acid fracturing technology in ultra-deep carbonate reservoir[J]. *Reservoir Eval Dev* (2019) 9(6):56–60.
39. Liu M, Zhang S, Mou J, Zhou F. Wormhole propagation behavior under reservoir condition in carbonate acidizing. *Transport in porous media* (2013) 96(1):203–20. doi:10.1007/s11242-012-0084-z
40. Zhu W, Liu Q, Yue M, Zhang L. Calculation of fracture conductivity considering proppant influence and simulation of proppant transport in fracture[J]. *Chem Eng Oil Gas* (2019) 48(2):75–8.
41. Zhou J, Zhou L, Jiang T, Zhang J. Experimental study on the fracture conductivity of ultra-deep carbonate reservoirs by channel sanding acid fracturing[J]. *Chem Eng Oil Gas* (2019) 48(2):75–8.
42. McDaniel G, Abbott J, Mueller F, Mokhtar A, Pavlova S, Nevvonen O, et al. Changing the shape of fracturing: new proppant improves fracture conductivity[C]. In: SPE Annual Technical Conference and Exhibition. Florence, Italy: OnePetro (2010).



## OPEN ACCESS

## EDITED BY

G. Cheraghian,  
Technical University of Braunschweig,  
Germany

## REVIEWED BY

Cuiying Jian,  
York University, Canada  
Lu Lee,  
University of Wyoming, United States

## \*CORRESPONDENCE

Yili Kang,  
✉ CWCT\_FDC@163.com  
Jingyi Zhang,  
✉ swpuzjy@163.com

RECEIVED 25 October 2022

ACCEPTED 18 April 2023

PUBLISHED 06 July 2023

## CITATION

Zhang J, Kang Y, Deng Y, Xu C, Yan X,  
Lin C and Cui X (2023), An experimental  
evaluation method of drilling fluid lost  
control efficiency considering loss types.  
*Front. Phys.* 11:1079345.  
doi: 10.3389/fphy.2023.1079345

## COPYRIGHT

© 2023 Zhang, Kang, Deng, Xu, Yan, Lin  
and Cui. This is an open-access article  
distributed under the terms of the  
[Creative Commons Attribution License  
\(CC BY\)](https://creativecommons.org/licenses/by/4.0/). The use, distribution or  
reproduction in other forums is  
permitted, provided the original author(s)  
and the copyright owner(s) are credited  
and that the original publication in this  
journal is cited, in accordance with  
accepted academic practice. No use,  
distribution or reproduction is permitted  
which does not comply with these terms.

# An experimental evaluation method of drilling fluid lost control efficiency considering loss types

Jingyi Zhang<sup>1,2\*</sup>, Yili Kang<sup>2\*</sup>, Yunhui Deng<sup>1</sup>, Chengyuan Xu<sup>2</sup>,  
Xiaopeng Yan<sup>3</sup>, Chong Lin<sup>4</sup> and Xiaojiang Cui<sup>1</sup>

<sup>1</sup>China Zhenhua Oil Co., Ltd., Beijing, China, <sup>2</sup>State Key Laboratory of Oil and Gas Reservoir Geology and Exploitation, Southwest Petroleum University, Chengdu, China, <sup>3</sup>School of Petroleum and Natural Gas Engineering, Changzhou University, Changzhou, China, <sup>4</sup>CCDC Drilling and Production Technology Research Institute, Guanghan, China

There are serious drilling fluid loss problems in fractured reservoirs during drilling and completion. Indoor evaluation of the drilling fluid lost control effect is an important basis for on-site plugging formula design, but there are some problems in drilling fluid lost control evaluation, such as the inability to evaluate specific loss types. Therefore, based on the classification of loss causes, this paper defines the main control factors of drilling fluid lost control efficiency of different loss types and puts forward a method for recognizing loss types. The influence of fracture module and experimental steps on the drilling fluid lost control efficiency was evaluated through laboratory experiments. Based on the analysis method of indoor and field drilling fluid lost control efficiency, the best laboratory experimental conditions of different loss types were recommended, and then, the experimental evaluation method of the drilling fluid lost control efficiency considering various loss types was established. This method can comprehensively evaluate and grade the lost control ability of the plugging formula. Through the verification in Block K of the Tarim Basin, the test results are closer to the field lost control results, and the evaluation results of the drilling fluid lost control efficiency are better, which can guide the field leakage control evaluation.

## KEYWORDS

lost circulation, fractured reservoir, loss control, reservoir protection, lost circulation formula, evaluation method

## 1 Introduction

The lost control of drilling fluid in deep fractured formation has become a common problem encountered in the field of oil and gas, and deep geothermal engineering. Lost circulation will not only directly cause significant economic losses and increase non-productive time but also induce safety accidents [1–3]. Reservoir loss will seriously hinder the discovery and production of oil and gas resources. Scholars have conducted a lot of research work on the drilling fluid loss control from aspects of the lost circulation type, lost circulation mechanism, new plugging materials, and plug formula optimization [4–8]. According to the causes of loss, loss can be divided into three categories, which include induced fracture type loss, fracture propagation type loss, and natural fracture type loss [9–11]. Induced fracture loss refers to the undisturbed intact

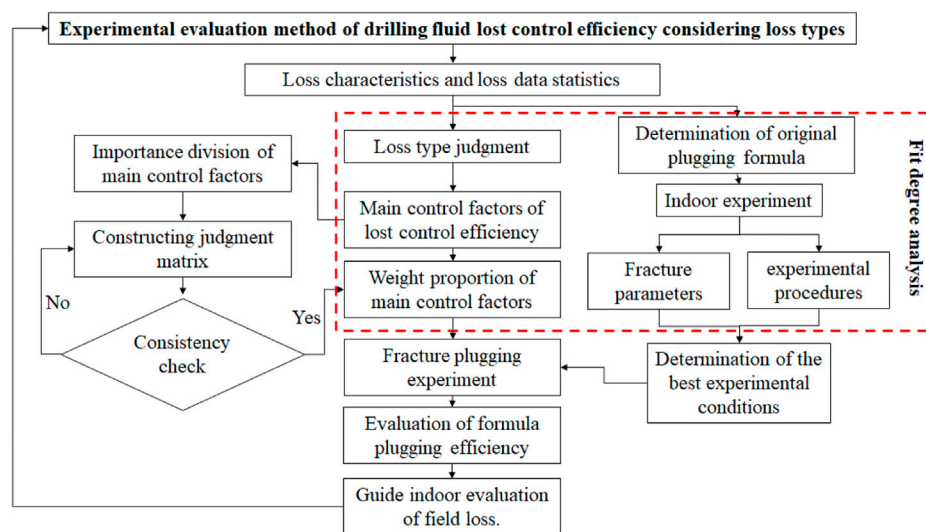


FIGURE 1

Flow chart of the experimental evaluation method for the drilling fluid lost control efficiency.

rock mass near the wellbore. When the effective pressure of the drilling fluid column is greater than the formation breakdown pressure, fracture occurs and extends. Fracture propagation type loss refers to the phenomenon that after the pressure of the drilling fluid column is transmitted to the fracture surface, the geometric size of the fracture increases due to the comprehensive influence of positive pressure difference, temperature, and seepage, and finally, the solid and liquid phases of the drilling fluid enter the formation. Natural fracture loss refers to the phenomenon that the drilling fluid enters formation freely through a natural fracture connecting wellbore and formation once pressure difference is observed.

Drilling fluid lost control efficiency is the comprehensive embodiment of the effect and ability of controlling loss. Laboratory experiments are often carried out to evaluate the plugging ability of the plugging formula. Since 1960s, scholars have been continuously improving the experimental means to simulate and evaluate the formation loss and to evaluate the appropriate plugging materials and technologies. However, at present, laboratory instruments are diversified, such as the API static plugging tester, crevice plugging tester, and high-temperature and high-pressure drilling fluid loss dynamic evaluation tester [8, 12–17]. There are different experimental methods, such as thin-fractured plate fracture plugging, standard core fracture plugging, and long core fracture plugging [17–25]. Therefore, this will lead to deviation of the experimental results, which cannot reflect the evaluation results of the drilling fluid lost control efficiency of specific loss types. Commonly used indicators to characterize the effect and ability of drilling fluid lost control include the pressure bearing capacity, sealing time, loss amount, and loss rate [24–32]. However, when evaluating the effect and ability of lost control, single or several indicators are mostly used, which lead to the evaluation results being not systematic, sufficient, and accurate. In order to comprehensively evaluate the effect and ability of drilling fluid

lost control in fractured formations, this paper presents an experimental evaluation method of the drilling fluid lost control efficiency considering loss types. By analyzing the control efficiency and main control factors of drilling fluid loss, the relative weight ratio of main control factors is defined. Based on the coincidence degree of the indoor and field drilling fluid lost control efficiency, the reasonable fracture module parameters and experimental steps for indoor evaluation of the drilling fluid lost control efficiency are put forward, and then, the application strategy of the experimental evaluation method of the drilling fluid lost control efficiency in fractured formation is formed. By the field test in Block K in the Tarim Basin, the feasibility of this method is verified, providing ideas for field drilling fluid lost control.

## 2 Methodology

The flow of the experimental evaluation method of the drilling fluid lost control efficiency is shown in Figure 1. First, according to the geological data on the work area and the drilling fluid loss situation, the drilling fluid loss type was determined, the main control factors of the lost control efficiency were analyzed, and the weight proportion of the main control factors was calculated. The formula of field plugging slurry is adopted, and the formula of indoor and field plugging slurry is consistent. The influence of fracture module parameters and experimental steps on the drilling fluid lost control efficiency is studied by a single factor. Based on the analysis of the coincidence degree between the indoor and field drilling fluid lost control efficiency, the best indoor experimental conditions for different types of losses are determined. Then, an indoor crack plugging simulation experiment is carried out, and the evaluation result of the plugging formula is obtained so as to guide the indoor evaluation of the field lost control.



## 2.1 Judgment of the drilling fluid loss type in fractured formation

The loss types of fractured formation can be divided into induced fracture loss, fracture propagation loss, and natural fracture loss. By collecting the field engineering geological characteristic data on fractured formation and referring to the dynamic model of drilling fluid loss, the drilling fluid loss rate–time characteristic curve of the loss model is made as the characteristic layout, the data on the drilling fluid loss rate in the early stage of drilling fluid loss in the well to be determined are recorded, the drilling fluid loss rate–time curve is drawn, and the field drilling fluid loss rate–time curve is compared with the characteristic charts of different loss types to determine the drilling fluid loss types in fractured formation.

## 2.2 Drilling fluid lost control efficiency and main control factors

### 2.2.1 Analysis of the drilling fluid lost control efficiency

The effect and ability of drilling fluid lost control are comprehensively influenced by the strength, efficiency, and compactness of the fracture plugging zone. Commonly used indicators to characterize the effect and ability of drilling fluid lost control include the pressure bearing capacity, sealing time, loss amount, and loss rate, but there is no uniform standard and requirement for the application of evaluation indicators at present. These conditions lead to differences in the evaluation results of indoor experiments. In this paper, the plugging strength, plugging efficiency, and plugging compactness of the fractured plugging zone are comprehensively considered; the control efficiency of the drilling fluid loss in fractured formation is determined by the three factors; and the plugging strength, plugging efficiency, and plugging compactness are measured by the pressure bearing capacity, initial loss, and cumulative loss. The strength of the bearing capacity is a comprehensive reflection of the strength and structural stability of a fracture sealing zone. The strength of the fracture sealing zone can be characterized by measuring the strength of bearing capacity [33]. Bearing capacity refers to the difference between the corresponding wellbore liquid column pressure and formation pressure when the fracture sealing zone is destroyed. The greater the bearing capacity, the stronger the resistance of the fracture sealing zone to external forces and the more stable the structure. The initial loss reflects the formation efficiency of the fracture sealing zone, that is, the sealing efficiency. Initial loss refers to the loss of drilling fluid before the formation of the fracture sealing zone after the plugging material enters the fracture, which is characterized by the loss 1 min before the formation of the sealing zone. The smaller the initial loss is, the shorter the time it takes for the lost circulation material (LCM) to bridge and form the fracture sealing zone. The cumulative loss is a comprehensive reflection of the structural compactness of the fracture sealing zone. The denser the fracture plugging zone structure, the less drilling fluid will be lost. Cumulative loss refers to the loss of drilling fluid from the time the LCM enters the fracture to the time when the fracture plugging

zone is destroyed. The smaller the cumulative loss, the denser the structure of the fracture sealing zone.

### 2.2.2 Controlling factors of the drilling fluid lost control efficiency

The main control factors of the drilling fluid lost control efficiency are different with different loss types, and the influence of plugging strength, plugging efficiency, and plugging compactness on the drilling fluid lost control efficiency is different, which makes the pressure bearing capacity, initial loss, and cumulative loss of the plugging zone have different weights in the comprehensive evaluation of the drilling fluid lost control efficiency.

Loss occurs when the working fluid density is very high for a low-pressure formation. The longer the fracture extends, the harder it is to plug. In addition, the more drilling fluid leaks, the harder it is to plug. Fluid lost control should include both prevention treatment and plugging treatment. The fluid lost control should be fast and efficient to avoid formation failure and further extension of fractures. The plugging effect depends on the fracture restart pressure and propagation pressure after the lost circulation control. For induced fracture loss, plugging fracture in time is the key to improving the plugging efficiency and drilling fluid lost control efficiency.

Fracture propagation type loss means the condition under a comprehensive influence of positive pressure difference, temperature and seepage, fracture propagation, and the solid–liquid two-phase drilling fluid flow. The fracture extends from the original width to loss fracture width and then a fracture network. The plugging effect depends on the fracture propagation pressure and plugging zone strength. For this type, the improving drilling fluid lost control efficiency should focus on plugging operation time and plugging intensity.

Natural fracture type loss refers to the type that the conventional plugging technology can successfully plug the fracture, which is often accompanied by fracture expansion and extension, making the conventional plugging method difficult to work.

The drilling fracture opening has reached the loss opening and is connected into a network. As the sealing range becomes wide, the number of weak sealing points increases. The main goal should be sealing the lost channel. The plugging effect depends on the strength and compactness of the plugging zone. Natural fracture type leakage does not require a high plugging efficiency as long as the leakage channel can be plugged to make the fracture plugging zone have a certain strength. The control efficiency of drilling fluid loss depends on whether it can be plugged and the plugging strength.

It is summarized that the main control factor of the induced fracture type lost control efficiency is the plugging efficiency. The main control factor of the fracture propagation type lost control efficiency is the plugging efficiency and plugging intensity. In addition, the main control factor of the natural fracture type lost control efficiency is plugging intensity and plugging compactness.

## 2.3 Analysis of weight proportion of main control factors

The main control factors of the drilling fluid lost control efficiency are different for different loss types, and the pressure

TABLE 1 Index quantification standard.

Score	1	2	3	4	5	6	7	8	9	10
Pressure bearing capacity (MPa)	<3.5	3.5–5	5–6	6–7	7–9	9–11	11–13	13–15	15–20	≥20
Initial loss (mL)	≥100	80–100	70–80	60–70	50–60	40–50	30–40	20–30	10–20	<10
Cumulative loss (mL)	≥250	200–250	170–200	150–170	120–150	100–120	70–100	50–70	30–50	<30

TABLE 2 Judgement matrix of the drilling fluid lost control efficiency.

Index	Pressure bearing capacity	Initial loss	Cumulative loss	$m_i$	$\psi_i$
Pressure bearing capacity	1	1	3	1.2286	0.5029
Initial loss	1/3	1/2	1	0.2445	0.0973
Cumulative loss	1	1	2	0.9719	0.3998

bearing capacity, plugging efficiency, and plugging strength have different influences on the drilling fluid lost control efficiency. The square root method is used to calculate the relative weight of each index, and the calculation steps are as follows.

- 1) Based on the analysis of the drilling fluid lost control efficiency in Section 2.2, the index quantification standard is established, as shown in Table 1.
- 2) Calculate the geometric mean  $m_i$  of all elements in each row of the judgment matrix by using the square root method, and form all the obtained  $m_i$  into vector  $M$ , as shown in Formula 1.

$$M = [m_1, m_2, m_3, \dots, m_i, \dots, m_n]^T. \quad (1)$$

$$\text{In the formula, } m_i = \sqrt[n]{\prod_{j=1}^n a_{ij}}, \quad i=(1,2,3, \dots, n)$$

$$\Psi = [\Psi_1, \Psi_2, \Psi_3, \dots, \Psi_i, \dots, \Psi_n]^T. \quad (2)$$

$$\text{In the formula, } \Psi_i = m_i / \sum_{j=1}^n m_{ij}, \quad i=(1,2,3, \dots, n).$$

- 3) After calculating the geometric average of each row of elements, calculate the relative weight of each influencing factor with Formula 2.
- 4) Construction of the judgment matrix: Taking natural fracture loss as an example, the sealing strength and sealing compactness of the fracture sealing zone determine the control efficiency of drilling fluid loss. According to the field test data, laboratory test results, and the experience of experts and engineers, the importance of the main control factors is divided and the judgment matrix of the drilling fluid lost control efficiency is constructed [34], as shown in Table 2.
- 5) Consistency test: In order to ensure the validity of the judgment matrix, it is necessary to test the consistency of the evaluation results of the judgment matrix (as shown in Formulas 3, 4).

$$C_R = \frac{C_I}{R_I}, \quad (3)$$

$$C_I = \frac{\lambda_{\max} - n}{n - 1}. \quad (4)$$

$R_I$ — the average random consistency index;

$C_I$ — the consistency coefficient, which is related to the order  $n$  and the maximum characteristic root of the matrix;

$\lambda_{\max}$ — the maximum eigenvalue of the judgment matrix;

$n$ — the order of the judgment matrix.

The consistency test results of the judgment matrix show that the evaluation system of the drilling fluid lost control efficiency for natural fractures meets the consistency standard.

Through the aforementioned steps, the weight proportion of main control factors of the drilling fluid lost control efficiency for natural fracture type loss can be obtained. Similarly, the weight proportion of main control factors of the induced fracture type and fracture propagation type drilling fluid lost control efficiency can be obtained, which is convenient for the analysis and calculation of subsequent experimental results. One decimal point is reserved. The results are shown in Table 3.

## 2.4 Fit analysis method of the lost control efficiency

There will be deviations between the indoor experiment results and the field application results. In order to further make the indoor experiment fit with the field, an analysis method of the lost control efficiency fit degree is proposed (as shown in Table 4). In the laboratory, the fracture plugging simulation experiment is carried out by different evaluation methods using the formula of the plugging slurry used in the field, including different fracture module parameters (the fracture module height, fracture module inclination angle, and fracture surface roughness) and different experimental steps (pressurization mode, single pressure increase, and pressure stabilization time). Differences between the indoor and field lost control results upon the pressure bearing capacity, initial loss, and cumulative loss are weighted in each loss type, according to the results shown in Table 4. In addition, the fit degree of this drilling fluid lost control efficiency evaluation method on each loss type is analyzed through the formula in Table 4. The grading of the evaluation results of the drilling fluid lost control efficiency is classified as “very good,” “good,” “general,” “poor,” and “very

**TABLE 3 Weight proportion of main control factors of different types of the drilling fluid lost control efficiency.**

Index		Pressure bearing capacity	Initial loss	Cumulative loss
Relative weight	Induced fracture type loss	0.1	0.6	0.3
	Fracture propagation type loss	0.4	0.4	0.2
	Natural fracture type loss	0.5	0.1	0.4

**TABLE 4 Fit analysis method of the indoor and field drilling fluid lost control efficiency.**

		Pressure bearing capacity	Initial loss	Cumulative loss
Field lost control results		$X_1$	$Y_1$	$Z_1$
Indoor experimental results		$X_2$	$Y_2$	$Z_2$
Deviation between indoor and field		$ X_2 - X_1 /X_1$	$ Y_2 - Y_1 /Y_1$	$ Z_2 - Z_1 /Z_1$
Weight proportion of main control factors of the drilling fluid lost control efficiency	Induced fracture type loss	0.1	0.6	0.3
	Fracture propagation type loss	0.4	0.4	0.2
	Natural fracture type loss	0.5	0.1	0.4
Comprehensive deviation of the drilling fluid lost control efficiency	Induced fracture type loss	$0.1 \times  X_2 - X_1 /X_1 + 0.6 \times  Y_2 - Y_1 /Y_1 + 0.3 \times  Z_2 - Z_1 /Z_1$		
	Fracture propagation type loss	$0.4 \times  X_2 - X_1 /X_1 + 0.4 \times  Y_2 - Y_1 /Y_1 + 0.2 \times  Z_2 - Z_1 /Z_1$		
	Natural fracture type loss	$0.5 \times  X_2 - X_1 /X_1 + 0.1 \times  Y_2 - Y_1 /Y_1 + 0.4 \times  Z_2 - Z_1 /Z_1$		
Fit degree between the indoor drilling fluid lost control efficiency and field drilling fluid lost control efficiency	Induced fracture type loss	$1 - (0.1 \times  X_2 - X_1 /X_1 + 0.6 \times  Y_2 - Y_1 /Y_1 + 0.3 \times  Z_2 - Z_1 /Z_1)$		
	Fracture propagation type loss	$1 - (0.4 \times  X_2 - X_1 /X_1 + 0.4 \times  Y_2 - Y_1 /Y_1 + 0.2 \times  Z_2 - Z_1 /Z_1)$		
	Natural fracture type loss	$1 - (0.5 \times  X_2 - X_1 /X_1 + 0.1 \times  Y_2 - Y_1 /Y_1 + 0.4 \times  Z_2 - Z_1 /Z_1)$		

poor,” according to the aforementioned values 90%, 80%–90%, 70%–80%, 60%–70%, and less than 60%, respectively.

## 2.5 Evaluation of the lost control ability of the plugging formula under different loss types

Since the best experimental conditions are determined, fracture plugging experiments should be carried out for further analysis. A comprehensive score of different loss plugging formulas can be calculated by the evaluation method shown in lines 5 to 7. Then, the leakage plugging formulas can be graded according to the lost control capability grading system. Through this method, these loss plugging slurry formulas are classified as “very good,” “good,” “general,” “poor,” and “very poor,” according to the aforementioned values 9.5, 8–9.5, 6.5–8, 5–6.5, and less than 5, respectively.

$$\text{Induced fracture type loss } R_1 = 0.1X + 0.6Y + 0.3Z, \quad (5)$$

$$\text{Fracture propagation type loss } R_2 = 0.4X + 0.4Y + 0.2Z, \quad (6)$$

$$\text{Natural fracture type loss } R_3 = 0.5X + 0.1Y + 0.4Z. \quad (7)$$

## 2.6 Laboratory evaluation experiment of the drilling fluid lost control efficiency

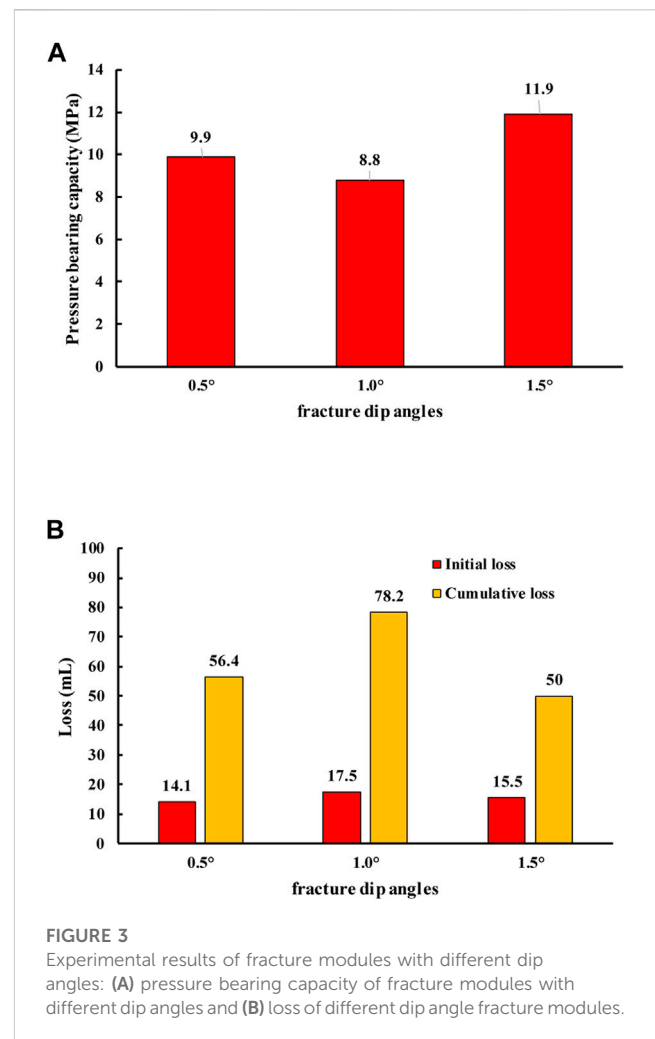
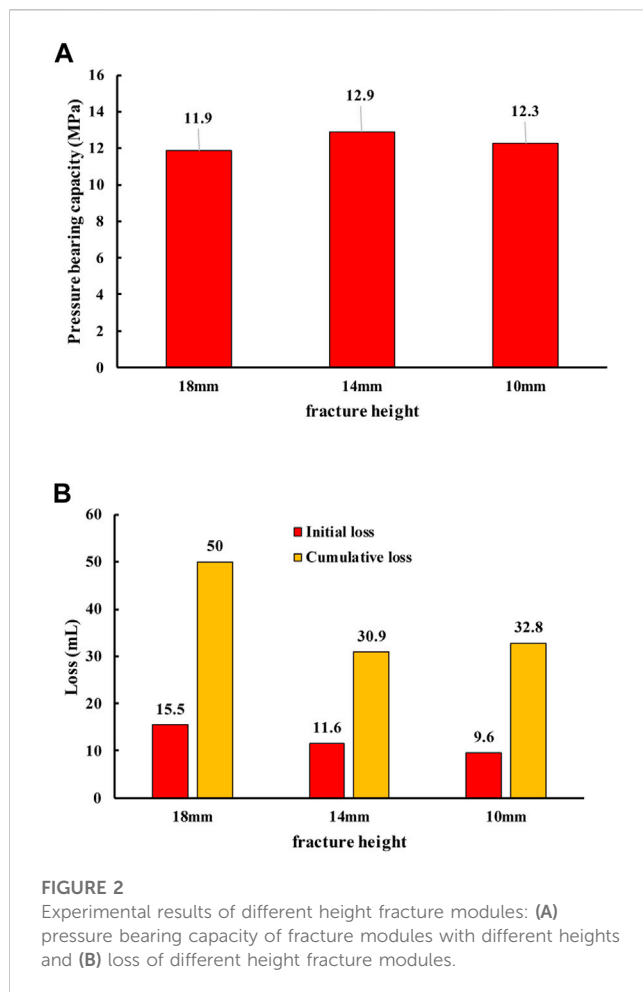
In order to establish the experimental evaluation method of the drilling fluid lost control efficiency, it is necessary to determine the best laboratory experimental conditions for the efficiency evaluation experiment of the plugging formula. It is necessary to adopt the original plugging formula used in the field and use different evaluation methods to compare the indoor and field drilling fluid lost control efficiency. Taking Well A in Block K of the Tarim Basin as an example, the results of well lost control show that the initial loss is 14.0 mL, the cumulative loss is 41.0 mL, and the pressure bearing capacity is 13.5 MPa, which successfully blocks the fracture. The field data analysis shows that the lost circulation interval of Well A is mainly induced fracture loss, and the maximum particle size in the lost circulation formula is basically less than 3 mm. The particle size distribution range of bridging material in the formula is 1.64–2.96 mm, and the particle size distribution range of filling material is 0.17–2.12 mm. The fracture type corresponds to the indoor 3–1 mm wedge fracture.

TABLE 5 Related parameters of each plunger.

Number	Fracture height (mm)	Fracture length (mm)	Fracture width (mm)
3-1-18	18	50	3–1
3-1-14	14	50	
3-1-10	10	50	
Number	Fracture dip angle (°)	Fracture length (mm)	Fracture height (mm)
3-1-100	0.5	100	50
3-1-70	1.0	70	
3-1-50	1.5	50	
Number	Coefficient of the surface fracture JRC	Fracture length (mm)	Fracture height (mm)
1#	1	18	50
2#	10		
3#	20		

TABLE 6 Experimental scheme of the influence of experimental steps on the drilling fluid lost control efficiency.

Number	Plugging formulation	Experimental procedure	Exploring factors
1#	Water-based drilling fluid+3% LCM-S2+5% LCM-F1+5% LCM-F2+0.5% LCM-X1	Stepped pressurization: 0–2.5 MPa, pressure stabilization for 2 min; 2.5–5 MPa, and the voltage is stabilized for 2 min; 5–7.5 MPa, and the voltage is stabilized for 2 min; 7.5–10 MPa, and the voltage is stabilized for 2 min; 10–12.5 MPa and voltage stabilization for 2 min; and then pressurizing until it is destroyed	Pressurization mode
2#		Pressurization: 0–20 MPa, with the pressure increasing rate of 7 mL/min until it is destroyed	
3#		Stepped pressurization: 0–1.25 MPa and pressure stabilization for 2 min; 1.25–3.5 MPa, maintaining the voltage for 2 min; 3.5–4.75 MPa, and the voltage is stabilized for 2 min; 4.75–6 MPa, and the voltage is stabilized for 2 min; 6–7.25 MPa and voltage stabilization for 2 min; 7.25–8.5 MPa and voltage stabilization for 2 min; 8.5–9.75 MPa, and the voltage is stabilized for 2 min; and then pressurizing until it is destroyed	Single pressure increment
4#		Stepped pressurization: 0–2.5 MPa and pressure stabilization for 2 min; 2.5–5 MPa, and the voltage is stabilized for 2 min; 5–7.5 MPa, and the voltage is stabilized for 2 min; 7.5–10 MPa, and the voltage is stabilized for 2 min; 10–12.5 MPa and voltage stabilization for 2 min; and then pressurizing until it is destroyed	
5#		Step pressure: 0–5 MPa and pressure stabilization for 2 min; 5–10 MPa, and the voltage is stabilized for 2 min; 10–15 MPa and voltage stabilization for 2 min; 15–20 MPa and voltage stabilization for 2 min	
6#		Stepped pressurization: 0–2.5 MPa and pressure stabilization for 2 min; 2.5–5 MPa, and the voltage is stabilized for 2 min; 5–7.5 MPa, and the voltage is stabilized for 2 min; 7.5–10 MPa, and the voltage is stabilized for 2 min; 10–12.5 MPa and voltage stabilization for 2 min; and then pressurizing until it is destroyed	Pressure stabilization time
7#		Step pressure: 0–2.5 MPa, and the pressure is kept for 4 min; 2.5–5 MPa, maintaining the voltage for 4 min; 5–7.5 MPa, and the voltage is stabilized for 4 min; 7.5–10 MPa, maintaining the voltage for 4 min; 10–12.5 MPa, maintaining the voltage for 4 min; and then pressurizing until it is destroyed	
8#		Step pressure: 0–2.5 MPa, and the pressure is kept for 6 min; 2.5–5 MPa, maintaining the voltage for 6 min; 5–7.5 MPa and voltage stabilization for 6 min; 7.5–10 MPa, and the voltage is stabilized for 6 min; 10–12.5 MPa, maintaining the voltage for 6 min; and then pressurizing until it is destroyed	



### 2.6.1 Laboratory sample

In the lost circulation case of well A, the formula for successful lost control is “water-based drilling fluid+3% LCM-S2+5% LCM-F1+5% LCM-F2+0.5% LCM-X1.” According to the formula of the basic plugging slurry on site, the LCMs used in indoor experiments are selected. In the experiment, 3D wedge-shaped plungers with the same fracture width (3 mm–1 mm) and different fracture heights, fracture inclination (defined as the ratio of the fracture height to fracture length in this paper), and fracture surface roughness were selected as experimental plungers to study the effects of fracture height, fracture inclination, and fracture surface roughness on the drilling fluid lost control efficiency. The parameters of each plunger are shown in Table 5.

To study the influence of experimental steps on the control efficiency of drilling fluid loss, the experimental plungers all use unified plungers. On the premise that the fracture width is fixed at 3–1 mm, the most commonly used 3D printing wedge plunger with the fracture height of 18 mm, the dip angle of 1.5, and the JRC coefficient of the fracture surface of 1 is selected.

### 2.6.2 Laboratory installation

An indoor fracture plugging simulation experiment was conducted with a self-made portable damage assessment instrument [31]. When exploring the influence of experimental

steps on the control efficiency of drilling fluid loss, different experimental steps are set. The preliminary preparation work and the experimental process remain unchanged. In addition, the pressurization mode, the single pressure increase, and the pressure stabilization time will be changed. Table 6 represents the specific scheme.

## 3 Results and discussion

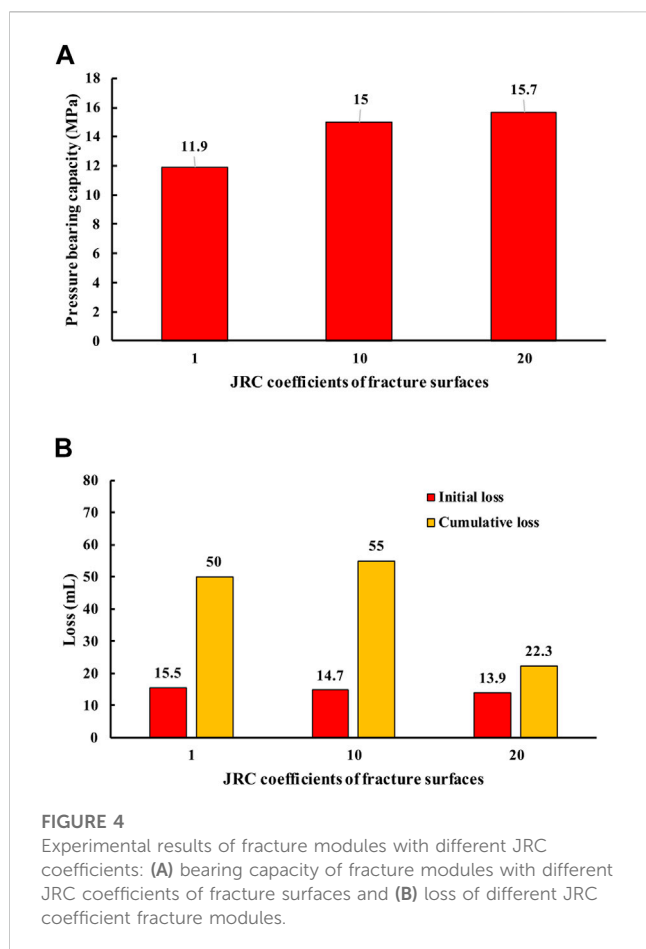
The loss control results of Well A in Block K were studied as an example, and the method was used to evaluate the induced fracture loss. In addition, the weighting proportion of main fluid lost control factors and the experimental steps were reconfirmed.

### 3.1 Effect of fracture parameters on the drilling fluid lost control efficiency

#### 3.1.1 Effect of fracture height

The experimental results of the influence of the fracture height on the drilling fluid leakage control efficiency are shown in Figure 2. Plungers with experimental heights of 18 mm, 14 mm, and 10 mm





were selected. According to the analysis method of the indoor and on-site drilling fluid lost control efficiency fit shown in Table 4, the calculation results of the indoor plunger with different fracture heights and the on-site drilling fluid lost control efficiency fit are obtained.

The results show that the lost control efficiency of the plunger drilling fluid with a fracture height of 18 mm is in the highest agreement with the field results, and the evaluation result of the drilling fluid lost control efficiency is “good.” The lost control efficiency of the plunger drilling fluid with a fracture height of 10 mm has the lowest agreement with the field results, and the evaluation result of the drilling fluid lost control efficiency is “average.” For the plunger with a fracture height of 18 mm, the fracture height: fracture entrance width is 6: 1. For a plunger with a fracture height of 10 mm, the fracture height: fracture entrance width is about 3: 1. Therefore, when the ratio of the fracture height to fracture entrance width is larger, the coincidence degree of indoor and field drilling fluid lost control efficiency is higher. Combined with this experimental data, when the fracture height: fracture entrance width is 6: 1, the evaluation result of the drilling fluid lost control efficiency is the best.

### 3.1.2 Effect of fracture dip angles

The experimental results of the influence of fracture inclination on the drilling fluid lost control efficiency are shown in Figure 3.

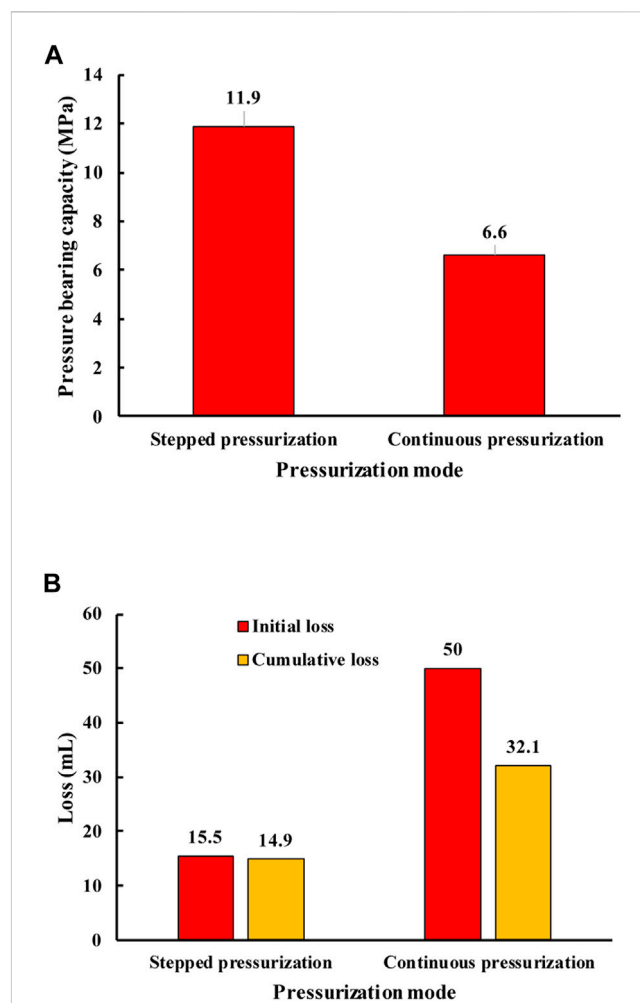
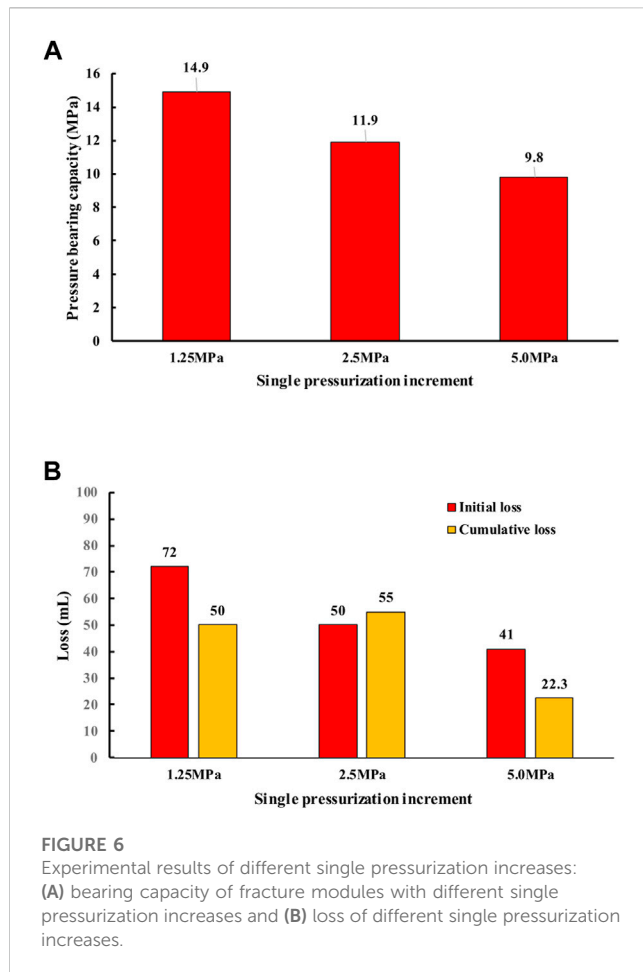


**FIGURE 5**  
Experimental results of different pressurization modes: (A) bearing capacity of fracture modules with different pressurization modes and (B) loss of different pressurization modes.

Select plungers with experimental inclination angles of 0.5, 1.0, and 1.5. According to the analysis method of indoor and field drilling fluid lost control effectiveness, the calculation results of indoor plungers with different inclination angles and field drilling fluid lost control effectiveness are obtained.

The results show that the lost control efficiency of plunger drilling fluid with fracture inclination angles of 0.5 and 1.5 is higher than that of the field, and the difference between them is very small. The evaluation results of both the drilling fluid lost control efficiency are “good.” However, the lost control efficiency of plunger drilling fluid with a fracture inclination of 1.0 is the lowest, and the evaluation result is “poor,” which is close to “very poor.” The length of plunger fracture with a crack inclination of 0.5 is 100 mm. The length of plunger fracture with a fracture inclination of 1.5 is 50 mm. When the fracture dip angle is greater than 1 and close to 1.5 or less than 1 and close to 0.5, the indoor and on-site drilling fluid lost control efficiency fits well. Combined with the experimental data, the fracture dip angle ranges from 0.5 to 1.5, and the evaluation effect of the drilling fluid lost control efficiency is the worst when the dip angle is 1.



Therefore, when evaluating the drilling fluid lost control efficiency, the value of the fracture dip angle should deviate from 1 as much as possible.

### 3.1.3 Effect of fracture surface roughness

The experimental results of the influence of the fracture JRC coefficient on the drilling fluid lost control efficiency are shown in Figure 4. The plunger with the JRC coefficient of the fracture surface of 1, 10, and 20 mm was selected in the experiment. According to the analysis method of indoor and field drilling fluid lost control effectiveness, the calculation results of the indoor JRC coefficient plunger and field drilling fluid lost control effectiveness are obtained.

The results show that the lost control efficiency of the plunger drilling fluid with the JRC coefficient of the fracture surface of 20 is the highest in accordance with the field, and the evaluation result of the drilling fluid lost control efficiency is “good.” The lost control efficiency of plunger drilling fluid with a fracture JRC coefficient of 1 is the lowest, and there is an obvious linear relationship between the lost control efficiency of indoor and field drilling fluid and the roughness of the fracture surface. In a certain range, the coarser the fracture surface is, the greater the JRC coefficient of the fracture surface is, and the higher the lost control efficiency of indoor and field drilling fluid is.

## 3.2 Effect of experimental steps on the drilling fluid lost control efficiency

### 3.2.1 Effect of the pressurization mode

The experimental results of the influence of different pressurization methods on the drilling fluid lost control efficiency are shown in Figure 5. The pressurization methods selected in the experiment are step pressurization and continuous pressurization. The calculation results of the coincidence degree between different pressurization methods and on-site drilling fluid lost control efficiency are obtained.

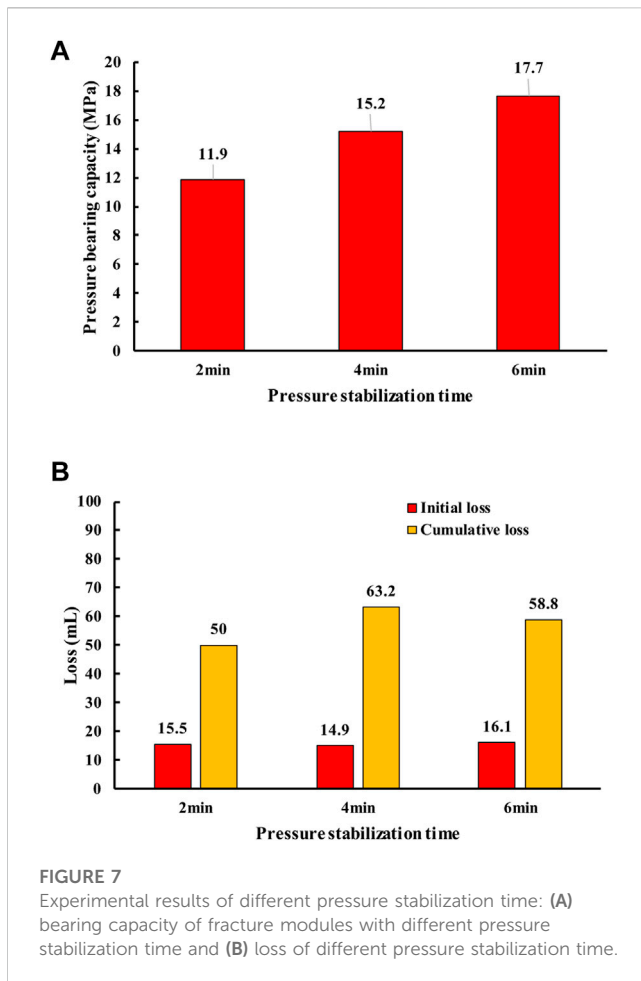
The results show that there is no obvious difference between the indoor and field drilling fluid lost control efficiency in two different pressurization methods, and the evaluation results of the drilling fluid lost control efficiency are all “good.” According to the analysis, stepped pressurization gradually pushes the plugging material into the fracture by pressurization–pressure stabilization–pressurization, while continuous pressurization pumps the displacement fluid at a constant rate. No matter which pressurization method is used, it has little influence on the initial loss, and the plugging efficiency has no obvious change. For the induced fracture loss, the plugging efficiency accounts for the largest proportion of the drilling fluid lost control efficiency, which is 0.6. Therefore, there is no obvious difference between the drilling fluid lost control efficiency of the two different pressurization methods and the on-site fit degree.

### 3.2.2 Effect of single pressurization increase

The experimental results of the influence of different single pressurization increases on the drilling fluid lost control efficiency are shown in Figure 6. Different single pressure increases of 1.25 MPa, 2.5 MPa, and 5.0 MPa were selected in the experiment. Determine the calculation results of the coincidence degree between different single pressure increases and the on-site drilling fluid lost control efficiency.

The results show that when the single pressure increase is 5 MPa, the drilling fluid lost control efficiency is the highest in accordance with the field, and the evaluation result of the drilling fluid lost control efficiency is “good.” When the single pressure increase is 1.25 MPa, the drilling fluid lost control efficiency is the lowest in correspondence with the field, and the evaluation result of the drilling fluid lost control efficiency is “poor.” Moreover, there is an obvious linear relationship between the coincidence degree of the drilling fluid lost control efficiency in the field and indoor and the single pressure increase. In a certain range, the greater the single pressure increase, the higher the coincidence degree.

The main control factor of the lost control efficiency for induced fracturing drilling fluid is the plugging efficiency, which is characterized by the initial loss in the experiment. The higher the plugging efficiency, the less time it takes to form an effective plugging zone and the lower the initial loss. When the single pressure increase is different, with the increase of the single pressure increase, the time required for the LCM to enter the fracture to form a plugging zone is less, the plugging efficiency is higher, and the initial loss is less, thus improving the drilling fluid lost control efficiency. When the single pressure increase is small and the indoor drilling fluid lost control efficiency is poor, with the increase of the single pressure increase, the lost control becomes



better and the coincidence degree of the indoor and field drilling fluid lost control efficiency is improved.

### 3.2.3 Effect of pressure stabilization time

The experimental results of the influence of different pressure stabilization time on the drilling fluid lost control efficiency are shown in Figure 7. In the experiment, the different pressure stabilization time is 2 min, 4 min, and 6 min. Determine the calculation results of the coincidence degree between different pressure stabilization time and the on-site drilling fluid lost control efficiency.

The results show that when the pressure stabilization time is 2 min, the coincidence degree of the indoor and field drilling fluid lost control efficiency is the highest and the evaluation result of the drilling fluid lost control efficiency is “good.” However, when the pressure stabilization time is 6 min, the fitting degree is the lowest and the evaluation result of the drilling fluid lost control efficiency is “average.” In a certain range, the coincidence degree of the indoor and field drilling fluid lost control efficiency is negatively correlated with the pressure stability time.

According to the above three series of analysis and experimental results, it can be seen that the evaluation method of out-of-control efficiency of experimental drilling fluid induces fracture loss. When the fracture height: fracture entrance width is 6: 1, the degree of fracture inclination deviation of 1° is high and the fracture surface is

rough; then, the indoor and field drilling fluid lost control efficiency fits well. For induced fracture loss, a perfect experimental evaluation method of the drilling fluid lost control efficiency will be supported by this result. As for the evaluation of experimental steps, in the pressurization mode, there is no significant difference between the indoor and field drilling fluid lost control efficiency. In addition, the drilling fluid lost control efficiency is less affected by the evaluation of the pressurization mode. However, the choice of the single pressure increase is more suitable for the evaluation of the drilling fluid lost control efficiency with a higher single pressure increase, and the evaluation results are more consistent with the field. Regarding the selection of pressure stabilization time, when the pressure stabilization time exceeds 1 min, the shorter the pressure stabilization time is and the higher the coincidence degree of the indoor and field drilling fluid lost control efficiency is. Aiming at the induced fracture loss, the perfect experimental evaluation method of the drilling fluid lost control efficiency will be supported by the aforementioned comprehensive analysis results.

## 3.3 Experimental evaluation method and application strategy of the drilling fluid lost control efficiency

Combined with the experimental analysis results of the influence of fracture module parameters and experimental steps on the drilling fluid lost control efficiency, as shown in Section 3.1 and Section 3.2, an experimental evaluation method of the drilling fluid lost control efficiency for the induced fracture loss is established.

### 3.3.1 Experimental method of the drilling fluid lost control efficiency considering various loss types

For induced fracture loss, the best fracture height, fracture dip angle, fracture surface roughness, the best pressurization mode, single pressure increase, and pressure stabilization time are defined so as to evaluate the drilling fluid lost control efficiency systematically. At the same time, experiments have been carried out on fracture propagation type loss and natural fracture type loss, and the experimental conditions, as shown in Table 7, have been established.

### 3.3.2 Application strategy

Considering that more than one type of drilling fluid loss can present in some cases, it is necessary to determine the loss types and analyze proportion of each loss type so as to determine the major and secondary loss types. The ideas are as follows:

- (1) Determine the loss type. Determine the primary and secondary loss types, and analyze the weight proportion of different loss types by AHP; refer to the analysis method of weight proportion of evaluation indicators in Section 2.4, analyze the weight proportion of different loss types, and determine that the proportion of induced fracture loss, fracture propagation loss, and natural fracture loss are M, N, and O (if there are three loss types at the same time), respectively, and if there are two loss types at the same time, determine the weight proportion of M and N, respectively (M, N, O are all  $\in [0,1]$ ).

TABLE 7 Experimental scheme of the influence of experimental steps on the drilling fluid lost control efficiency.

Loss type	Evaluation content	Evaluating indicator	Main points of the method
Induced fracture type loss	Fracture module	Fracture height	Height of fracture: width of fracture entrance = 6: 1, the coincidence degree of the indoor and field drilling fluid lost control efficiency is high, and the evaluation result is good
		Fracture dip angle	When the dip angle of the fracture is 0.5, the coincidence degree of the indoor and field drilling fluid lost control efficiency is higher and the evaluation result is better
		Roughness of the fracture surface	The rougher the fracture surface, the higher the coincidence degree of the indoor and field drilling fluid lost control efficiency, and the better the evaluation result
	Experimental procedure	Pressurization mode	The pressurization method has no significant effect on the experimental evaluation results of the drilling fluid lost control efficiency
		Single pressure increase	When the single pressure increase is larger, 5 MPa, indoor and present The coincidence degree of the drilling fluid lost control efficiency is high, and the evaluation result is good
		Pressure stabilization time	When the pressure stabilization time is short, it is 2 min, the coincidence degree of the indoor and field drilling fluid lost control efficiency is higher, and the evaluation result is better
Fracture propagation type loss	Fracture module	Fracture height	Height of fracture: width of the fracture entrance = 6: 1, and the coincidence degree of the indoor and field drilling fluid lost control efficiency is high, and the evaluation result is good
		Fracture dip angle	When the dip angle of the fracture is 0.5, the coincidence degree of the indoor and field drilling fluid lost control efficiency is higher, and the evaluation result is better
		Roughness of the fracture surface	The rougher the fracture surface, the higher the coincidence degree of the indoor and field drilling fluid lost control efficiency, and the better the evaluation result
	Experimental procedure	Pressurization mode	Choosing the stepped pressurization mode, the indoor and on-site drilling fluid lost control efficiency fits well, and the evaluation results are good
		Single pressure increase	When the single pressure increase is 5 MPa, the efficiency of indoor and field drilling fluid lost control is in good agreement, and the evaluation result is good
		Pressure stabilization time	When the pressure stabilization time is moderate and it is 4 min, the coincidence degree of the indoor and field drilling fluid lost control efficiency is high, and the evaluation result is good
Natural fracture type loss	Fracture module	Fracture height	Height of fracture: width of the fracture entrance ≈ 3: 1, the coincidence degree of the indoor and field drilling fluid lost control efficiency is high, and the evaluation result is good
		Fracture dip angle	When the dip angle of the fracture is 0.5, the coincidence degree of the indoor and field drilling fluid lost control efficiency is higher and the evaluation result is better
		Roughness of the fracture surface	The rougher the fracture surface, the higher the coincidence degree of the indoor and field drilling fluid lost control efficiency, and the better the evaluation result
	Experimental procedure	Pressurization mode	Choosing the stepped pressurization mode, the indoor and on-site drilling fluid lost control efficiency fits well, and the evaluation results are good
		Single pressure increase	When the single pressure increase is moderate, 2.5 MPa, the coincidence degree of the indoor and field drilling fluid lost control efficiency is high, and the evaluation result is good
		Pressure stabilization time	When the pressure stabilization time is moderate, and it is 4 min, the coincidence degree of indoor and field drilling fluid lost control efficiency is high, and the evaluation result is good

- Use the experimental evaluation method of the drilling fluid lost control efficiency aiming at different loss types; after the main loss types are determined, the evaluation method corresponding to the main loss types is selected to evaluate the drilling fluid lost control efficiency through Table 7. If the main loss type is induced fracture type, the drilling fluid lost control efficiency will be evaluated according to induced fracture type loss, and the remaining cases are the same.
- Make a comprehensive evaluation on the lost control ability of the plugging slurry formula and give the grading results.

According to step 1), among the loss types of fractured formation, the determined proportions of induced fracture type loss, fracture propagation type loss, and natural fracture type loss are M, N, and O (if there are three types of leakage at the same time), respectively. Determine the comprehensive score of the lost control ability of plugging slurry.

$$R_M = M \times (0.1X + 0.6Y + 0.3Z), \quad (8)$$

$$R_N = N \times (0.4X + 0.4Y + 0.2Z), \quad (9)$$

$$R_O = O \times (0.5X + 0.1Y + 0.4Z), \quad (10)$$

TABLE 8 Indoor experiment evaluation method.

Experimental method	Experimental fracture module parameter	Experimental procedure
Indoor routine evaluation method	The fracture width is 3 mm–1 mm. Under the condition of this width, the commonly used plunger in the room generally has a fracture height of 18 mm and a fracture inclination of 1.5°	The commonly used indoor pressurization method is stepped pressurization, with a single pressure increase of 2.5 MPa and a stable pressure time of 6 min
Experimental evaluation method of the lost control efficiency of natural fractured drilling fluid	For cracks with a fracture width of 3 mm–1 mm, the height of the fracture module: the crack entrance width is 6: 1, and the height is 18 mm. The fracture inclination is 1.5°, and the JRC coefficient is 20	Step-by-step pressurization method, the experiment was carried out with a single pressure increase of 2.5 MPa and a constant pressure of 4 min

where  $x$ ,  $y$ , and  $z$  are the specific scores of bearing capacity, initial loss, and cumulative loss in the lost control results, respectively, which are obtained by combining the specific values of the three indicators with Table 1.

For the final  $R$  value, refer to Table 8 to determine the grading result of the lost control ability of the plugging slurry formula.

## 4 Field test

Well D is an evaluation well located in Block K of the Tarim Basin, and it has developed micro-fractures. When drilling to the well depth of 5694–5819 m, loss occurred. The on-site plugging slurry formula was oil-based drilling fluid (1.88) +4%NTS-M (medium coarse) +7% NTS-S (type II, medium coarse) +5% NTS (type I, coarse) +2%GYD-coarse +3%GYD-medium coarse +5%GYD-fine. Carry out indoor experiments with the same formula.

According to the evaluation method proposed in this paper, the coincidence degree with the on-site drilling fluid lost control efficiency exceeds 90%, and the evaluation result is rated as “very good.” The indoor conventional evaluation method, which is just over 80% consistent with the on-site drilling fluid lost control efficiency, has a rating between “good” and “general.” Two different indoor evaluation methods are used to evaluate the effectiveness of drilling fluid lost control. The evaluation method proposed in this paper is closer to the field lost control result, and the evaluation result of drilling fluid lost control effectiveness is better.

When the conventional laboratory experiment method is adopted, the evaluation method of the lost control ability of the natural fracture type loss plugging slurry formula is adopted, where the value of  $X$  can be determined as 2 by referring to Table 1 with the pressure bearing capacity of 4.6 MPa, and similarly,  $Y$  and  $Z$  can be determined as 8 and 7, respectively.  $R = 4.6$  can be obtained, and the result is graded as “very poor,” according to the lost control ability grading system of the loss slurry formula.

When the method proposed in this paper is adopted, according to the judgment result of loss type,  $R = 0.5 \times 3 + 0.1 \times 7 + 0.4 \times 5 = 4.2$  can be obtained, and the result is classified as “poor,” according to the classification system of the lost control ability of the slurry loss formula. The evaluation method proposed in this paper is the same as the conventional indoor evaluation method in grading the evaluation results of the same plugging slurry formula, which verifies the feasibility of the evaluation method proposed in this

paper. In addition, the evaluation method can realize the reasonable evaluation of on-site lost control, and the efficiency of indoor and on-site drilling fluid lost control is in high agreement with good evaluation results. This method can effectively guide on-site lost control evaluation, such as oil and gas fractured reservoirs and EGS of deep hot-dry rock.

## 5 Conclusion

In this paper, the control efficiency of drilling fluid loss is analyzed and the relative weight ratio of main control factors is defined. Based on the correspondence between the indoor and field drilling fluid lost control efficiency, the reasonable fracture module parameters and experimental steps for indoor evaluation of the drilling fluid lost control efficiency are put forward, and the experimental evaluation methods for the drilling fluid lost control efficiency in fractured formations with different loss types are established. The main achievements and understandings are as follows

- (1) The control efficiency of drilling fluid loss is the comprehensive embodiment of the strength, sealing efficiency, and sealing compactness of the fracture sealing zone formed when controlling the loss. These three important indexes are characterized by the pressure bearing capacity, initial loss, and cumulative loss in the laboratory.
- (2) The main control factors of the drilling fluid lost control efficiency of different loss types and the weight ratio of main control factors are defined. For induced fracture loss, the best fracture height, fracture dip angle, fracture surface roughness, the best pressurization mode, single pressure increase, and pressure stabilization time are defined so as to evaluate the drilling fluid lost control efficiency systematically. Make a comprehensive evaluation on the lost control ability of the plugging slurry formula and give the grading results. A method for judging drilling fluid loss types in fractured formations is proposed based on the relationship between the loss rate and time.
- (3) The experimental evaluation method of the drilling fluid lost control efficiency considering various loss types is established. According to the analysis method of the experimental results of the drilling fluid lost control efficiency, the indoor evaluation method with the highest coincidence degree with the on-site drilling fluid lost control efficiency is obtained, including the height of the fracture



module with the highest coincidence degree, fracture inclination, fracture surface roughness, pressurization mode, single pressure increase, and pressure stabilization time. Considering the simultaneous existence of multiple losses, a comprehensive evaluation and grading method of the lost control ability of the plugging slurry considering multiple loss is put forward. Through the aforementioned method, the field lost control evaluation can be effectively guided, which is of great significance to drilling fluid lost control and reservoir protection.

## Data availability statement

The original contributions presented in the study are included in the article/Supplementary Material; further inquiries can be directed to the corresponding authors.

## Author contributions

JZ comprehensively contributed to the work of the manuscript, including the design of the study, organized the data, and performed the statistical analysis. YK and CX mainly contributed to the design of the study. XY and CL mainly contributed to the organization of the database. All authors contributed to manuscript revision, and read and approved the submitted version.

## References

- Klungtvedt KR, Khalifeh M, Saasen A, Berglund B, Vasshus KJ. Preventing drilling fluid induced reservoir formation damage. In: SPE/IADC Middle East Drilling Technology Conference and Exhibition; Abu Dhabi, UAE (2021).
- Lavrov A. *Lost circulation: Mechanisms and solutions*. Gulf Professional Publishing, Elsevier (2016).
- Windarto GAY, Sukarno P, Soewono E. Modelling of formation damage due to mud filtrate invasion in a radial flow system. *J Pet Sci Eng* (2012) 100:99–105. doi:10.1016/j.petrol.2012.11.003
- Sun JS, Bai YR, Cheng RC, Lv KH, Liu F, Feng J, et al. Research progress and prospect of plugging technologies for fractured formation with severe lost circulation. *Pet Exploration Dev* (2021) 48:732–43. doi:10.1016/s1876-3804(21)60059-9
- Feng Y, Gray KE. *Lost circulation and wellbore strengthening*. Switzerland: Springer (2018).
- Wang H, Sweatman R, Engelman R, Deeg W, Whitfill D, Soliman M, et al. Best practice in understanding and managing lost circulation challenges. *SPE Drilling and Completion* (2008) 23:168–75. doi:10.2118/95895-pa
- Mortadha A, Mohammed F, Runar N. Updated criterion to select particle size distribution of lost circulation materials for an effective fracture sealing. *J Pet Sci Eng* (2017) 149:641–8.
- Beda G, Carugo C. Mud microloss analysis while drilling improves fractured-reservoir evaluation. *J Pet Tech* (2002) 54:0149–2136.
- Kang YL, Xu CY, Tang L, Li S. Constructing a tough shield around the wellbore: Theory and method for lost-circulation control. *Pet Exploration Dev* (2014) 41:520–7. doi:10.1016/s1876-3804(14)60061-6
- Zeng YJ, Li DQ, Yang CH. Leakage prevention and control in fractured formations. *Chin J Rock Mech Eng* (2016) 35:2054–61.
- Xu CY, Kang YL, You LJ, You Z. Lost-circulation control for formation-damage prevention in naturally fractured reservoir: Mathematical model and experimental study: Mathematical model and experimental study. *SPE J* (2017) 22:1654–70. doi:10.2118/182266-pa
- Ivan CD, Bruton JR, Thiercelin M, Bedel JP. Making a case for rethinking lost circulation treatments in induced fractures. In: SPE Annual Technical Conference and Exhibition. San Antonio, Texas (2002).
- He YC, Han TF, Zhao JG. Development of high-temperature visual plugging instrument. *Equipment Geotechnical Eng* (2017) 18:3–5.
- Duan MX, Zhang XF, Zhang QM. BDY-1 portable plugging device for drilling fluid. *Drilling Fluid and Completion Fluid* (2002) 19:30–1.
- Li J. *Study on improvement of experimental technology of drilling fluid plugging evaluation*. Beijing: China University of Petroleum (2010).
- Yu WC, Su CM, Huang XR, Zhang CY. Development of high temperature high pressure (HTHP) dynamic sealing evaluating system. *J oil gas Technol* (2000) 28:13–4.
- Albattat R, Hoteit H. A semi-analytical approach to model drilling fluid leakage into fractured formation. *Rheologica Acta* (2021) 60(6):353–70. doi:10.1007/s00397-021-01275-3
- Al-saba MT, Nygaard R, Saasen A, Nes OM. Lost circulation materials capability of sealing wide fractures. In: SPE Deepwater Drilling and Completions Conference. Society of Petroleum Engineers (2014).
- Al-saba MT, Nygaard R, Saasen A, Nes OM. Laboratory evaluation of sealing wide fractures using conventional lost circulation materials. In: SPE annual technical conference and exhibition. Society of Petroleum Engineers (2014).
- Wang G, Cao C, Pu X, Zhao Z. Experimental investigation on plugging behavior of granular lost circulation materials in fractured thief zone. *Particulate Sci Tech* (2016) 34:392–6. doi:10.1080/02726351.2015.1089963
- Zhong H, Shen G, Yang P, Qiu Z, Jin J, Xing X. Mitigation of lost circulation in oil-based drilling fluids using oil absorbent polymers. *Materials* (2018) 11:2020. doi:10.3390/ma11102020
- Xu C, Kang Y, Chen F, You Z. Analytical model of plugging zone strength for drill-in fluid loss control and formation damage prevention in fractured tight reservoir. *J Pet Sci Eng* (2017) 149:686–700. doi:10.1016/j.petrol.2016.10.069
- Kang YL, Zhang JY, Xu CY, You LJ, L C. The effect of geometrical morphology of rigid lost circulation material on its retention behavior in fractures. *Pet Drilling Tech* (2018) 46:26–34.
- Majidi R, Miska SZ, Ahmed R, Yu M, Thompson LG. Radial flow of yield-power-law fluids: Numerical analysis, experimental study and the application for drilling fluid losses in fractured formations. *J Petrol Sci Eng* (2010) 70(3–4):334–43. doi:10.1016/j.petrol.2009.12.005

## Acknowledgments

The authors would like to thank the support of the National Natural Science Foundation of China (52004233) and the support of the Natural Science Foundation of Sichuan Province (23NSFSC1596). Finally, the authors would like to thank the paper reviewers for their valuable comments and suggestions. They gratefully acknowledge the financial support from the China Postdoctoral Science Foundation (Grant No. 2022M723501).

## Conflict of interest

JZ and YD were employed by the company China Zhenhua Oil Co., Ltd.

The remaining authors declare that the research was conducted in the absence of any commercial or financial relationships that could be construed as a potential conflict of interest.

## Publisher's note

All claims expressed in this article are solely those of the authors and do not necessarily represent those of their affiliated organizations, or those of the publisher, the editors, and the reviewers. Any product that may be evaluated in this article, or claim that may be made by its manufacturer, is not guaranteed or endorsed by the publisher.

25. Qiu ZS, Bao D, Liu YJ, Chen J, Chen X Microcosmic mechanism of fracture-plugging instability and experimental study on pressure bearing and tight plugging. *Acta Petrolei Sinica* (2018) 39:587–96.
26. Mostafavi V, Hareland G, Belayneh M, Aadnoy BS. *Experimental and mechanistic modeling of fracture sealing resistance with respect to fluid and fracture properties*. U.S. symposium on rock mechanics. American rock mechanics association (2011).
27. Nasiri A, Ghaffarkhah A, Dijvejin ZA, Mostofi M, Moraveji MK. Bridging performance of new eco-friendly lost circulation materials. *Pet Exploration Dev* (2018) 45:1154–65. doi:10.1016/s1876-3804(18)30119-8
28. Xu CY, Yan XP, Kang YL, You LJ, You ZJ, Zhang H, et al. Friction coefficient: A significant parameter for lost circulation control and material selection in naturally fractured reservoir. *Energy* (2019) 174:1012–25. doi:10.1016/j.energy.2019.03.017
29. Grant P, Lassus L, Savari S, Whitfill DL. Size degradation studies of lost circulation materials in a flow loop. In: IADC/SPE Drilling Conference and Exhibition; Fort Worth, Texas, USA (2016).
30. Omid R, Ali KV, Eric VO, Munir A, Sudarshan G. Optimum particle size distribution design for lost circulation control and wellbore strengthening. *J Nat Gas Sci Eng* (2016) 35:836–50.
31. Xu CY, Zhang HL, Kang YL, Zhang JY, Bai YR, Zhang J, et al. Physical plugging of lost circulation fractures at microscopic level. *Fuel* (2022) 317:123477. doi:10.1016/j.fuel.2022.123477
32. Albattat R, AlSinan M, Kwak H, Hoteit H. Modeling lost-circulation in natural fractures using semi-analytical solutions and type-curves. *J Pet Sci Eng* (2022) 216(2022):110770. doi:10.1016/j.petrol.2022.110770
33. Lavrov A. From fracture gradient to spectrum of lost-circulation pressures: A paradigm shift. *Energy Proced* (2017) 114:3185–92. doi:10.1016/j.egypro.2017.03.1447
34. Xu CY, Xie ZC, Kang YL, Yu GY, You ZJ, You LJ, et al. A novel material evaluation method for lost circulation control and formation damage prevention in deep fractured tight reservoir. *Energy* (2020) 210:118574. doi:10.1016/j.energy.2020.118574



## OPEN ACCESS

## EDITED BY

Chengyuan Xu,  
Southwest Petroleum University, China

## REVIEWED BY

Xiaohui Mao,  
University of Alberta, Canada  
Daobing Wang,  
Beijing Institute of Petrochemical  
Technology, China

## \*CORRESPONDENCE

Yang Wang,  
✉ wangyang0996@petrochina.com.cn

RECEIVED 24 May 2023

ACCEPTED 03 July 2023

PUBLISHED 13 July 2023

## CITATION

Wang Y, Fan Y and Wang X (2023), Study on migration law of multiscale temporary plugging agent in rough fractures of shale oil reservoirs.

*Front. Phys.* 11:1228006.

doi: 10.3389/fphy.2023.1228006

## COPYRIGHT

© 2023 Wang, Fan and Wang. This is an open-access article distributed under the terms of the [Creative Commons Attribution License \(CC BY\)](https://creativecommons.org/licenses/by/4.0/). The use, distribution or reproduction in other forums is permitted, provided the original author(s) and the copyright owner(s) are credited and that the original publication in this journal is cited, in accordance with accepted academic practice. No use, distribution or reproduction is permitted which does not comply with these terms.

# Study on migration law of multiscale temporary plugging agent in rough fractures of shale oil reservoirs

Yang Wang\*, Yu Fan and Xiaojiao Wang

Engineering Technology Research Institute of Southwest Oil and Gas Field Company, PetroChina, Chengdu, China

For unconventional oil and gas reservoirs and deep carbonate reservoirs, temporary plugging fracturing is an important technology to improve oil and gas production. At present, the research of temporary plugging fracturing is mainly focused on the development of high-performance temporary plugging agent, the simulation of fracture growth morphology and the test of plugging ability of temporary plugging agent. There is limited research on the migration law of temporary plugging agents in fractures, which affects the optimization of temporary plugging processes and parameters. Through a crack sealing experimental device, taking into account the influence of rough cracks and crack width, a temporary plugging agent sealing pressure test was conducted. The sealing pressure and the thickness of the dense layer formed by the temporary plugging agent were used to quantitatively characterize the migration law of the temporary plugging agent. This article elucidates the influence of different types, combinations, and concentrations of temporary plugging agents on the sealing pressure. The research results show that the granular temporary plugging agent has better plugging ability than fiber, and it is easier to plug the fractures with small width. Increasing the concentration of temporary plugging agent is beneficial to plugging fractures, and high concentration of temporary plugging agent can achieve higher plugging pressure compared with low concentration of temporary plugging agent. At the same concentration, the plugging pressure of the temporary plugging agent combined with fiber and small particles is lower than that of the temporary plugging agent combined with fiber, small particles and large particles. Increasing the fiber concentration in the composite temporary plugging agent can effectively increase the temporary plugging pressure and shorten the pressure starting time. Compared to smooth fractures, temporary plugging agents are more likely to accumulate and seal in rough fractures. Temporary plugging fracturing technology has been widely used in unconventional fields such as tight gas and shale oil in the Sichuan Basin. The analysis of fracturing injection pressure data shows that fractures will turn several times in the formation after the temporary plugging agent is added to the fracturing fluid, thus increasing the stimulation range.

## KEYWORDS

migration, multi-scale, temporary plugging agent, rough fracture, fracturing

# 1 Introduction

China has a large number of unconventional oil and gas resources, and unconventional resources such as tight gas, shale oil and shale gas are playing an increasingly important role in oil and gas production [1–3]. Unconventional oil and gas reservoirs are often characterized by low porosity, low permeability and strong heterogeneity. Hydraulic fracturing is an important technology to improve the utilization of unconventional oil and gas resources [4–8]. Affected by reservoir heterogeneity and mutual interference between fractures, hydraulic fractures often expand unevenly, which seriously affects oil and gas production [9]. Improving the uniformity of multiple fractures is the key to unconventional fracturing technology. By adding temporary plugging agent to the fracturing fluid, temporary plugging fracturing can form a plugging layer in the fracture, change the flow direction of subsequent fracturing fluid, and open a new hydraulic fracture in the horizontal section [10, 11]. This technology can greatly improve the uniform expansion of the fracture, thus improving the stimulation effect. Temporary plugging fracturing can form a plugging layer in the fracture by adding temporary plugging agent to the fracturing fluid, forcing the subsequent fracturing fluid to change the flow direction and open a new hydraulic fracture in the horizontal section [12, 13]. This technology can greatly improve the uniform expansion of the fracture, thus improving the stimulation effect.

Yang Wang et al. [14] evaluated the applicability of fiber and granular temporary plugging agent in acid fracturing of ultra-deep carbonate reservoir, and optimized the formula of temporary plugging agent with plugging pressure greater than 15 MPa. Yang Wang et al. [15] proposed a compound staged acid fracturing method for horizontal wells using packers and temporary plugging agents, which greatly increased the stimulation range by adding temporary plugging agents several times. Lishan Yuan et al. [16] used 3D printing technology to create rough fractures and evaluated the migration law of 1 mm fibers and particles in the fractures, and the experimental results shows that fibers and particles are easy to accumulate in the narrow area of fractures. Wei Feng et al. [17] proposed new parameters to analyze fracture morphology and introduced an integrated experimental method as well to study plugging behavior within fractures with different morphologies. Hao Qin et al. [18] used the coupling method of computational fluid dynamics (CFD) and discrete element method (DEM) to establish the mathematical model of temporary plugging agent migration, through which the migration law of temporary plugging agent in artificial fractures during temporary plugging and fracturing of hot and dry rocks can be accurately grasped. Daobing Wang et al. [19] first present a comprehensive workflow to model hydraulic fracture by accounting for interactions with numerous crosscutting natural fracture or joint sets, as well as the effect of temporary plugging in opened fractures. This model is a fully coupled seepage flow in porous media, fluid flow in fractures, and rock deformation finite element model with adaptive insertion of cohesive elements as crosscutting natural fracture or joint sets. Bo Wang et al; [20] modified the commonly used true triaxial hydraulic fracturing system to study the influence of various factors in the process of diversion on the injection pressure response and fracture geometry. According to the physical and mechanical parameters of tight rocks, Yin Zhang et al; [21] poured artificial simulated rock samples (AARS) of sandstone reservoirs in Shengli Oilfield. The true triaxial TP fracturing test under different TP is concentrated on AARS. With the aid of nano-

boron crosslinker (NBC) and sleeve, the initiation and propagation of hydraulic fractures are monitored by acoustic emission (AE) system. Chen Yang et al. [22] established a large-scale visual experimental system based on similarity criteria, which can observe the dynamic plugging performance of fibers and particles. The experimental results show that the plugging process begins with the fiber adhering to the bottom, top and surface of the crack, and then the attached fiber continuously captures the flowing particles to form a dispersed blocking area, and finally forms a flow channel and gradually narrows until it is completely blocked. The fiber causes plugging, and the particles as the skeleton accelerate the subsequent plugging process. Lufeng Zhang et al; [23] carried out experimental research on plugging behavior of degradable fibers and particles in acid-etched fractures, and the results showed that the fracture surface morphology affected the formation time of temporary plugging, but did not affect whether temporary plugging was formed. Ahmed M. Gomaa et al; [24] evaluated the temporary plugging agent suitable for far field (FF) and near well (NW) applications through bridging test, filling permeability test and dissolution test under static and dynamic conditions. Based on Jimusar shale, Minghui Li et al. [25] investigated the plugging performance of fibers and particles and diverting fracturing behavior under three different TPDF application scenarios: near-wellbore in-plane TPDF, multistage TPDF in the horizontal wellbore, and far-field TPDF within fractures. C. E. Cohen et al; [26] developed an acid containing fiber and has been successfully used in matrix acidizing of highly heterogeneous carbonate formations. The fiber is designed to be inert under surface and pumping conditions. Its geometry enables it to form a strong and stable fiber network, which can effectively cross natural cracks, wormholes, and perforated tunnels. Finally, the fiber degrades into water-soluble organic liquid, which will return to the surface during the reflux process. Vanessa Williams et al; [27] proposed an acid fracturing technology that uses solid particles to improve the stimulation effect and enhance the far-field conductivity. This method can not only enhance the conductivity of fractures, but also increase the complexity of fractures. Wang Liwei et al; [28] used the physical simulation method and combined with the on-site temporary plugging process to study the indoor verification of the opening and coupling extension of natural fractures at different levels. The experimental results show that the fracture aperture has a great influence on the temporary plugging steering pressure, and not all fractures with any apertures can be temporarily plugged and steered into new fractures. Ruxin Zhang et al; [29] used five shale outcrops to carry out large-scale real triaxial temporary plugging fracturing simulation research, and the results showed that the temporary plugging agent effectively plugs up induced fractures at two different positions, which are its heel or tip, and results in three main fracture diversion patterns: fracture diversion at the old fracture heel, fracture diversion with an old fracture, and a new fracture induced at a new position. Based on past experience, Mary S. Van Domelen et al; [30] optimized modern diversion practices with self degradable particles and developed diverter design guidelines that provide a basis for temporary plugging fracturing design. The research of temporary plugging fracturing mainly focuses on two aspects: performance evaluation of temporary plugging agent and numerical simulation of fracture propagation, among which performance evaluation of temporary plugging agent is an important component of temporary plugging fracturing technology. The performance evaluation of temporary plugging agents often uses smooth steel plates instead of fracturing fractures to test the plugging pressure of

temporary plugging agents under different width fracture conditions. However, the fracturing fracture walls in the formation are actually not smooth, and they often present a rough and uneven state. Therefore, using smooth steel plates to conduct experiments has certain errors, which cannot accurately characterize the impact of rough walls on the plugging process of temporary plugging agents. Chengyuan Xu et al; [31] used a microscopic visualization experimental device formed by the blockage zone to observe the dynamic blockage performance of spherical materials, sheet materials, and fibers in fractures. Chengyuan Xu et al; [32] used the microscopic visualization experimental device formed by the crack plugging zone to analyze the plugging behavior of different types and different concentrations of irregular shape plugging materials in the fracture. The experimental results show that the main factors affecting the formation of fracture plugging zone are flatness, roundness, convexity and concentration. Huang Liuke et al; [33] studied the effects of rock intrinsic heterogeneity and grain size on the initiation and propagation of hydraulic fractures under different propagation modes by using a two-dimensional discrete element model. Yixin Chen et al; [34] proposed the liquid solid phase transition self-generated proppant fracturing fluid system (LSPCAP), which converts into solid particles at formation temperature to resist closure stress in fractures. Daobing Wang et al. [35] established a discrete network model of complex fracture distribution in HDR reservoirs. The numerical simulation results show that the main factors affecting the thermal recovery efficiency of HDR reservoirs include fracture width, fracture density, fracture permeability and matrix permeability. Daobing Wang et al. [36] used the extended finite element method to study the repeated fracture propagation paths at different initiation angles. The rich function method and magic mode technique are introduced into the repeated crack model, which ensures that the repeated crack can spread freely on the structural grid without any refinement near the crack tip.

Through literature research, it can be found that the research on temporary plugging fracturing of Shale oil mainly focuses on the development of high-performance temporary plugging agent, numerical simulation of fracture growth, and the distribution of temporary plugging agent in the petrophysical model, lacking the research on the migration law of temporary plugging agent in fractures. It is necessary to accurately understand the migration law of temporary plugging agents in rough fractures, as it can provide important basis for the selection of temporary plugging materials and the parameter design of temporary plugging fracturing.

Through a fracture plugging experimental device, taking into account the impact of rough fractures and fracture widths on temporary plugging effectiveness, this paper conducted a plugging pressure test of temporary plugging agents, demonstrating in detail the impact of different types, combinations, and concentrations of temporary plugging agents on plugging pressure, and revealing the migration and bridging process of temporary plugging agents under rough fracture conditions. This study has guiding significance for improving temporary plugging fracturing technology, which has been widely used in unconventional oil and gas reservoirs such as shale oil, tight gas, and shale gas in the Sichuan Basin, achieving good stimulation effects and improving the development effect of gas reservoirs.

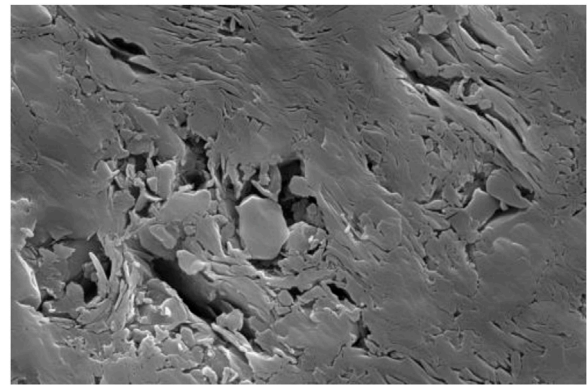


**FIGURE 1**  
Reservoir pore structure of well XQ1.

## 2 Results and discussion

Sichuan Basin is rich in conventional and unconventional oil and gas resources [37]. Its main shale gas production layer is the Wufeng Formation-Longmaxi Formation. Shale oil is mainly distributed in the Jurassic Daanzhai and Lianggaoshan Formations [38], and the tight gas production layer is the Jurassic Shaximiao Formation [39]. The unconventional oil and gas resources in the Sichuan Basin are characterized by low porosity, low permeability, and strong heterogeneity [40, 41]. Hydraulic fracturing is an important technology to enhance unconventional oil and gas production.

Taking the Jurassic shale oil as an example, the Jurassic reservoir is mainly composed of limestone and sandstone, with an average porosity of 5.7%, an average permeability is 0.42 mD, organic carbon content of 1.2%–2.4%, movable hydrocarbon content of 0.6 mg/g–2.5 mg/g, and brittle mineral content of 50%–60%. The compressive strength of shale is 165 MPa, the compressive strength of sandstone is 415 MPa, the elastic modulus of shale is  $5.2 \times 10^4$  MPa, the elastic modulus of sandstone is  $6.1 \times 10^4$  MPa, the horizontal stress difference of reservoir is 6.6–10.4 MPa, and the stress difference coefficient is 0.14–0.18. As can be seen from Figure 1, the reservoir structure of Well XQ1 is composed of residual intergranular pores, clay mineral intergranular pores, and microfractures.

### 2.1 Effect of temporary plugging agent morphology on plugging pressure

This experiment uses a crack sealing tester, which is composed of an injection system, a fracture simulation system, and a data acquisition system. The injection system consists of a high-pressure displacement pump, with an upper limit of 300 mL/min. The fracture simulation system uses a set of parallel steel plates to simulate fracturing cracks, and simulates fractures of different widths by adjusting the gap between two steel plates. Because the fracture wall in the formation is rough, in order to truly simulate the rough fracture in the formation, we first obtained the fracture wall data of Shale oil core through 3D scanning technology,



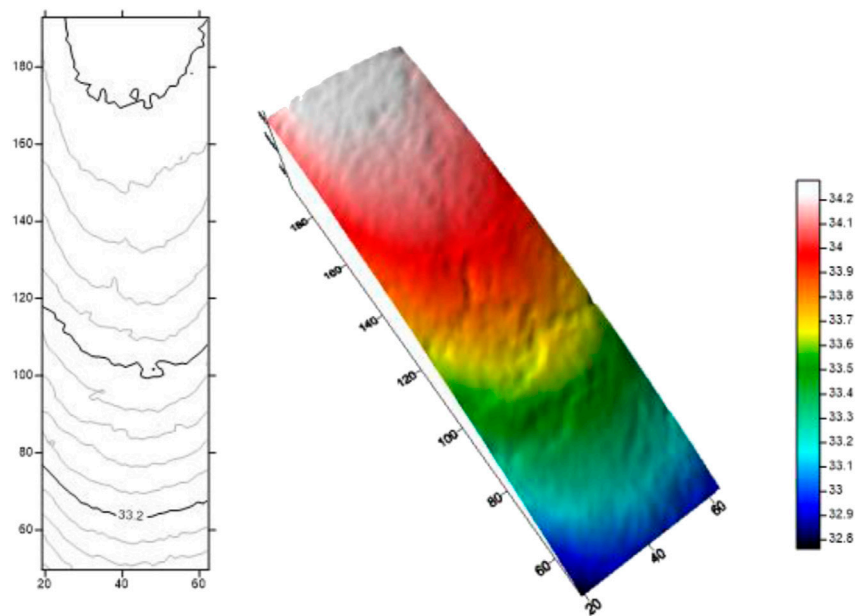


**FIGURE 2**  
Wall scanning cloud map of the fracturing fracture.

and then polished the steel plate according to the obtained 3D laser scanning data, so as to ensure that the roughness of the simulated fracture is consistent with that of the fracture in the real formation. The data collection system mainly records the injection pressure and displacement in real-time through high-performance pressure sensors.

Figure 2 is a scanned cloud map of the wall of a hydraulic fracturing fracture. From this image, it can be seen that the wall of the fracturing fracture is not smooth, but rather very rough and uneven. Using rough wall fractures for experiments is helpful to truly reflect the migration law of temporary plugging agents in fracturing fractures. We create a simulated crack system based on the crack wall data in Figure 2.

Linear gel is a commonly used fracturing fluid, mainly composed of guar gum and water. In this experiment, a linear gel with a viscosity of 30 mPas was selected as the carrier fluid, and fibers and granular temporary plugging agents of different concentrations and proportions were mixed in the linear gel. The mixed liquid was injected into the simulated fracture through a displacement pump, and the injection pressure and displacement were recorded in real-time through a data acquisition system. The chemical composition of fiber, 100 mesh and 10/40 mesh particles in the experiment is polyvinyl alcohol resin modified by poly lotion. The length of the fiber is 6 mm, the diameter of 100 mesh particles is 0.15 mm, and the diameter of 10/40 mm particles is 0.425 mm–2 mm. The density of fibers and particles is 1.26 g/cm<sup>3</sup>, and the above temporary plugging agents were all purchased from Southwest Oil and Gas Field Company.

We inject 0.5% fiber, 0.5% 100 mesh particulate temporary plugging agent, and 0.5% 10/40 mesh particulate temporary plugging agent into a simulated rough fracture with a width of 4 mm through an injection system, while recording the plugging pressure through a data acquisition system.

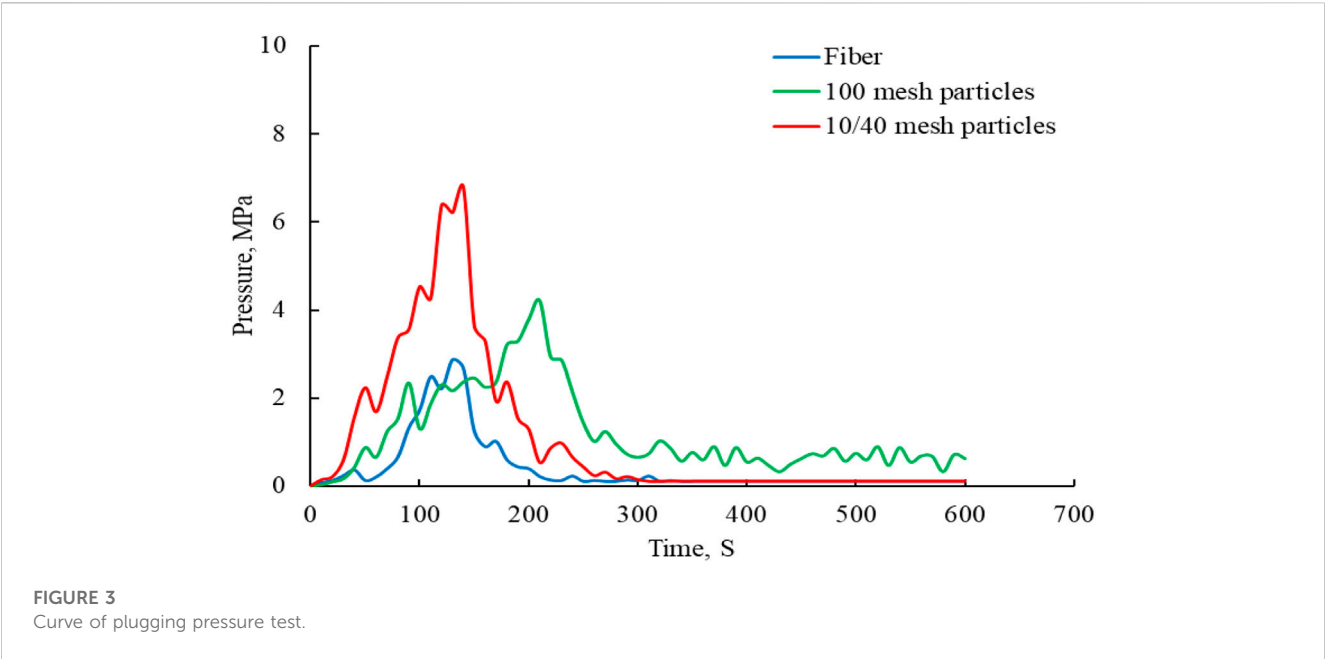
As can be seen from Figure 3 and Table 1, compared to fiber and 10/40 mesh granular temporary plugging agent, the peak plugging pressure of the 100 mesh granular temporary plugging agent is the highest, and the plugging pressure increases rapidly after the injection of the fiber, with the shortest pressure build-up time. The peak plugging pressure of 10/40 mesh granular temporary plugging agent can reach 6.78 MPa, which is 136% larger than the peak fiber plugging pressure.

Compared to fiber and 100 mesh granular temporary plugging agent, the reason why 10/40 mesh granular temporary plugging agent has the best plugging effect is that large particle temporary plugging agent has a good match with the fracture [42], which can quickly fill and accumulate at the fracture opening to form a sealing layer, thereby increasing the plugging pressure and shortening the plugging pressure rise time.

## 2.2 Effect of temporary plugging agent concentration on plugging pressure

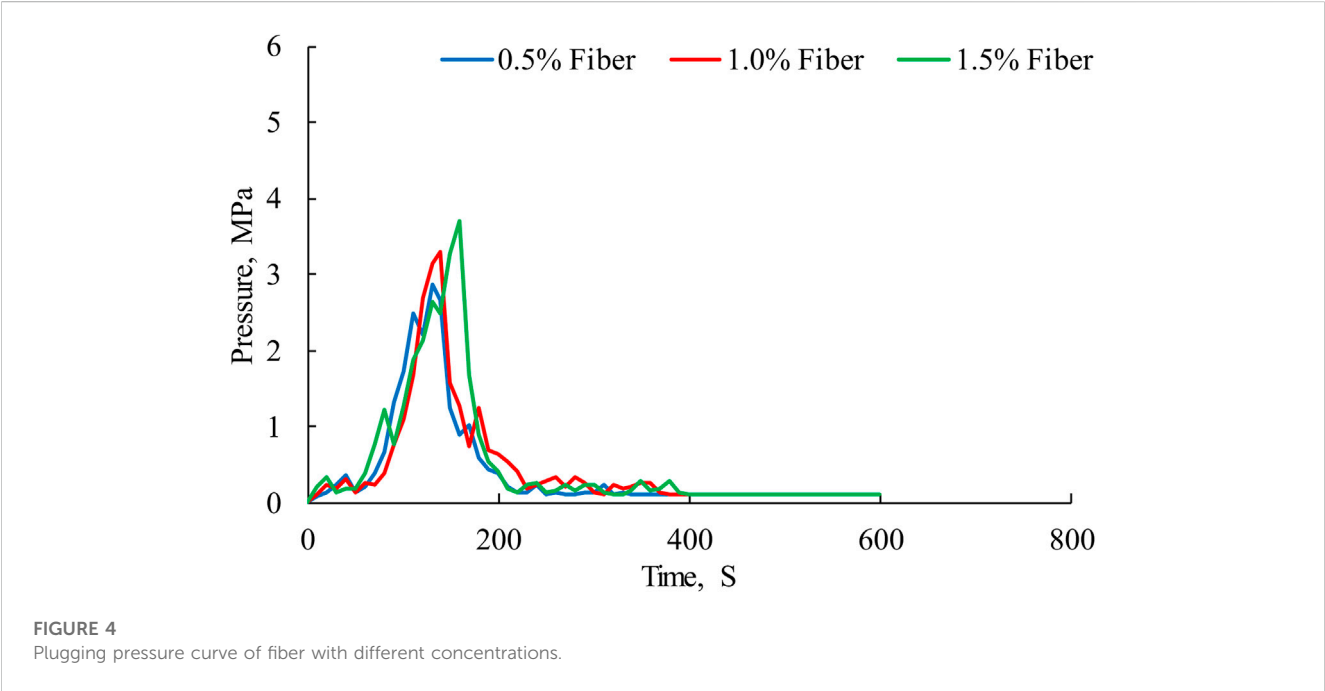
We injected different concentrations of fiber, 100 mesh granular temporary plugging agent, and 10/40 mesh granular temporary plugging agent into the simulated rough fractures, with a fracture width of 4 mm and a carrier fluid injection displacement of 250 mL/min. In the experiment, the plugging pressure data was recorded by the data acquisition system. After the experiment, the parallel steel plate used to simulate the crack was opened, and the thickness of the dense layer formed by the temporary plugging agent in the crack was measured by the vernier caliper. The migration of the temporary plugging agent in the fracture is judged by the plugging pressure and the thickness of the dense layer.





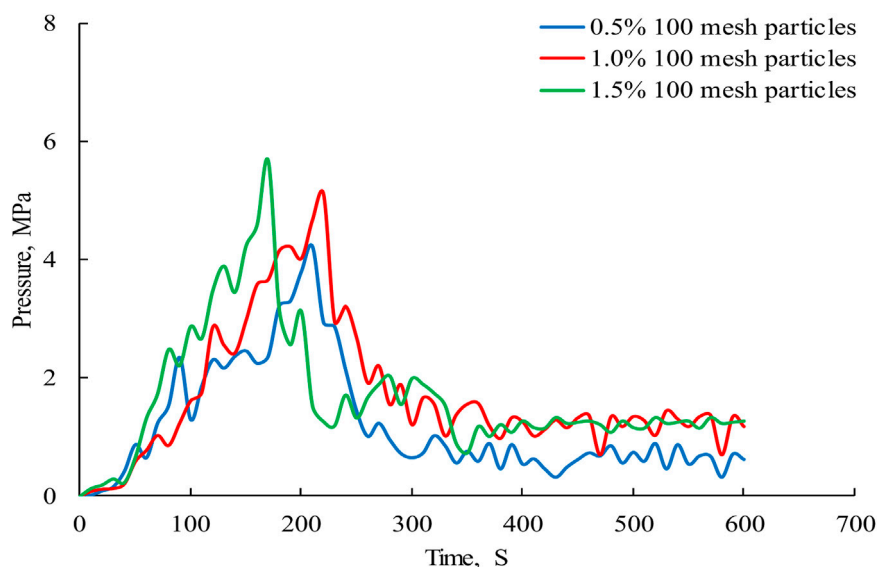
**TABLE 1** Comparison of plugging peak pressure and starting time of different forms of temporary plugging agents.

Type of temporary plugging agent	The time when the plugging pressure starts to rise(S)	Peak plugging pressure (MPa)
Fiber	51	2.87
100 mesh particles	35	4.21
10/40 mesh particles	29	6.78



**TABLE 2** Comparison of plugging effects of temporary plugging agents with different concentrations.

Type of temporary plugging agent	Concentration of temporary plugging agent (%)	Thickness of sealing layer (cm)	Peak plugging pressure (MPa)
Fiber	0.5	2.2	2.87
	1.0	2.6	3.29
	1.5	3.1	3.71

**FIGURE 5**

Plugging pressure curve of 100 mesh particles plugging agents with different concentrations.

As can be seen from Figure 4, as the fiber concentration increases from 0.5% to 1.5%, the peak plugging pressure of the fiber increases, but the increase in plugging pressure is not significant. Especially when the fiber concentration is 1.5%, the peak plugging pressure is 3.71 MPa, which is only 0.84 MPa more than the peak plugging pressure when the fiber concentration is 0.5%. Shale oil and gas reservoirs in Sichuan Basin have strong heterogeneity, with a horizontal two-way stress difference of over 10 MPa. The plugging pressure of fibers is low and cannot meet the requirements for temporary plugging and fracturing of shale oil and gas reservoirs.

As can be seen from Table 2, with the increase in fiber concentration, the peak plugging pressure gradually increases, while the thickness of the sealing layer gradually increases. The fiber concentration has a significant impact on the performance of the plugging layer. The sealing layer formed by compaction of high concentration fibers is very dense, and the pressure bearing capacity of the sealing layer is significantly improved.

As can be seen from Figure 5, with the concentration of 100 mesh granular temporary plugging agent increasing from 0.5% to 1.5%, the peak plugging pressure does not increase significantly. Especially, the peak plugging pressure of 100 mesh granular temporary plugging agent with a concentration of 1.5% is

only 0.91 MPa higher than the peak plugging pressure of 100 mesh granular temporary plugging agent with a concentration of 0.5%, and the peak plugging pressure of 100 mesh granular temporary plugging agent with a high concentration is still very low, which is only 5.67 MPa. It still cannot meet the requirements for temporary plugging and fracturing of shale oil and gas reservoirs in the Sichuan Basin.

As can be seen from Figure 6, under the same concentration, the plugging pressure of 10/40 mesh granular temporary plugging agent is much greater than that of fiber and 100 mesh granular temporary plugging agent. The plugging pressure of 10/40 mesh granular temporary plugging agent with a concentration of 1.5% is the highest, which can reach 9.42 MPa. However, temporary plugging fracturing of shale oil and gas reservoirs in Sichuan Basin requires a plugging pressure of more than 15 MPa, and using fiber or particles cannot meet the reservoir stimulation requirements.

Compared to fiber and 100 mesh granular temporary plugging agent, the reason why the plugging pressure of 10/40 mesh granular temporary plugging agent is high is that the temporary plugging agent has a large size and can quickly form accumulation at the simulated fracture opening with a width of 4 mm to improve the plugging pressure. However, due to the obvious gap between various particles in the accumulation process of granular temporary

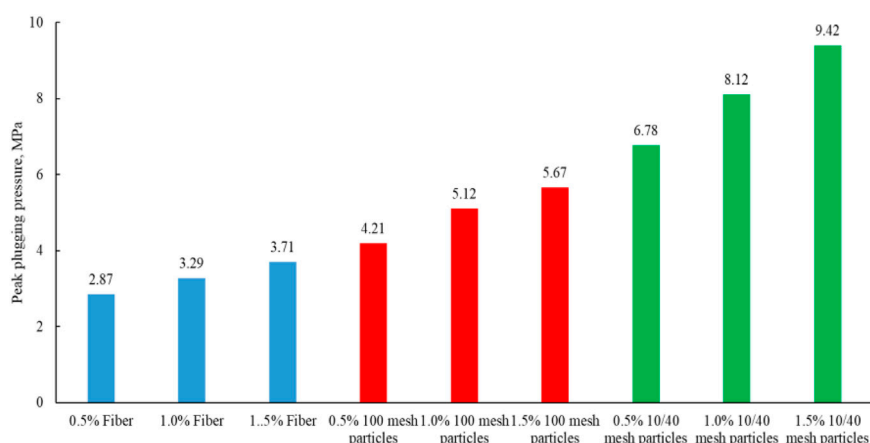


**FIGURE 6**  
Comparison of peak plugging pressures of different temporary plugging agents.



**FIGURE 7**  
Accumulation of 10/40 mesh granular temporary plugging agent at the fracture opening.

plugging agents (Figure 7), the plugging layer formed by the granular temporary plugging agent has obvious gaps, which makes the liquid easily flow through the gaps, resulting in the low plugging pressure of the granular temporary plugging agent.

## 2.3 Effect of temporary plugging agent combination on plugging pressure

Tight gas, shale oil, and ultra-deep carbonate reservoirs in the Sichuan Basin have strong heterogeneity and large stress differences. Temporary plugging fracturing requires high plugging performance of temporary plugging agents. Neither fiber nor granular temporary plugging agent can meet the requirements of temporary plugging and fracturing in the Sichuan Basin. Composite fiber and granular temporary plugging agent can improve the plugging pressure [43]. This paper evaluates the plugging effect of composite fiber and granular temporary plugging agent by plugging pressure testing.

We maintain the concentration of temporary plugging agent at 2% and adjust the proportion of fiber, 100 mesh granular temporary plugging agent, and 10/40 mesh granular temporary plugging agent. The experiment injected a mixture of fiber and granular temporary plugging agent into the simulated rough fractures, and recorded the change in plugging pressure in real time. The fracture width was 4 mm, and the carrier liquid injection displacement was 250 mL/min.

From Figure 8 and Table 3, it can be seen that the plugging pressure increases significantly after mixing fibers and particles together, especially when the proportion of granular temporary plugging agents is high. As the concentration of 10/40 mesh granular temporary plugging agent increases, the peak plugging pressure of the dense layer formed by the mixture of fiber and granular temporary plugging agent significantly increases, especially when the concentration of 10/40 mesh granular temporary plugging agent is 1.5%, the peak plugging pressure is 37.5% higher than the peak plugging pressure when the concentration of 10/40 mesh granular temporary plugging agent is 0.5%.

The strength of the sealing layer is characterized by the sealing pressure, and the higher the sealing pressure, the greater the strength of the sealing layer. As can be seen from Figure 9, the mixture of fiber and granular temporary plugging agent forms a very thick dense layer at the fracture opening, in which the fiber and granular temporary plugging agent are wrapped together, especially in the interior of the fracture, where a large amount of the mixture of fiber and granular temporary plugging agent is also filled. By comparing Figure 7, it can be seen that if only granular temporary plugging agents are used, there are obvious gaps between the particles, and using a mixture of fibers and particles can well compensate for this disadvantage. Fibers capture granular temporary plugging agents like fishing nets. After the granular temporary plugging agent is wrapped in fibers, the strength of the plugging layer is further improved, while fibers can be filled in the gaps between the granular temporary plugging agents, which improves the compactness of the plugging layer. The plugging pressure formed by fibers and particles is higher than that of a single fiber or particle, mainly because when fibers and particles are mixed together, they can wrap and fill each other, thereby reducing the gap in the sealing layer.

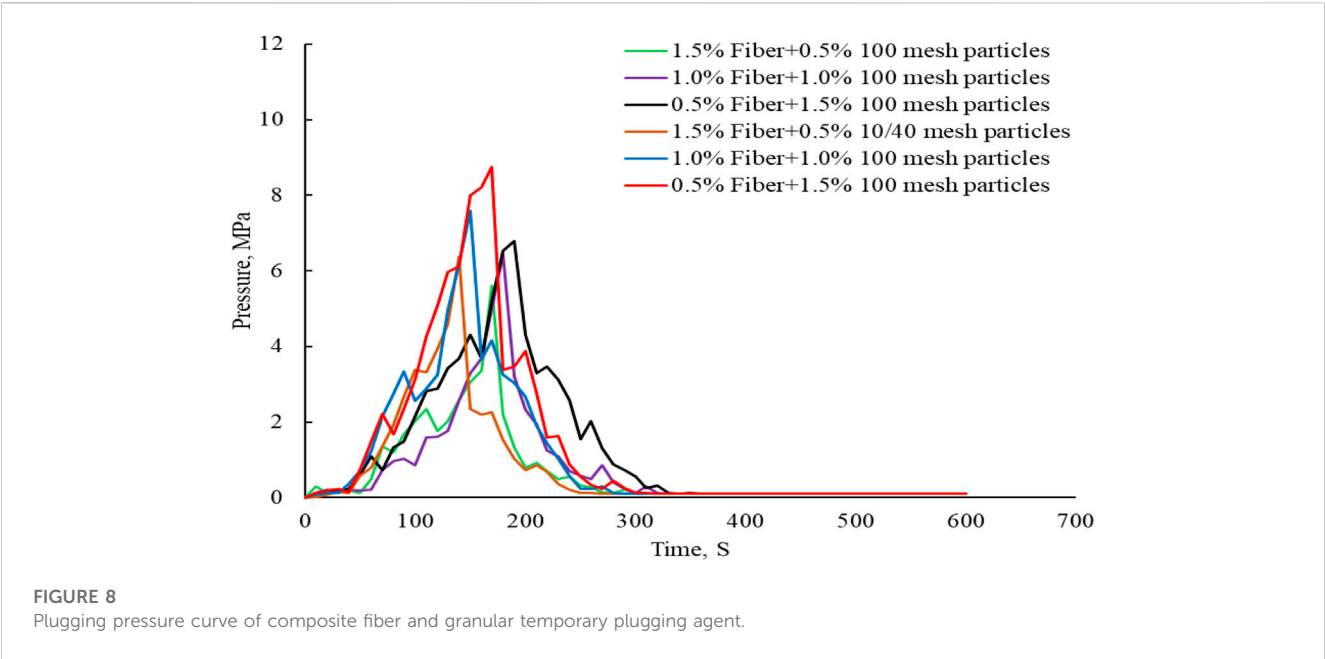
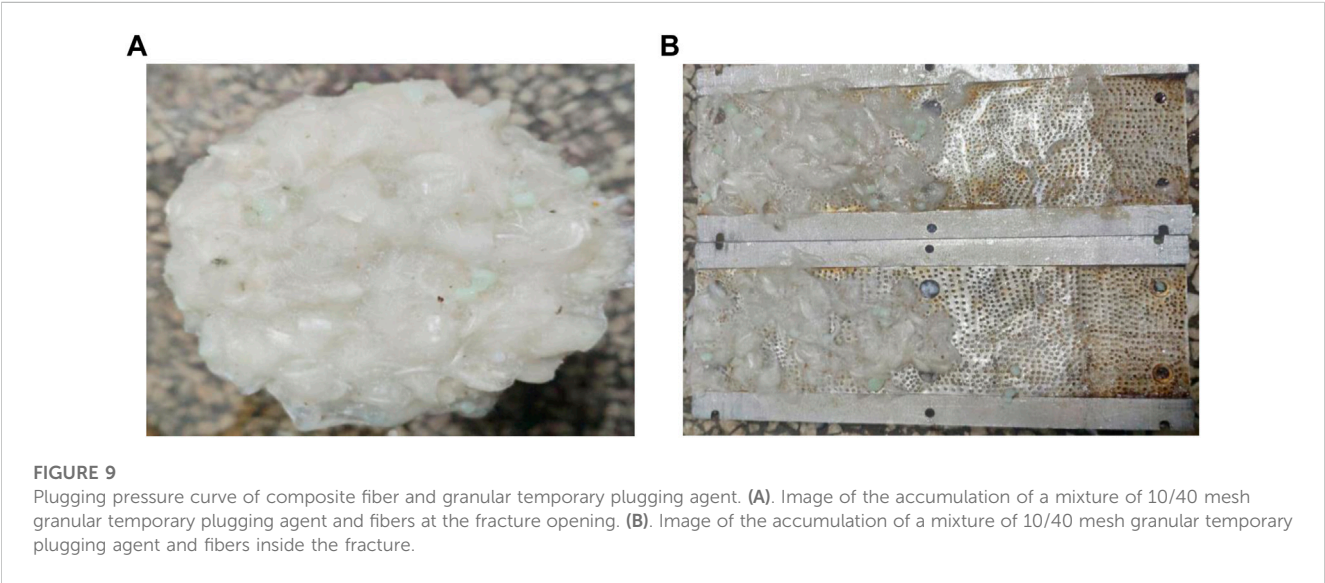
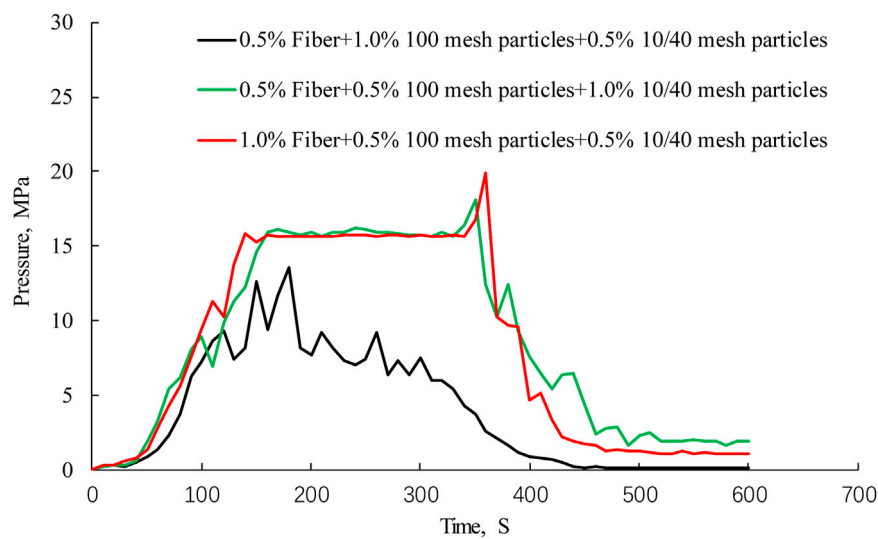


TABLE 3 Comparison of peak plugging pressure.

Concentration of fibers (%)	Concentration of 100 mesh granular temporary plugging agent (%)	Concentration of 10/40 mesh granular temporary plugging agent (%)	Peak plugging pressure (MPa)
0.5	1.5	—	6.79
1.0	1.0	—	6.45
1.5	0.5	—	5.61
0.5	—	1.5	8.79
1.0	—	1.0	7.59
1.5	—	0.5	6.39





**FIGURE 10**  
Plugging pressure curves of different combinations of temporary plugging agents.

We used a mixture of fiber, 100 mesh granular temporary plugging agent, and 10/40 mesh granular temporary plugging agent to conduct plugging tests. The plugging layer consists of the above three temporary plugging agents. We adjusted the ratio of fiber, 100 mesh granular temporary plugging agent, and 10/40 mesh granular temporary plugging agent to test the plugging performance of different combinations of temporary plugging agents. In the experiment, the simulated fracture width is 4 mm, and the carrier liquid injection displacement is 250 mL/m.

As can be seen from Figure 10, when the concentration of fiber is 0.5%, increasing the concentration of 10/40 mesh granular temporary plugging agent is beneficial to improving the plugging pressure, especially when the concentration of 10/40 mesh granular temporary plugging agent increases from 0.5% to 1.0%, the peak plugging pressure increases from 13.54 MPa to 18.12 MPa. In the experiment, the fiber concentration was increased from 0.5% to 1.0%, and the peak plugging pressure was increased from 18.12 MPa to 19.86 MPa. The peak plugging pressure was not significantly increased after increasing the fiber concentration, but the pressure onset time was shortened from 20 s to 10 s. Increasing the fiber concentration is conducive to the formation of a network structure between fibers, which can quickly capture granular temporary plugging agents and shorten the formation time of the plugging layer.

## 2.4 Effect of fracture width on plugging pressure

We injected a mixture of 100 mesh temporary plugging agent with a concentration of 0.1% and 10/40 mesh temporary plugging agent with a concentration of 0.1% into the simulated rough fractures. The widths of fractures are 2 mm, 4 mm, and 6 mm, respectively, while carefully recording the changes in plugging pressure. The displacement of this experiment is 250 mL/min.

As can be seen from Figure 11, temporary plugging agents have a better sealing effect on narrow fractures. As the fracture width decreases, the peak sealing pressure increases rapidly, and the pressure onset time becomes shorter. During the plugging process of temporary plugging agent, the larger the width of the fracture, the larger the cross section of temporary plugging agent migration, and the greater the difficulty of temporary plugging agent bridging. In order to achieve rapid and high-strength plugging, it is recommended to reduce the injection displacement before injecting temporary plugging agent in acid fracturing, thereby reducing the fracture width, and improving the plugging pressure and effectiveness.

## 2.5 Effect of fracture roughness on plugging pressure

The wall of a fracture formed by hydraulic fracturing is rough and uneven. We use two types of roughness to simulate the fracture for experiments, one is a simulation fracture with a smoother wall surface, and the other is a simulation fracture with a very rough wall surface. Through experiments, we evaluate the impact of fracture roughness on the plugging effect of temporary plugging agents. The experiment uses a mixture of 0.5% fiber, 1.0% 100 mesh granular temporary plugging agent, and 0.5% 10/40 mesh granular temporary plugging agent. The simulated fracture width is 4 mm, and the injected liquid displacement is 250 mL/min.

As can be seen from Figure 12, compared to the smooth fractures, temporary plugging agents have a better plugging effect on the rough fractures, mainly because there are a large number of bumps on the surface of rough fractures, which will intensify the collision of granular temporary plugging agents. The granular temporary plugging agent will stop moving and accumulate at the depressed position of the fracture, while the bumps on the fracture wall will slow down the migration speed of fibers within the

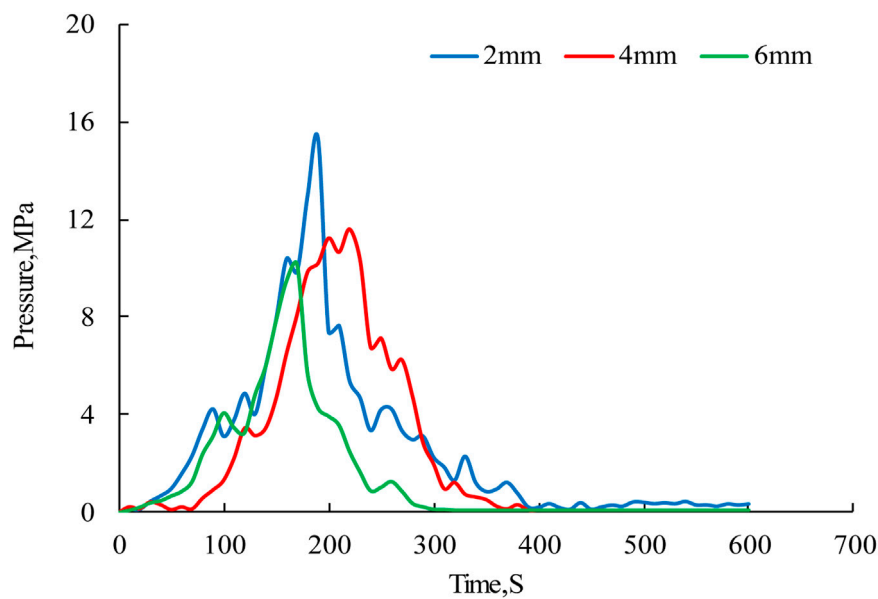


**FIGURE 11**  
Influence curve of fracture width on plugging pressure.

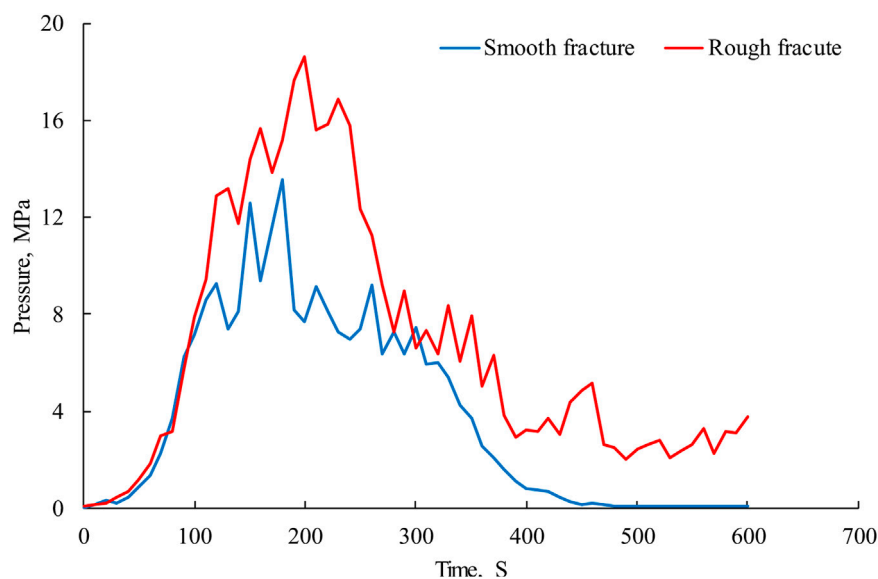


**FIGURE 12**  
Influence curve of fracture width on plugging pressure.

fracture, which will further slow down the migration speed of granular temporary plugging agent, so as to achieve effective plugging [44].

## 2.6 Field application

More than 40 wells in the Sichuan Basin have undergone temporary plugging fracturing, which has significantly improved

the stimulation effect of tight gas, shale oil and gas, and ultra-deep carbonate oil and gas reservoirs. Well SC1 is a horizontal well in the Daanzhai section of the Sichuan Basin, with a reservoir temperature of 89°C and a reservoir pressure coefficient of 1.65. The horizontal section of SC1 is 1000 m long, with strong reservoir heterogeneity and significant differences in porosity and permeability. In order to improve the complexity of fracturing fractures, temporary plugging fracturing technology was used in Well SC1. A total of 1700 kg of fiber and 1700 kg of granular temporary plugging agent were added



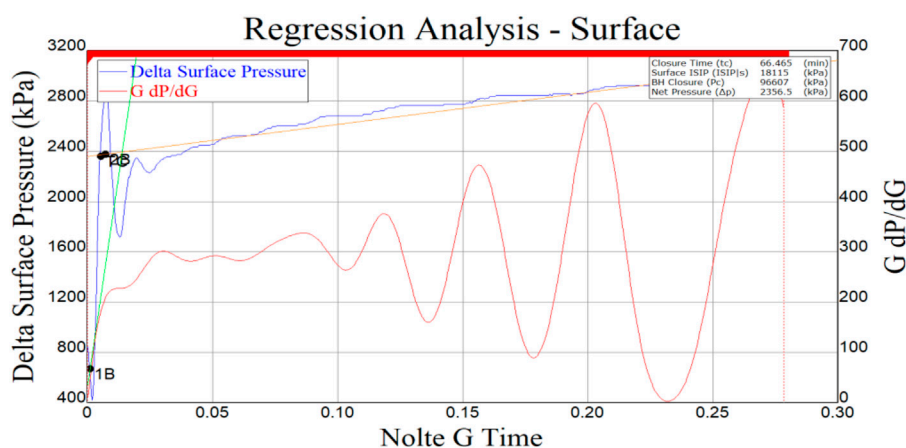


FIGURE 13

The pump injection pressure analysis of well SC1.

to the fracturing of Well SC1, and among them, there is 850 kg of 100 mesh granular temporary plugging agent, and 850 kg of 10/40 mesh granular temporary plugging agent. During the fracturing process, the temporary plugging agent is uniformly mixed in the linear glue with a viscosity of 30 mPa·s, and the mixed liquid is injected into the formation through the fracturing pump truck with an injection displacement of 1 m<sup>3</sup>/min.

After adding the temporary plugging agent, the fracturing pressure increased by an average of 6 MPa. The pump injection pressure analysis of well SC1 (Figure 13) shows that the G function exhibits multiple jumping peaks and troughs, indicating that the fracturing fracture has undergone multiple deflections and expansion in the formation, which proves that the research results in this paper can be used to guide the fracturing design of Shale oil.

### 3 Conclusion

In this study, we clarified the migration rule of temporary plugging agent in rough fractures through visualization and plugging pressure testing, and confirmed that using fiber, 100 mesh granular temporary plugging agent, and 10/40 mesh granular temporary plugging agent can achieve rapid and high-strength plugging. Especially when the fiber concentration is increased, the pressure onset time is significantly shortened, which is conducive to the rapid formation of a sealing layer to force the fracture to turn. This study has been widely used in the stimulation of tight gas, shale oil and gas, and ultra deep carbonate oil and gas reservoirs in the Sichuan Basin, and has achieved good stimulation effects. Although this paper has studied the migration law of temporary plugging agent in the fracture, it still needs to be further improved. For example, it is suggested to use high-strength transparent resin to make a fracture seal pressure test system, and to be equipped with high-speed cameras to capture the migration state of temporary sealing agent in the fracture in real time, so as to have a more intuitive understanding of the results.

### Data availability statement

The original contributions presented in the study are included in the article/supplementary material, further inquiries can be directed to the corresponding author.

### Author contributions

YW: Conceptualization, funding acquisition, project administration, re-sources, writing—original draft and software, formal analysis, methodology, writing—review and editing project administration. YF and XW: Investigation, Data curation funding. All authors contributed to the article and approved the submitted version.

### Funding

This work was financially supported by the project of the PetroChina Southwest Oil and Gas Field Company (Grant Nos. 20200302-14, 20210302-19, and 20220302-11).

### Conflict of interest

Authors YW, YF, and XW were employed by Engineering Technology Research Institute of Southwest Oil and Gas Field Company, PetroChina.

### Publisher's note

All claims expressed in this article are solely those of the authors and do not necessarily represent those of their affiliated organizations, or those of the publisher, the editors and the reviewers. Any product that may be evaluated in this article, or claim that may be made by its manufacturer, is not guaranteed or endorsed by the publisher.

## References

- Suyun HU, Jianzhong LI, Tongshan W, Zecheng WA, Tao YA, Xin LI, et al. CNPC oil and gas resource potential and exploration target selection. *P Geo Exp* (2020) 42(5): 813–23.
- Li L, Tan J, Wood DA, Zhao Z, Becker D, Lyu Q, et al. A review of the current status of induced seismicity monitoring for hydraulic fracturing in unconventional tight oil and gas reservoirs. *Fuel* (2019) 242:195–210. doi:10.1016/j.fuel.2019.01.026
- Chen S, Xu G, Yang J, Li Y-F, Zhang J, Zhao H-W, et al. Foundational geological survey for oil and gas resources in Songliao Basin and its periphery areas: Progress and prospect. *Geology Resour* (2021) 30(3):221–31.
- Guoxin L, Rukai Z. Progress, challenges and key issues in the unconventional oil and gas development of CNPC. *China Pet Exploration* (2020) 25(2):1. doi:10.3969/j.issn.1672-7703.2020.02.001
- Qin L, Zhang X, Zhai C, Lin H, Lin S, Wang P, et al. Advances in liquid nitrogen fracturing for unconventional oil and gas development: A review. *Energy and Fuels* (2022) 36(6):2971–92. doi:10.1021/acs.energyfuels.2c00084
- Boak J, Kleinberg R. Shale gas, tight oil, shale oil and hydraulic fracturing. *Future Energy* (2020) 67–95. doi:10.1016/b978-0-08-102886-5.00004-9
- Aslannezhad M, Kalantariasl A, You Z, Iglauer S, Keshavarz A. Micro-proppant placement in hydraulic and natural fracture stimulation in unconventional reservoirs: A review. *Energy Rep* (2021) 7:8997–9022. doi:10.1016/j.egyr.2021.11.220
- Wang D, Wang X, Ge H, Sun D, Yu B. Insights into the effect of spontaneous fluid imbibition on the formation mechanism of fracture networks in brittle shale: An experimental investigation. *ACS omega* (2020) 5(15):8847–57. doi:10.1021/acsomega.0c00452
- Wang D, Dahi Taleghani A, Yu B, Wang M, He C. Numerical simulation of fracture propagation during refracturing. *Sustainability* (2022) 14(15):9422. doi:10.3390/su14159422
- Wang Y, Yang J, Wang T, Hu Q, Lv Z, He T. Visualization experiment of multi-stage alternating injection acid fracturing. *Energy Rep* (2022) 8:9094–103. doi:10.1016/j.egyr.2022.07.031
- Wang Y, Zhou C, Zhang H, He T, Tang X, Peng H, et al. Research and application of segmented acid fracturing technology in horizontal wells of ultra deep carbonate gas reservoirs in southwest China. In: International Petroleum Technology Conference; March 2021. OnePetro (2021).
- Wang D, Qin H, Zheng C, Sun D, Yu B. Transport mechanism of temporary plugging agent in complex fractures of hot dry rock: A numerical study. *Geothermics* (2023) 111:102714. doi:10.1016/j.geothermics.2023.102714
- Wang Y, Zhou C, Yi X, Li L, Chen W, Han X. Technology and application of segmented temporary plugging acid fracturing in highly deviated wells in ultradeep carbonate reservoirs in southwest China. *ACS omega* (2020) 5(39):25009–15. doi:10.1021/acsomega.0c01008
- Wang Y, Fan Y, Zhou C, Luo Z, Chen W, He T, et al. Research and application of segmented acid fracturing by temporary plugging in ultradeep carbonate reservoirs. *ACS omega* (2021) 6(43):28620–9. doi:10.1021/acsomega.1c03021
- Wang Y, Fan Y, Wang T, Ye J, Luo Z. A new compound staged gelling acid fracturing method for ultra-deep horizontal wells. *Gels* (2022) 8(7):449. doi:10.3390/gels8070449
- Yuan L, Zhou F, Li B, Gao J, Yang X, Cheng J, et al. Experimental study on the effect of fracture surface morphology on plugging efficiency during temporary plugging and diverting fracturing. *J Nat Gas Sci Eng* (2020) 81:103459. doi:10.1016/j.jngse.2020.103459
- Feng W, Yang C, Zhou F. Experimental study on surface morphology and relevant plugging behavior within acid-etched and unetched fractures. *J Nat Gas Sci Eng* (2021) 88:103847. doi:10.1016/j.jngse.2021.103847
- Qin H, Wang D, Deng Y, Han D, Yu B, Sun D. Study on transport law of temporary plugging agent in artificial fractures of hot dry rocks. *J Eng Thermophys* 43(9):2397–403.
- Wang D, Dong Y, Sun D, Yu B. A three-dimensional numerical study of hydraulic fracturing with degradable diverting materials via CZM-based FEM. *Eng Fracture Mech* (2020) 237:107251. doi:10.1016/j.engfracmech.2020.107251
- Wang B, Zhou F, Yang C, Wang D, Yang K, Liang T. Experimental study on injection pressure response and fracture geometry during temporary plugging and diverting fracturing. *SPE J* (2020) 25(2):573–86. doi:10.2118/199893-pa
- Zhang Y, Yu R, Yang W, Tian Y, Shi Z, Sheng C, et al. Effect of temporary plugging agent concentration and fracturing fluid infiltration on initiation and propagation of hydraulic fractures in analogue tight sandstones. *J Pet Sci Eng* (2022) 210:110060. doi:10.1016/j.petrol.2021.110060
- Yang C, Zhou F, Feng W, Tian Z, Yuan L, Gao L. Plugging mechanism of fibers and particulates in hydraulic fracture. *J Pet Sci Eng* (2019) 176:396–402. doi:10.1016/j.petrol.2019.01.084
- Zhang L, Zhou F, Feng W, Pournik M, Li Z, Li X. Experimental study on plugging behavior of degradable fibers and particulates within acid-etched fracture. *J Pet Sci Eng* (2020) 185:106455. doi:10.1016/j.petrol.2019.106455
- Gomaa AM, Nino-Penaloza A, Castillo D, McCartney E, Mayor J. Experimental investigation of particulate diverter used to enhance fracture complexity. In: SPE International Conference and Exhibition on Formation Damage Control; February 24–26, 2016; Louisiana, USA. OnePetro (2016).
- Li M, Zhou F, Sun Z, Dong E, Zhuang X, Yuan L, et al. Experimental study on plugging performance and diverted fracture geometry during different temporary plugging and diverting fracturing in Jimusar shale. *J Pet Sci Eng* (2022) 215:110580. doi:10.1016/j.petrol.2022.110580
- Cohen CE, Tardy PM, Lesko T, Lecerf B, Pavlova S, Voropaev S, et al. Understanding diversion with a novel fiber-laden acid system for matrix acidizing of carbonate formations. In: SPE annual technical conference and exhibition; September 19–22, 2010; Florence, Italy. OnePetro (2010).
- Williams V, McCartney E, Nino-Penaloza A. Far-field diversion in hydraulic fracturing and acid fracturing: Using solid particulates to improve stimulation efficiency. In: SPE Asia Pacific hydraulic fracturing conference; August 24–26, 2016; Beijing, China. OnePetro (2016).
- Liwei W, Xiuling H, Chunming X, Bo W, Zhanwei Y, Ying G. Multi-fracture temporary blocking steering mechanism and experimental research in ultra-deep fractured reservoir. In: 5th ISRM Young Scholars' Symposium on Rock Mechanics and International Symposium on Rock Engineering for Innovative Future; December 1–4, 2019; Okinawa, Japan. OnePetro (2019).
- Zhang R, Hou B, Tan P, Muhadasi Y, Fu W, Dong X, et al. Hydraulic fracture propagation behavior and diversion characteristic in shale formation by temporary plugging fracturing. *J Pet Sci Eng* (2020) 190:107063. doi:10.1016/j.petrol.2020.107063
- Van Domelen MS. A practical guide to modern diversion technology. In: Spe oklahoma city oil and gas symposium; March 27–31, 2017; Oklahoma, OK. OnePetro (2017).
- Xu C, Zhang H, Kang Y, Zhang J, Bai Y, Zhang J, et al. Physical plugging of lost circulation fractures at microscopic level. *Fuel* (2022) 317:123477. doi:10.1016/j.fuel.2022.123477
- Xu C, Zhang H, She J, Jiang G, Peng C, You Z. Experimental study on fracture plugging effect of irregular-shaped lost circulation materials. *Energy* (2023) 276:127544. doi:10.1016/j.energy.2023.127544
- Huang L, Liu J, Zhang F, Dontsov E, Damjanac B. Exploring the influence of rock inherent heterogeneity and grain size on hydraulic fracturing using discrete element modeling. *Int J Sol Structures* (2019) 176:207–20. doi:10.1016/j.ijsolstr.2019.06.018
- Chen Y, Sang Y, Guo J, Yang J, Chen W, Zeng J, et al. Experimental study on a liquid–solid phase-change autogenous proppant fracturing fluid system. *ACS omega* (2023) 8(10):9101–10. doi:10.1021/acsomega.2c04853
- Wang D, Zhu H, Micheal M, Tang X, Li Q, Yi X, et al. Coupled heat-fluid-solid numerical study on heat extraction potential of hot dry rocks based on discrete fracture network model. *Energy Geosci* (2023):100159. doi:10.1016/j.engeos.2023.100159
- Wang DB, Zhou FJ, Li YP, Yu B, Martyushev D, Liu XF, et al. Numerical simulation of fracture propagation in Russia carbonate reservoirs during refracturing. *Pet Sci* (2022) 19(6):2781–95. doi:10.1016/j.petsci.2022.05.013
- Guo X, Hu D, Huang R, Wei Z, Duan J, Wei X, et al. Deep and ultra-deep natural gas exploration in the Sichuan Basin: Progress and prospect. *Nat Gas Industry B* (2020) 7(5):419–32. doi:10.1016/j.ngib.2020.05.001
- Chen S, Zhu Y, Wang H, Liu H, Wei W, Fang J. Shale gas reservoir characterisation: A typical case in the southern Sichuan Basin of China. *Energy* (2011) 36(11):6609–16. doi:10.1016/j.energy.2011.09.001
- Zhang X, Fu M, Deng H, Li Z, Zhao S, Gluyas JG, et al. The differential diagenesis controls on the physical properties of lithofacies in sandstone reservoirs from the Jurassic Shaximiao Formation, Western Sichuan depression, China. *J Pet Sci Eng* (2020) 193:107413. doi:10.1016/j.petrol.2020.107413
- Dai J, Zou C, Liao S, Dong D, Ni Y, Huang J, et al. Geochemistry of the extremely high thermal maturity Longmaxi shale gas, southern Sichuan Basin. *Org Geochem* (2014) 74:3–12. doi:10.1016/j.orggeochem.2014.01.018
- Liang C, Jiang Z, Yiting Y, Wei X. Shale lithofacies and reservoir space of the wufeng-longmaxi formation, Sichuan Basin, China. *Pet Exploration Dev* (2012) 39(6): 736–43. doi:10.1016/s1876-3804(12)60098-6
- Wang D, Zhou F, Ge H, Shi Y, Yi X, Xiong C, et al. An experimental study on the mechanism of degradable fiber-assisted diverting fracturing and its influencing factors. *J Nat Gas Sci Eng* (2015) 27:260–73. doi:10.1016/j.jngse.2015.08.062
- Al-Enezi A, Al-Othman M, Al-Shtail M, Sadeeqi YA, Bhatia K, Alboueshi A, et al. Application of integrated far-field diversion technology in multistage acid-fracturing: Lesson learnings from unconventional field north Kuwait. In: SPE International Hydraulic Fracturing Technology Conference and Exhibition; January 11–13, 2022; Muscat, Oman. OnePetro (2022).
- Zheng C, Wang D, Yu B. Numerical investigation on the migration law of temporary plugging agent in rough fractures based on CFD-DEM coupling. *Journal Engineering Thermophysics* (2013) 44(2):422–8.



## OPEN ACCESS

## EDITED BY

Chong Lin,  
CCDC Drilling & Production Technology  
Research Institute, China

## REVIEWED BY

Yuanqing Wu,  
Shenzhen University, China  
Ying Zhong,  
Chengdu University of Technology,  
China

## \*CORRESPONDENCE

Xiangwei Kong,  
✉ kongxw\_yangtze@163.com

RECEIVED 24 May 2023

ACCEPTED 10 July 2023

PUBLISHED 26 July 2023

## CITATION

Xing X, Wu G, Zhou J, Zhang A, Hou Y,  
Xie X, Wu J, Kong X and Li S (2023), Finite  
element study on the initiation of new  
fractures in temporary  
plugging fracturing.  
*Front. Phys.* 11:1227917.  
doi: 10.3389/fphy.2023.1227917

## COPYRIGHT

© 2023 Xing, Wu, Zhou, Zhang, Hou, Xie,  
Wu, Kong and Li. This is an open-access  
article distributed under the terms of the  
[Creative Commons Attribution License  
\(CC BY\)](https://creativecommons.org/licenses/by/4.0/). The use, distribution or  
reproduction in other forums is  
permitted, provided the original author(s)  
and the copyright owner(s) are credited  
and that the original publication in this  
journal is cited, in accordance with  
accepted academic practice. No use,  
distribution or reproduction is permitted  
which does not comply with these terms.

# Finite element study on the initiation of new fractures in temporary plugging fracturing

Xuesong Xing<sup>1</sup>, Guangai Wu<sup>1</sup>, Jun Zhou<sup>1</sup>, Anshun Zhang<sup>1</sup>,  
Yanan Hou<sup>1</sup>, Xin Xie<sup>1</sup>, Jianshu Wu<sup>1</sup>, Xiangwei Kong<sup>2,3\*</sup> and Song Li<sup>2</sup>

<sup>1</sup>CNOOC Research Institute Co., Ltd., Beijing, China, <sup>2</sup>School of Petroleum Engineering, Yangtze University, Wuhan, China, <sup>3</sup>Hubei Key Laboratory of Oil and Gas Drilling and Production Engineering, Yangtze University, Wuhan, China

Hydraulic fracturing technology is an important means to efficiently exploit unconventional oil and gas reservoirs. As the development of oil and gas fields continues at a high rate, the life cycle of oil and gas wells has been significantly shortened. Fracture sealing is often used to transform oil and gas reservoirs, maintaining long-term economic development benefits. Multiple high-conductivity channels were created between the borehole and the reservoir through temporary sealing of fractures near the contaminated zone. This extended the recovery range and further improved the recovery of oil and gas. A mathematical model was developed to predict the distribution of stress around the artificial fracture prior to the rupture of the seal. Finite element software was used to model the stress distribution around a reservoir containing natural and artificial fractures. We discuss the mechanical conditions for the initiation of a new fracture and the optimal timing for fracture sealing. The prediction of the propagation and propagation trajectories of the new fracture is revealed, and the behavior rules for the initiation and steering propagation of the new fracture are clarified. These results can facilitate theoretical studies and on-site technical optimization of fracture sealing.

## KEYWORDS

temporarily block the steering, fracture initiation and expansion, geostress reconstruction, fracture diversion, temporary plugging

## 1 Introduction

Hydraulic fracturing technology is one of the important means to efficiently exploit unconventional oil and gas reservoirs. It plays a crucial role in reducing costs and maximizing production efficiency in the development of unconventional oil and gas reservoirs. With the continuous and high-speed development of oil and gas fields, the life cycle of oil and gas wells has been significantly shortened. Therefore, it is essential to utilize temporary plug fracturing to transform oil and gas reservoirs and maintain long-term economic development benefits. Temporary plug fracturing technology is designed to increase the reconstruction effort of the target layer, reduce the difficulty of fracture construction, and increase the efficiency of unit well section reconstruction. The creation of multiple high-conductivity channels between the wellbore and the reservoir through the temporary plug of the fracture extends the recovery range and further improves oil and gas recovery. This approach not only reduces the cost of fracturing but also ensures production maximization in the efficient development of tight oil and gas [1–6].

Research and field testing on temporary plugging fracturing technology began in the 1950s and 1960s, leading to significant progress in understanding the mechanisms, materials, numerical simulation, design, and construction of temporary plugging fracturing [1–3, 7, 8]. Field experiments have shown that several factors, such as initial artificial fractures, changes in reservoir pore pressure and temperature fields due to long-term production, artificial fractures in adjacent wells, and production/injection activities, can affect the size and direction of the *in situ* stress field [5, 9–11]. According to the theory of rock and fracture mechanics, artificial fractures are always perpendicular to the direction of minimum horizontal stress. Therefore, performing temporary plug fracturing on a reservoir where stress reorientation has already occurred may result in a new fracture reorientation, which is fracturing and extending in a different direction from the initial fracture.

Refracturing old wells in low permeability oil fields has been established, mainly through intra-fracture diversion fracturing, which has become a leading technology for tapping potential and stabilizing production in many blocks [11–16]. By developing numerical models of the stress field and fracture propagation, we obtain new fracture propagation behaviors and optimal fracture timing based on different geological features and fracture design parameters generated by temporary plug fracturing [17–19]. Compared to theoretical calculations and numerical simulation methods, indoor fracture propagation experiments are more realistic and intuitive. The use of true triaxle fracturing experiments to study fracture propagation behavior reveals geological and engineering factors that affect changes in fracture morphology. Zhang et al. [20] used large-scale true triaxle simulation experiments to believe that perforations change the distribution of ground stress around the well, thereby affecting the initiation and propagation of fracturing fractures. Wu et al. [21] studied the impact of perforating parameters on the initiation and propagation of fracturing fractures under different ground stress differences through true triaxle physical model experiments, thereby optimizing perforating parameters that improve reconstruction efficiency. Yuanqing et al. [22] simulated matrix acidification in a fractured porous medium using the CF model and DBF framework and validated it by comparing it with the simulations of Khoei. In addition, the thermal DBF framework was utilized to investigate the impact of temperature on the acidification of the matrix. Yue et al. [23] used CT scanning technology to describe large physical model experiments to simulate the fracture morphology after primary fracturing and temporary plugging fracturing; analyzed the effects of ground stress difference, natural fractures, and fracturing fluid viscosity on the fracture morphology; and discussed the theory of temporary plugging and fracturing. Liu et al. [24] improved the commonly used model of fracture-hole duality scaling by proposing a pseudo-fracture model in which the cavity consists of a cluster of anomalous matrices with high porosity. They proposed a new method for generating stochastic pore-breaking models. The finite volume method was used to obtain the sensitivity of the solution dynamics to the fracture and hole parameters. The aforementioned studies have gained much understanding in terms of fracture formation mechanisms, fracture simulation, and process techniques, effectively guiding

the field testing of temporary plug fracture techniques. However, due to the “complexity” of temporary plugging fracturing technology in creating new fractures and the diversity of factors affecting the initiation and diversion of fractures, the consideration of factors affecting the initiation and diversion of new fractures is not perfect.

The aforementioned studies have given us a better understanding of the experimental procedures and other aspects of TCEF, which have effectively guided the field testing of the technique. However, due to the complexity of creating new fractures and the diversity of factors that influence the initiation and diversion of such fractures in the technique of temporary plug fracturing, a more comprehensive consideration of these factors is required. Therefore, a mathematical model for the distribution of the stress field around the artificial fracture prior to the rupture of the temporary plug was developed. The stress distribution around a reservoir containing both natural and artificial fractures is accurately modeled using finite element software. Therefore, we discuss the mechanical conditions sufficient for the initiation of new fractures and the optimal timing of temporary plug fracturing. The propagation and propagation trajectories of the new fracture are predicted, and the mechanism of initiation and diversion of the new fracture in the temporary stop fracture is revealed.

## 2 Analysis of formation stress field before temporary plugging fracturing

### 2.1 Temporary plugging fracturing mechanism

Temporary plug fracturing is the refracking of wells and formations that have undergone one or more fracturing measures. From a fracture and formation perspective, there are currently one or more mechanisms for temporarily plugging and fracturing a well:

- ① Reopen the fractures that were originally opened: after fracturing, the water injected into the fracture during the previous fracturing process failed to keep up, resulting in a decrease in the formation pressure, which significantly increased the closing pressure. The fracture was closed, and the fracture failed. During temporary plug fracturing, enhanced water injection into the corresponding formation during fracturing and re-energization will effectively open the fracture that was originally opened.
- ② Effectively extend the original fracture system, increase the contact surface between the fracture and the oil-bearing layer, expand the oil drainage area, and increase the oil flow channel of the original fracture system: this requires applying a high sand ratio and large sand volume fracturing techniques in the temporary plug fracturing of old wells to operate in the original fracture system and effectively extend the original fracture system.
- ③ Flush the fracture surface: on the fracture surface that was originally fractured due to being blocked by insoluble substances (residues) of the fracturing fluid or the filter



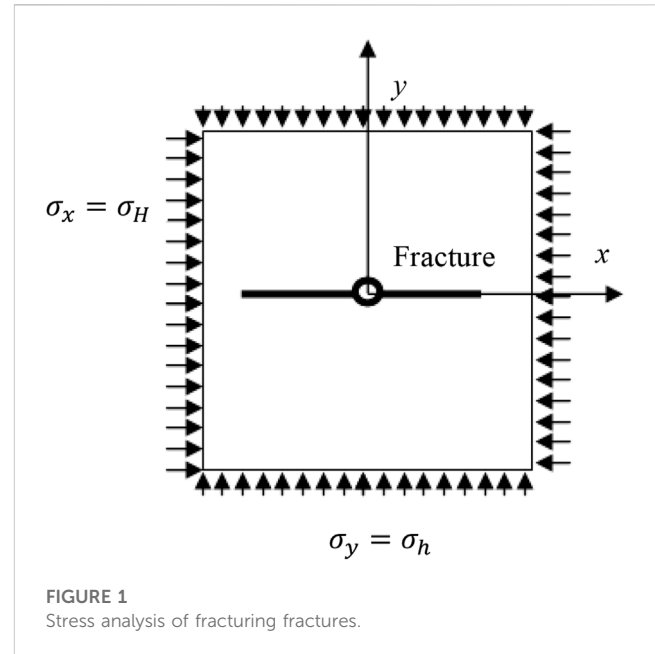
cake formed by the fracturing fluid being too thick or too strong, which affects the seepage of the fracture surface, it should be effectively cleaned, and the blocked substances should be returned to the oil well. Due to the current presence of certain residues in the fracturing fluid used for fracturing, the study of the mechanism and measures for flushing the fracture surface is still at an exploratory stage and requires further in-depth investigation.

- ④ Refill with proppant: fracking and proppant embedding in hydraulically fractured wells will continue to increase over time, requiring temporary plug fracturing, refilling with high-conductivity proppants, and improved sand addition methods to increase production in temporary plug fracturing wells.
- ⑤ Press open new fractures: the new fracture generated by temporary plugging fracturing starts and extends in a different direction from the previous artificial fracture, which can open new oil and gas flow channels in the oil and gas reservoir, communicate with the unused oil and gas reservoir of the old fracture in a wider range, and greatly increase production.

According to the theory of elastic mechanics and the rock fracture criterion, the fracture always starts along the direction perpendicular to the minimum horizontal principal stress. Therefore, the distribution of stress fields in temporary plugging fracturing wells determines whether temporary plugging fracturing will expand along old fractures or generate new fractures, as well as the optimal time to generate new fractures, the location and orientation of the initiation of new fractures, the direction and trajectory of the extension of new fractures, and the length of new fractures. Therefore, the distribution of the stress field around the fracture prior to temporary plug fracturing is very important for studying the mechanism of temporary plug fracturing.

A large number of field and indoor experimental studies have shown that the existence of previous artificial fractures in oil and gas wells, changes in pore pressure caused by long-term production activities in oil and gas wells, and changes in temperature fields will lead to changes in the size and direction of the *in situ* stress field in the reservoir, resulting in stress redirection. After fracturing an oil and gas well, the presence of artificial fractures can alter the magnitude and direction of the ground stress near the borehole, as confirmed by field and laboratory tests. Operations such as production and water injection in oil and gas wells can cause changes in the formation pore pressure, and if such changes are not uniform, then so are changes in the stress field, resulting in a redistribution of stress. The prolonged injection of cold water inevitably leads to a decrease in the temperature inside the reservoir, which also induces a change in the stress field. These induced stresses alter the distribution of the reservoir stress field in wells with hydraulic fracturing fractures and may cause stress reorientation, making it possible for temporary plug fracturing to generate new fractures with different orientations from the initial fracture, achieving the goal of reforming the reservoir and improving oil recovery.

The total stress field in the borehole and in the vicinity of the fracture prior to temporary plug fracturing can be viewed as a superposition of the following four stress fields: 1) the *in situ* stress field, which is the unperturbed far-field *in situ* stress field; 2) the stress field induced by the first artificial fracture: the stress



field is induced by the variation of the pore pressure; 3) variation of the stress field induced by the temperature field: for a well, it is necessary to calculate the aforementioned three stress fields separately and then add them together to obtain the total stress field; and 4) the stress field induced by the initial artificial break: the direction of fracture resulting from temporary plug fracturing still depends on the stress state, and its geometry is still controlled by the mechanical properties of the strata and the parameters of the construction. Therefore, it is important to investigate the mechanism of temporary plug fracturing by studying the variation of the *in situ* stress field after the initial fracturing. The magnitude of the initial artificial fracture-induced stress decreases as the distance from the fracture surface increases. The pressure field is induced by the pore pressure change. During the exploitation of oil and gas reservoirs, changes in the pressure of the pore fluid, on the one hand, cause changes in the stress of the rock skeleton, which in turn cause changes in the rock properties. On the other hand, these variations affect the flow and pressure profiles of the pore fluid. As oil and gas production progresses, the distribution of the pore pressure around the fracture becomes very inhomogeneous, which changes the pore pressure gradient around the fracture in the formation, leading to a redistribution of the *in situ* stress throughout the reservoir. The stress field is induced by the change in the formation temperature. During the exploitation of oil and gas reservoirs, water injection is commonly used to maintain formation energy. The injection of water into the injection well also causes changes in the ground stress, which are mainly reflected in two ways: one is that the injection well enters the reservoir and generates pore elastic stress; conversely, due to the temperature difference between the injected water and the reservoir rock, long-term cold water injection is necessary to lead to a decrease in the temperature in the reservoir, causing rock shrinkage. Thermal elastic tensile stress is generated, which can also lead to changes in the geostress field.



## 2.2 Mathematical model of stress distribution before temporary plugging fracturing

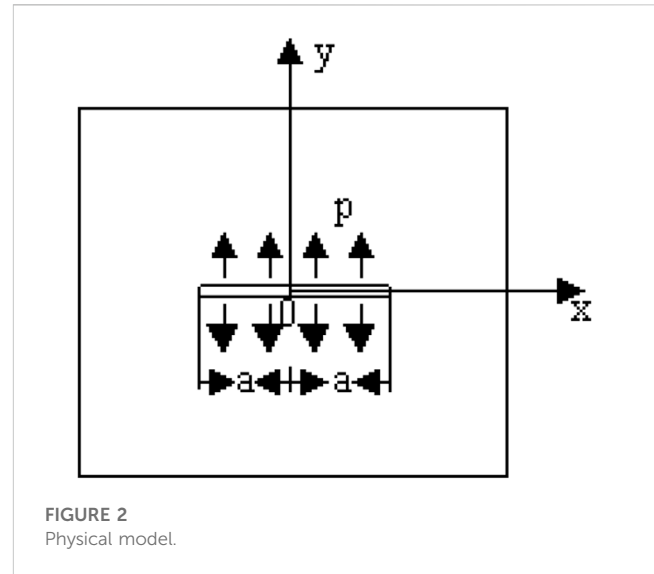
The total stress field in the borehole and the vicinity of the fracture prior to temporary plug fracturing can be viewed as a superposition of the following four stress fields. First, a small deformation is assumed under the assumption of a planar strain state inside the reservoir. This satisfies the superposition principle and results in an *in situ* stress field representing the unperturbed long-range force exerted on the region. Second, the stress field induced by the first artificial break is considered. In addition, the pressure field induced by the pressure change at the pore is calculated, and finally, the variation of the stress field induced by the temperature field is noted. The aforementioned four stress fields are calculated individually and then added together to obtain the total stress field.

When studying the induced stress field in temporary plugging fracturing wells, for ease of expression, the coordinate system shown in Figure 1 is used: the fracture length direction of the initial artificial fracture is the  $x$ -axis, and the direction perpendicular to the initial fracture through the wellbore is the  $y$ -axis. Obviously, the  $x$ -axis is parallel to the initial maximum horizontal principal stress  $\sigma_H$  direction, and the  $y$ -axis is parallel to the initial minimum horizontal principal stress  $\sigma_h$  direction. This determines the relationship between the coordinate system and the initial geostress and fractures. The direction of the stress field before temporary plugging and fracturing in vertically fractured wells is determined jointly by the superimposed stress. For vertically fractured wells, no shear stress is generated in the direction of the initial fracture length and the direction of the vertical fracture length, and the superimposed stress in these two directions represents the maximum and minimum horizontal stress directions. If the current stress in the initial maximum horizontal stress direction is less than the current stress in the initial minimum horizontal principal stress direction, stress redirection occurs.

If the stress variation values induced by the aforementioned factors are known, it is feasible to calculate the stress distribution in time and space before fracturing of the well plug, which can determine whether new fractures will be generated during the temporary plugging fracturing operation, as well as the direction in which new fractures initiate and extend. In the following, the stress field induced by temperature variations is neglected, and only the stress field induced by hydraulic fracture and formation pore pressure is considered. In addition, the mechanical mechanism by which the temporary plug breaks to produce a new fracture was investigated.

## 2.3 Primary fracturing-induced stress field

In order to analyze the stresses induced by artificial fractures, it is necessary to first develop mathematical and mechanical models. These models rely on an understanding of the rock medium and the mechanical environment surrounding the fracture. In real reservoirs, the rock surrounding a fracture may undergo plastic deformation under complex stress conditions during fracturing. The



presence of heterogeneity and anisotropy in the formation, coupled with natural micro-fractures, voids, and other factors in the reservoir, makes mathematical analysis quite challenging. The following assumptions are made to simplify the analysis of the stress field around artificial fractures: 1) the fractures are vertical; 2) the reservoir is homogeneous and isotropic; 3) the reservoir is in a linear elastic state; and 4) the interaction between the reservoir and proppant is not considered.

A vertical fracture containing a symmetric double wing in an infinite reservoir can be simplified to the physical model shown in Figure 2: a linear fracture in the center of an infinite flat plate (which can be regarded as the limit case of an ellipse with a short half axis), with a length of  $2a$ , the fracture penetrating the thickness of the plate, and the tension acting on the fracture surface of  $-p$ .

Clearly, the horizontal hydraulic fracture-induced *in situ* stress field, the formation pore pressure-induced stress field, and the stress field plate problem induced by the change of the formation temperature in the physical model described previously belong to the plane strain problem. According to the theory of elasticity, the equilibrium differential equation of the plane strain problem (excluding physical force) is as follows:

$$\begin{cases} \frac{\partial \sigma_x}{\partial x} + \frac{\partial \tau_{xy}}{\partial y} = 0, \\ \frac{\partial \sigma_y}{\partial y} + \frac{\partial \tau_{xy}}{\partial x} = 0. \end{cases} \quad (1)$$

The geometric equations for planar problems are as follows:

$$\begin{cases} \epsilon_x = \frac{\partial u}{\partial x}, \\ \epsilon_y = \frac{\partial u}{\partial y}, \\ \gamma_{xy} = \frac{\partial v}{\partial x} + \frac{\partial u}{\partial y}, \end{cases} \quad (2)$$

where  $u$  is the displacement in the direction  $x$  and  $v$  is the displacement in the direction  $y$ .

The physical equation for plane strain problems is the stress-strain equation:

$$\begin{cases} \varepsilon_x = \frac{1}{E} [(1-\mu^2)\sigma_x - \mu(1+\mu)\sigma_y], \\ \varepsilon_y = \frac{1}{E} [(1-\mu^2)\sigma_y - \mu(1+\mu)\sigma_x], \\ \gamma_{xy} = \frac{1+\mu}{E}\sigma_{xy}, \end{cases} \quad (3)$$

where  $\mu$  is Poisson's ratio and  $E$  is the modulus of elasticity.

The boundary conditions of the aforementioned physical model are shown in the Figure 2:

$$y = 0, |x| \leq a: \sigma_y = p, \tau_{xy} = 0, \quad (4)$$

$$y = 0, |x| > a: \tau_{xy} = 0, v = 0, \quad (5)$$

$$\sqrt{x^2 + y^2} \rightarrow \infty, \sigma_x \rightarrow 0, \sigma_y \rightarrow 0, \tau_{xy} \rightarrow 0. \quad (6)$$

Equations 1–6 are the equilibrium equations, geometric equations, physical equations, and boundary conditions that describe the aforementioned physical model. These six equations constitute a mathematical model that facilitates quantitative analysis of this physical problem.

## 2.4 Formation of pore pressure-induced stress field

Long-term production and water injection in an oil well can decrease or increase the formation pore pressure, resulting in a change in the *in situ* stress state. There is some gradient in the pore pressure around the hydraulic fracture. As oil and gas production progresses, the distribution of the pore pressure around the fracture becomes very inhomogeneous, which changes the pore pressure gradient around the fracture in the formation, resulting in a redistribution of the *in situ* stress throughout the reservoir.

The production process of oil and gas reservoirs is a dynamic coupling process of multiphase fluid (oil, gas, and water) seepage and deformation of porous media in reservoir rock and soil, which is mainly manifested as follows: 1) with the development of oil and gas fields, production and injection will cause changes in pore pressure; 2) changes in pore pressure lead to changes in rock and soil deformation and effective stress field. Changes in *in situ* stress and rock deformation will lead to changes in reservoir physical properties, such as porosity, permeability, rock and soil density, and pore compression coefficient, affecting pore fluid seepage and production. As a result, oil, gas, water seepage, and rock and soil deformation are mutually affected and constrained during the exploitation of oil and gas reservoirs, with strong coupling effects between them. Therefore, when studying the changes in geostress caused by changes in pore pressure during the production of oil and gas reservoirs, it is necessary to consider the flow laws of fluids, including liquids (oil or water) and gases (e.g., natural gas) in porous media and their impact on the deformation or strength of the rock mass itself, as well as the interaction between the stress field and the seepage field within the rock mass.

The following assumptions are made: 1) assume that the thickness of the reservoir does not vary with space, that the

height of the fracture is equal to the thickness of the reservoir, and that the rock is in a plane strain state; 2) it is assumed that rock deformation during mining can be linear, nonlinear, elastic, and elastic-plastic small deformations, but no fracturing occurs; 3) the seepage flow in a reservoir is planar, two-dimensional, and isothermal, and the fluid is compressible; 4) the flow of each phase in the matrix obeys Darcy's law relative to the rock particle, and the flow in the fracturing support fracture obeys Forchheimer's high-speed non-Darcy flow; and 5) consider the effects of gravity and capillary forces.

(1) The equation of motion is as follows:

$$U_\alpha = 1/(\varphi S_\alpha) \bullet V_\alpha + V_s = \frac{-KK_{ra}\delta_\alpha}{\varphi S_\alpha \mu_\alpha} (\nabla P_\alpha - \rho_\alpha g \nabla D) + V_s. \quad (7)$$

(2) The continuity equation is as follows:

$$\begin{aligned} -\nabla \bullet \left[ \sum_{\alpha=o,g,w} X_{i\alpha} \varphi \rho_\alpha S_\alpha V_\alpha \right] + \tau_\alpha (P_\alpha - P_{f\alpha}) + q_{f\alpha} \\ = \partial \left[ \varphi \sum_{\alpha=o,g,w} X_{i\alpha} \rho_\alpha S_\alpha \right] / \partial t. \end{aligned} \quad (8)$$

(3) The partial equation of seepage flow is as follows:

$$\begin{aligned} \nabla \bullet \left[ \sum_{\alpha=o,g,w} \frac{X_{i\alpha} \rho_\alpha K K_{ra} \delta_\alpha}{\mu_\alpha} (\nabla P_\alpha - \rho_\alpha g \nabla D) \right] + \tau_\alpha (P_\alpha - P_{f\alpha}) + q_{f\alpha} \\ = \partial \left[ \varphi \sum_{\alpha=o,g,w} X_{i\alpha} \rho_\alpha S_\alpha \right] / \partial t. \end{aligned} \quad (9)$$

Equation 9 is multiphase and multicomponent fluid-solid coupling in a fracturing fracture system.

## 3 Finite element model of stress distribution before temporary plugging fracturing

### 3.1 Near wellbore *in situ* stress field

The *in situ* stress around the borehole is redistributed due to the phenomenon of stress concentration around the borehole. In order to better analyze the stress distribution in boreholes with artificial fractures, the phenomenon of stress concentration around boreholes was first studied. The *in situ* stress field distribution around the borehole was modeled by a finite element analytical model using Abaqus software.

#### 3.1.1 Basic parameters of the model

The geological parameters used in the numerical model are based on the reservoir parameters of tight oil and gas reservoirs in the Ordos Basin, China, as shown in Table 1 and Table 2.

#### 3.1.2 Establishment of the finite element model

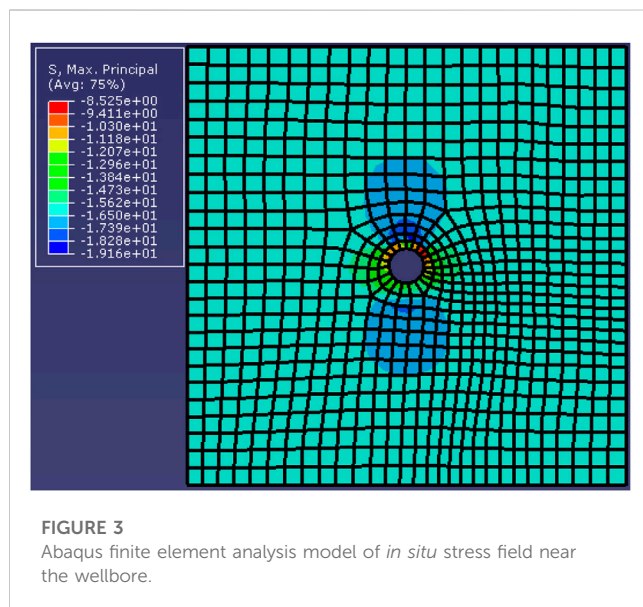
This is sufficient to establish a small reservoir boundary region due to the main studies on the distribution of *in situ* stress fields in the vicinity of boreholes and the fact that the induced stress due to boreholes generally vanishes within a few times the extent of the

TABLE 1 Reservoir physical parameters.

Reservoir thickness $H(m)$	20	Primary porosity $\phi$	0.05
Permeability ( $um^2$ )	$4 \times 10^{-3}$	Permeability $K_y(um^2)$	$1 \times 10^{-3}$
Oil viscosity $\mu_o(Pa \cdot s)$	$2 \times 10^{-3}$	Formation water viscosity $\mu_w(Pa \cdot s)$	$5 \times 10^{-4}$
Original formation pressure (MPa)	30	Initial oil saturation	0.05
Oil density $\rho_o(kg/m^3)$	$0.85 \times 10^3$	Original formation temperature $T_i(K)$	360
$\sigma_H(MPa)$	40	$\sigma_h(MPa)$	32

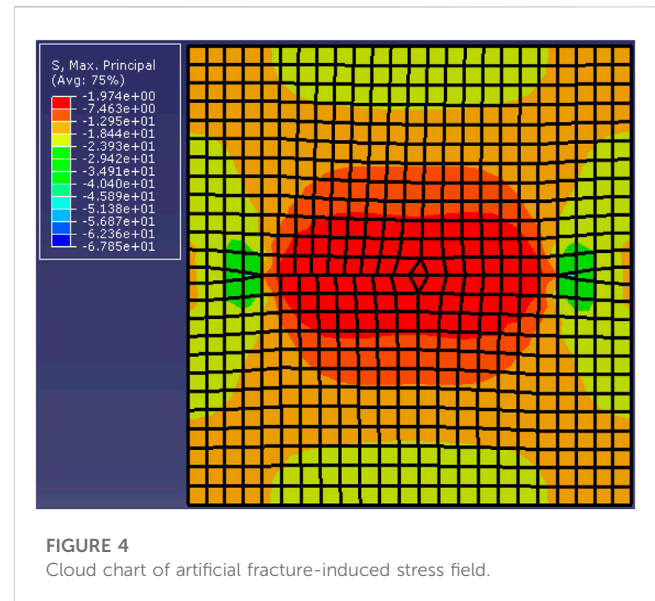
TABLE 2 Initial artificial fracture parameters.

Half-length of fracture $L_f(m)$	60	Fracture width $w_f(m)$	$3 \times 10^{-3}$
Fracture height $H_f(m)$	20	Closing net pressure $p_{net}(MPa)$	5
Bottom hole temperature (K)	300	Borehole diameter $r_w(m)$	0.15



borehole. The boundary of a  $100 \times 100$ -cm square oil reservoir is centered on an oil well with a hole diameter of 21.59 cm.

The maximum principal stress loaded in the X direction is 60 MPa, that in the Y direction is 55 MPa, and that in the formation pore pressure is 40 MPa. The purpose is to study the phenomenon of stress diversion near boreholes caused by boreholes without considering the effect of changes in borehole pressure during production. Figure 3 shows the Abaqus finite element analytical model for the near-well bore geostress field. A quadrilateral free mesh is used for mesh partitioning, with the element type being pore fluid/stress element. A total of 9,260 elements and 9,490 nodes are partitioned. Figure 3 shows the scheme for the *in situ* stress field around the bore. Figure 3 shows that a significant stress concentration is formed around the borehole due to the compression of the largest principal stress in the formation, with the X direction being the direction of the largest principal stress.



### 3.1.3 Simulation analysis

The condition of the well before temporary plugging and fracturing can be simplified as a straight fracture with a length of  $2a$  penetrating the plate thickness in the center of a plate, which can be regarded as the limit case of an ellipse with a short half-axis tending to 0. According to the theory of elasticity, calculating the induced stress field in the presence of fractures belongs to a plane strain problem. Based on the stress-strain equation and boundary conditions, the integration formula of the Fourier transform, inverse transform, and Bessel function is introduced. The fracture-induced stress is as follows:

$$\frac{1}{2}(\sigma_y - \sigma_x) + i\tau_{xy} = p \frac{r}{a} \left( \frac{a^2}{r_1 r_2} \right)^{\frac{1}{2}} i \sin \theta e^{-3i(\theta_1 + \theta_2)/2}, \quad (10)$$

$$\frac{1}{2}(\sigma_y + \sigma_x) = -p \operatorname{Re} \frac{1}{a} \left[ 1 - r e^{i\theta} (r_1 r_2)^{-\frac{1}{2}} e^{-i(\theta_1 + \theta_2)/2} \right], \quad (11)$$

where  $P$  is the fluid pressure in fractures, MPa, and  $h$  is the fracture height, m.

$$c = \frac{h}{2}, \quad r = \sqrt{x^2 + y^2}, \quad r_1 = \sqrt{x^2 + (y+c)^2}, \\ r_2 = \sqrt{x^2 + (y-c)^2}, \quad \theta = \tan^{-1}(x/y), \\ \theta_1 = \tan^{-1}[x/(-y-c)], \quad \theta_2 = \tan^{-1}[x/(c-y)]$$

This software is used to construct finite element analytical models of *in situ* stresses in artificial fracture wells. A rectangular stratum boundary with a semi-length of 80 m, a width of 1.0 cm, and a borehole diameter of 10.0 cm was used. The maximum and

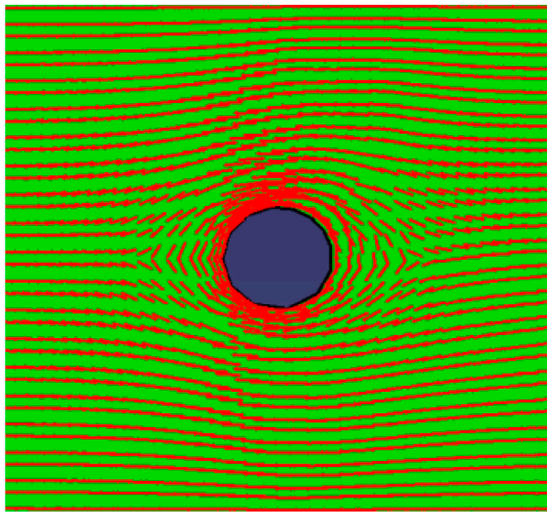


**FIGURE 5**  
Vector diagram of maximum principal stress in the near-well zone.

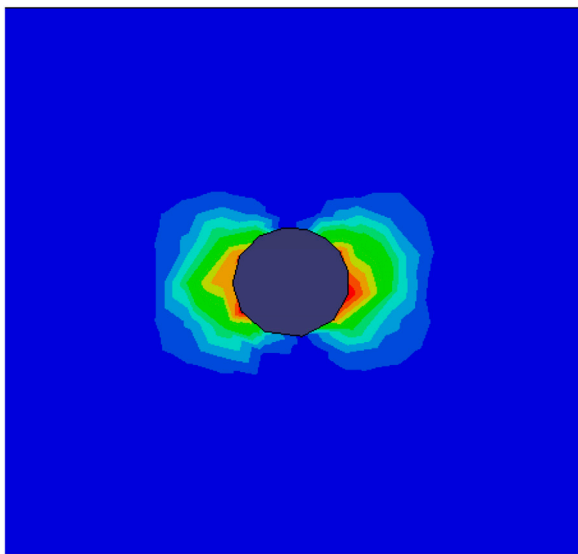


**FIGURE 6**  
Cloud chart of the difference between the maximum principal and the principal stress in the X direction (Smax-S11).

minimum principal stresses in the horizontal direction of the formation were taken to be 40 and 25 MPa, respectively. The cloud pattern of the artificial fracture-induced stress field is shown in Figure 4, which shows that a distinct induced stress field is formed around the artificial fracture, with the maximum principal stress in this region being much higher than in the other regions. The maximum principal stress is in the *x*-axis direction, with a significant increase in the *in situ* stress in the *y*-axis direction, which is much larger than the maximum principal stress value around the borehole in the absence of fracture. The

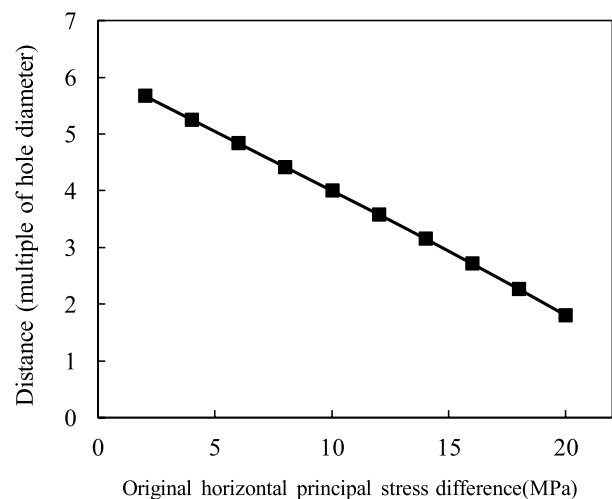


**FIGURE 7**  
Relationship curve between stress steering area length and stress difference in the *x*-axis direction.

occurrence of this phenomenon provides a basis for the diversion of new fractures in the temporary plug fracture.

Figure 5 shows the maximum principal stress scheme for near-well formation, with a large maximum principal stress value in the *y*-axis direction. The maximum principal stress in the borehole is generated in the *Y* direction of the borehole. Figure 5 shows a significant stress shift near the bore, with the stress direction generally following the tangential direction of the bore. In the *x*-axis direction, the stress deviates most from the direction of the initial maximum principal stress. In the *y*-axis direction, the stress hardly changes direction.

In order to study the effect of *in situ* stress difference on the size of the stress diversion region near the wellbore, a user-defined field variable Smax-S11 was established, which is the difference between the maximum principal stress and the *X* direction stress. As the initial maximum principal stress is in the *X* direction, when the difference between the maximum principal stress in the vicinity of the well and the *X* direction is zero, the maximum principal stress can be considered to have recovered to the *X* direction. Figure 6 shows the nephogram of the difference between the maximum principal stress and the stress in the *X* direction. The difference is large in the *X* direction of the wellbore, and the stress steering angle is the largest.

By customizing the field variable Smax-S11 and changing the stress difference, the impact of the stress difference on the size of the stress steering region can be analyzed. Figure 7 shows the relationship curve between the length of the steering area and the stress difference in the *x*-axis direction. With the increase in the stress difference, the stress turning area shows a significant decrease trend. It can be restored to the original stress field direction within the range of 3–5 times the diameter of the borehole.

For initial fracturing, the direction of fracture initiation may not necessarily follow the direction of the maximum principal stress in



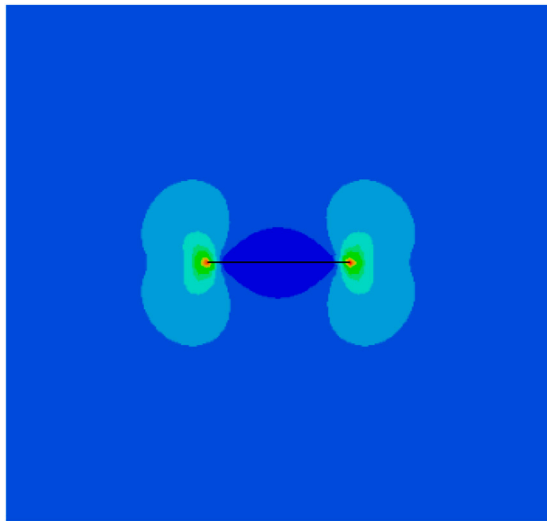


**FIGURE 8**  
Maximum principal stress field induced by artificial fractures.

the original formation due to changes in the direction of the *in situ* stress near the borehole. As the fracture is extended and the direction of the stress field is restored, it gradually transitions to the original maximum principal stress direction. Due to the generally small stress-turning region near the borehole, the process of fracture turning and extending along the direction of the original maximum principal stress will be completed quickly.

## 3.2 Stress field around artificial fractures

### 3.2.1 Establishment of the finite element model

A zone of 640 m × 640 m was constructed with a 0.15 m diameter borehole in the center. A symmetric artificial fracture

was established in the X direction of the borehole. The fracture has a half-length of 80 m and a width of 1.0 cm. Divide a rectangular area around the fracture for subsequent mesh generation. The maximum principal stress loaded in the X direction is 60, that in the Y direction is 55 MPa, and that in the formation pore pressure is 40 MPa. Because the permeability in the artificial fracture is far greater than the formation permeability, the fluid pressure drop in the artificial fracture is ignored, and the production flow rate of the fluid is loaded on the fracture wall. For the artificial fracture-induced stress field, the impact of pore pressure changes during production will not be considered temporarily.

### 3.2.2 Simulation analysis

The induced stress field due to a single artificial fracture is shown in Figure 8, without considering the effect of the pore pressure change on the ground stress during the production process. The induced stress field forms around the fracture, and the stress concentration are pronounced at the fracture tip. The induced stress field due to a single artificial fracture is shown in Figure 9. The induced stress field forms around the fracture, and the stress concentration is evident at the fracture tip.

Figure 9A shows the maximum principal stress vector diagram of the whole model, and Figure 9B shows the maximum principal stress vector diagram near the fracture displayed in magnification. Perpendicular to the fracture wall, the principal stress direction changes little and essentially remains the same as the original maximum principal stress direction. At the tip of the fracture, the principal stress changes considerably, and the direction of the maximum principal stress is almost perpendicular to the original stress direction. The direction of the maximum principal stress does not change much in the direction of the vertical fracture wall, but the change in the direction of the maximum principal stress outside the fracture tip is very pronounced. The shift in the ground stress prior to temporary plug fracturing is mainly caused by the production of multiple wells in a local area, and the effect of the artificial fracture-induced stress field on the shift toward the new fracture is limited.

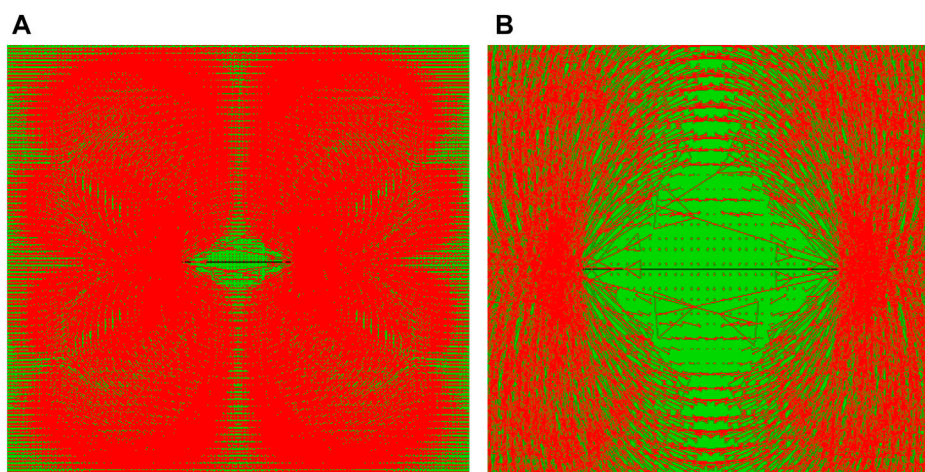


**FIGURE 9**  
Maximum principal stress vector diagram around fractures. (A) the maximum principal stress vector diagram of the whole model. (B) the maximum principal stress vector diagram near the fracture.



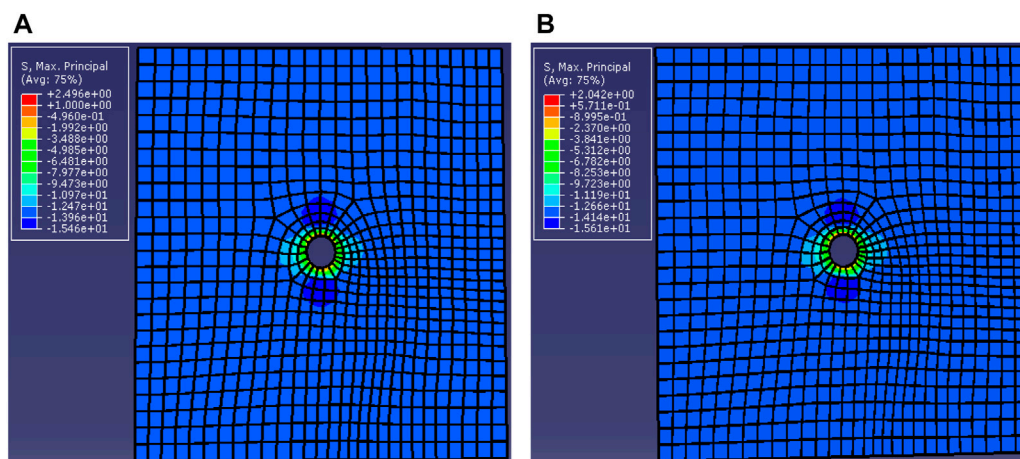


FIGURE 10

Comparison of the maximum principal stress nephogram around wellbore (A) before production and (B) after production.

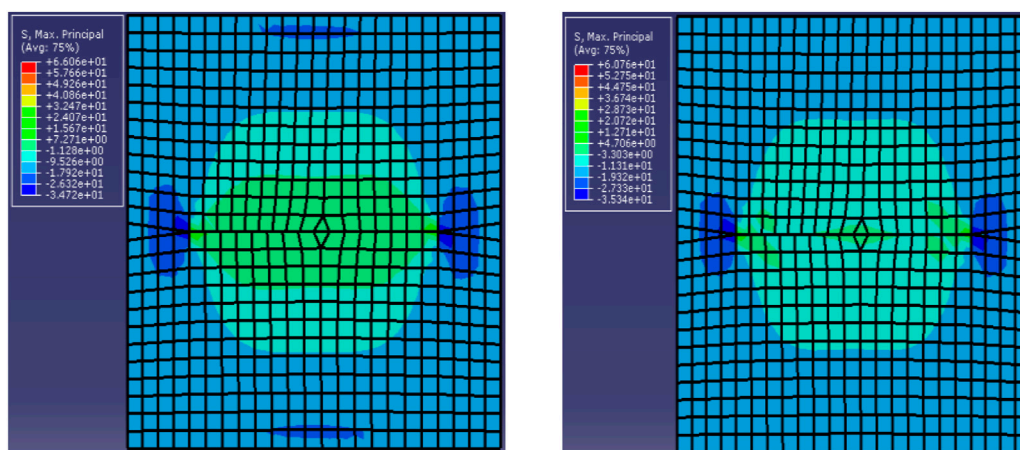


FIGURE 11

Comparison of maximum principal stress nephograms around artificial fractures (A) before production and (B) after production.

### 3.2.3 Stress field induced by pore pressure change after operation

With the progress of production, the formation pore pressure will change, and there is a certain gradient of pore pressure around hydraulic fractures (its graph is shown in Figure 10). Based on the finite element analysis model of artificial fracture, the formation pore pressure was loaded with 40 MPa, and a certain production rate was assigned to the fracture wall to simulate the effect of pore pressure on the stress field in the production process. Figure 10 compares the program of the maximum principal stress distribution around the borehole before and after production. It shows that after a production period, the maximum principal stress value decreases to a certain extent, and the decrease is the largest in the direction of the maximum principal stress.

Considering the effect of a change in the pore pressure due to production on the stress field around the artificial fracture, the pore pressure is applied at the formation boundary, and the production rate is set at the fracture wall. Figure 11 shows that the maximum principal stress around the artificial fracture is distributed along the  $x$ -axis before production. After a period of production, the maximum principal stress around the artificial fracture significantly decreases, the direction of the maximum principal stress is not clearly located in the  $x$ -axis direction, and there is a tendency for the principal stress to turn. This opens up the possibility of refracturing fracture diversion.

Figure 12A shows the maximum principal stress vector diagram of the whole model, and Figure 12B shows the maximum principal stress vector diagram near the fracture displayed in magnification. As shown in Figure 12B, when the pore pressure of the local layer is

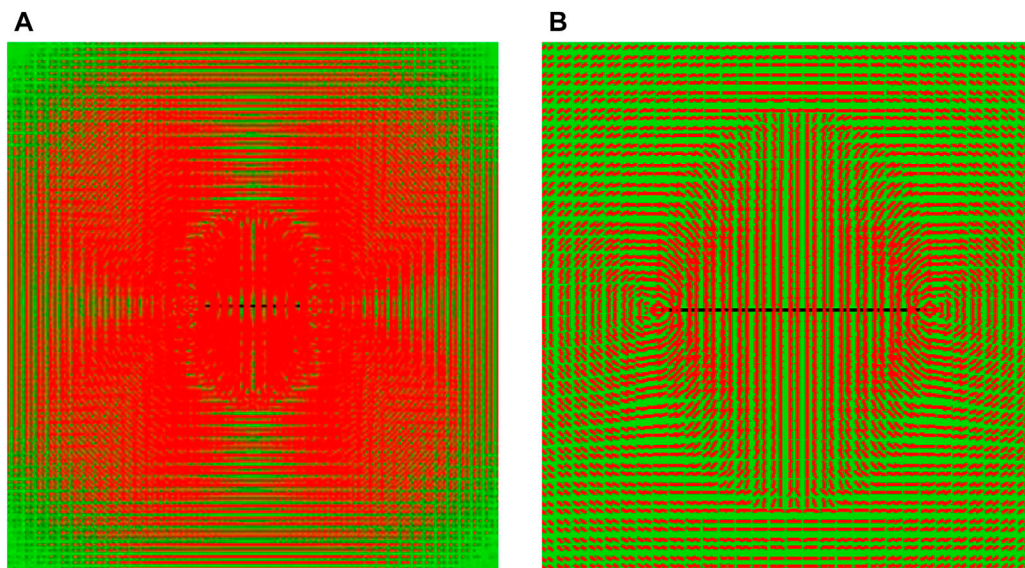


**FIGURE 12**

Vector diagram of the maximum principal stress field around artificial fractures. (A) the maximum principal stress vector diagram of the whole model. (B) the maximum principal stress vector diagram near the fracture.

sufficiently reduced, the maximum principal stress undergoes a sharp turn, which occurs over a large area, making it possible for temporary plug fracturing to generate new turn fractures.

## 4 Fracture initiation and extension mechanism of temporary plugging fracturing

Before temporarily plugging a vertically fractured well, the initial artificial fracture can cause induced stress, and the pore pressure decrease caused by the production of oil and gas wells can lead to stress direction changes in and around the wellbore. If a temporary fracture is created perpendicular to the initial fracture at this time, it may be possible to temporarily plug and break the new fractures. However, this effect is valid only within a finite distance from the wellhead. As the new fracture extends during temporary plugging, the stress distribution in the reservoir constantly changes and directly affects the direction of the fracture extension. When the stress steering vanishes due to certain conditions, such as the influence of adjacent wells, the new fracture may continue to extend in the direction parallel to the primary fracture length under heavy pressure. If the stress direction is not reoriented, the new fracture may acquire a longer twist fracture as temporary plugging fracturing extends.

Suppose a vertically fractured well with an initial fracture half-length  $L_{xf}$  and direction perpendicular to the direction of minimum horizontal principal stress. The direction of the new fracture in temporary plugging fracturing is formed from the direction of the initial fracture length. Along the direction of the new fracture length in temporary plugging fracturing, the distance from the borehole to the isotropic point is defined as  $L'_{xf}$  and the length of the new fracture penetrating the reservoir vertically when the stress isotropic point is exceeded is defined as  $L''_{xf}$ .

## 4.1 Mechanical conditions of temporary plugging fracturing for new fractures

In the vicinity of the initial artificial fracture of a vertically fractured well, tensile stresses are induced by factors such as hydraulic fractures and changes in pore pressure in both parallel and vertical directions along the length of the initial hydraulic fracture. However, they are balanced by the compressive stresses induced at locations far away from the fracture. The induced tensile stress perpendicular to the fracture surface is initially larger than the tensile stress in the direction parallel to the fracture length. If the stress difference induced by factors, such as hydraulic fracture and pore pressure change, is greater than the initial horizontal stress difference, the initial maximum horizontal stress direction becomes the current minimum horizontal stress direction.

According to fracture mechanics in rocks, fractures always start and extend perpendicular to the direction of the minimum horizontal principal stress. If a temporary plug fracture is performed at this time, the new fracture will start and extend perpendicular to the direction of the initial fracture length. Thus, the mechanical conditions for the generation of new fractures in a vertically fractured well by temporary plug fracturing are stress reorientation in the pretemporary plug stress profile at and near the borehole.

If the initial maximum horizontal stress direction at the wellbore changes to the current minimum horizontal stress direction, and the initial minimum horizontal stress direction changes to the current maximum horizontal stress direction, then temporary plugging fracturing will generate a new fracture perpendicular to the length direction of the primary fracture. The mechanical conditions for generating new fractures at the wellbore are as follows:

$$\sigma_{Hmax0}(0,0) + \Delta\sigma_{Hmax}(0,0,t) < \sigma_{Hmin0}(0,0) + \Delta\sigma_{Hmin}(0,0,t). \quad (12)$$

If stress redirection does not occur at the wellbore but occurs at a point  $(x,0)$  in the length direction of the initial fracture, the stress conditions for the fracture to fracture at a point  $(x,0)$  in the direction of the initial fracture and generation of a new fracture are as follows:

$$\sigma_{Hmax0}(x,0) + \Delta\sigma_{Hmax}(x,0,t) < \sigma_{Hmin0}(x,0) + \Delta\sigma_{Hmin}(x,0,t). \quad (13)$$

Shear stress may be induced by a variety of factors affecting stress changes in a temporarily capped fracking well, resulting in an increase in the maximum shear stress. If the maximum shear stress causes a shear fracture of the formation, new fractures in temporary plugging fracturing may start and extend along the shear plane, and the direction of the new fracture may not be perpendicular to the direction of the initial fracture length, but there may be a certain angle with it.

## 4.2 The best time for temporary plugging fracturing

In order to quantitatively determine the optimal time for a temporary plug fracture to generate a new fracture, it is necessary to consider the length of the fracture before it changes direction and the pore pressure distribution at that time. Tests showed that the longer the interval between temporary plug fracturing, the longer the time before the fracture turned. Although the pore pressure of oil and gas wells continues to decrease after a few years of production, the length of the fracture before turning increases slowly. The best time to break a temporary plug is when the fracture length can reach a very long length or when the pore pressure in the area where the fracture will extend is still high. When the local layer stress profile and other factors governing the pressure profile, such as porosity, permeability, geostress, and reservoir properties, are known, the optimal time to perform temporary plug fracturing can be determined. When the distribution of the pore pressure cannot be accurately determined, the stress distribution can still be used to better estimate the optimal timing of temporary plug fracturing.

Stress reorientation must occur at a point in the borehole or in the direction of the initial fracture length to generate new fractures during temporary plug fracturing. The optimal time for temporary plug fracturing can initially be determined using the time at which stress reorientation occurs at a point in the borehole or in the direction of the initial fracture length. According to Eqs 12, 13 and the stress calculation model, the optimal timing of temporary plugging fracturing can be accurately calculated. The optimal time  $t$  to initiate a new fracture at the borehole is as follows:

$$\sigma_{Hmax0}(0,0) + \Delta\sigma_{Hmax}(0,0,t) = \sigma_{Hmin0}(0,0) + \Delta\sigma_{Hmin}(0,0,t). \quad (14)$$

The best time  $t$  to initiate a new fracture at a point in the initial fracture length direction is as follows:

$$\sigma_{Hmax0}(x,0) + \Delta\sigma_{Hmax}(x,0,t) = \sigma_{Hmin0}(x,0) + \Delta\sigma_{Hmin}(x,0,t), \quad (15)$$

where  $\Delta\sigma_{Hmax}$  is the stress change in the direction of the initial maximum horizontal stress and  $\Delta\sigma_{Hmin}$  is the stress change in the

direction of the initial minimum horizontal stress. From Eqs 14, 15, the critical time for stress redirection can be obtained, which is the best possible opportunity for temporary plugging fracturing.

## 4.3 New fracture extension law of temporary plugging fracturing

During the extension of a new fracture during temporary plugging fracturing, the induced stress gradually changes as it moves away from the wellbore and gradually enters an isotropic point on the regional boundary along the expected direction of fracture extension under heavy pressure (equal horizontal stress point: the maximum horizontal stress equals the minimum horizontal stress). After the temporary plugging fracturing new fracture exceeds the isotropic point (the distance from the wellbore is  $L'_{xf}$ ), due to the possibility of restoring the stress state to the initial fracturing state, as the temporary plugging fracturing continues, the fracture gradually reorients (turning to the vertical distance is  $L''_{xf}$ ) and ultimately will likely extend in a direction parallel to the initial fracture.

### 4.3.1 Factors affecting isohorizontal stress points

Numerous studies and numerical calculations have shown that the stress isotropic point is generally located within half of the initial fracture length. The distance between the stress isotropic point and the borehole depends on parameters such as the magnitude of the initial horizontal stress difference, the initial fracture penetration depth, the production speed, the reservoir permeability, and the difference in the elastic modulus between the production layer and the interlayer.

Dimensionless time  $\tau$  is as follows:

$$\tau = \frac{4ct}{L_{xf}^2} = \frac{4kt}{\mu L_{xf}^2 \left( c_{fl} \varphi + \frac{\alpha(1+\nu)(1-2\nu)}{(1-\nu)E} \right)}. \quad (16)$$

Dimensionless stress deflection tensor  $\Pi$  is expressed as the ratio of stress difference to the production pressure difference:

$$\Pi = \frac{S_0}{\sigma_*}, \quad (17)$$

$$\sigma_* = \frac{\eta q}{4\pi\kappa}. \quad (18)$$

Dimensionless fracture toughness  $\chi$  is the ratio of fracture toughness to the product of production pressure difference and the square root of the initial fracture half-length:

$$\chi = K_{Ic} / \left( \sigma_* \sqrt{L_{xf}} \right). \quad (19)$$

The dimensionless fracture height ratio  $\gamma$  is as follows:

$$\gamma = H / L_{xf}. \quad (20)$$

The dimensionless shear modulus ratio  $\beta_G$  is as follows:

$$\beta_G = G_b / G_f, \quad (21)$$

where  $c$  is the diffusion coefficient ( $\kappa/S, S = 1/M + \alpha/(K + 4G_f/3)$ ,  $K = E/[3(1-2\nu)]$ ),  $M$  is the Biot ( $M = K_{fl}/\varphi$ ),  $K_{fl}$  is the reservoir fluid bulk modulus ( $K_{fl} = 1/c_{fl}$ ),  $c_{fl}$  is the reservoir fluid compressibility,  $G_f$  is the shear modulus of the pay zone ( $G_f =$

$E/[2(1+\nu)]$ ,  $G_b$  is the shear modulus of the interlayer,  $\kappa$  is the mobility coefficient ( $\kappa = k/\mu$ ),  $k$  is the original permeability,  $\mu$  is the fluid viscosity,  $K$  is the dry bulk modulus,  $2S_0$  is the initial stress difference,  $\eta$  is the pore elasticity coefficient  $\eta = \alpha(1-2\nu)/[2(1-\nu)]$ ,  $\nu$  is Poisson's ratio,  $K_{Ic}$  is fracture toughness, and  $q$  is the production.

### 4.3.2 Distance between equal horizontal stress points

According to Eq. 16, the distance  $L'_{xf}$  from the initiation point to the isotropic point of a new fracture for temporary plugging fracturing is calculated from the following two equations:

The distance  $L'_{xf}$  from the wellbore to the isotropic point where a new fracture is temporarily blocked and fractured due to fracturing initiation at the wellbore is as follows:

$$\sigma_{Hmax}(0, L'_{xf}) + \Delta\sigma_{Hmax}(0, L'_{xf}, t) = \sigma_{Hmin}(0, L'_{xf}) + \Delta\sigma_{Hmin}(0, L'_{xf}, t). \quad (22)$$

The distance  $L'_{xf}$  from the initiation point  $(x, 0)$  to the isotropic point in the initial fracture direction where a new fracture is temporarily blocked for fracturing occurs is as follows:

$$\sigma_{Hmax}(x, L'_{xf}) + \Delta\sigma_{Hmax}(x, L'_{xf}, t) = \sigma_{Hmin}(x, L'_{xf}) + \Delta\sigma_{Hmin}(x, L'_{xf}, t). \quad (23)$$

As the time in Eqs 22, 23 has been determined, it is convenient to calculate the vertical penetration distance of a new fracture under heavy pressure, that is, the length  $L'_{xf}$  of the straight-line fracture, based on the stress change in the direction of the initial maximum horizontal stress and the stress change in the direction of the initial minimum horizontal stress.

## 5 Summary

A mathematical model of the stress field around the artificial fracture prior to the temporary plug fracture was developed, and the stress distribution around the reservoir containing the artificial fracture was simulated using finite element software. The results indicate that the maximum horizontal principal stress in the induced stress field around artificial fractures is much higher than that in other regions, with its  $x$ -axis direction, and the horizontal principal stress in the  $y$ -axis direction significantly increases, which is greater than the maximum horizontal principal stress value around the wellbore without fractures.

*In situ* stress simulations before and after the production of artificial fracture wells show that the magnitude of the induced stress in the initial artificial fracture decreases with increasing distance from the fracture surface. The artificial fracture tip exhibits a concentration of stress, while the area in the direction perpendicular to the fracture wall where the stress direction changes is relatively small and insufficient to generate a new kink fracture. When the production time is sufficiently long and the pore pressure around the fracture is significantly reduced, the maximum stress is shifted perpendicular to the fracture wall and the turning area is large. Repeated fracturing can create new artificial fractures. Changes in the pore pressure are the main effect in the occurrence of directional fractures during repeated fracturing.

We calculated the mechanical conditions for the initiation of new fractures and the optimal timing of temporary plug fracturing and predicted the propagation of new fractures. The longer the interval between the temporary plug and the break, the longer the fracture length before turning. The initial maximum horizontal stress direction at the bore changes to the current minimum horizontal stress direction, and the initial minimum horizontal stress direction changes to the current maximum horizontal stress direction. At this point, repeated fracturing generates new fractures perpendicular to the direction of the initial fracture length.

## Data availability statement

The original contributions presented in the study are included in the article/supplementary material; further inquiries can be directed to the corresponding author.

## Author contributions

GW and XuX: Conceptualization, funding acquisition, project administration, resources, writing—original draft and software. YH: Data curation, formal analysis, methodology. GW and SL: writing—original draft, and writing—review and editing. XK: Project administration, resources. JZ: Investigation, methodology, software, and visualization. XiX and JW: Conceptualization, funding acquisition, methodology. XK: Investigation, methodology, project administration. All authors have read and agreed to the published version of the manuscript.

## Funding

This research was funded by “Research on Offshore Large-Scale Fracturing Engineering Technology (KJGG2022-0704), Key Parameter Characterization and Dessert Area Evaluation Technology of Coalbed Methane Geological Engineering (KJGG2022-1001), and Research on Inter-Well Disturbance Integral Fracturing Technology of Coalbed Gas (2021-YXKJ-010).”

## Acknowledgments

The authors are grateful to the reviewers and editors for their careful review of this manuscript.

## Conflict of interest

XX, GW, JZ, AZ, YH, XX, and JW were employed by CNOOC Research Institute Co., Ltd.

The remaining authors declare that the research was conducted in the absence of any commercial or financial relationships that could be construed as a potential conflict of interest.



## Publisher's note

All claims expressed in this article are solely those of the authors and do not necessarily represent those of their affiliated

organizations or those of the publisher, the editors, and the reviewers. Any product that may be evaluated in this article, or claim that may be made by its manufacturer, is not guaranteed or endorsed by the publisher.

## References

- Lindsay GJ, White DJ, Miller GA, et al. Understanding the applicability and economic viability of refracturing horizontal wells in unconventional plays. In: Proceedings of the SPE hydraulic fracturing technology conference; February 2016; The Woodlands, Texas, USA (2016).
- Barree RD, Miskimins JL, Svatek KJ. Reservoir and completion considerations for the refracturing of horizontal wells. *SPE Prod Operations* (2018) 33(01):1–11. doi:10.2118/184837-pa
- Goehtz F, Evers SC, Prommersberger KJ. Re-fracture of the distal radius with lying palmar plate Handchirurgie, Mikrochirurgie, plastische Chirurgie: Organ der Deutschsprachigen Arbeitsgemeinschaft Fur Handchirurgie: Organ der Deutschsprachigen Arbeitsgemeinschaft Fur Mikrochirurgie der Peripheren Nerven und Gefasse. *Organ der V* (2020) 52(3):218–9. doi:10.1055/a-1170-8515
- Nolan EK, Chen HY. A comparison of the cox model to the Fine-Gray model for survival analyses of re-fracture rates [J]. *Arch Osteoporos* (2020) 15:1–8. doi:10.1007/s11657-020-00748-x
- Artun E, Kulga B. Selection of candidate wells for re-fracturing in tight gas sand reservoirs using fuzzy inference. *Pet Exploration Develop* (2020) 47(2):413–20. doi:10.1016/s1876-3804(20)60058-1
- Singh A, Bierrum WRN, Wormald JCR, Eastwood D. Non-operative versus operative management of open fractures in the paediatric population: A systematic review and meta-analysis of the adverse outcomes. *Injury* (2020) 51(7):1477–88. doi:10.1016/j.injury.2020.03.055
- Zhao L, Chen Y, Du J, Liu P, Luo Z, et al. Experimental Study on a new type of self-propping fracturing technology. *Energy* (2019) 183:249–61. doi:10.1016/j.energy.2019.06.137
- Xu CY, Zhang HL, Kang YL, Zhang J, Bai Y, Zhang J, et al. Physical plugging of lost circulation fractures at microscopic level. *Fuel* (2022) 317:123477. doi:10.1016/j.fuel.2022.123477
- Zhao H, Li W, Wang L, et al. A novel numerical simulation method for predicting the initiation position of refracturing technology using temporary plugging for fluid diversion. *FREsENIU's ENVIRONMENTAL BULLETIN* (2020).
- Shammam FO, Alkinani HH, Al-Hameedi AT, et al. Assessment of the production gain from refractured wells in the major shale plays in the United States. In: Proceedings of the 55th US Rock Mechanics/Geomechanics Symposium; June 2021; Santa Fe, New Mexico, USA. (2021).
- Zhang J, White M, McEwen J, Schroeder S, Cramer DD. Investigating near-wellbore diversion methods for refracturing horizontal wells. *SPE Prod Operations* (2020) 35(04):836–51. doi:10.2118/199703-pa
- Zhang G, Chen M. Study on optimal re-fracturing timing in anisotropic formation and its influencing factors [J]. *Acta Petrolei Sinica* (2008) 29(6):885–93.
- Jiang X, Cheng M, Zhang G, et al. Effect of directional perforation on the initiation and extension of hydraulic fractures [J]. *J Rock Mech Eng* (2009) 28(7):1321–6.
- Zhu H, Deng J, Liu S, et al. Prediction model for fracturing initiation pressure in directional perforation hydraulic fracturing [J]. *Acta Petrolei Sinica* (2013) 34(3):556–62.
- Guo TK, Liu BY, Qu ZQ, Gong DG, Lei X. Study on initiation mechanisms of hydraulic fracture guided by vertical multi-radial boreholes. *Rock Mech Rock Eng* (2017) 50(7):1767–85. doi:10.1007/s00603-017-1205-3
- Huang L, Liu J, Zhang F, Donstov E, Damjanac B. Exploring the influence of rock inherent heterogeneity and grain size on hydraulic fracturing using discrete element modeling. *Int J Sol Struct*. (2019) 176:207–20. doi:10.1016/j.ijsolstr.2019.06.018
- Zhu X, Cheng F, Shi C, Chen K. Mechanical plugging—Solid expandable tubular refracturing technology. *J Mech Sci Technol* (2020) 34:2357–64. doi:10.1007/s12206-020-0512-x
- Lei Y, Wang H, Wu X, et al. Analysis of fracture geometry for refractured vertical wells in tight conglomerate reservoir. *Pet Reservoir Eval Develop* (2021) 11(5):782–92. doi:10.13809/j.cnki.cn32-1825/te.2021.05.017
- Hou B, Chen M, Cheng W, et al. Fracture mechanism on shale gas reservoir fracturing with variable pump rate. *Chin J Geotechnical Eng* (2014) 36(11):2149–52.
- Zhang X, Jiang T, Jia C, Zhang B, Zhou J. Physical simulation of hydraulic fracturing of shale gas reservoir. *Pet Drilling Tech* (2013) 41(2):70–4.
- Wu Y, Hou B, Han H, et al. Study on the optimization of helical perforation parameters for horizontal wells in the condition of high horizontal stress difference. *Chin J Underground Space* (2019) 15(1):226–31.
- WuKouSun YJS. Matrix acidization in fractured porous media with the continuum fracture model and thermal Darcy-Brinkman-Forchheimer framework. *J Pet Sci Eng* (2022) 211:110210. doi:10.1016/j.petrol.2022.110210
- Yue L, Mou J, Qiong J, et al. Experimental study on fracture propagation during in-fracture temporary plugging and diverting fracturing in carbonate rock. *Oil Drilling Prod Technol* (2022) 44(2):204–10. doi:10.13639/j.odpt.2022.02.011
- Liu P, Kong X, Feng G, Zhang K, Sun S, Yao J. Three-dimensional simulation of wormhole propagation in fractured-vuggy carbonate rocks during acidization. *Adv Geo-Energy Res* (2023) 7(3):199–210. doi:10.46690/ager.2023.03.06





## OPEN ACCESS

## EDITED BY

Chong Lin,  
CCDC Drilling & Production Technology  
Research Institute, China

## REVIEWED BY

Jiajia Bai,  
Changzhou University, China  
Jun Li,  
Southwest Petroleum University, China  
Chinedu J. Okere,  
Texas Tech University, United States  
Mingzheng Yang,  
Louisiana State University, United States

## \*CORRESPONDENCE

Jun Zhou,  
✉ zhoujun23@cnooc.com.cn  
Xiangwei Kong,  
✉ 501074@yangtzeu.edu.cn

RECEIVED 16 February 2023

ACCEPTED 11 July 2023

PUBLISHED 21 August 2023

## CITATION

Chen Z, Wu G, Zhou J, Ai C, Zhang A,  
Xie X, Wu J, Kong X and Li S (2023),  
Optimization of degradable temporary  
plugging material and experimental study  
on stability of temporary plugging layer.  
*Front. Phys.* 11:1167215.  
doi: 10.3389/fphy.2023.1167215

## COPYRIGHT

© 2023 Chen, Wu, Zhou, Ai, Zhang, Xie,  
Wu, Kong and Li. This is an open-access  
article distributed under the terms of the  
[Creative Commons Attribution License](https://creativecommons.org/licenses/by/4.0/)  
(CC BY). The use, distribution or  
reproduction in other forums is  
permitted, provided the original author(s)  
and the copyright owner(s) are credited  
and that the original publication in this  
journal is cited, in accordance with  
accepted academic practice. No use,  
distribution or reproduction is permitted  
which does not comply with these terms.

# Optimization of degradable temporary plugging material and experimental study on stability of temporary plugging layer

Zhengrong Chen<sup>1</sup>, Guangai Wu<sup>1</sup>, Jun Zhou<sup>1\*</sup>, Chuanzhi Ai<sup>1</sup>,  
Anshun Zhang<sup>1</sup>, Xin Xie<sup>1</sup>, Jianshu Wu<sup>1</sup>, Xiangwei Kong<sup>2,3\*</sup> and  
Song Li<sup>2</sup>

<sup>1</sup>CNOOC Research Institute Co., Ltd., Beijing, China, <sup>2</sup>School of Petroleum Engineering, Yangtze University, Wuhan, China, <sup>3</sup>Hubei Key Laboratory of Oil and Gas Drilling and Production Engineering, Yangtze University, Wuhan, China

Temporary plugging technology is an important drilling technique for maintaining wellbore stability and resolving lost circulation problems. The key to its success lies in the use of materials that can form a tight and stable “temporary plugging layer” with certain pressure bearing capacity and a permeability close to zero in the loss channel near the wellbore. Experimental studies have been conducted to develop adhesion formulations for optimal temporary plugging materials, as the matching relationship between particle size and fracture width is critical [(0.5–1)/1]. By measuring the permeability of the temporary plugging layer under varying confining pressure with a soap foam flowmeter, researchers have been able to evaluate the effectiveness, degradation, and dosages of temporary plugging agents. It has been shown that a single-particle material, such as a walnut shell, has a smaller permeability than a hyperfine  $\text{CaCO}_3$  coated temporary plug layer. The latter, however, is less capable of bearing pressure. By combining different materials, such as walnut shells and hyperfine  $\text{CaCO}_3$  particles, the researchers were able to create a temporary plug layer that had the lowest permeability and did not change much at variable confining pressures. Its pressure-bearing capacity is strong and the temporary plug works well. Experiments have shown that a ratio of 2:1–3:1 of hyperfine  $\text{CaCO}_3$  and walnut shell particles work well for plugging a fracture system with particles of size 2–3 times the fracture width. It developed an evaluation method for temporary plugging agents, studied their plugging capability and degradation performance for reservoir conversion, and evaluated degradation performance after successful temporary plugging. The temporary plugging rate of the temporary plugging agent increased from 98.10% to 99.81%, and the maximum temporary plugging pressure is 50.39 MPa, which can be completely reduced at 150°C for 4 h, meeting the technical requirements of “dense temporary plugging, two-way pressure bearing” to some extent.

## KEYWORDS

temporary blockage, temporary plugging layer, pressure bearing capacity, degradation, permeability

# 1 Introduction

The problem of lost circulation, the most serious form of reservoir damage, is common during deep and ultra-deep drilling. However, leakage from karst caves and large fracture vent types with large production intervals is rare and leakage control techniques are difficult to implement. Leakage control techniques should temporarily plug the fracture as a leaky channel. Studies of reservoir fracture stress sensitivity, multiple fracture dynamic widths, and ideal matching models for temporary plug materials with special properties such as high strength, high permeability, and high recovery rate are fundamental to the successful application of shielded temporary plug technology in fractured reservoirs [1–8].

As one of the core technologies for protecting oil and gas reservoirs, temporary plugging technology has been deeply studied by researchers [9–16]. The temporary plugging technology is mainly aimed at porous reservoirs with high permeability. Abrams first proposed the famous “one-third bridging rule” for the drilling fluid used to protect oil and gas reservoirs [17]. Luo et al. put forward the “two-thirds bridge building criterion” that can improve the stability of bridge building on the basis of the “one-third bridge building rule”. They believed that the average particle size of bridge blocking particles should be  $1/2\text{--}2/3$  of the average pore throat size of the formation. On this basis, they put forward the temporary shielding plugging technology [18]. Zhang et al. began to use the ideal temporary plugging theory and D90 temporary plugging new method (on the cumulative distribution curve of particle size composition, when the cumulative volume fraction of 90% of the particle diameter (D90) is equal to the maximum diameter of the formation pore throat, the temporary plugging effect is the best) to temporarily plug medium and high permeability reservoirs [19]. Liu Jing et al. considered the shielding temporary plugging of fracture pore type reservoirs with different fracture widths and pressure differences, studied the reasonable positive pressure difference of drilling fluid shielding temporary plugging and the temporary plugging effect under different fracture widths, and provided a reasonable basis for the effective application of shielding temporary plugging protection technology [20]. Yang et al. added appropriate bridging particles, filling particles, and deformation particles into the original working fluid according to the  $2/3$  bridging theory, pore throat size distribution, fracture characteristics, and particle size and distribution of various particles in the working fluid, and achieved good reservoir protection effect [21]. Based on the concept of temporary plugging, a technology called “temporary plugging” is proposed for fractured porous reservoirs with a crack width of  $150\text{ }\mu\text{m}$ . According to the “ $1/3$  bridging theory,” the particle size and crack width of the bridging temporary blockage should meet certain requirements. The best combination of temporary plugging materials is 2.0% bridging particles + 1.5% deformed particles, and the recovery rate of the natural flowback permeability is greater than 65.0% [22]. Bao et al. discussed the instability failure mechanism of a high-temperature temporary plugging layer by using a self-made high-temperature high-pressure fracture temporary plugging simulation experimental device. Three kinds of plugging

materials, including micro filling particles, elastic deformation particles, and sheet filling particles, which are resistant to temperatures up to  $220^{\circ}\text{C}$ , were selected from the experiment. Two new plugging materials were made, namely, rigid bridging particles with high temperature resistance, high strength, and low density, and high temperature resistance and high strength fibers [23]. In view of the characteristics of high temperature, high pressure, and natural fracture development in ultra-deep fractured carbonate reservoir, based on the study of rock mineral composition, microstructure characteristics, and damage factors, a reservoir protection strategy of “drilling fluid performance control acid soluble temporary plugging system” is proposed, and a high-temperature acid soluble temporary plugging system consisting mainly of acid soluble fibers, acid soluble filler materials and elastic graphite is developed. The reservoir protection goal of “plugging and unlocking” has been realized [24]. Addagalla et al. designed the new phase-transforming loss circulation material (PTLCM) to pump easily and achieve thixotropic behavior under downhole conditions, resisting losses in the thief zone before setting it as a rigid plug with high compressive strength [25]. Vickers et al. investigated the effects of additive particle size and pore size dispersion on the performance of LCMs, ultimately reducing reservoir damage. It is shown that if the particle size and pore dispersion parameters of LCMs D10, D50, and D90 are the same, the reduction of drilling fluid leakage will be minimized [26]. All these studies indicate that the reduction of drilling fluid leakage must take into account the grain size distribution of LCMs. Alsaba et al. introduced the fibrous and flaky type LCMs, which can be capable of creating a tight defensive plugged zone against fractures and big, porous, and permeable voids in the reservoir formation. These LCMs can be effective to prevent heavy mud losses in drilling engineering [27]. Alireza et al., experimentally studied the productivity of various loss control materials (LCMs) in bentonite mud, evaluated the particle size distribution of LCMs based on API standards, investigated the loss of bentonite mud in various fractures via Bridging Testing Materials (BMT) apparatus [28]. Bao et al. experimentally studied the effect of LCM type, concentration, and particle size distribution on seal integrity through an LCM apparatus with a long fracture slot. The breaking pressure, fluid loss values, position, and thickness of plugging zone are the parameters for evaluating LCM performance [29]. Souza et al. experimentally studied the water-based fluid containing polymers as viscosifiers and lost-circulation materials (LCM), which evaluated the behavior of granular and fibrous materials and mixtures of them and their behavior and mechanisms of action in different sealing processes [30]. Temporary plugs are a proposed method for controlling leaks in channels ranging from tens of microns to millimeters. This is an important direction for potential lost circulation reservoir protection technology. By studying the change in the stability of the temporary plugging layer of plugging materials in fractures, we can extend the coverage of shielding temporary plugging technology to protect the width of fractures, quickly and efficiently achieving the goal of temporary plugging integration, and thus eliminating most induced losses in the “embryonic state.” The proposed technology has both

advantages and limitations, and examples can help to better illustrate these aspects. By providing a more specific analysis, we can evaluate the effectiveness and potential of this technology in various scenarios.

The technical idea of temporary plugging and unplugging is also widely applied in the field of simulation and reconstruction of oil and gas reservoirs. In the aspect of temporary plugging and fracturing and acidizing for stimulation and reconstruction, degradable materials are mainly used as temporary plugging and diverting agents, which rely on the acid liquid to carry into the layer with good permeability and large flow coefficient, so as to achieve temporary plugging and diverting, thus achieving the purpose of reasonable placement of acid liquid in strongly heterogeneous reservoirs [31–34]. Multiple types of temporary plugging agents are selected according to the formation conditions to implement composite temporary plugging [35], which is conducive to improving the temporary plugging effect. Li et al. simulated and studied the non-mechanical temporary plugging steering process under different completion methods based on the 3D printing fracture rock plate simulation technology, selected the temporary plugging steering material with temperature resistance and pressure capacity, and evaluated the design parameters such as the content of temporary plugging steering material and the combination of particle size under different fractures and their temporary plugging capacity [36]. Wu et al. proposed a novel water-soluble polymer plug for fracturing, which was completely degraded at 70°C for 5–8 h by carrying out experimental evaluation tests, such as water absorption expansion rate [37].

Temporary plugging materials play a vital role in drilling engineering and in the development and stimulation of oil and gas fields. In this study, different temporary plugging materials were evaluated for their permeability and temporary plugging effect, and the temporary plugging layer formed by different compositions of temporary plugging materials was tested under varying confining pressure conditions. Moreover, the bridge temporary plugging formula of “tight temporary plugging and bidirectional pressure” was optimized, and the pressure stability and degradation performance of the plugging layer were experimentally evaluated. These results provide a useful reference for the use of temporarily effective blocking and bearing fracture systems in drilling and oil extraction. This paper describes an experimental design for various temporary plugging materials, evaluates the permeability and temporary plugging effect of different temporary plugging material compositions under varying confining pressure conditions, optimizes the bridge temporary plugging formula of “tight temporary plugging and bidirectional pressure,” and evaluates the pressure stability and degradation performance of the plugging layer experimentally. The experiments provide valuable reference information for temporary plugging techniques. In addition, we investigate the capability and degradation performance of temporary plugging, develop an evaluation method for temporary plugging for reservoir conversion, and evaluate the degradation performance after successful temporary plugging. Our findings can contribute to the improvement of temporary plug technology and the efficient development of oil and gas fields technology. In addition, the authors investigated the capability and degradation performance of temporary plugging, developed an evaluation method for reservoir conversion, and evaluated the degradation performance after successful temporary plugging.



**FIGURE 1**  
Fractured rock sample for experiment.



**FIGURE 2**  
Walnut shell granule.

## 2 Formulation optimization of temporary plugging agent

### 2.1 Experimental materials and instruments

Dense carbonate outcrops were selected and treated with Brazil splitting. The fractures in the walls were then filled with experimental material. To prepare the fracture for the experiment, a pretreatment of 20 MPa confining pressure was applied. This resulted in a fracture width of approximately 100 mesh (as shown in Figure 1). We selected walnut shell and coated ultra-fine  $\text{CaCO}_3$  as the indoor plugging materials to be tested, as shown in Figure 2 and Figure 3.

A gas flow meter was used in the experiment to measure the gas permeability of the fractured rock sample. This equipment, independently developed, is composed of a nitrogen cylinder, core gripper, and special measuring cylinder (Figure 4), which is mainly based on the Darcy formula and is suitable for on-site measurement of the permeability of low porosity and low permeability rock samples. Measurements were performed by



**FIGURE 3**  
Superfine  $\text{CaCO}_3$ .

using nitrogen gas to penetrate the sample in a core holder, connecting a flow meter containing bubble water and creating bubbles to drive the gas upward through the holder. Due to the small bubble mass, the effect of gravity can be neglected and the rise velocity can be measured. By using Darcy's formula, the permeability of the sample can be calculated.

## 2.2 Experimental scheme

- (1) The design involves uniformly placing equal amounts of the plug material formula on the fracture surface as a temporary plug layer, and then tightly wrapping the fractured rock sample in the core holder.
- (2) The oil pressure pump provides and controls the confinement pressure of the core gripper, while the nitrogen cylinder provides the gas and flow pressure.
- (3) The pipes are connected according to the drawing procedure. The soapy water is placed in a rubber tube at the bottom of a special measuring cylinder and the tube is squeezed to create soap bubbles. These bubbles are driven upwards by the passage of  $\text{N}_2$  gas through the fractured rock sample, creating a driving force. The permeability of the fractured rock sample at varying confining pressures was then calculated by recording the rate of rise of a single soap bubble in the measuring cylinder to obtain the flow rate of gas at the exit.
- (4) Five confining pressures were chosen for the gripper: 5, 10, 15, 20, and 30 MPa. At least five different flow pressure points are reasonably chosen to provide the confining pressure sequentially. After each pressure change, it is necessary to stabilize the system for 30 min. The rise rate of the foam was recorded at each flow pressure and the steady-state time was varied by 1–2 min. The error rate is ensured to be as small as possible.
- (5) The gas flow rates for the different plug formulations were obtained by successively using the temporary plug formation in

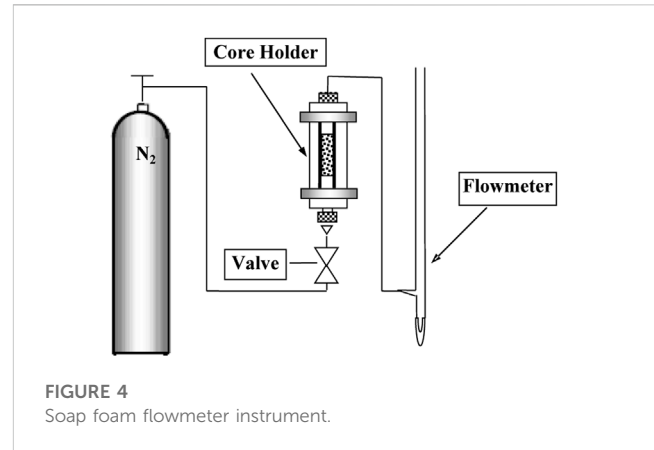


**FIGURE 4**  
Soap foam flowmeter instrument.

Table 1 as the temporary plug layer for the fractured rock samples.

- (6) According to Eq. 1, the gas flow measured at the outlet is converted into the permeability of the fractured rock sample to obtain the permeability change rule of the temporary plugging layer with different plugging materials under the action of varying confining pressure.

$$K = \frac{Q\mu_g L}{A(p_1^2 - p_2^2)} \quad (1)$$

Where,  $K$  is the permeability,  $10^{-3} \mu\text{m}^2$ .  $Q$  is the average flow of gas, mL/s.  $\mu_g$  is the gas viscosity,  $10^{-3} \text{Pa}\cdot\text{s}$ .  $L$  is the length of the rock sample, cm.  $p_1$ ,  $p_2$  are respectively the pressure before and after gas passes through the fractured rock sample, MPa.

## 2.3 Experimental results and discussion

### 2.3.1 Experimental results

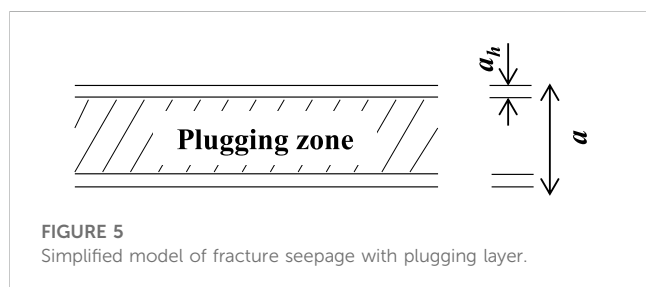
Soap-foam flow meters were used to obtain permeability variations for nine species of plug material in fractured rock samples. The goal of the present study is to investigate the permeability of different temporary plug layers formed in fractured rocks under various confining pressures. As shown in Figure 6, the permeability is highest for the temporary plug layer formed by 200 meshes coated with ultra-fine  $\text{CaCO}_3$ , indicating that the mismatch between particle size and fracture width makes the bridge unstable and vulnerable to destruction, resulting in a large permeability for the temporary plug layer. On the other hand, the permeability of the temporary plug layer formed by 150 mesh walnut shell particles is minimal and decreases with increasing confining pressure. This suggests that the temporary plug layer formed by walnut shell particles is the densest compared to other plug materials.

Comparing the permeability of the individual plug materials, Figure 7 shows that the permeability of the temporary plug layer formed by the walnut shell particles is smaller than that of the ultrathin  $\text{CaCO}_3$ -coated film. Figure 7



TABLE 1 Plugging layers with different materials.

No.	I	II	III	IV	V	VI	VII	VIII	IX
Temporary blocking materials	150 mesh covered $\text{CaCO}_3$	200 mesh covered $\text{CaCO}_3$	200 mesh walnut shell	150 mesh walnut shell	200 mesh + 150 mesh covered $\text{CaCO}_3$	200 mesh walnut shell + 200 mesh covered $\text{CaCO}_3$	200 mesh walnut shell + 150 mesh covered $\text{CaCO}_3$	150 mesh + 200 mesh walnut shell	150 mesh walnut shell + 150 mesh covered $\text{CaCO}_3$



shows that the permeability of the temporary plug layer formed by walnut shell particles is smaller than that of the ultrathin  $\text{CaCO}_3$ -coated film, suggesting that the temporary plug layers formed by walnut shell particles in fractures tend to be denser due to their higher persistence at confining pressures compared to coated hyperfine  $\text{CaCO}_3$ . Moreover, although walnut shells cannot form temporary plugs on their own due to their weak solubility, they can be an effective component in the production process of oil and gas development as temporary plugs.

An ideal temporary plug layer requires a mixture of different plug materials as shown in Figure 8. To compare and analyze the permeability of the temporary plug layer formed by 150 mesh-coated hyperfine  $\text{CaCO}_3$  and 200 mesh-coated hyperfine  $\text{CaCO}_3$ , a temporary plug layer is formed by stabilizing bridges constructed by coating the fracture with ultrathin  $\text{CaCO}_3$ , using the assistance of walnut-shell particles of small grain size and weak stiffness. As the confining pressure is increased, the coated hyperfine  $\text{CaCO}_3$  and walnut-shell particles become more compacted, thereby decreasing the permeability of the temporary plug layer. Although coated hyperfine  $\text{CaCO}_3$  can act as a bridge, it cannot effectively act as a compact temporary plug by deformation, as coated hyperfine  $\text{CaCO}_3$  films are brittle and nearly incompressible. However, the small deformation of the walnut-shell particles at confining pressure makes the temporary plug more compact, indicating that the gas permeability of the fractured rock sample is minimal at the macroscopic level. Moreover, the coated hyperfine  $\text{CaCO}_3$  is acid-soluble and easily unplugged. When calcium carbonate is dissolved by acid, the walnut shells in the temporary plug are destabilized and the temporary plug is destroyed. Therefore, it has been suggested that a mixture of coated hyperfine  $\text{CaCO}_3$  and walnut shell particles can form an ideal temporary plug layer.

The particles in the temporary plugging layer make “point” contact with the fracture wall, and are pressed against the fracture wall due to the confining pressure. When there is a temporary plug layer within the fracture width, its percolation state can be divided into three zones. The boundary “fractures” near the fracture wall can be considered as the equivalent hydraulic fracture width of  $A_h$ , and the temporary plugging layer with a thickness of  $A - A_h$  in the middle (Figure 5). Thus, the gas flow measurement of the fractured rock

sample with the temporary plugging layer consists of two parts. In conclusion, utilizing appropriate paragraph structures and connective words, replacing technical vocabulary with more accessible language, and correcting grammar and syntax errors will significantly enhance the cohesiveness and clarity of the essay.

$$Q = Q_1 + Q_2 \quad (2)$$

$$Q_1 = \frac{2ga_h^3}{12\nu} LJ \quad (3)$$

$$Q_2 = K(a - 2a_h)LJ \quad (4)$$

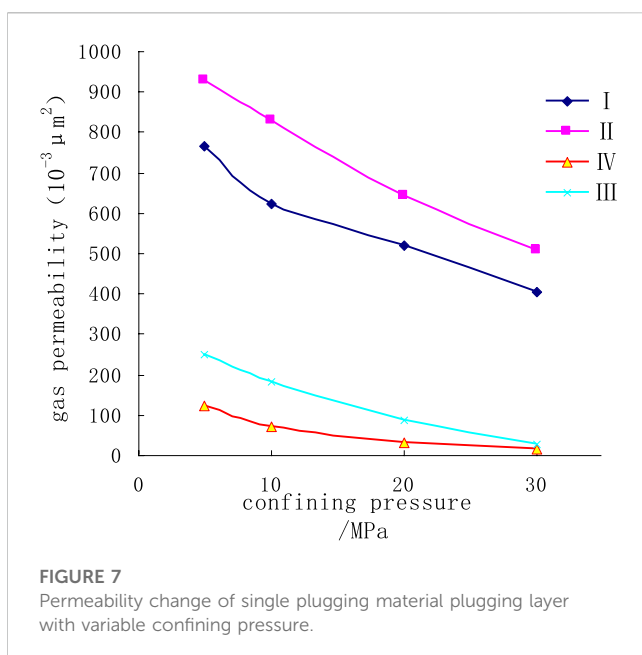
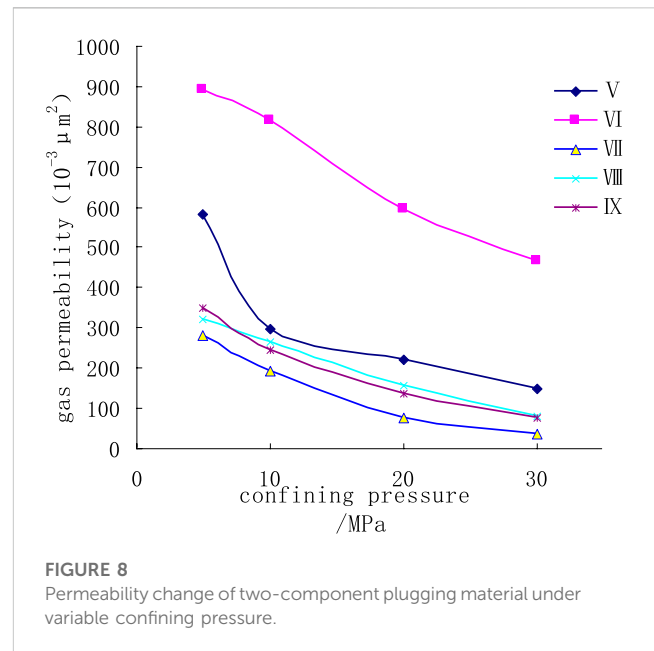
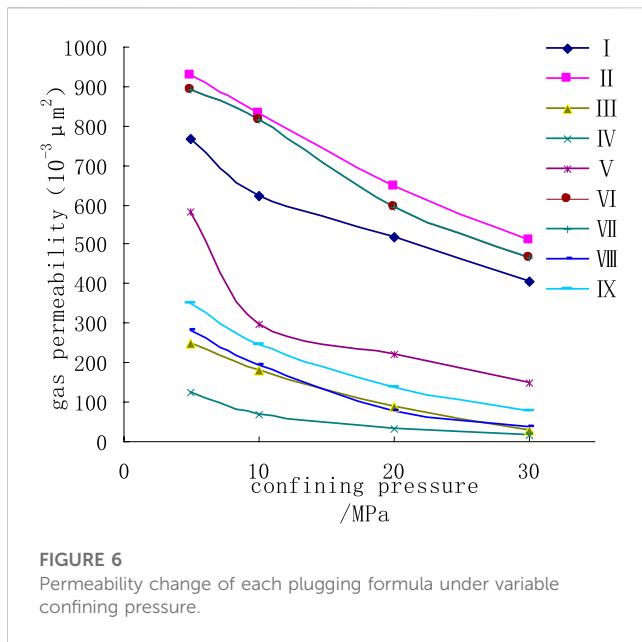
Where,  $K$  is the permeability coefficient of the temporary plugging layer,  $10^{-3} \mu\text{m}^2$ .  $L$  is the fracture height, cm.  $J$  is the hydraulic gradient.

It can be seen from Equation 4 that when the width of the temporary plugging layer  $a$  is much larger than  $a_h$ , and  $Q_2 \approx kaLJ$ . This means that the permeability  $k$  of the temporary plug layer contributes significantly to the permeability of the fractured rock sample, and the permeability of the temporary plug layer determines the permeability of the fractured rock sample. The denser the temporary plug layer in the fractured rock sample, the lower the permeability and the better the temporary plug.

Comparing the experimental results (Figures 6–8) that shown in Table 2, we can draw the following conclusions:

- (1) Both walnut shells and calcium carbonate are rigid particles. However, walnut shells have lower hardness and larger deformation as pressure increases. They also exhibit increased pressure-bearing regions, making them less likely to break at high pressures. In contrast, calcium carbonate (such as quartz sand and glass beads) has a higher hardness and minimal deformation.
- (2) Changes in confining pressure produce relatively gentle alterations to the permeability of the rigid particle filling layer, mainly due to small deformation that is insufficient to reduce the fracture’s permeability. The coordination between particle size and fracture width means that smaller calcium carbonate particles (150 mesh) will cause less permeability than larger ones (200 mesh).
- (3) The best composite formula for sealing purposes comprises 150 mesh calcium carbonate particles and 200 mesh walnut shells (Figure 8). The rigid 150 mesh calcium carbonate particles perfectly match the fracture width, while the smaller 200 mesh walnut shell particles deform under the confining pressure, resulting in the lowest permeability and the best sealing effect. When filled solely with deformed particles, such as walnut-shell particles, the fracture undergoes larger deformations at confining pressure. By using larger rigid particles as bridging materials, fractures become more resistant to confinement pressure deformation. Optimal





sealing can be achieved over a wide range of confining pressures by using rigid particles with appropriate grain sizes in combination with deformable materials with smaller grain sizes. Fine and dense composite fillings can better block fractures than fillings with larger grain sizes under fracture width requirements.

In summary, the experimental results suggest that the combination of 150 mesh calcium carbonate particles and 200 mesh walnut shells yields the best sealing. This can be attributed to the fact that rigid 150 mesh calcium carbonate particles perfectly match the fracture width and small 200 mesh

walnut shell particles deform under pressure, resulting in the lowest permeability and best sealing. In addition, we find that the permeability of rigid granular packing layers changes only modestly due to the small deformations involved, and that the fracture permeability can be lower with smaller calcium carbonate particles than with larger ones.

## 2.4 Micro analysis of temporary plugging layer

### (1) Micro state of temporary plugging agent

The temporary plug of the artificial nucleus was observed by scanning electron microscopy (Figure 9). The results show that the temporary plug effectively adhered to and blocked off all pores, without any open pores observed at a magnification of 1,500, indicating its strong ability to block pores. This could potentially have significant implications for the development of new methods to improve the stability and functionality of artificial nuclei, but further studies are needed to fully understand its potential applications. Overall, this experiment provides valuable insights into efficient blocking capabilities. The use of temporary plugs for artificial nuclei warrants further investigation.

### (2) Adhesion of temporary plugging agent to wall surface under pressure

As shown in Table 3, under the condition of 5 MPa ring pressure, after 30 min, the separation pressure of the temporary plugging agent from the fracture wall was 4.0 N by using the method of removing pieces.

### (3) Deformation and elongation capacity of temporary plugging agent under pressure, as shown in Table 4

TABLE 2 Permeability and bear strength results of different plugging zones under variable confining pressure.

No.	Plugging zone materials	Flow pressure (MPa)	Confining pressure (MPa)	Kg ( $\times 10^{-3} \mu\text{m}^2$ )	Bearing strength/MPa	
					20°C	80°C
I	150 mesh ultra-fine calcium carbonate	0.1	5	766.59	0.36	0.35
			10	623.40		
			20	519.75		
			30	403.82		
II	200 mesh ultra-fine calcium carbonate	0.1	5	927.44	0.22	0.2
			10	830.13		
			20	644.73		
			30	509.83		
III	200 mesh peanut shells	0.1	5	249.73	0.5	0.3
			10	182.58		
			20	88.63		
			30	27.06		
IV	150 mesh peanut shells	0.1	5	123.96	1.1	0.5
			10	69.66		
			20	32.76		
			30	17.65		
V	200 mesh + 150 mesh ultra-fine calcium carbonate	0.1	5	582.60	4.8	4.3
			10	296.83		
			20	222.06		
			30	149.28		
VI	200 mesh peanut shells + 200 mesh ultra-fine calcium carbonate	0.1	5	893.39	4	3.1
			10	816.03		
			20	595.04		
			30	466.64		
VII	200 mesh peanut shells + 150 mesh ultra-fine calcium carbonate	0.1	5	281.45	5	3.9
			10	191.47		
			20	76.58		
			30	36.43		
VIII	150 mesh + 200 mesh peanut shells	0.1	5	319.47	1.3	0.6
			10	266.25		
			20	155.13		
			30	80.46		
IX	150 mesh peanut shells + 150 mesh ultra-fine calcium carbonate	0.1	5	347.56	4.5	2.4
			10	243.18		
			20	137.61		
			30	74.42		

**TABLE 3 Adhesion between temporary plugging agent and wall under pressure.**

Sample	Annular compression (MPa)	External force (N)	Breaking	Strength (MPa)
Temporary plugging agent	5.0	4.0	Fracture along seam	$\sigma_{g-w} > \sigma_g$

Note:  $\sigma_g$  self-tensile strength,  $\sigma_{g-w}$ , adhesion strength between colloid and wall surface.

**TABLE 4 Deformation and elongation capacity of temporary plugging agent under pressure.**

Sample	Initial length (mm)	Length after pressing (mm)	Extensibility (%)
Temporary plugging agent	23.5	30.7	30.6

The maximum elongation of the temporary plugging agent is 30.6% (Table 4), and it has good compressive elongation and toughness.

## 3 Stability evaluation of temporary plugging layer

### 3.1 Performance evaluation method

#### 3.1.1 Evaluation method of temporary plugging effect

Existing evaluation methods for temporary plugging agents are mainly formulated based on the process characteristics of water plugging, profile control of water injection wells, and drilling fluids for oil and gas wells. However, they are not fully applicable to the reservoir reconstruction process because there is no uniform evaluation standard or recognized method for temporary plugs for domestic and international reservoir reconstruction. To address this, a new evaluation method for temporary plugging agents in reservoir reconstruction is proposed in this paper, focusing on the temporary plugging ability and plugging removal performance of the temporary plugging agent.

The temporary plugging agent is used to temporarily plug high permeability layers or fractures to create a plugging layer, which forces the subsequent injected liquid into the low permeability layer or creates a new fracture. After the operation, the plugging layer can be dissolved/degraded under the formation conditions to remove the temporary plugging agent. To evaluate temporary plugging agents, the temporary plug rate and fracture pressure at the reservoir temperature are investigated to determine the properties of the temporary plug on fracture, matrix, and other reservoirs. Additionally, the high-temperature solubility/degradability of the temporary plug is evaluated to determine if the temporary plugging agent will cause damage to the reservoir after being removed.

The evaluation of the temporary plug rate and break pressure can be achieved through core flow devices. When evaluating the temporary plug rate, the percentage decrease in permeability after the temporary plug with a temporary plugging agent should be calculated. The break pressure of a temporary plug is the lowest pressure at which the reservoir reconstruction fluid can break through a temporary plug layer of a certain thickness, indicating the pressure at which the reservoir reconstruction fluid cannot penetrate the temporary plug layer in large quantities.

In conclusion, the proposed evaluation method for temporary plugging agents in reservoir reconstruction focuses on the temporary plugging ability and plugging removal performance of the temporary plugging agent. Through the evaluation of the

temporary plug rate and break pressure, the properties of the temporary plug on fracture, matrix, and other reservoirs, as well as the high-temperature solubility/degradability of the temporary plug, can be determined more accurately and effectively.

#### (1) Experimental condition

The experimental conditions are shown in Table 5 below.

#### (2) Experimental methods (Figure 10)

Breakthrough pressure after temporary plugging of matrix:

- Measure the initial permeability of the core by using standard saline solution at 80°C, regardless of temperature effects on permeability.
- To achieve complete wetting, add an appropriate amount of reservoir conversion liquid until completely mixed with the temporary blocking agent.
- Fill the core's front end with a wetted temporary blocking solution of some thickness.
- Inject standard brine at a constant flow rate (10 mL/min) into the end face of the core filled with temporary blocking solution. Record the following parameters: displacement time, flow rate, pressure, and liquid volume at the outlet.
- If the core does not break after increasing the displacement pressure to 40 MPa, switch on constant pressure control and continue injecting standard brine while observing stability.
- The experiment concludes when there is a sudden decrease in pressure (usually over 30%) or a sudden increase in liquid flow at the outlet (usually over 30%), indicating core breakthrough.
- Remove the core and examine it to conclude the experiment.

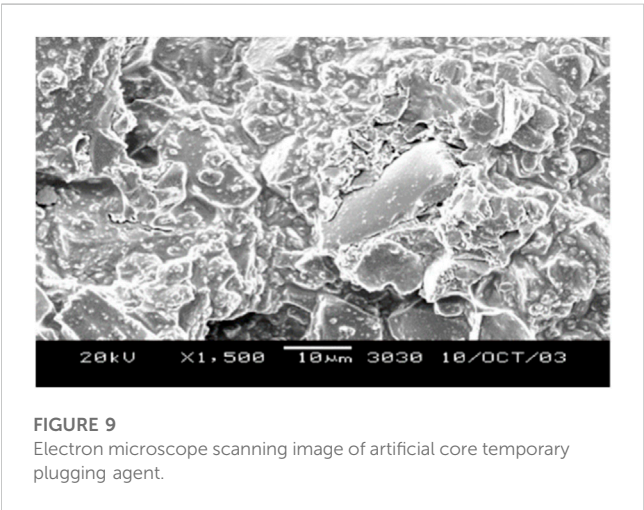
Breakage pressure after temporary plugging of the fracture.

To measure the rupture pressure of the temporary plug diverter on the fracture, the artificial core was first split in half along the central axis. A layer of Teflon of a certain thickness is then applied to the edges of the split core, which is reassembled to mimic the formation of a fracture. Finally, the breakthrough pressure is measured according to the experimental method of temporary plugging of the matrix.

The temporary blockage rate is calculated according to the following formula:

TABLE 5 Experimental condition.

Experimental core	Artificial core (φ 25.2 mm, L ≥ 40 mm)
Experimental equipment	Core flow test device, temperature resistance 177°C, pressure resistance 55 MPa
Experimental temperature	150°C



$$\eta = \frac{K_0 - K_1}{K_0} \times 100 \tag{5}$$

Where,  $\eta$  is the temporary blockage rate, %.  $K_0$  is the permeability of the core before temporary plugging,  $10^{-3} \mu\text{m}^2$ .  $K_1$  is the permeability of the core after temporary plugging,  $10^{-3} \mu\text{m}^2$ .

3.1.2 Evaluation method for degradability of temporary plugging agent

The temporary plug in the reservoir reconstruction plays a crucial role in this process. This is necessary in order for the temporary plug not to dissolve or slowly dissolve when injected into the formation with the reservoir reconstruction fluid. A temporary stop should act as a torsion by bridging, expanding, and performing other functions to temporarily block the fracture or pore of the reservoir, thus forcing the subsequent reservoir reconstituted fluid into a low permeability layer or

secondary sweet spot region. Later, under the influence of the reservoir temperature and the fluid, the temporary plug will gradually dissolve or degrade to remove the plug. It is therefore necessary to assess the solubility of the temporary plug, mainly by investigating its dissociation in water at different temperatures.

(1) Experimental condition

Experimental equipment: thermostatic drying oven, high-temperature aging tank (with PTFE inner cylinder), which can be heated to 150°C.

Test temperature: 150°C. Test time: 4 h.

The experimental conditions are shown in Table 6 below.

(2) Experimental methods

To prepare the drilling fluid, 10 g of a temporary blocking agent is added to 200 mL of water, mixed vigorously, and poured into the aging tank. The mixture is then heated in a 150°C oven for 4 h, after which the tank is taken out of the oven and observed for any solid residue at the bottom.

3.2 Evaluation results

3.2.1 Evaluation of temporary plugging performance

Take a standard core with a permeability of  $1.41 \times 10^{-3} \mu\text{m}^2$  at 40 MPa, and connect an iron ring with a length of 1.0 cm at the end face. A temporary plug test is performed by adding a temporary plug to the iron ring. The injection rate is 10 mL/min. The pressure was first limited to 40 MPa to test the temporary plug rate and then increased to 50 MPa to test the

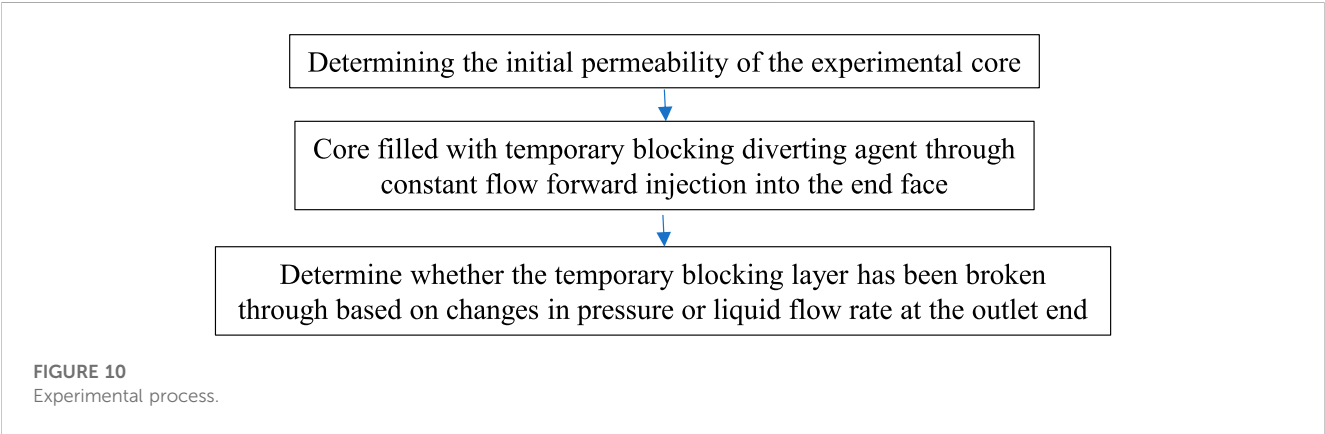


TABLE 6 Experimental condition.

Experimental material	Temporary plugging agent (10 g)
Experimental equipment	Thermostatic drying oven, high-temperature aging tank (PTFE inner cylinder)
Experimental temperature	150°C
Experimental time	4 h

TABLE 7 Evaluation results and effects of temporary plugging experiment.

Sample	Initial permeability ( $10^{-3} \mu\text{m}^2$ )	Temporary plugging permeability ( $10^{-3} \mu\text{m}^2$ )	Temporary plugging efficiency (%)	Maximum temporary plugging pressure (MPa)	Flow after temporary blockage (mL/min)
Old sample	1.41	0.02679	98.10	51.72	0.73
New sample	1.41	0.00263	99.81	50.39	0.07

maximum temporary plug pressure. The temporary plug test data before and after the optimization is shown in Table 7. Experimental results showed that while the pressure bearing capacity of the temporary plug did not improve significantly, its density did, and the flow rate of fluid through the sealing layer decreased from 0.73 to 0.07 mL/min. This improved performance not only reduces working fluid intrusion and prevents permeability damage to seals, but also reduces reservoir damage.

After the pressure rise to 50 MPa, the test was stopped due to the limitation of the core pressure resistance, and it can be seen that the temporary plugging rate of the new sample has been improved to a certain extent (Figure 11). From the appearance of the experimental results, a sealed layer of approximately 0.5 cm thickness can be seen at the end of the core.

3.2.2 Evaluation of degradation ability of temporary plugging agent

(1) Thermal rolling treatment in drilling fluid

To prepare the temporary stopper, 10 g of the stopper was thoroughly mixed by hand with 200 mL of water before being added to the aging tank containing the drilling fluid. The mixture was then heated in an oven at 150°C for 4 h. The



FIGURE 11  
Temporary blocking test.

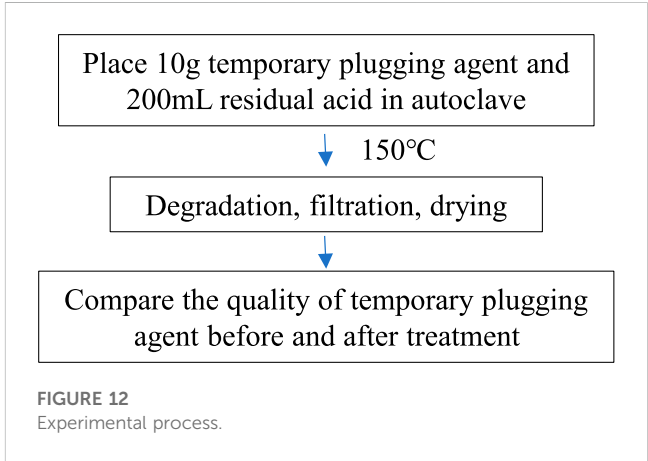


FIGURE 12  
Experimental process.

experimental results, shown in Figure 12, demonstrate that the agent completely dissolves, leaving no residue at the bottom of the tank. This successful application of a temporary blocking agent highlights its potential for use in future drilling applications.

(2) Acid resistance

The main equipment of the degradation experiment is a high-precision oven and autoclave with PTFE lining. During the experiment, put 10 g temporary plugging agent and 200 mL residual acid in an autoclave and put them in an oven at 150°C to degrade, filter, dry, and weigh the remaining temporary plugging agent mass  $W_d$ . The experimental steps are shown in Figure 12. The degradation rate =  $(10 - W_d)/10\% \times 100\%$ .

The evaluation results demonstrate that the temporary blocking material in the residual acid can achieve a degradation rate of more than 98% within 12 h with minimal damage to the reservoir, thus meeting the requirements. The degraded material left no solid residue and did not contaminate the reservoir. When particle impingement optimization is employed, the impingement rate is improved from 98.10% to 99.81%, and the maximum impingement pressure is increased to 50.39 MPa. Also, it can fully degrade at 150°C for 4 h, satisfying all design performance requirements.



## 4 Summary

- (1) For temporary plugging, different temporary plug materials were tested for their ability to form a denser temporary plug layer. It has been shown that walnut-shell particles have a smaller permeability than coated hyperfine  $\text{CaCO}_3$ , and that the denser the temporary plug layer, the better the particle size agrees with the fracture width.
- (2) Mixing the coated hyperfine  $\text{CaCO}_3$  with the walnut shell resulted in a lower permeability of the temporary plug layer. In addition, the temporary plug layer formed from the multi-component temporary plug material is more compact and stable under variable confining pressure, thus allowing for better temporary plugging of fractures.
- (3) The best results were obtained by coating hyperfine  $\text{CaCO}_3$  with walnut-shell particles, yielding a temporary plug layer with little change in permeability under variable confining pressure conditions and strong pressure bearing capacity. Experimental optimization of the two temporary plug materials resulted in a 2:1–3:1 mixing ratio of coated hyperfine  $\text{CaCO}_3$  and walnut-shell particles with particle sizes 2–3 times the fracture width. The temporary plugging rate increased from 98.10% to 99.81% with a maximum temporary plugging pressure of 50.39 MPa, which could be completely reduced at 150°C for 4 h. To some extent, this satisfies the temporary plugging technical requirements of “dense temporary plugging, two-way pressure bearing, low damage degradation.”

## Data availability statement

The original contributions presented in the study are included in the article/Supplementary Material; further inquiries can be directed to the corresponding authors.

## Author contributions

ZC: Conceptualization, funding acquisition, project administration, resources, writing—original draft and software. GW and CA: Data curation, formal analysis, and methodology. SL: writing—original draft,

and writing—review and editing. XK: Project administration and resources. AZ: Investigation, methodology, software, and visualization. XX and JW: Conceptualization, funding acquisition, and methodology. XK: Investigation, methodology, and project administration. All authors contributed to the article and approved the submitted version.

## Funding

This research was funded by “Research on offshore large-scale fracturing engineering technology (KJGG2022-0704), Key parameter characterization and desert area evaluation technology of coalbed methane geological engineering (KJGG2022-1001), and Research on Inter-well Disturbance Integral Fracturing Technology of Coalbed Gas (2021-YXKJ-010).”

## Acknowledgments

The authors are grateful to the reviewers and editors for their careful review of this manuscript.

## Conflict of interest

Authors ZC, GW, JZ, CA, AZ, XX, and JW were employed by CNOOC Research Institute Co., Ltd.

The remaining authors declare that the research was conducted in the absence of any commercial or financial relationships that could be construed as a potential conflict of interest.

## Publisher’s note

All claims expressed in this article are solely those of the authors and do not necessarily represent those of their affiliated organizations, or those of the publisher, the editors and the reviewers. Any product that may be evaluated in this article, or claim that may be made by its manufacturer, is not guaranteed or endorsed by the publisher.

## References

1. Yan F, Kang Y, Li S, Du C, Li D. Simulated experiment on stress sensitivity in fractured-vuggy reservoir. *Nat Gas Geosci* (2010) 21(3):489–93.
2. Li S, Kang Y, Li D, You L, Lian Z. ANSYS simulation of fracture width variation in fracture-cavity reservoirs. *Nat Gas Geosci* (2011) 22(2):340–6.
3. Kang Y, Yan F, You L, Du C, Li D. Loss and control in regular reservoir formations in block Tahe. *Drilling Fluid & Cementing Fluid* (2010) 27(1):41–3.
4. Chen S, Kang Y, Ma X. Application of the screen bridging technology on the new drilling area. *Drilling Prod Technol* (2005) 28(6):99–101.
5. You L, Kang Y, Chen Y, Hao S, Cheng Q. Application of temporary and shielding plugging technology to improve well-logging responses for tight sandstone gas reservoir. *Oil Drilling Prod Technol* (2007) 29(1):113–7.
6. Okere CJ, Su G, Zheng L, Cai Y, Li Z, Liu H. Experimental, algorithmic, and theoretical analyses for selecting an optimal laboratory method to evaluate working fluid damage in coal bed methane reservoirs. *Fuel* (2020) 282:118513. doi:10.1016/j.fuel.2020.118513
7. He J, Okere CJ, Su G, Hu P, Zhang L, Xiong W, et al. Formation damage mitigation mechanism for coalbed methane wells via refracturing with fuzzy-ball fluid as temporary blocking agents. *J Nat Gas Sci Eng* (2021) 90:103956. doi:10.1016/j.jngse.2021.103956
8. Yan Z, Okere CJ, Zeng X, Yao Z, Su G, Gan M, et al. Preventing sour gas kicks during workover of natural gas wells from deep carbonate reservoirs with anti-hydrogen sulfide fuzzy-ball kill fluid. *Energ Sci Eng* (2022) 10(8):2674–88. doi:10.1002/ese3.1158
9. Okere CJ, Sheng JJ, Fan L, Huang X, Zheng L, Wei P. Experimental study on the degree and damage-control mechanisms of fuzzy-ball-induced damage in single and multi-layer commingled tight reservoirs. *Pet Sci* (2023). doi:10.1016/j.petsci.2023.05.017
10. Kang Y, You L, Xu X, Liao Z. Practices of formation damage control for deep fractured tight gas reservoir in Western Sichuan basin. In: Proceedings of the CPS/SPE International Oil & Gas Conference and Exhibition in China; June 2010; Beijing, China (2010). doi:10.2118/131323-MS
11. Moghadasi J, Jamialahmadi M, Müller-Steinhagen H, Sharif A. Formation damage due to scale formation in porous media resulting from water injection. In: SPE: 86524 presented at SPE International Symposium and Exhibition on Formation Damage Control held in Lafayette; February 2004; Louisiana (2004). doi:10.2118/86524-MS
12. Collins N, Kharitonov A, Whitfill D, Miller M. Comprehensive approach to severe lost circulation problems in Russia. In: Proceedings of the SPE Russia Oil & Gas

Technical Conference and Exhibition held in Moscow; October 2010; Russia (2010). p. 26–8. doi:10.2118/135704-MS

13. Cui Y. A new method for the optimal selection of temporary plugging particles. *Geoscience* (2000) 14(1):91–4.

14. Qian Z, Lu Z, Bai H, Li J, Guan J. Leak resisting and plugging techniques for oil-based drilling fluid. *Pet Geology oilfield Develop Daqing* (2017) 36(6):101–4. doi:10.19597/j.issn.1000-3754.201610058

15. Xu CY, Zhang HL, Kang YL, Zhang J, Bai Y, Zhang J, et al. Physical plugging of lost circulation fractures at microscopic level. *Fuel* (2022) 317:123477. doi:10.1016/j.fuel.2022.123477

16. Xu CY, Zhang HL, She JP, Jiang G, Peng C, You Z. Experimental study on fracture plugging effect of irregular-shaped lost circulation materials. *Energy* (2023) 276:127544. doi:10.1016/j.energy.2023.127544

17. Abrams A. Mud design to minimize rock impairment due to particle invasion. *JPT* (1977) 29(2):586–92. doi:10.2118/5713-pa

18. Luo P. A temporary plugging technique on formation damage control during drilling and completion. Beijing: Encyclopedia of China Publishing House (1997). p. 68–98.

19. Zhang J, Yan J, Zhao H. Optimization of bridging particle size distribution of drilling fluid for formation protection. *Drilling Fluid & Cementing Fluid* (2004) 21(5):4–7.

20. Liu J, Kang Y, Liu D, You L, Gao B. Research on the temporary shielding plugging experiment in considering fracture-pore reservoir of fracture width and pressure difference. *Drilling Prod Technol* (2006) 29(2):97–8.

21. Yang J, Kang Y, Lan L, Hu Y, Chen J. Study of shielding temporary plugging technology for the fractured sandstone reservoir protection in the center of Sichuan basin. *Drilling Fluid & Cementing Fluid* (2006) 23(4):25–7.

22. Yan F, Kang Y, Sun K, Zhang J, Wang H. The temporary sealing formula for fractured-vuggy carbonate reservoir. *Pet Drilling Tech* (2012) 40(1):47–51.

23. Bao D, Qiu Z, Qiu W, Wang B, Guo B. Experiment on properties of lost circulation materials in high temperature formation. *Acta Petrolei Sinica* (2019) 40(7):846–57. doi:10.7623/syxb201907009

24. Fang J, Zhang Y, Li S, Yu P, Li Y. Acid-soluble temporary plugging technology for ultra-deep fractured carbonate reservoirs in block 1 of the Shunbei area. *Pet Drilling Tech* (2020) 48(2):17–22.

25. Addagalla AK, Jadhav P, Yadav P, Sarmah P, Maley I, Anerao A. A novel phase transition loss circulation solution for severe losses scenario: Case histories from the Middle East and africa. In: Proceedings of the SPE Asia Pacific Oil & Gas Conference and Exhibition; November, 2020; Virtual (2020). doi:10.2118/202234-MS

26. Vickers S, Cowie M, Jones T, Twynam AJ. A New methodology that surpasses current bridging theories to efficiently seal a varied pore throat distribution as found in natural reservoir formations. *Wiertnictwo, Nafta, Gaz* (2006) 23(1):501e515.

27. Alsaba M, Nygaard R, Hareland G, Contreras O. Review of lost circulation materials and treatments with an updated classification. In: Proceedings of the prepared for presentation at the 2014 AAE Fluids Technical Conference and Exhibition; April 2017; Houston, Texas (2014).

28. Nasiri A, Ghaffarkhah A, Moraveji MK, Ali G, Valizadeh M. Experimental and field test analysis of different loss control materials for combating lost circulation in bentonite mud. *J Nat Gas Sci Eng* (2017) 44:1875–5100. doi:10.1016/j.jngse.2017.04.004

29. Bao D, Qiu Z, Zhao X, Zhong H, Chen J, Liu J. Experimental investigation of sealing ability of lost circulation materials using the test apparatus with long fracture slot. *J Pet Sci Eng* (2019) 183:106396. doi:10.1016/j.petrol.2019.106396

30. Souza TM, Filho MNB, Calçada LA, Scheid CM. Evaluation of the effect of temperature and pressure on the process of combating loss of circulation using fibrous and granular materials. *J Pet Sci Eng* (2022) 219:111115. doi:10.1016/j.petrol.2022.111115

31. Luo Y, Zhang Y, Yang Z, Chang L, Zhang J. Application of temporary plugging and acidization in Changqing low permeability reservoirs. *Chem Eng Oil Gas* (2008) 37(3):229–32.

32. Xiong Y, Xueqin Z, Long S. Research and application of a new type of temporary plugging diverting agent for reservoir reconstruction. *Chem Eng Oil Gas* (2017) 46(2):59–67.

33. Wang Y, Zhou C, Yi X, Li L, Chen W, Han X. Technology and application of segmented temporary plugging acid fracturing in highly deviated wells in ultradeep carbonate reservoirs in southwest China. *ACS omega* (2020) 5(39):25009–15. doi:10.1021/acsomega.0c01008

34. Wang Y, Fan Y, Zhou C, Luo Z, Chen W, He T, et al. Research and application of segmented acid fracturing by temporary plugging in ultradeep carbonate reservoirs. *ACS omega* (2021) 6(43):28620–9. doi:10.1021/acsomega.1c03021

35. Lu Z. Progress and prospect study on temporary plugging agent for diverting fracturing[J]. *Sci Technol Eng* (2020) 20(31):12691–701.

36. Li S, Zhang H, Wang M, Zhang X, Zhou C, Hu Q. Experimental investigation into temporary acidizing of fractured Carbonate reservoirs in Sichuan Basin. *Chem Eng Oil Gas* (2021) 50(3):90–5.

37. Wu G, Chen Z, Zhang A, Zhou J, Hou Y, Xie X, et al. Experimental studies on the performance evaluation of water-soluble polymers used as temporary plugging agents. *Front Phys* (2023) 11:1174268. doi:10.3389/fphy.2023.1174268

# Frontiers in Physics

Investigates complex questions in physics to understand the nature of the physical world

Addresses the biggest questions in physics, from macro to micro, and from theoretical to experimental and applied physics.

## Discover the latest Research Topics

[See more →](#)

### Frontiers

Avenue du Tribunal-Fédéral 34  
1005 Lausanne, Switzerland  
[frontiersin.org](https://frontiersin.org)

### Contact us

+41 (0)21 510 17 00  
[frontiersin.org/about/contact](https://frontiersin.org/about/contact)

